Seismicity in the Vicinity of Yucca Mountain, Nevada, for the Period October 1, 1997, to September 30, 1999

D. H. von Seggern, K. D. Smith, and G. P. Biasi

Nevada Seismological Laboratory

Final Issue

05/11/2001

Prepared for the U.S. DOE/UCCSN Cooperative Agreement
Number DE-FC08-98NV12081
Task 12
Southern Great Basin Seismic Network Operations

TABLE OF CONTENTS

Status of the Data

The earthquake location and magnitude data (Appendix 3) and focal mechanism data (Table 6-1) are the main data in FY98-99 developed for this report. The location/magnitude data was generated under appropriate quality-assurance controls. A preliminary set of this data has been submitted to the TDMS under DTN UN0007SPA012DV.002 as "non-Q" data, pending final review and approval of this report. The FY98-99 focal mechanism data was submitted to the TDMS under DTN UN0009SPA012DV.005; again, this was submitted as "non-Q" pending report approval.

This report makes use of prior location/magnitude datasets that have been submitted to the TDMS by the Nevada Seismological Laboratory; their DTN's and status are as follows:

Period of Data	DTN #	Status
FY97	MO9906SEISYMNV.000	Q
FY96	MO970483117412.002	Q
1995 (01/01-09/30)	UN0009SPA012DV.004	non-Q
1994 (01/01-12/31)	GS950383117412.003	Q
1993 (01/01-12/31)	GS950183117412.001	Q
1992 (10/01-12/31)	UN0009SPA012DV.003	non-Q

The reason for the non-Q status of the 1992 and 1995 datasets is complex. We intend to qualify these two datasets with one of the alternative methods of AP-SIII.2Q.

Other FY98-99 data shown in graphs and tables herein were generated from the raw source data which has been submitted to the Records Processing Center under the titles "Raw seismic data collected by the Southern Great Basin Digital Seismic Network -- 10/01/97 to 09/30/98", "Raw seismic data collected by the Southern Great Basin Digital Seismic Network -- 10/01/98 to 9/30/99", and "YMP Strong Motion Network: Data: Period ... to ..." where "..." covers several specific dates within FY9899; these data were collected under appropriate quality-assurance procedures.

This report meets the requirements of the QARD in regard to seismic monitoring activities. Data collection and analysis are governed by applicable UCCSN Implementing Procedures and by the UCCSN Scientific Investigation Plan (SIP-004). There are no "models" treated in this report.

Abstract

Starting on October 1, 1995, the monitoring of seismicity within the southern Great Basin near Yucca Mountain was performed with a new digital network. This network features three-component recording with 24-bit A/D conversion in the field. Continuous data is collected at 20 sps, and event triggered windows are collected at 100 samples per second. A seismic bulletin of events is made by associating triggers occurring within a prescribed time window, classifying the local earthquake events, and locating the earthquakes and computing their magnitudes with conventional methods. This report covers the operational and seismic results of the third and fourth full years (FY98-99) of the improved, digitally based, monitoring.

The FY98-99 bulletin of earthquakes contains approximately 5700 events within approximately 50 km of Yucca Mountain. The largest event in FY98-99 had a magnitude (M_W) of 4.7. Nearly 40% of the seismicity was still concentrated in the aftershock zone of the 1992 Little Skull Mountain earthquake. Besides Little Skull Mountain, there were two notable seismically active areas: 1) a swarm-like cluster of over 1000 earthquakes (maximum $M_L = 3.6$) in Thirsty Canyon, approximately 40 km NNW of Yucca Mountain from late 1997 through the middle of 1998; 2) the M_L 4.7 earthquake near Frenchman Lake on January 27, 1999, approximately 45 km east of Yucca Mountain, with hundreds of aftershocks. Hypocentral depths, whose accuracy is greatly aided by the ability to time S-waves on horizontal components, are largely concentrated in the range of 7-12 km. The observed detection thresholds for earthquakes within the network are in the range of M_L from -0.5 to 0.5 or greater, with the lower threshold achieved for earthquakes in the Little Skull Mountain and Yucca Mountain areas.

Nearly 100 new focal mechanisms were reliably determined from the FY98-99 earthquakes. These, and the nearly 160 from the previous two years, show a fairly clear picture of the overall stress field in the region of the digital network. The tension axis is oriented at roughly 60° west of north, at shallow dip, and the pressure axis at roughly 30° east of north, with variable dip to allow for strike-slip and dip-slip motion on faults. A composite diagram of events in the zone of the Little Skull Mountain earthquake shows very consistent tension axis orientation. All known focal mechanisms were collected and reviewed for the area within roughly 65 km of Yucca Mountain. These show a consistent WNW tension axis over time and space. Focal mechanisms in the immediate vicinity of Yucca Mountain are consistent with the overall data.

The new digital network has enabled a significant increase in the detected numbers of earthquakes within or near the Yucca Mountain block itself. The overall threshold in the immediate Yucca Mountain vicinity (10-15 km from the ESF) is near $M_L = -0.5$. Aside from the change in threshold, the recurrence data for the past four years for earthquakes near Yucca Mountain overlays well with that formed from the previous 17 years of monitoring with the analog network. This recurrence rate is 20 times less than a typical area of comparable size in the southern Great Basin. In FY98-99, five additional events within or near Yucca Mountain were located; however, first-motion focal mechanisms could not be determined for any of these.

Event locations in this area of Yucca Mountain since 1992 were reworked to include station corrections. The resulting seismicity pattern after the relocation process shows clearer features and has some interesting correlations with gravity data.

Recordings from regional earthquakes were used to estimate a distance-dependent *kappa* of 0.24 ms/km and an average site *kappa* of 27 ms. Both estimates agree well with previous estimates made from local earthquakes. An analysis of signals from local earthquakes recorded at AL5 (Alcove 5-ESF) and at RPY (on surface above ESF) showed that, in the band of 2-15 Hz, RPY amplitude exceeded AL5 amplitude by approximately 3:1 to 4:1 for all three components of motion.

1. Introduction

This report covers the seismicity observed within the Yucca Mountain region during the third and fourth year of operation of the digital network, termed the Southern Great Basin Digital Seismic Network (SGBDSN). The differences between this and the former analog network, which was operational from 1978 to 1995, and the benefits of the digital network relative to the analog network are discussed in von Seggern and Smith (1997) and von Seggern and dePolo (1998). The largest changes in collection and processing of seismic data were made at the transition to the digital network, and the past two years have seen only minor improvements.

This report is organized to first present the basic information on the network performance. This comprises a brief description of the data recording, an explanation of recording problems, a discussion of the processing procedures, and some analysis of the event types. A more extensive presentation of these topics was made in von Seggern and Smith (1997). The report then presents the seismicity as seen by the network in FY98-99. A more detailed treatment of special events or topics is given; among these are earthquakes for which focal mechanisms could be determined, earthquakes that were close to Yucca Mountain, or earthquakes that had relatively large magnitude or some other aspect of interest. Lastly, the specific ground motion issues of kappa and of ESF-tunnel versus surface spectral ratios are addressed.

2. Data Collection and Processing

Station Description

The SGBDSN comprised a 26-station configuration as shown in Figure 2-1 by September 1999. Only 2 stations were added during FY98-99 to the network: SGR and AL5. A map of a larger area showing the analog (SGBSN) stations along with the digital (SGBDSN) stations is shown in Figure 2-2 because data from analog stations were used to determine focal mechanisms and to aid in the relocation of events, both topics covered later in this report. The SGBDSN stations transmitted to one of the five telemetry nodes shown in Figure 2-3. The exact installation dates of the digital stations, along with the location information for each, are listed in Appendix 1. Most digital stations use Geotech S-13 seismometers. A few use Guralp CMG-40 seismometers. The AL5 station within Alcove 5 of the ESF (Exploratory Studies Facility) uses a Mark Products 3-component L4 seismometer and also has a Geotech FPS-11A, 3-component, strong-motion instrument. Neither the Guralp nor Mark Products seismometers are used in magnitude computations.

The response in digital counts to ground displacement versus frequency of the SGBDSN instruments is shown in Figure 2-4. These responses are nominal for all instruments in the two main groups, S-13 or CMG-40. Actual calibration data show that there is only a maximum of ±10% deviation for any particular instrument from the nominal curves. Calibration pulses were analyzed monthly to ensure that none of the instruments drifted outside of this range. The free period of the S-13 instruments was set to 1.0 s and that of the CMG-40 instruments to 30 s. The damping coefficient

was set to 0.7 of critical damping in all cases. Also shown is the response of a typical instrument of the analog network (WCT). The S-13 recording response for the SGBDSN peaks at roughly 40 Hz compared to 20 Hz for the instruments of the analog network. The 40 Hz cutoff is due to antialiasing filters in the DAS (Digital Acquisition System) units. It is important to point out that the much higher noise floor of the analog recording makes a much narrower usable recording band in the frequency domain than for the SGBDSN recordings. Figure 2-5 shows a typical local earthquake recorded at the sites WCT (analog) and WLD (digital) which are within 20 m of one another. The higher background noise of the analog recording is evident before the P-wave arrival at 5 seconds. Figure 2-6 shows the spectra of the signal and prior noise at both sites. The digital signal has a usable bandwidth from 1 to 45 Hz while the analog is usable only from 5 to 25 Hz. A 20-Hz low-pass filter operates on the analog signal at the site. The overall higher background of the analog recording is due to noise in the analog telemetry. The CMG-40 instruments are recorded at a lower gain than the S-13 instruments in order to provide some on-scale recording for the network in the case of a larger earthquake because the S-13 instruments clip at close distances (< 10 km) for earthquakes as small as $M_L = 3$.

Station locations were determined with a Trimble GPS unit. Data recorded in the field was downloaded and corrected to base station readings taken at the YMP Field Operations Center. This differential GPS location procedure is accurate to within approximately 10 meters in the horizontal plane. The elevation is taken from the GPS readings also but may be in error by up to 20 meters or more. Locations in Appendix 1 are for the seismometers themselves, not the antenna position.

Data Collection Method

The field data acquisition systems are described in von Seggern and Smith (1997). During the time period covered by this report, two data streams were in effect at all stations: 1) a 20-sps, 3-component, continuous data stream and 2) a 100-sps, 3-component, triggered data stream. The former was enabled with a "continuous" trigger specification which creates contiguous trigger windows of 30 minutes duration each. The latter was controlled by an "event" trigger specification with the following parameters:

short-term average (STA) length	0.4 seconds
long-term average (LTA) length	10.0 seconds
STA/LTA trigger threshold	3.5
pre-trigger record length	30 seconds
total record length	150 seconds
channels included in trigger	Z, N, E
threshold exceeded by at least *n* channels	1

The manner of data collection at the Nevada Seismological Laboratory is also as previously described in von Seggern and Smith (1997). The result of the automated data collection is basically two data sets:

1) large 24-hour files (one per station) holding all the original data packets sent from the field acquisition units,

2) "trigger" files of 150-sec length, at a sample rate of 100 sps, in SEGY format, three per station trigger, one for each component of motion (Z,N,E).

The triggered data is then available for review and manipulation with standard seismic processing software. For each trigger, an entry was made in a file called trigger.log. The contents of this file give a complete history of the triggering of the network by time and station, and so it serves as a valuable resource for analyzing network performance.

Downtime and Problems

The reliable collection of data is subject to the following problems:

* seismometer malfunction or failure
* DAS malfunction or failure
* radio transmission interference
* telemetry interference or failure
* hardware failure at the central recording site
* software failure at the central recording site

Except for seismometer failures, the effect is almost always to record no data rather then to record corrupt data. Corrupt data intervals are reported on Non-Conformance Reports (NCR). Seismometer malfunctions are covered by IPR-001 and are also reported on NCR's. In the third and

fourth years of operation, various examples of all of these types of problems occurred. Downtime information was entered into an online computer file when it occurred. A printout of that file for FY98-99 is shown in Appendix 2. This downtime log was used to note only major recording problems that affected most or all of the stations, with consequent loss of data over a certain significant time period. "Significant" in this context means more than roughly 10 or 15 minutes. Often, short downtimes were associated with computer reboots and program changes; and these were not recorded. If one sums the downtime hours indicated by Appendix 2, the overall FY98-99 network downtime is 0.38% of total time. Figure 2-7 shows that, after the first six quarters of SGBDSN operation, the downtime has reached more or less a steady state. This improvement was achieved with several software and hardware "hardening" steps, with the most significant probably being the installation of a paging system which detects when the data collection program fails or when the data collection computer stops. At the end of 1999, this paging system was implemented with a cellular phone.

There were numerous occasions where individual stations were down; these times were not recorded though. Such single-station situations only marginally impact the ability to locate events within the network. A statistical analysis of the first year of SGBDSN recording in von Seggern and Smith (1997) revealed that, on average, station downtime may have been as high as 15%. This figure is considered an upper limit for recording in FY98-99 because of the measures taken to "harden" the data collection. A very rough indication of each station's downtime in FY98-99 could be estimated though from the trigger.log file mentioned above, but this was not attempted on a station-by-station basis.

Daily Processing

Trigger windows from the 100 sps stream were automatically converted to SEGY files as mentioned above. These files became the pool of data from which seismic events could be associated, classified, and located. The data flow is illustrated in Figure 2-8. A processing scheme which treated a single day's data was applied within one to three days typically after the day's recording was complete, as outlined in Figure 2-8.

The association of triggers to common events was described in von Seggern and Smith (1997). Basically, because the areal size of the network is small, a simple method based on a short time delay between triggers (< 15 s) can be used successfully. After waveforms for the associated triggers are moved to an event directory, the triggers that are left behind are usually non-earthquake noise triggers. However, all unassociated trigger waveforms were examined for possible earthquakes. Any signals believed to be from local earthquakes were moved to a special event directory reserved for small events. Sometimes, true event signals were missed by the association process because the field acquisition unit triggered early on some prior event or noise burst and thus an inappropriate start time for the signal file was registered. Signals meeting this late criteria and which appeared to be associated with local events already created by the automatic association process were moved to the event directory.

In the event directory, the analyst reviews all the files with the PASSCAL program called *pql*. At this time an annotation is made of event type in the online file *Event_list*. which contains a list of all the associated trigger files for a given day. The annotations and their criteria are:

L = local	an event whose S-P time is t < 3 sec at one or more stations
R = regional	an event which does not meet the local criterion but appears to be < 20° distant from the network (20° is the accepted cutoff for classifying events as regional or teleseismic)
T = teleseismic	an event which appears to be > 20° from the network
P = blast	an event which appears to have been a manmade explosion
N = noise	an event which appears to be some kind of non-seismic noise
C = calibrations	an event consisting of calibration pulse recordings (programmed to occur regularly at 08:00:00 UTC each day)

All "local" events were later picked and located, if possible. There are uncertainties in applying the above criteria, and seismological judgement is often involved. The reading of P times is not always clear for signals which are near the background noise level, and the reading of S times is often uncertain to within a few tenths of a second. The classification of teleseismic versus regional events is very uncertain around the 20° epicentral distance cutoff between them. There is really no practical effect of a misclassification between these two types because all regional and teleseismic event files are archived for later possible use anyway. Subsequent referral to NEIS or various regional network bulletins could determine the exact location of the event if that were required.

Once the events are classified for a given day, all the files belonging to "noise" events are removed from the directory. Using the Event_list file, a summary sheet is printed out with the trigger time of the first station for each event and the event type as given above. This sheet serves as a guide in

locating the day's events.

The arrival times are picked in a program called *dbpick*, and events are located simultaneously in a program called *dbloc2* to give the preliminary locations. Both these programs are graphics application tools associated with the Datascope database (Quinlan, 1998). In order to use these programs, the waveform file names are first entered into the database, along with parametric data necessary to read and display the waveforms.

The location program *dbloc2* enables the user to add and delete picks from the set used to locate an earthquake, choose one of several velocity models, and constrain the depth if necessary. It provides graphical feedback on the quality of the location. A significant number of events which were classified as local events cannot be actually located, and this fact is entered on the event summary sheet. Reasons for failure to locate an event are: 1) less than three stations, 2) less than five total picks, 3) unacceptable residuals (usually an rms > 0.2 s, but subject to case-by-case judgement) or 4) inability of the location algorithm to converge. Any other pertinent comments are also entered on the event summary sheet.

The magnitude M_L is calculated after the locations are made. The original Richter (1935) formulation for local magnitude is used:

$$M_L = \log_{10}A - \log_{10}A_0$$

where A is the maximum amplitude in mm on a horizontal seismogram of a Wood-Anderson (W-A)

instrument with a magnification of 2800 and $\log_{10}(A_0)$ is the distance-correction term as tabled by Richter to make a magnitude 3 earthquake have an amplitude of 1 mm at 100 km from the source on a W-A seismogram. Application of this formulation requires a conversion of the S-13 response, which is constant in the velocity spectrum, to the Wood-Anderson response, which is constant in the displacement spectrum. In so doing, the actual magnification of the S-13 recordings is accounted for. The response reshaping is done using a 5-s window of the seismogram starting 1 s prior to the S-wave arrival. If no S wave was picked but a P wave was, the window is set to start at the P time and to have a duration of 15 sec, which is long enough to catch the S arrival for local earthquakes within or near the network. The maximum amplitude on the converted horizontal seismograms is used as A in the formula above. If neither P nor S was picked at a station, no attempt is made to calculate magnitude at the station. The event magnitude is the average of all available station magnitudes.

When all locations and magnitudes are complete for a day's data, the arrival times, hypocenters, and magnitudes are all contained in the Datascope database files (Quinlan, 1998). These files are organized into individual calendar months and kept online. Among other capabilities, the Datascope utility programs allow one to retrieve data according to various selection criteria; create, delete, or change records; plot numeric parameters; and convert data to various specifications. All of the site information is kept in the Datascope database also for easy reference and for ease in access by other programs. Datascope now contains four years of data for the SGBDSN (October 1, 1995 to September 30, 1999).

Event Classification Results

During FY98-99, the total number of associated triggers was 286,786 from a pool of 1,077,610 original triggers. From these associated triggers, the number of events which fell in each category were as follows:

L (local):	7,812
R (regional):	15,738
T(teleseism):	2,445
P (blast):	360
N (noise):	14,773
C (calibration):	730
Total	41,858

Thus in forming a catalog of earthquakes for the two years, nearly 42,000 events were reviewed, or approximately 57 per day. It is emphasized that all triggered seismograms, whether associated or not, are reviewed; therefore, the identification of local earthquakes is nearly as complete as possible. Only by reviewing the continuous data at each station could more events be found; it is believed that such massive effort would only produce a minor decrease in the threshold, perhaps 0.1 or 0.2 magnitude units. Note that local earthquakes are only about 20% of the events that are reviewed. It must be remembered that not all the events classified as "local" were actually located. In fact, only 5733 of the possible 7,812 local events appear in the final catalog. One reason for this decrease is that many events identified as local had actual signals on only one or two of the triggered stations; the other triggered stations would be simply noise or otherwise. Of those local events with three or

more legitimate station triggers, many were unlocatable due to the fact that there were less than five pickable arrival times or that the location algorithm did not converge (rare). These latter cases were mostly in the outlying parts of the network where the station coverage was poor or at the network fringe and beyond, where the azimuthal gap of the observing stations was too large to determine a location. Finally, a few events were eliminated by hand in the final review of the catalog (see below).

Picking Errors

The program *dbpick* allows the analyst to set a value for the picking error. This varies greatly depending on the how impulsive the arrival is and how its amplitude compares to that of the seismic background noise. This value has a significant subjective component and cannot be quantitatively determined in any precise sense except where the first arrivals of P waves are very clear and impulsive; such arrivals intrinsically have an error no more than the sample interval (0.01 s for the SGBDSN data). Especially for S waves, the setting of picking error is very subjective. During FY98-99, the SGBDSN picks were made by the authors and three other individuals; a comparison of the distribution of picks made by each did not show any significant differences, and so they are lumped together here for presentation.

All the picking error values for FY96-99 (4 years) were extracted from the data base for arrivals associated with preliminary hypocenters; there were 105,173 such arrivals. Cumulative distributions were computed for the assigned P and S pick errors separately. These distributions for P and S are plotted in Figure 2-9 as large circles and squares, respectively. Note that nearly 95% of the P picks

had the timing error set at less than 0.05 s while less than 40% of the S picks fell in this range. Cases of errors greater than 0.15 s assigned to either P or S are extremely rare. This information is seemingly difficult to reconcile with the other curves on the plot showing the distributions of absolute values of P and S residuals as determined by the location program (predicted - actual travel time); these curves do not reach their 90% values until the 0.20 to 0.25 s range, with the S curve showing a significantly broader distribution. The large discrepancy between assigned picking errors and location residuals is partly explained by significant error in the assumed velocity model used in the locations, probably in a 3-D sense. It is also explained by the fact that the designated picking errors will tend to be smaller than actual. In fact, in the case of grossly mistimed arrivals, the assigned picking error will bear little relation to the actual error. It will be important at some future time to refine the velocity model in order to reduce the location residuals. However, even then their distribution will not likely approach closely that of the picking errors because full 3-D models only typically reduce the location rms residual by about one-half and because the picking errors may be underestimated in many cases. Von Seggern and dePolo (1998) showed that there is only weak correlation between picking errors and location residuals. This result is not surprising, for the assigned picking errors generally contribute to the location residuals but only as a second-order effect.

Finalizing the Earthquake Catalog

The final locations and magnitudes for the FY98-99 earthquakes were obtained according to UCCSN procedures IPR-002 and IPR-003. The location program specified in IPR-002 is HYPOINVERSE (Klein, 1989), and the magnitude program specified in IPR-003 is MLCALC which was internally

developed and implements the magnitude calculation outlined above.

The preliminary earthquake catalog for FY98-99 contained a total of 6023 earthquakes. The procedure for computing final locations (IPR-002, "Determining the Location of Earthquakes Recorded by the Yucca Mountain Seismic Network") directs that the arrival times and preliminary locations be extracted from the Datascope tables and reformatted for input to the program HYPOINVERSE (Klein, 1989). It requires that arrivals with residuals larger than 0.3 s not be used. It also requires that a single velocity model be used for the entire suite of earthquakes; this model, called the "moonhof" model (Hoffman and Mooney, 1984), has the following structure:

Depth (km)	P velocity (km/s)
0.0	3.00
1.0	5.85
25.0	6.35
30.0	6.60
35.0	7.80

HYPOINVERSE was then run in batch mode with this input. A few hypocenters were eliminated because they had four or less arrivals. At this point, events with large azimuthal gaps (>330°) and with large horizontal error (> 5 km for one sigma) were culled out for review. Events which were just west of the Little Skull Mountain area were also reviewed because several of them were considered unreliable. This unreliability was due to the fact that, for many of these events, the only observing stations were LSC, FMW, and CAF, which are nearly in a linear configuration (see Figure

2-1). This review eliminated over 100 events. The procedure then calls for removing arrivals having residuals greater than 0.3 seconds. The program was rerun with the same input and with this constraint, and a few additional events could not be located because the number of acceptable arrivals fell below five. A total of 5733 events remained in the final catalog which is listed in Appendix 3.

Note that the catalog of events in Appendix 3 includes error bars (+/- one standard deviation) for the horizontal (erh) and vertical (erz) precision of the hypocenters. These are indicative of the location quality. These errors are considerable in some cases, on the order of several km, and are generally greater for the erz values than the erh ones. The density of these errors, in 1-km bins, is shown in Figure 2-10. In the case of horizontal errors, 90% of the events have standard errors < 1.8 km. For a 95% confidence ellipse and assuming a normal distribution of errors, this should be doubled to 3.6 km. Assuming a circular 95% confidence region, this becomes the radius of a circle with area given by $\pi(3.6)^2 = 41$ km^2.

The results here must be weighed in relation to the constraints (mostly programmatic) used in producing the final locations. One of these constraints was the use of a single 1-D velocity model for the entire network region. Another was the fact that, although numerous analog stations still were operating within the southern Great Basin, arrival times from these stations were not used. Aside from the location precision indicated by the erh and erz values, there is the question of accuracy. Especially for events near the fringe of the SGBDSN network, the addition of analog readings, if available, would have improved both location precision and accuracy in nearly every case. It is important to note, however, that even with excellent station coverage in both distance and

azimuth, locations can be significantly off. The non-proliferation explosion (NPE) of September 22, 1993, was recorded by the entire analog network and had excellently timed arrivals; but its computed location, with depth constrained to the known 0.4 km, was off by approximately 2 km horizontally (von Seggern and dePolo, 1994). The 95% confidence ellipse had a semimajor axis of only 0.5 km and thus failed to cover the true location. This inaccuracy is due to the significant 3-D velocity variations in the southern Great Basin which are not accounted for in routine location with a 1-D flat-layered velocity model.

3. Seismicity Characteristics

Spatial Pattern of Earthquakes

Previous reports on seismicity in the southern Great Basin using the analog network (SGBSN) have shown that the area immediately around Yucca Mountain itself is rather aseismic and that the seismicity tends to be clustered spatially (von Seggern et al., 1995, and references therein). For reference, an epicenter plot for the historical seismicity of 1868 to 1978 (Meremonte and Rogers, 1987) is shown in Figure 3-1 and another for the years 1978-1995, when the area was monitored with the analog network (see Figure 2-2), is shown in Figure 3-2. The epicenters in the plot of historical data have large uncertainties, and spatial representation of actual seismicity is probably very distorted. The 1978-1995 data has much lower uncertainties, and spatial patterns can be inferred reliably. However, many of the epicenters in the NW part of the NTS are probably induced seismic events associated with high-yield, underground, nuclear explosions. Since June 29, 1992, the date of the Little Skull Mountain earthquake, the majority of earthquakes within the monitored region have occurred in the aftershock zone of this earthquake (roughly 20 km southeast of the ESF). Since October 1, 1995, the seismicity within the Yucca Mountain region has been located with the digital network (SGBDSN); the epicenter plots from this network for FY96 (von Seggern and Smith, 1997) and FY97 (von Seggern and dePolo, 1998) are shown in Figures 3-3 and 3-4, respectively. These show the continued dominance of the Little Skull Mountain aftershocks.

For the period of this report (FY98-99), Figure 3-5 shows the epicenters of 2744 earthquakes located

with the SGBDSN in FY98; similarly, Figure 3-6 shows the 3002 earthquakes located in FY99. Notable features of the FY98-99 seismicity pattern are: 1) the large number of continuing aftershocks near Little Skull Mountain (roughly 20 km southeast of the ESF); 2) the cluster of events near 37.2N, 116.6W which is termed the Thirsty Canyon swarm; 3) the large cluster of events on the east boundary of NTS, which are aftershocks of the $M_L = 4.7$ Frenchman Lake earthquake of January 27, 1999. Approximately 39% of the events in the FY98-99 catalog are in the area of the Little Skull Mountain earthquake, as defined by the rectangle (36.68N, 116.35W) to (36.78N, 116.20W). Roughly 20% are in the Thirsty Canyon swarm and roughly 19% in the Frenchman Lake sequence. Later sections of this report will focus on the seismicity in each of these two clusters. Additional notable zones of activity include a small FY98 cluster near 37.0N, 115.9W and a small FY99 cluster near 37.3N, -116.2W. Neither of these clusters seems to be represented in the prior known seismicity.

Figure 3-7 shows those events in FY98-99 larger than $M_L = 2$. The largest earthquake in the FY98-99 catalog is the Frenchman Lake earthquake ($M_L = 4.70$, January 27, 1999, 10:44:22 UTC). The next three largest events were aftershocks of this event, with magnitudes 4.03, 3.85, and 3.59. The only other event with $M_L > 3.5$ during the two years occurred in the Thirsty Canyon swarm ($M_L = 3.57$, April 2, 1998, 19:20:16 UTC). The $M_L > 3$ event within the 25-km circle around Yucca Mountain was in the northeast part of Jackass Flats near the $M_L = 3.9$ Calico Hills earthquake discussed in the FY97 report (von Seggern and dePolo, 1998). The immediate area around this earthquake has continued to be active through FY99. Missing from this and previous maps is the M 5.7 earthquake and its aftershocks at Scotty's Junction (August 1, 1999, 16:06:22 UTC), approximately 37.4N, -117.0W. These events are considered to lie outside the network, and

locations with only SGBDSN stations would be subject to significant inaccuracies. We note that the Scotty's Junction earthquake was the largest in the southern Great Basin since the 1994 Eureka Valley earthquake and the largest within 75 km of Yucca Mountain since the 1992 Little Skull Mountain earthquake.

Figure 3-8 shows the FY98-99 seismicity overlain on a fault map of the NTS region. These faults are taken from the GENISES dataset labelled "fnyesu" on the *Yucca Mountain Project GIS CDROM for 1998*. In preparing this plot, only FY98-99 epicenters with magnitudes ≥ 1.0 were used; this subset amounted to less than 10% of the total number of epicenters. In general, these are the best located earthquakes due to the fact that a majority of the network usually detects any event above magnitude 1.0. The spatial relation of earthquakes to mapped faults must be subjected to careful interpretation because: 1) faults may have significant dip and therefore not overlay a plotted epicenter which lies directly above the hypocenter of a particular earthquake; 2) epicenters, even for well located earthquakes, may have inaccuracies of 2 km or more; and 3) many earthquakes are known to occur on faults that have no mappable surface expression. With these items in mind, the fact that there is little apparent correlation between earthquake locations and mapped faults in Figure 3-8 is not surprising.

A meaningful comparison of the seismicity as seen by the digital network in FY96-99 can be made to that seen by the analog network in prior years (1978-1995) if two adjustments are made. Firstly, the thresholds of the digital and analog networks are different, with the digital one being much lower; and a common cutoff should be made on both catalogs such that complete detection above this cutoff is assured. Secondly, the magnitudes of the analog network catalog in the years of 1992-

1995 were duration magnitudes and must be converted to equivalent local magnitudes. The magnitude adjustment is made according to the M_L-vs-M_D formula given in von Seggern and Smith (1997):

$$M_L = -1.24 + 1.31\ M_D$$

The threshold adjustment is then made by cutting the catalogs at $M_L = 1$. (That this cutoff ensures nearly complete detection for the analog catalog is shown in Figure 3-20 at the end of this section.)

With these adjustments, we make three plots. The first in Figure 3-9 shows the $M \geq 1$ earthquakes of the digital (FY96-99) catalog compared to $M < 1$ earthquakes in this catalog. The purpose of this side-by-side comparison is to highlight areas of seismicity which are revealed by having a low threshold; such areas should show up only in the plot of the $M < 1$ earthquakes on the right. Certainly, the immediate area around Yucca Mountain is one of these; no earthquakes with $M > 1$ were located by the SGBDSN within 10 km of the proposed repository. This comparison also shows that, with only a few exceptions, the seismicity just north of and just south of the reposed repository, but within 25 km of it, is comprised of $M < 1$ events. Otherwise, the $M < 1$ seismicity appears to be occurring in areas which have $M \geq 1$ seismicity, and vice-versa.

The second and third comparisons show the $M > 1$ seismicity of Figure 3-9 in comparison with that for the analog catalog after the $M = 5.6$ Little Skull Mountain (LSM) earthquake and then before it. The date of this earthquake, June 28, 1992; is a natural break in the instrumental catalog for the Yucca Mountain vicinity because of the dominance of its aftershocks in the post-LSM catalog.

Figure 3-10, having the post-LSM data, has a time span for the analog catalog of roughly 3 years and 3 months while the span for the digital catalog is 4 years; therefore a good comparison is possible. This figure shows that the LSM aftershocks have continued through 1999, at about 20 km southeast of the proposed repository, but at a lesser rate and in a more confined area than that in the initial years after the LSM earthquake. The M = 4.7 Frenchman Flat earthquake and its aftershocks of early 1999, near the eastern boundary of NTS, show up clearly on the plot of the digital catalog, but this area was evidently active in the post-LSM years of the analog catalog. Aside from these two notable areas, there is not a great difference between the seismicity patterns for the two periods. Figure 3-11 shows the pre-LSM data for the analog catalog in comparison to that of the digital catalog. However, the time span of the analog catalog here is roughly 3.5 times that of digital catalog and so the comparison is somewhat obscured. With this difference in mind, it is notable that both the LSM earthquake area and the Frenchman Flat earthquake area were active before the occurrence of their respective main shocks. A further matter in obscuring the pre-LSM data is the presence of many events induced by underground nuclear explosions in the northern part of the NTS. Disregarding the influence of the explosions and the occurrence of the two large earthquakes, the patterns of seismicity again do not appear to differ in significant ways.

Temporal Distribution

Figure 3-12 shows the plot of cumulative number of earthquakes versus time for the FY96 through FY99 catalog of earthquakes; this spans the operation of the SGBDSN. Except for the Thirsty Canyon swarm and the Frenchman Lake sequence, the slope of the line is fairly constant, with the average rate being roughly 5 to 6 earthquakes per day after removal of their effects. In the FY98-99

reporting period, only two new sites, SGR and AL5 (see Figure 2-1), were installed in the network; and the addition of these sites has no significant effect on the observed earthquake rate. A more meaningful temporal plot is the cumulative moment release over the same four years, as shown in Figure 3-13. The moments were computed from the relations

$\log10(M_0) = 1.5(M_L + 10.7)$	$M >= 3$	(Hanks and Kanamori, 1979)
$\log10(M_0) = M_L + 17.55$	$M < 3$	(von Seggern and Smith, 1997)

This is dominated by the Frenchman Lake earthquake ($M_0 = 1.26*10^{23}$ dyne-cm from formula above) which occurred after an anomalously low rate of moment release for approximately the previous 300 days. The end of FY99 appears to again be characterized by this low rate. Compared to the 1992 Little Skull Mountain earthquake with a moment reported in the range of 2.5 to $5.5*10^{24}$ dyne-cm (Anderson et al., 1992), the cumulative moment observed with the SGBDSN, even with the Frenchman Lake earthquake, is insignificant for the region within the network.

As stated previously, the seismicity rate at LSM continues to be a dominant feature of the SGBDSN catalog. The main shock occurred on June 29, 1992; and we have consistently located events in the aftershock zone since October 1, 1992, when we took over operation of the analog network. The location of events has continued with the SGBDSN since October 1, 1995. In order to combine the SGBDSN data of the past four years with the analog network data of the previous three years, a magnitude adjustment was required on the M_D (coda) magnitudes of the analog network. From the linear relation developed in von Seggern and Smith (1997), the M_D's were converted to equivalent SGBDSN M_L's for the 1992-1995 dataset. Then the combined catalog was cut at a minimum

magnitude of 0.5, well above the threshold of location for LSM events; this high value was chosen so that a comparison can be made with time prior to 1992 when the network's threshold was higher around LSM. The event count per month of $M_L > 0.5$ LSM aftershocks is then shown in Figure 3-14 for the 7 years of NSL reporting. Note that the rate of such events at the end of FY99 appears to be less than ten per month. In comparison, the background rate of $M_L > 0.5$ earthquakes in the identical LSM zone as seen by the analog network in the period 1982 to 1991 averaged approximately two per month. We emphasize that the network threshold for LSM earthquakes was at least as low as $M_L = 0.5$ prior to 1992. Thus, the apparent rate of seismicity at LSM is still roughly 4-5 times the pre-LSM earthquake rate.

It is important to note that month 79 in Figure 3-14 corresponds to January 1999, the month in which the Frenchman Lake earthquake occurred. The number of LSM aftershocks increased significantly in this month and in the four following months, compared to the rate prior to January 1999. The distance from the Frenchman Lake earthquake to the LSM aftershock zone is roughly 20 km. Because it is likely that the LSM main shock was triggered by the M = 7.3 Landers earthquake which occurred one day prior to it at a distance of 240 km (Hill et al., 1993), we should not be surprised that the aftershock zone may have responded to this closer event. A rough estimate of the influence of the two events on the zone around the LSM earthquake can be obtained from the M_L values for the two events, 4.7 versus 7.3, and the distance terms in the M_L formula appropriate to the two events. In the Richter formula for M_L, the displacement predicted for an event is given by:

$$\log A_{mm} = M_L - \log A_0(r)$$

where $\log A_0(r)$ is the variable distance term, 1.6 and 3.7 in the case of Frenchman Lake (20 km) and Landers (240 km), respectively. Thus, the comparative amplitudes are the antilogs of 3.1 and 3.6, or an amplitude ratio given by the antilog of the difference, which is 0.5. Although this amounts to a amplitude factor of 3 in favor of the Landers earthquake, this seems to be not highly significant, given other uncertainties in making this rough comparison. One can only speculate that the LSM aftershock zone did indeed respond to the Frenchman Lake earthquake even though it was nearly seven years since the LSM main shock. One should also consider here the rise in aftershock rate at 50 months (September 1995) in Figure 3-14. This increase is not accompanied by any events of magnitude greater than 3.5 within the entire southern Great Basin, as seen from the earthquake catalog of the SGBSN.

The aftershock decay rate for the LSM earthquake sequence was reported in von Seggern and dePolo (1998), and here we will repeat the analysis with two additional years of data. The number of aftershocks versus time is often fit with a model called the "modified Omori law" (Kisslinger, 1993); the equation of this model is:

$$N(t) = \frac{K}{(t+c)^p} + r$$

where

N = rate of aftershocks at time t

K = constant

t = time since start of sequence (usually $t = 0$ at time of main shock)

c = adjustment term for modified law

p = exponent of decay rate

r = constant background rate of seismicity

The parameter p is the important one in this formulation, with a low value indicating a persistent aftershock sequence. In this case, the NSL catalog of aftershocks did not begin until October 1, 1992; and so this is taken as $t = 4$ (four month from the occurrence of the LSM main shock). The events were binned into monthly intervals, and so the rates in the above will be in units of number per month. A non-linear fitting algorithm was used to determine the parameters K, c, and p with r held to the known background rate of 2.1 per month. Figure 3-14 shows the resulting curve along with the data; it appears to be an excellent fit to the data, and the parameters of the fitted model are $K = 5053$, $p = 1.555$, and $c = 3.557$. The decay exponent of 1.555 is higher than the 1.08 determined by Gross (1996) using events of the LSM aftershock series. The value 1.555 would lie in the upper quartile of values determined by Kisslinger (1993) for 29 different aftershock series. However, it is not much greater than the 1.24 found for the nearby Eureka Valley, California, sequence by Gross. It should be pointed out that there are at least three significant differences between the LSM dataset used here and the LSM one used by Gross: 1) the dataset here started with three month's delay from the time of the main shock while the dataset in Gross started shortly after the main shock, 2) the magnitude cutoff used by Gross (1.5) is a whole unit higher than the one used here, and 3) the length of the dataset here is seven years versus two years in Gross. All these reasons may contribute to obtaining different values of p. Using the fitted parameters, the modified Omori Law predicts that in the year 2010 there will still be an excess of one event per month over the background rate of 2.1.

Depth Distribution

For the FY98-99 catalog, the distribution of hypocenter depths is shown in Figure 3-15. The data was binned in 1 km intervals (0-1, 1-2, etc.), and bin counts are plotted at the midpoints of the bins. Due to the dominance of LSM seismicity and to the large contributions of the Thirsty Canyon swarm and the Frenchman Lakes sequence, the catalog was subsetted around these groupings and separate depth distributions were formed. Overall, most events occur in a fairly limited source zone of 6-12 km. The increase in number of events at 1-4 km depth is probably contaminated by a significant number of events whose depth was not well determined; however, many earthquakes in the Rock Valley area are known to have shallow depth. The significant number of events with zero depth, 52, is probably more indicative of poor location quality than actual shallow depth of faulting. The depth distributions for all events in FY96 (von Seggern and Smith, 1997) and FY97 (von Seggern and dePolo, 1998) are very similar.

Figure 3-15 shows that events in the LSM zone have a very narrow peak in depth from 8 to 13 km. Given the probable errors in location depths, this peak could actually be somewhat narrower. For events in the Thirsty Canyon swarm, the depths are heavily concentrated in the narrow range of 6 to 8 km. For the Frenchman Lake sequence of aftershocks, the depths are broadly distributed over the range of 0 to 16 km. The location of these latter events was impaired by emergent P-waves, uncertain S waves, and lack of stations to the east; consequently location control, especially depth, was very poor. This will be discussed more fully in a later section.

For comparison with previous data, the catalog for the analog network for October 1992 through

October 1995 was searched for events within 50 km of station RPY and the depth distribution formed from the result. The result is shown in Figure 3-16 along with the FY98-99 data. Note that the hypocenters of prior years show a very narrow peak in the depth distribution at 9-10 km. This can be explained mostly by the fact that the LSM aftershocks comprised 75% of the analog SGBSN catalog in these years and that these events seem to occupy a narrow range of depths. Furthermore, the LSM aftershock zone was well instrumented in FY92 through FY95, with 7 stations added to the network immediately after the main shock (Figure 2-2). Consequently, depth control was better. For FY98-99 the LSM aftershocks only comprised 39% of the SGBDSN catalog. Although the peak in the range of 9-11 km for FY98-99 data reflects the prior years' peak, it is somewhat broader and shifted upward by perhaps one km. The hypocenters for FY98-99 include relatively more shallow depths. This is due in part to the influence of the poorly located Frenchman Lakes sequence. Also for FY98-99 a significant number of events are still on the fringe of the network where large azimuthal gaps in recording stations result in poor hypocentral depth control. The events in the FY92-95 catalog generally did not have this problem because the SGBSN network extended well beyond the SGBDSN network.

If the epicenters of the events with $z < 4$ km are plotted as in Figure 3-17, it can be seen that they are mostly associated with the Thirsty Canyon swarm and Frenchman Lake sequence. Otherwise, they are somewhat broadly distributed. The events with shallow depths on the fringes in the western part of the network (> 116.7 W) always have poor azimuthal coverage of detecting stations, and it is presumed that most of their depths are actually greater. It is notable that only 14 of the events on this plot have magnitude > 2 (some points obscured) while, for the entire FY98-99 catalog, approximately 100 events had magnitude > 2. This suggests that shallow depths may occur for the

smaller events due to less location control. The one area known to have truly shallow depths is Rock Valley (Shields et al., 1995), which lies to the southeast and east of the LSM aftershock zone. Several of the events which plot there in Figure 3-17 have excellent picked times and good azimuthal coverage, and their computed shallow depths are thought to be accurate. Shallow depths for events in this area have been previously determined with the aid of portable seismic stations by Shields et al. (1995).

On the other end of the depth distribution of Figure 3-15, only a very few events (132) were located with depths greater than 14 km. The locations of these epicenters are shown in Figure 3-18. Note that many of these are associated with the Frenchman Lake sequence, whose events are often poorly located. Other clusters of deeper events to the southwest at the California-Nevada boundary and to the north of the NTS have poor network control (Figure 2-1). The remainder of the deeper events are also suspect and of small magnitude.

Magnitude Distribution and Threshold

As discussed in a previous section, the SGBDSN catalog magnitudes were computed by the original Richter (1935) M_L formula, except for the fact that SGBDSN velocity seismograms had to be converted to pseudo-Wood-Anderson seismograms. Analysis of SGBDSN magnitudes in von Seggern and Smith (1997) showed that the Richter M_L formula applies sufficiently well to the SGBDSN region of coverage and should not introduce any bias. A good check on SGBDSN magnitudes can be made by comparing magnitudes of larger earthquakes with published magnitudes from the NEIC catalog. Taking the earthquakes with $M_L > 3$ in the FY98-99 catalogs, we searched

for local magnitudes (M_L) assigned by the NEIC (National Earthquake Information Center) for these events. Table 3-1 lists the events, their SGBDSN M_L , and the NEIS M_L found for them. The average of the difference (NEIS - SGBDSN) for the eight events with M_L magnitudes listed by NEIS is +0.01. A similar result of +0.10 was found in von Seggern and dePolo (1998) based on nine earthquakes in FY97. These results strongly imply that there is no significant magnitude bias associated with the SGBDSN magnitudes relative to those determined by a broader network.

For the entire suite of earthquakes in the SGBDSN FY98-99 catalogs, Figure 3-19 shows the cumulative recurrence curve. The threshold of complete detection appears to somewhere in the range M_L 0.0 to 0.3. In von Seggern and dePolo (1998), the threshold was stated as M_L = -0.3 for the catalog of FY97. We do not believe the intrinsic network threshold has increased in FY98-99, and one can look at the distribution of events for the answer to this difference. In FY98-99, the proportion of LSM events decreased substantially while the number of events in the Thirsty Canyon and Frenchman Lake zones became significant. Both the latter zones had earthquakes which were more difficult to detect and locate than the LSM earthquakes of identical magnitude. Thus, these changes in seismicity altogether pushed the apparent threshold up somewhat. As shown in von Seggern and Smith (1997), the network threshold for events near the perimeter of the network is significantly greater, more on the order of $M_L = 1$.

The *b* value in the equation

$$\log_{10}(N) = a - b\, M_L$$

was determined by the method given in Aki (1965) for the data in Figure 3-19. The estimated slope (b value) of 0.863 appears to be slightly greater than a visual fit might obtain. The fit to the FY96-97 data by von Seggern and dePolo (1998) gave b = 0.77, and so the current data agree reasonably well with the earlier SGBDSN results.

Extrapolation of the line in Figure 3-19 should be done with caution. A more reasonable approach would be to include all seismicity in the SGBDSN region back to the start of the analog SGBSN operation and then select a threshold of complete detection for the SGBDSN area. This was done using the catalog of events reported by the USGS through September 30, 1992, and the NSL catalog thereafter. Duration magnitudes were converted to local magnitudes for the NSL catalog from October 1, 1992, through September 30, 1995. A search on epicenters within 65 km of station RPY was performed to obtain the 1978-1999 catalog. The recurrence data from this catalog is shown in Figure 3-20. A maximum-likelihood fit to this curve does not seem possible because it lacks linearity over a large portion. We have instead lifted the curve of slope –0.863 from Figure 3-19 and adjusted the intercept for a visual fit to magnitudes in the range of 1 to 3. This curve also falls close to the largest magnitude point corresponding to the LSM earthquake. It may be a reasonable approximation to the underlying recurrence rate. From this curve, a magnitude 6.3 earthquake within 65 km of Yucca Mountain has a return period of 100 years.

4. Observed Explosions

In previous years, explosions were routinely observed within the southern Great Basin on the seismic recordings of the SGBSN stations. These explosions were recognized simply by their signal character in almost all cases and were generally ignored in post-processing. A few special cases, such as known tests on the Nevada Test Site, were located and analyzed to varying degrees. Signal features characteristic of explosions include: 1) all compressional first arrivals, 2) emergent arrivals due to ripple-firing in quarry blasting, 3) "ringing" appearance due to the same ripple firing, 4) prominent surface waves due to very shallow or surficial sources, 5) lack of clear S waves, and 6) similarity among the envelopes of the traces on all three recordings. The three-component recording of SGBDSN stations has made it easier to positively identify blasts than with the SGBSN which mostly had single-component stations.

During FY98-99 a uniform approach was used in dealing with explosions seen on the recordings of the SGBDSN stations. Appendix 4 lists the 282 events which were detected by three or more SGBDSN stations, which appeared to be near or within the network, and which were identified as explosions based on several of the criteria above. Because they were not located, the times are approximate, to the nearest minute of the actual origin time. Handwritten comments made at the time of identification are included, unless they were simply "blast". Most of these events identified as blasts occurred in the known mining areas within Bare Mountain (on the west side of Crater Flat) and to the west and north of Beatty, Nevada. The signals would arrive first at either station TAR or station WLD, and these events are the ones simply listed without comment in Appendix 4. A few

of these events were strong enough to trigger all, or nearly all, the SGBDSN stations.

The more interesting blasts were those which were located outside of known mining areas, some being on the Nevada Test Site. In prior years of 1995 through 1997, numerous blasts associated with ESF construction were recorded, but this activity has stopped. A few FY98-99 blasts were seen at stations CAF and TPW (see Figure 2-1) and may be attributable to military exercises in the Calico Hills area. Most of the events identified as blasts near the station STC are presumed to be due to weaponry tests on Nellis AFB but cannot be confirmed. A few other events identified as blasts are at random locations around the NTS and are probably due to miscellaneous construction activity. The threshold of detection for blasts with the SGBDSN has been established from a few confirmed blasts to be roughly 100# of explosive. This threshold will vary considerably around the network though.

5. Possible UNE Hole Collapses

Some unusual seismic events have occurred near the eastern edge of Yucca Flat during FY98-99 and into the current year. Our previous monitoring experience suggests that they are probably underground nuclear test hole collapses. One of these events occurred on 04/04/2000, which is not in the period of this report; but has been included anyway in this discussion. Due to the importance of such events in the framework of the Comprehensive Test Ban Treaty (CTBT) and possibly other interests, a discussion of them together in this report seems important. Previously, we reported on probable collapse events in the Pahute Mesa area (Smith et al., 1997; von Seggern and dePolo, 1998).

The locations of the four known events of this type near Yucca Flat are given in Table 5-1 and shown in Figure 5-1 on top of digital terrain data. We have also plotted the locations of announced underground nuclear explosions (UNE). The locations of the presumed collapses were made with the standard location program dbloc2 used for Yucca Mountain seismic monitoring, and the depth of zero was either the depth determined by the program (3 cases) or held fixed (1 case). Two events are nearly coincident and are not distinct on this map. The easternmost 04/04/2000 event is also the smallest one; for this reason, it's location would be considered the least accurate. On the other hand, YFT (installed in mid 1999) was used only in the location of the 04/04/2000 event; and its close proximity would justify believing that this event is the best located.

Except for the easternmost event, the presumed collapse locations fall in the region of known UNE's.

Without the UNE epicenter overlay, the digital terrain indicates many surface depressions, indicative of former collapses, in this area. Our experience with location accuracy indicates that a mislocation error of 1-2 km is not unreasonable for shallow events; for instance the NPE in September 1992 was located off by approximately 2 km with the former analog network even though the azimuthal coverage was better than what the digital network affords for these recent events. 3-D velocity models would help to resolve location of shallow events in this area.

The closest SGBDSN stations to these events, prior to mid 1999, when the Sandia station YFT was installed, are TWP and PUV, also shown on the map. The seismograms for these two stations alone reveal the unusual signal character of these events. Figure 5-2 shows the recordings at TWP for the four events and Figure 5-3 shows the same for PUV. A comparative earthquake, discussed below, is shown at the bottom of each plot. Note that the recordings of the four presumed collapse events have strong low-frequency signals, emergent P waves, and long codas. The entire network triggered for the largest event on 07/19/1998, and the first motion was dilatational at all stations that showed a clear P-wave first motion. Dilatational first motions would be consistent with a collapse.

The recordings for thirteen events in the SGBDSN catalog within 5 km of these unusual events were retrieved and examined to make sure no other similar collapse events existed. These thirteen events were confirmed as natural earthquakes. The waveform character of the natural earthquakes is illustrated by the TWP and PUV recordings in Figures 5-2 and 5-3 for one of these events with a magnitude of 0.38. It occurred on 04/20/1998 at 17:49:17 UTC and was located at 37.0805, 116.0300 with a depth of 7.7 km. These waveforms show much higher frequency, distinct P and S arrivals (at least on TWP recordings), and relatively short coda in comparison with the waveforms

of the presumed collapses.

Given the areal locations of the four events, the zero depth determination by the hypocenter location program, the negative first motions, and the waveform character that is distinctly different from those of nearby earthquakes, we tentatively identify these events as hole collapses. The only negative argument is the fact that one of the events, but perhaps the best located one, lies 1 km east of the nearest known UNE. Evidence in the form of pre-event and post-event aerial photographs, satellite images, or SAR (side-aperture radar) could make the identifications absolute.

6. Focal Mechanisms

The determination of focal mechanisms for earthquakes in the SGBDSN FY98-99 catalog was done in a manner closely following that reported in von Seggern and Smith (1997) using observed P-wave polarities. The actual program used for determining focal mechanisms is FPFIT (Reasenberg and Oppenheimer, 1985). This program was qualified in 1998 and entered into the YMP Software Configuration Management (SCM) system with reference number 10083-1.0-00. We have not only used FPFIT to compute the FY98-99 focal mechanisms, but we have recomputed all the focal mechanisms in our annual seismicity reports for Yucca Mountain, beginning with 1993, with the qualified software. This earlier data will be treated in a section on review of all known focal mechanisms later in this report.

For the current reporting period, earthquakes in the FY98-99 SGBDSN catalog, beginning with a lower cutoff of $M_L = 1.0$, were collated with those of the NSL CUSP catalog which used the analog network. When matches were found, the first motions from both data bases were merged for these common events. It is important to note that first motions for SGBDSN P waves are determined automatically in the program *dbpick*. Consequently, every SGBDSN P-wave first motion for all events was reviewed, and numerous first motions were changed as a result of this review. Due to the effort required to restore waveforms to online status, the data from the analog network were not reviewed, except for a few important events; however, first motions for the analog stations were always determined by human analysts. Note also that the number of analog stations which were recorded by CUSP steadily decreased during FY98-99 so that by the end of FY99 there were

essentially no data from analog sites to add to the SGBDSN data for determining focal mechanisms.

With the merged datasets, it was necessary to recompute the earthquake locations in order to generate a single-reference set of data for each focal mechanism. The relocation process resulted in improved locations in many cases due to the more complete coverage of the combined networks, especially for events in the SGBDSN catalog near the edge of the SGBDSN or just outside of it. After the relocation process, several events were dropped from the list due to lack of sufficient first-motion data (minimum of 15 picks), significant azimuthal gaps (greater than 180 degrees), or other data quality problems which would make a focal mechanism solution unreliable.

Program FPFIT was run on the data of the remaining 168 events. Details describing the methodology of this program are given in von Seggern and Smith (1997). After an initial run of FPFIT, discrepant first motions were reexamined for the SGBDSN readings; several cases where they were clearly wrong were corrected, and a second run of FPFIT was then made. Not all mechanisms were well defined. Most of the events showing multiple solutions were rejected. However, in a few cases it was reasonable to prefer one solution over the other(s). For instance, where only one of the multiple solutions was tectonically viable (for instance, no near-horizontal fault plane), this solution was accepted. Another situation in which one solution might be objectively preferred over the others is when one or more critical stations with clear first motions agrees with only one of the solutions.

Table 6-1 lists the 93 events for which acceptable focal mechanisms were determined. This table uses the ".fps" format in which FPFIT outputs its results. Figure 6-1 shows all the focal mechanisms

listed in the table. A significant number of the focal mechanisms in this table, as marked with asterisks, are associated with events in the aftershock zone of the LSM earthquake. Focal mechanisms of these events are usually well constrained due to the density of SGBDSN stations in the LSM area. The presence of analog stations in this area contributed further to the first-motion database; NSL installed 6 additional analog stations around the LSM area immediately after the June 29, 1992, earthquake; but these were removed in late 1998 and are no longer available.

In order to look at the individual focal mechanisms in relation to the location of each earthquake, we plot the tension and pressure vectors in Figures 6-2 and 6-3, respectively. These vectors are projected to the horizontal plane; thus, shorter vectors represent higher dip of the pressure or tension axis. The tails of the vectors are placed at the earthquake epicenters. In the tension axes plot, we see that the axes which are anomalous lie mostly to the west and southwest, in Sarcobatus Flat and Amargosa Desert. One event just south of the Nevada Test Site boundary, near the west end of Rock Valley, also shows an anomalous east-west tension axis. These anomalies are somewhat reflected in the pressure axes plot.

The area of the LSM aftershocks is too densely filled in the previous plots to adequately show the vectors. Therefore, in Figures 6-4 and 6-5 we plot the tension and pressure vectors, respectively, again projected to the horizontal plane, at a larger scale around LSM. The tension axes especially show a remarkable consistency among the focal mechanisms.

7. Special Sequences

Thirsty Canyon Swarm

A notable sequence of earthquakes occurred from October 1997 through about August 1998 in the Thirsty Canyon area just off the northwest corner of NTS. Figure 7-1 shows the epicenter of the largest event in this sequence, an M_L 3.57 event on 04/02/1998 at 19:20:16 UTC, displayed on a digital terrain map. Over 1100 events were eventually located and included in the FY98-99 catalog. Unfortunately, the early part of the sequence was not well located because the station TYM was down and the remainder of the network had a small azimuthal range in relation to the epicenters. Station STC would have been valuable except for the fact that its P arrivals were emergent and could only be accurately timed for the larger events.

On 01/05/1998, a portable station (THC) was placed near the epicenters of the sequence, as shown in Figure 7-1. This station should have helped greatly in hypocenter control; however, the S arrivals were emergent and difficult to time in most cases. Figure 7-2 shows some typical THC recordings of Thirsty Canyon earthquakes. Moreover, the geometry is such that, with THC over the hypocenters, they can swing perpendicular to the azimuth at which the remainder of the network lies, generally SSE of Thirsty Canyon, without changing travel-time residuals significantly. By the time that TYM became operational again in late 1998, the portable had been removed. The threshold of TYM was observed to be much higher than the stations to the SSE, partly due to its broadband seismometer character; but it helped constrain locations well when P arrivals could be picked on its

recordings.

The epicenters for the period when the portable site at THC was running (January-August 1998) are shown in Figure 7-3. The events have been heavily culled to eliminate the more poorly located ones. Even with the culled dataset, there is no apparent trend to the cluster and many outliers exist. 3-D projections did not help to reveal any trend to the aftershocks. The epicenters for the period when TYM was working again (January-September 1999) are shown in Figure 7-4. Again, the full dataset was culled to eliminate poorer locations. Here a fairly clear linear trend along the strike of roughly N20°E is seen. 3-D perspectives of the events are shown in Figures 7-5a and 7-5b. Note that the view from the SSW reveals an apparent high-angle fault oriented parallel to the view angle.

Several focal mechanisms for the Thirsty Canyon swarm were determined, as listed in Table 6-1. They show a fairly consistent trend for the T axis of roughly W to WNW. Figure 7-6 shows the mechanism for the largest shock. This implies strike-slip on a high-angle fault oriented either to the NW or to the NE. Note, however, that the NE-trending nodal plane is not well controlled; some adjustment to the dip of the NW plane could allow the NE plane to rotate somewhat more northward to agree with the epicenter trend in Figure 7-4.

A fault striking northeast to north would agree with focal mechanisms determined for the aftershocks of underground nuclear explosions in the northwest corner of NTS (Hamilton and Healy, 1969) and reasonably well with the trend of faults in this area (Carr, 1984). The Thirsty Canyon earthquake swarm lies at the edges of three known calderas: Silent Canyon to the northeast, Timber Mountain to the southeast, and Black Mountain to the northwest (Grauch et al, 1997). Some stress adjustment

such as occurred in this swarm would not be unexpected along these major structural boundaries. It is noteworthy that this swarm location was also active in the analog network years of 1978-1995 (Figure 3-2). In fact, there is a suggestion of a NNW-trending fault in this prior activity.

The cumulative recurrence curve for the Thirsty Canyon sequence of earthquakes is shown in Figure 7-7. Due to the non-linear character of this recurrence curve, no attempt was made to compute the *b*-value according to Aki (1965). Instead, a line with slope equal to that found for the entire FY98-99 catalog (Figure 3-16) is shown, adjusted downward to lie close to the Thirsty Canyon data. It can be seen that this line apparently overestimates the *b*-value of the Thirsty Canyon data by a small amount. This sequence had a maximum earthquake of $M_L = 3.57$ but several within one magnitude unit of that value. It is also notable that the largest earthquake came late in the sequence, six months after the initiation of activity. These characteristics are more representative of an earthquake swarm than a normal sequence with main shock and aftershocks.

The cumulative moment release for the Thirsty Canyon swarm is shown in Figure 7-8. The line is dominated by the moment of the M_L 3.57 earthquake on 04/02/1998. Total moment release is equivalent to roughly a magnitude 4 earthquake. The swarm was basically over about 270 days after the start although nearly one hundred earthquakes of small magnitude have been located there from September 1998 through September 1999. We would not be surprised to see activity increase again at this location.

Scotty's Junction Earthquake

The M_L 5.7 Scotty's Junction earthquake occurred on August 1, 1999, at 9:06 AM PDT (or 16:06 UTC) about 11 km north of Scotty's Junction, Nevada. This is about 85 km NW of Yucca Mountain and in a similar tectonic environment. The area includes several known or suspected Quaternary faults (Piety, 1996) of a variety of orientations. The earthquake involved primarily normal faulting on a moderately dipping north-northeast striking fault plane, although no detailed relocation process has been undertaken to refine the structures from the aftershock distribution. Aftershocks (Figure 7-9) show a slight alignment with the Sarcobatus Flat fault bordering the volcanic tuffs to the east of the mainshock with down-to-the-west displacement, although without detailed investigations we can only speculate on the active structure.

Several NE striking faults with Quaternary offsets are present to the east of the Scotty's Junction event and show an intersecting relation to the Sarcobatus fault (Piety, 1996). The Sarcobatus fault has been identified as a known or suspected Quaternary structure (Piety, 1996). These NE striking structures east of the Scotty's Junction event appear to be related to the northern termination of the Furnace Creek fault, where it transitions westward into the southern end of the Fish Lake Valley fault zone and eastward into distributed faults of the eastern Walker Lane belt.

The Scotty's Junction mainshock depth is estimated to be approximately 7 km by standard location methods, although permanent station coverage in the epicentral area is poor. The mainshock was preceded by a notable foreshock sequence that included 13 events $M > 2$ beginning at 9:17 PM PDT (or 16:17 UTC) on July 31, 1999. Two aftershocks of M 4.8 and 4.9 occurred within the first two

days of the sequence. The Scotty's Junction earthquake can be considered to be an analog to the 1992 M 5.6 Little Skull Mountain earthquake that occurred 20 km SE of Yucca Mountain. The magnitude and sense of displacement are similar and the surface geology is also dominated by ash fall tuffs from the Miocene Silent Canyon caldera complex.

Frenchman Flat Earthquake

The January 27, 1999, M_w 4.7 Frenchman Flat earthquake was the largest event within NTS since the M 5.6 Little Skull Mountain earthquake. This event also appears to be associated, in an indirect way, with the Rock Valley fault zone. Whereas the Little Skull Mountain earthquake occurred near the western end of Rock Valley, the Frenchman Flat event took place at its eastern extent where the Rock Valley fault zone appears to terminate into the basin at Frenchman Flat. Neither the 1992 Little Skull Mountain nor the Frenchman Flat events appear to involve faulting in the Rock Valley fault zone. The Frenchman Flat mainshock was preceded by an extended foreshock sequence that included an M 4.2 earthquake. Portable instrumentation installed in the aftershock zone shortly after the mainshock recorded the early aftershock period; aftershock locations constrained with portable instrument phase data are shown in Figure 7-10. Sandia National Lab participated in the aftershock deployment, and near-source data provided by some of their instruments improved hypocentral control. P-wave first motions (Figure 6-1) and waveform modeling (Ichinose, personal communication, 1999) give a normal faulting mechanism for the mainshock although the alignment of Frenchman Flat aftershocks and constraints on depth of faulting from portable data suggest an oblique slip mechanism at mid-seismogenic depth (~7 km). Broadband waveforms were difficult to model due to the significant velocity contrasts associated with Frenchman Flat basin sediments

and may not be reliable for depth control. Also, the Frenchman Flat sequence showed unusually poor P-wave arrivals to the network stations, which lie mostly to the west and northwest. Station SHP, 80 km ESE, showed clearer P-wave arrivals than station PUV in southern Yucca Flat at 20 km epicentral distance. The generally poor P-wave arrivals make it difficult to constrain Frenchman Flat locations, and portable data was critical for understanding the sequence.

Depths of Frenchman Flat aftershocks based on control from portable stations range from about 5 to 10 km. They follow a NE trend (Figure 7-10) which is offset to the northwest from the southeast boundary of the Frenchman Flat basin, with the mainshock at the southwestern edge of the aftershock distribution. The set of relocated aftershocks shows a weak dip to the northwest, consistent with the northwest dipping fault plane from waveform modeling. The short period P-wave first motion mechanism using near-source portable control shows a normal faulting mechanism consistent with the orientation of aftershock locations (Fig. 7-10). Fault-plane dips are not tightly constrained and an oblique slip mechanism cannot be ruled out. Waveform modeling returned a much shallower source than is determined from using near-in portable data. The fault from waveform modeling is rotated slightly counterclockwise from the aftershock alignment and from the P-wave focal mechanism. This misalignment may result partly from inadequate accounting of low velocities for basin sediments in the regional waveform modeling.

The magnitude of the Frenchman Flat earthquake was problematic. NEIS reported $M_L = 4.7$. But the determination of the magnitude M_L using MLCALC yielded 4.13 with 17 stations (one S-13 station was eliminated due to clipping). NEIS (Berkeley) reported an M_W of 4.8 from waveform modeling, and the same methodology using data from SGBDSN network stations yielded M_W 4.7

(Ichinose, personal communication). This earthquake produced abnormally strong waves below 1 Hz, the corner frequency of the S-13 seismometers. The CMG-40 broadband seismometers show these lower frequencies well, as exemplified by TIM in Figure 7-11. In Figure 7-12, we have plotted the spectrum of the N-S component recording at TIM, corrected from velocity to displacement. Except for the effect a 2-pole corner at 1.25 Hz, this would be the spectrum seen by a hypothetical Wood-Anderson seismometer at the same location. Note that the broadband spectrum as seen by the CMG-40 continues to rise below 1 Hz, by approximately a whole log unit. This explains the larger M_W's computed for this earthquake because M_W is dependent on the amplitude at lowest observable frequencies. It is not, however, known why the NEIS M_L was 0.6 higher than the SGBDSN M_L because both should be drawn from the same higher frequency band above 1 Hz. Table 3-1 showed that SGBDSN and NEIS M_L's are roughly equivalent based on several events in the range of 3-4; thus we had no reason to expect the Frenchman Flat M_L discrepancy.

8. Earthquakes Near Yucca Mountain

In the previous reports of von Seggern and Smith (1997) and von Seggern and dePolo (1998), 14 earthquakes within 10 km of RPY, which is over the ESF, and six earthquakes in the southern part of the Yucca Mountain block were listed for the period of May 1995 through September 1997. Figure 8-1 shows a plot of the seismicity in FY98-99 within 15 km of station RPY which is sited above the proposed repository. For FY98-99 we located just four earthquakes within the radius of 10 km from station RPY, although three earthquakes were just barely outside the 10-km radius, and one additional earthquake within the southern part of the Yucca Mountain block. The four inside the 10-km radius and the south Yucca Mountain one, plus the others reported previously, are listed in Table 8-1. The FY98-99 five earthquakes were all very small and detected by 6 stations or less.

All the events of Table 8-1 are plotted in Figure 8-2. Note that the southernmost seven events are beyond the circle at 10 km radius from RPY. Station coverage (see Figure 2-1) is generally excellent for these earthquakes, with one or more stations at a distance that is less than the focal depth. We gathered any possible arrival times from the analog stations still operating in the area to determine the locations of these events; and thus the locations of Table 8-1 may differ from the ones obtained from the SGBDSN stations only, as listed in Appendix 3 here and in von Seggern and Smith (1997) or von Seggern and dePolo (1998) for the pre-FY98-99 events. We regard the locations of Table 8-1 as generally somewhat better where a difference exists. Magnitudes were determined in all cases from the data of the SGBDSN stations only.

The recurrence rate established by these earthquakes was examined in von Seggern and Smith (1997) and again in von Seggern and dePolo (1998) and shown to be significantly less than for the entire area enclosed by the SGBDSN or for the wider southern Great Basin as a whole. In Figure 8-3, the recurrence curve (labeled "norm. 95-99 digital") for earthquakes in the Yucca Mountain vicinity is shown updated with the FY98-99 event data of Table 8-1. Two other recurrence curves are shown in this figure, and each of the recurrence curves is normalized to a period of one year. The normalization factors are 18 years for the analog network and 4.5 years for the digital network. The SGBDSN data is directly compared with pre-SGBDSN data (labeled "norm. 78-95 analog") taken from the analog network catalog for the years 1978 to 1995. The magnitudes for the analog network are equivalent to M_L used for the SGBDSN, as described in von Seggern and Smith (1997). Note that the thresholds of completeness for the two networks are different, with the threshold of the SGBDSN being perhaps a half unit less in magnitude than that of the analog network. Disregarding the threshold difference, the analog and digital networks agree fairly well in the recurrence rate. The other curve in Figure 8-3 is for the entire analog network monitoring area. The curve for the whole analog network catalog (1978-1995) for the southern Great Basin, besides being normalized by the 18-year period, is normalized to an area of 10-km radius by the ratio of surface areas covered. For the analog network, we take the area as having a radius of roughly 150 km; thus this ratio is $(10/150)^2$. The resulting curve is labeled "norm. all 78-95 analog" in Figure 8-3.

The curves of Figure 8-3 enable us to compare the rate of earthquakes within the 10-km area around Yucca Mountain (actually station RPY) with the average rate for the southern Great Basin in an equivalent area of 10-km radius. This comparison is approximate only. A line was first visually fit to the straight portion of the entire 78-95 analog catalog data. This line is moved downward,

keeping the same slope, to visually fit the composite digital-analog Yucca Mountain data. The difference in $\log_{10}(N)$ is 1.55 vertically between the lines. Thus, the seismicity rate within the immediate vicinity of Yucca Mountain is roughly $10^{1.55} \sim 35$ times less than the average in an equivalent area of the whole southern Great Basin. This, as mentioned, is an approximate result; and several assumptions could be changed. Firstly, the 10-km area around station RPY is arbitrary. Figure 8-1 suggests that, if a circle somewhat more northerly were used, more events would be encompassed. Perhaps one could change the seismicity rate upwards as much as 50% at Yucca Mountain by adjusting the 10-km circle slightly for all of 1995-1999. This would reduce the comparison rate to roughly 23 from 35. Even if we removed the Little Skull Mountain aftershocks from the "all 1978-1995 analog" catalog (~25% of the total), the result would only reduce to 19. Thus, our comparison suggests that the seismicity rate at Yucca Mountain is at least 20 times less than the general seismicity rate around the southern Great Basin.

9. Review of Focal Mechanisms in the Yucca Mountain Region

Methodology

All P-wave, first-motion focal mechanisms were collected and reviewed for the area within approximately 65 km of Yucca Mountain. These fall into 3 time frames: 1) mechanisms for a few earthquakes in papers and reports for the time prior to 1978, 2) mechanisms produced with the southern Great Basin analog network from 1978 to 1995, and 3) those produced since 1995 by a combination of the analog network and the new digital network around Yucca Mountain. The digital network has significantly lowered the threshold at which focal mechanisms from P waves can be determined. More than half of the collected mechanisms are associated with the Little Skull Mountain earthquake of 1992. Several mechanisms are available for events within the Yucca Mountain block itself.

These mechanisms were not determined in a uniform manner. Those from the period prior to 1978 (Fisher et al., 1972; Hamilton and Healy, 1969) were determined with programs that were forerunners of FPFIT. Those in the period of 1978-1992, when the USGS operated the analog Southern Great Basin Seismic Network, were determined with a program by Snoke et al. (1984). They were taken from the reports by Harmsen and Rogers (1986), Harmsen and Bufe (1991), Harmsen (1991), Harmsen (1992), and Harmsen (1993). Those in the most recent period (since

1992), when NSL operated first the analog network and then the new digital network (1995 to present), were determined with the program FPFIT. They were taken from Table 6-1 of this report and from von Seggern and dePolo (1994), von Seggern et al. (1995), von Seggern and Smith (1997), and von Seggern and dePolo (1998). We have not been able to review thoroughly the quality of focal mechanisms prior to NSL operations but have included them in this study nonetheless. For those since 1992, we recomputed and reviewed the solutions carefully. We utilized the quality parameters "F" and "STDR" produced by the FPFIT program to further cull the data, eliminating several events with $F > 0.1$ and $STDR < 0.5$. For many earthquakes in this group, multiple solutions were generated; and careful judgement was used to either reject all solutions or to accept the most likely one. Those events whose tensional axis deviated from the large mass of data were most carefully reviewed. Of approximately 30 such events, 12 were removed due to poor data quality.

The total number of accepted mechanisms is 447. Only events within the 65-km circle around Yucca Mountain (specifically, station RPY) are treated here. The number produced since the inception of the digital network (October 1995) is 238, which is over half of the total. This is one of the clear benefits reaped from the digital network. Focal mechanisms have been determined for earthquakes as small as magnitude 0.5 in the middle of the digital network. It is important to note that, even after inception of the digital network operation in late 1995, data was still routinely available from the analog network (see Figure 2-2); this data was incorporated everywhere possible for the focal mechanism determined since October 1995.

Results

The orientation of the P (pressure) and T (tension) axes within the focal sphere is the major product of the focal mechanism determinations. We have projected the points where these axes exit the lower half of the focal sphere to the horizontal plane in Figure 9-1. Note, that with very few exceptions, the T axes align in the WNW to ESE direction. The average azimuth of all T axes, with those < 180° flipped by 180°, is 301°. The plunge of the T axes is remarkably shallow on the whole, with only 46 mechanisms (10 % of the total) showing plunges > 30°. The placement of the P axes is more diffuse, but they generally follow the orthogonal direction of SSW to NNE. Overall, the stress regime is clearly WNW-ESE tensional, with the response ranging from strike-slip (shallow P axis plunge) to dip-slip (steep P axis plunge).

The T and P axes have been projected onto the digital terrain map of the Yucca Mountain region in Figures 9-2 and 9-3, respectively. The placement of the vectors is such that their midpoint lies on the epicenters; their length is given by the projection to the horizontal plane. The T-axis vectors show an overall consistency in the WNW-ESE direction all across this map. Correspondingly, the P-axis vectors show a consistency in the orthogonal direction, but with much larger variation in length due to the complete range of plunge angles. Thus, within a tensional regime, mechanisms indicate the full range from pure strike-slip to pure dip-slip. The consistency of tension axes is reflected by the few mechanisms determined within the immediate Yucca Mountain block itself. The cluster to the southeast of Yucca Mountain comprises aftershocks of the June 29, 1992, Little Skull Mountain earthquake (M = 5.6) which is the largest event in the dataset. The P and T axes of this event and over two hundred aftershocks are shown in Figures 9-4 and 9-5, respectively.

Altogether, the tension and pressure axes orientation for LSM events only is very similar to that for all the events although it has more consistency. The mean pressure and tension axes directions are essentially identical, and therefore one can say that the LSM focal mechanisms and the remainder of focal mechanisms reflect a uniform stress field over the SGBDSN area. This composite result is also in good agreement with von Seggern and Brune (2000) who used the entire suite of published focal mechanisms from the analog network in the southern Great Basin, an area of roughly 100-150 km radius around Yucca Mountain.

Discussion

The current seismicity in the vicinity of Yucca Mountain is a response to the orientation of the stress field present in the southern Great Basin, with local adjustments for pre-existing structural patterns and for the influence of the large volcanic calderas present in the area. In this review we have found the average azimuth of the tension axis to be N61°W, approximately WNW. The azimuths of the T axes were remarkably consistent, and the inclination of the T axes to the horizontal were generally small. In contrast, the inclination of the P axes were well distributed, indicating a mixture of strike-slip and dip-slip faulting within the dominant tensional stress field. The stress field inferred from focal mechanisms is corroborated by several other lines of evidence taken around the Nevada Test Site and Yucca Mountain: 1) hydrofracturing and overcoring (Haimson, 1982); 2) field observations of the direction of slip on known active faults (Piety, 1996); 3) geodetic measurements near Yucca Mountain (Savage et al., 1999); and 4) geomorphological indications of quaternary movements (Carr, 1984). In particular, at Yucca Mountain itself there is support for a WNW-ESE tension axis from drill-hole measurements made by Stock et al. (1985); they studied hydraulic fracturing with

televiewers in wells from approximately 300 to 1300 m and noted the WNW orientation of fractures and breakouts. Although, the principal stresses have magnitudes such that normal faulting is most probable, these authors make the case that strike-slip as well as dip-slip faulting can occur within this stress regime. In a more recent study at Yucca Mountain, Lee (1996) conducted hydraulic stress measurements in a shallow borehole in the Thermal Test Facility Alcove of the ESF. These tests agreed with the results of Stock et al.; specifically, a normal faulting stress regime was found at this alcove, with the least principal stress oriented at N75°W. Altogether, the earthquake focal mechanisms and the deep and shallow hydraulic fracturing indicate a uniform WNW tensional axis in the vicinity of Yucca Mountain.

On a more regional scale, in a thorough integration of modern geophysical data for the California-Nevada region, Flesch et al. (2000) indicate that the dominant stress at the Nevada Test Site is oriented with tension approximately WNW, having a value of approximately 5 MPa. Because the geologic forces which control this are changing on very large time scales (Ma), this stress field should continue to control seismicity and inferred focal mechanims in the vicinity of Yucca Mountain for the effective life of the potential repository.

Numerical Experiment on the Accuracy of Focal Mechanism Determinations

During 1999 we completed a software qualification exercise on the USGS program FPFIT so that the focal mechanisms determined in our Yucca Mountain work would be "qualified" data. This exercise concentrated on usage of the program for our particular network and was thus limited to a hypothetical network within 50 km of Yucca Mountain. Two station sets were randomly created

within this 50 km radius, one having 30 sites and the other having 15 sites. Suites of 50 hypothetical strike-slip earthquakes and 50 hypothetical dip-slip earthquakes were created at random locations within the network. The two sets were oriented such that P and T axes were identical. Using the definitions in Aki & Richards (1980, p. 114), these sets have the following parameters:

	SET 1 (strike-slip)	SET 2 (dip-slip)
Strike	0	45
Dip	90	45
Rake	180	270

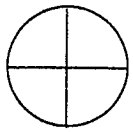

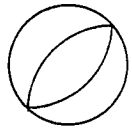

It is well known that, given an appropriate station configuration, these two mechanisms can mimic one another in first motion patterns and be effectively indistinguishable. (See the cover page of FPFIT manual by Reasenberg and Oppenheimer, 1985.)

Synthetic data sets of first motions were created for the 100 events using ray tracing in flat-layered models and the first-motion equation of Aki & Richards (1980, p. 115). All event depths were set at 10 km and the following velocity model was used:

Layer #	Velocity (km/s)	Depth (km) at top of layer
1	5.85	0.0
2	6.00	7.0

3	6.70	22.1
4	7.85	28.1

Two variations were then used to create "perturbed" data sets. One variation was to change the estimated depth of the event for calculating the takeoff angles while generating the first motions with the true 10-km depth. Estimated depths of 5 and 15 km were used. This variation simulates the problem of often having a poor estimated event depth from a location made with P times and even S times. A second variation was to use the 10-km event in the original velocity model to generate the first motions but then to change the velocity model for calculating the takeoff angles. This variation simulates the problem of imperfect knowledge of the travel time model, including strong 3-D effects in the vicinity of Yucca Mountain. The perturbed velocity model was:

Layer #	Velocity (km/s)	Depth (km) at top of layer
1	3.00	0.0
2	5.85	1.0
3	6.35	25.0
4	6.60	30.0
5	7.80	35.0

A naming scheme for the tests was devised as follows:

#stations_earthquake type_assumed depth_model perturbed

such that

30_SS_10	strike-slip fault at 10 km with 30 stations
30_SS_10_m	strike-slip fault at 10 km with 30 stations, modified model
30_SS_05	strike-slip fault at 5 km with 30 stations
30_SS_05_m	strike-slip fault at 5 km with 30 stations, modified model
30_SS_15	strike-slip fault at 15 km with 30 stations
30_SS_15_m	strike-slip fault at 15 km with 30 stations, modified model
15_SS_10	strike-slip fault at 10 km with 15 stations
15_SS_10_m	strike-slip fault at 5 km with 15 stations
15_SS_05_m	strike-slip fault at 5 km with 15 stations, modified model
15_SS_15	strike-slip fault at 15 km with 15 stations
15_SS_15_m	strike-slip fault at 15 km with 15 stations, modified model
30_DS_10	dip-slip fault at 10 km with 30 stations
30_DS_10_m	dip-slip fault at 10 km with 30 stations, modified model
30_DS_05	dip-slip fault at 5 km with 30 stations
30_DS_05_m	dip-slip fault at 5 km with 30 stations, modified model
30_DS_15	dip-slip fault at 15 km with 30 stations
30_DS_15_m	dip-slip fault at 15 km with 30 stations, modified model
15_DS_10	dip-slip fault at 10 km with 15 stations
15_DS_10_m	dip-slip fault at 10 km with 15 stations, modified model
15_DS_05	dip-slip fault at 5 km with 15 stations
15_DS_05_m	dip-slip fault at 5 km with 15 stations, modified model
15_DS_15	dip-slip fault at 15 km with 15 stations
15_DS_15_m	dip-slip fault at 15 km with 15 stations, modified model

The program FPFIT was run on all the test data sets in a uniform manner. In the following figures, multiple event solutions were not culled out. The first set of plots, Figures 9-6 through 9-9, show the P and T axes projections on the lower focal hemisphere for the 10-km events, with no perturbations, as determined for strike-slip or dip-slip events from either the 15-station or the 30-station network. Note that, for the strike-slip cases, the P and T axes are generally well estimated by FPFIT for either network while the axes for the dip-slip events are not nearly as well estimated. A second set of plots, Figures 9-10 and 9-11, deals with the estimated errors. Figure 9-10 shows the mean error of the three parameters (azimuth, dip, rake) for the different tests. Note that the errors

for the dip-slip events are higher for azimuth and rake but lower for dip than the strike-slip errors. Figure 9-11 shows how often the FPFIT 90% confidence bars on the estimates of azimuth, dip, and rake actually cover the true values. Note that the estimates for the dip-slip cases fail to cover the true values, especially rake, in a large percentages of cases.

Many focal mechanisms in the real data set were determined with a limited number of stations in non-ideal configurations, for instance, with less than 180° of station coverage. This was true in the synthetic data sets also. Although the FPFIT output includes several statistics for assessing solution quality, the distribution of stations in azimuth around the epicenter is not one of these. To see how station gaps may affect the solution quality, four plots, Figures 9-12 through 9-15, were made showing solution errors versus the maximum azimuthal gap in the station coverage for dip-slip events and strike-slip events, with either 15-station or 30-station networks. Although the strike-slip mechanisms are apparently fairly well estimated for large gaps, even for the 15-station network, the dip-slip mechanisms are often poorly estimated with the 15-station network. However, there is only a weak trend indicating that increasing azimuthal gap is detrimental to solution quality.

The numerical experiment designed to test the reliability of solutions determined with FPFIT had several important results:

* While strike-slip event P and T axes were usually well estimated, those for dip-slip events showed larger scatter, occasionally mimicking strike-slip events.
* The number of times that the confidence ranges failed to cover the true values of the parameters strike, dip, and rake were much higher for the dip-slip cases than the strike-slip ones.

* While perturbing the velocity model and assumed depth of the event caused little degradation in strike-slip solutions, the dip-slip solutions seemed to be much more adversely affected.
* Significant values for maximum azimuthal gap, even up to 200° or more, had only a slight adverse effect on the solution quality; here again the worst case is for dip-slip events with a small number of observing stations.

The results of the numerical experiments have implications for the real results in the following ways:

* Although there is likely some scatter in true results due to poor station configurations, it is not possible that a uniform mechanism, say pure strike-slip, is being cast into a full range of strike-slip to dip-slip solutions. (Physical evidence also indicates a range of true mechanisms.)
* Strike-slip mechanisms determined with as few as 15 stations are fairly robust; but more care should be taken with dip-slip ones because the confidence bars may not cover the true parameters.
* Even though both the velocity model and the depths of the real earthquakes have error, the artifacts due to these errors are not sufficient to significantly bias the majority of actual solutions.
* Although many real solutions were determined with station sets showing large maximum azimuthal gaps, they should not generally be discriminated against on this basis.
* Because the tension axis would rotate up to 90° in some numerical cases, one should be cautious about inferring a locally deviant stress field from actual solutions which show the tension axis considerably off the WNW-ESE trend.

* One always needs to be careful in accepting any one particular solution made with even as many as 30 stations.

10. Relocations of 1992-1999 Earthquakes in the Southern Great Basin: Constraints on Regional Tectonic Models

Introduction

Earthquakes from October 1992 through September 1999 have been relocated to provide a context for interpretating active tectonic processes in the southern Great Basin in the vicinity of Yucca Mountain. Although significant work has been carried out by the DOE and the USGS in characterizing the active faults near Yucca Mountain, the active seismicity provides an independent source of information to constrain kinematic models and view currently active structures that may not be accounted for in surface studies. Several tectonic models have been considered "viable" in current Yucca Mountain site characterization activities, and some can be evaluated in terms of the current seismicity. Although there have been few significant earthquakes in southern Nevada since late 1992, micro-earthquake activity represents, in a complex way, deformation processes that are ongoing in the low strain-rate environment of the southern Great Basin. Also, the lack of any significant seismicity in the Yucca Mountain block itself restricts testing site-specific tectonic models. Constraints on tectonic processes local to Yucca Mountain based on seismicity must be inferred from regional and near-regional observations.

The southern Nevada seismic belt is, in some way, related to an EW trending approximately 100 mgal bouguer gravity gradient that differentiates the northern and southern provinces of the Nevada Basin and Range Province (Rogers et al., 1991; Thompson et al., 1995). Regional gravity data is from the National Geophysical Data Center (Hittleman et al., 1992). This broad gravity gradient

extends through the Yucca Mountain area, with lower gravity to the north in central Nevada and high gravity values to the south. This gravity gradient is clearly expressed in the physiography of the southern Great Basin. This relationship can be simply interpreted as higher relief supported by low-density upper mantle to the north, in contrast to lower elevation and higher-density upper mantle to the south. This observation may reflect the state of the lithosphere in the southern Great Basin (Thompson et al., 1995). In this interpretation, the lower lithosphere is relatively thin or absent in northern Nevada where hotter low-density asthenospheric rocks are nearer the surface, whereas high-gravity low-elevation in southern Nevada reflects a thicker mature lithosphere.

From historical earthquake catalogs the EW trending southern Nevada seismic belt is spatially continuous through the NTS region. This apparent continuity can be attributed to both comprehensive earthquake monitoring near NTS and a dense concentration of earthquakes in northern NTS that were triggered by megaton-range underground nuclear explosions in the late 1960's and early 1970's (Hamilton, 1973). These large underground tests generated a prolific sequence of earthquakes that included many $M > 3$ events and extensive seismicity that aligned with numerous north-northeast striking faults. Tectonic release has been documented during these megaton-range underground explosions (Wallace et al., 1973 and 1975). How this large concentration of induced seismicity can be accounted for in developing regional recurrence relations for the southern Great Basin has been a challenge; i.e., Probabilistic Seismic Hazard Analysis [PSHA] teams addressed the triggered seismicity issue in a number of ways.

In late 1992 NSL assumed the operation the southern Great Basin analog network and had upgraded to a totally three-component digital network by 1999. The USGS had operated the network since

its inception in 1978. Since 1995 the southern Great Basin analog network has been incrementally replaced with a three-component digital network with a different, notably smaller but more dense, geographic configuration with different objectives (Smith et al., 1996). This has resulted in a decrease of about one magnitude unit in the detection threshold in certain areas and an increase in the number of earthquakes located. S-wave arrivals from the 3-component stations provide better constraints on locations, generally requiring fewer station recordings for an event to be included in the final earthquake catalog. Overall, there is a more improved data set by which to observe active tectonics in the Yucca Mountain area.

During the phasing out of the analog network, both networks were in operation, resulting in an increase in the previous or expected level of station coverage for basic earthquake monitoring. In this study, phase data from both the analog and digital networks have been combined to develop a single set of locations for this overlap period.

Earthquake Relocation Process

This analysis represents a first pass at developing an improved a set of locations to isolate active structures in the southern Great Basin. At present, Quality Assurance (QA) restrictions limit the available software for earthquake relocation, and in this study we only attempt to develop a more comprehensive view of the active structures and the regional tectonic processes that the seismicity reflects. Our objectives in this regional approach are not to refine the detailed structure in all earthquake sequences that have taken place since 1992, but to develop constraints on active tectonic processes provided by improved locations.

About 15,500 events are included in the relocation process with the dominant source of earthquakes being the aftershock zone of the 1992 Little Skull Mountain earthquake. Whereas S-waves are poorly constrained from the mostly single-component stations of the analog network, S-waves arrivals contribute significantly to digital network locations. Due to the increased sensitivity of the digital net, very small events in the Little Skull Mountain aftershock zone observed at digital stations did not trigger the CUSP-based analog network processing system. Therefore, there are some differences in location constraints for the smallest earthquakes between the analog and digital nets. To apply a common magnitude scale, duration magnitudes (M_d), developed from the analog data, have been corrected to an M_L equivalent using an M_L-M_d relation developed during the digital-analog overlap period.

To establish station corrections, the complete event set was located using the 1-D velocity model of Hoffman and Mooney (1984) for the Yucca Mountain area. The Hoffman and Mooney (1984) 1-D model is used in routine earthquake analysis for earthquakes in the Yucca Mountain and southern NTS regions. A subsequent location was performed, following removal of large travel-time residuals and S-wave arrivals more distant than 40 km from an epicenter. Average P-wave and S-wave residuals were developed from the set and applied in a final location. Due to the variability of the geology in the southern Great Basin, there is no assurance the Hoffman and Mooney model is a good representation of the velocity outside of the Yucca Mountain area and further refinements of the regional velocity model will improve earthquake locations in general.

The four figures (10.1-10.4) show subsets of the relocated earthquakes with location quality thresholds applied (rms residual: < 0.15 sec; number of stations > 5; location gap < 270 degrees). Because the two networks were operated independently in the transition, there are completeness issues that have not been addressed but are not considered to be critical to this first-pass regional analysis. By incorporating both P-wave and S-wave station corrections, the epicentral control has been significantly improved based on visual inspection of the relocated catalog and a composite catalog compiled for the overlap period from independent analog-digital network operations. In order to more precisely constrain earthquake depth distributions a more rigorous relocation effort must be undertaken.

Summary of "Viable" Tectonic Models for Yucca Mountain

Five basic tectonic models are considered "viable" or "working hypotheses" for characterizing the deformation in the Yucca Mountain area. These tectonic models arose from a PSHA conducted for the site area and are an integration of nearly one dozen tectonic models that were considered in that exercise. These models, discussed in *NRC Issue Resolution Status Report: Key Technical Issues: Structural Deformation and Seismicity, Rev. 2, 1999*, are summarized below. Although these models primarily focus on Yucca Mountain and Crater Faults specific faults and deformation, the regional seismicity provides a context for evaluating these models. The lack of seismicity at the Yucca Mountain site limits the use of detailed earthquake locations and focal mechanisms for placing constraints on site-specific processes.

The viable tectonic models from NRC Issue Resolution Status Report are:

1. Half-Graben with Moderate Depth Detachment (Young et al., 1992; Ferrill et al., 1996)
2. Half-Graben with Deep Detachment (Young et al., 1992; Ferrill et al., 1996).
3. Crater Flat Pull-Apart Basin (Fridrich, 1999).
4. Elastic-Viscous Graben
5. Amargosa Desert Fault (Schweichert and Lahren, 1997).

Details of these structural models can be found in the references and are only summarized here. Half-graben and graben models employ some form of upper to mid-crustal detachment (*Models 1 and 2*) or mobile, ductile mid-crust with thin elastic crust (Model *4*). For Crater Flat and Yucca Mountain area faults, a half-graben model would imply that either the west dipping Yucca Mountain faults or the east dipping Bare Mountain fault are the primary structure. This may or may not involve a single defined detachment, but would require the antithetic faults to intersect the primary structure. If potential antithetic faults shallow with depth prior to intersecting or encountering the primary structure at depth then there is an implied detachment, or horizontal slip transfer mechanism.

A primary question with regard to these models is at what depth does the detachment become operative. If the Bare Mountain fault is the primary structure of the half-graben, faults at Yucca Mountain would "toe" into it at some angle within the seismogenic crust. Detachment models must account for the geometric relationship between Bare Mountain and Yucca Mountain faults to the proposed detachment. Additional seismicity in the Crater Flat basin could provide sets of

earthquake focal mechanisms that could potentially constrain the dips and orientation of the basin faults, but there have been very few site area earthquakes.

There has been little to no evidence in the seismological literature for detachment systems that have a seismic signature and there has been no evidence shown from southern Great Basin earthquake monitoring that such systems exist. This may be a data resolution issue implying that more rigorous earthquake location efforts need to be applied. On the other hand, shallow detachments may not be seismogenic. If detachments are aseismic, then there may be a signal in the character of upper-plate versus lower-plate seismicity.

The Crater Flat pull-apart model (*Model 3*) requires as yet unrecognized seismic sources that account for strike-slip faulting within Crater Flat to accommodate the southerly increase in slip rate along Yucca Mountain block faults. These strike-slip features would be sites of earthquakes that would tend to limit the extent of Yucca Mountain site faults and be locations of potential moderate sized background earthquakes that have been accounted for in the PSHA. The Crater Flat "pull-apart" model addresses the clockwise vertical-axis rotation of southern Yucca Mountain and opening of Crater Flat. *Model 5* attempts to account for the alignment of basaltic cones in Crater Flat on fault systems but requires offset on currently unrecognized predominantly north-trending strike-slip structures. This model provides some consistency with strike-slip faulting observed southeast of Amargosa Valley in Stewart and Pahrump Valleys (Piety, 1996).

Observations

Low-magnitude earthquake activity is present throughout the southern Great Basin (Meremonte et al., 1987). The spatial distribution of earthquake activity over the past 7 years has been consistent with the historical record with a few exceptions (Figures 10-1 and 10-2). Areas of concentrated seismicity following large underground nuclear explosions (UNE) in the 1960's and early 1970's at Pahute Mesa have remained quiet, with one exception. The 1998 Thirsty Mountain swarm (largest event M 3.6), just west of Pahute Mesa, may represent some association with UNE triggered seismicity, although this is difficult to assess (Fig. 10-2). The past 7 years have also seen an increase in the earthquake activity in southern and southeastern NTS. It has continued to be a source of notable background seismicity, consistent with the historical catalog, although increases in 1992-1999 activity has been unique. This is predominantly the result of the 1992 Little Skull Mountain sequence, which by itself would have led to an increase in seismicity in the southern NTS. Also, out of character from 1978-1992 seismicity, other noteworthy, but minor, sequences have occurred in southern NTS. Southern NTS has been the dominant source of the moment release in the 1992-1999 monitoring period. This earthquake activity has included the 1992 Little Skull Mountain (Meremonte et al., 1995; Smith et al., 2000), 1993 Rock Valley (Smith et al., 2000), 1993 Spotted Range (von Seggern and Smith, 1995), 1999 Frenchman Flat (this report) and 1997 Calico Hills (von Seggern and dePolo, 1998) sequences. These sequences have shown a variety of faulting mechanisms and hypocentral depths.

There is about a 100 mgal bouguer gravity gradient extending through the study area (Figure 10-3). This results from a large south-to-north, high-to-low, regional gradient and the gravity signature of

the Timber Mountain-Silent Canyon Caldera complex in northern NTS (Crowe et al., 1996). Within this overall setting is the Kawich-Greenwater "rift" originally proposed by Carr (1984) and defined by a regionally extensive NS trending bouguer gravity low extending through SE Amargosa Valley northward into the Timber Mountain complex. The southern portion is the Amargosa Desert Trough (Blakely et al., 1998). The geometry of this gravity anomaly led Carr (1984) to define the kinematics of the "rift" zone as accommodating a large right step in Miocene deformation between the then active Las Vegas Valley shear zone, northward, to what was interpreted to be an expression of the ancestral Walker Lane.

The Yucca Mountain Crater Flat domain represents a local gravity low within the "rift" (Fig. 10-3). Snyder and Carr (1984) interpreted the local gravity low in Crater Flat to be the expression of a caldera. This model is not accepted in modern interpretations of the structure of Crater Flat (Fridrich, 1999). A general observation that can be made from Figure 10-3 is that the seismicity appears to be less energetic within the gravity defined "rift" than in the southern NTS-Rock Valley area, being characterized by small-magnitude localized clusters, most notably the 1997-1998 Thirsty Canyon swarm.

The conspicuous linear trend of low-magnitude earthquake activity that extends along the western edge of the Bare Mountain-Timber Mountain zone (western margin of the Kawich-Greenwater "rift") is pervasive through the historical and recent monitoring period (Figs. 10-1 to 10-3). It does not appear to correspond or align with any obvious structural features or Quaternary faults expressed in the surface geology. Local north-striking Quaternary faults (Piety, 1996) dip to the west, and these are only expressed in short segments most likely representing minor structures. This trend of

low-magnitude earthquakes remarkably corresponds to a sharp gravity gradient that bounds the western margin of the Timber Mountain - Kawich-Greenwater zone (Fig. 10-4). This observation implies that lower crustal and/or upper mantle properties have implications for understanding the distribution of seismicity. The lower-crustal and/or upper-mantle properties expressed in the gravity are remnants of Miocene deformation and volcanism that shaped the southern Great Basin physiography. A simple hypothesis is that the strain rates are so low, gravitational forces are being expressed in the background seismicity in addition to what plate boundary driven strain may be accompanying Yucca Mountain area deformation.

Within low gravity regions there are few extensive fault zones capable of large earthquakes, suggesting that the Miocene tectonic environment that has established the state of the lower crustal and upper mantle places important constraints on the current earthquake hazard. Quaternary faulting at Yucca Mountain is a continuation of episodes of Miocene extension (Fridrich, 1999; O'Leary, 2000), but the implication for understanding the distribution of historical seismicity from the perspective of the tectonic history has been underestimated.

The Yucca Mountain-Crater Flat tectonic domain is marked by a local gravity low within the overall Kawich-Greenwater zone. This, in turn, is gradational to the lowest gravity values in Timber Mountain and Pahute Mesa to the north. Based on the gravity, the Crater Flat domain bounds the western edge of the Kawich-Greenwater zone against Bare Mountain. In this context, Bare Mountain is in the footwall along the western margin of the "rift". The gravity-low at Crater Flat gives the appearance of being "scalloped" from south to north into the Kawich-Greenwater rift against Bare Mountain. The observation of minimal seismicity in the Yucca Mountain area is

consistent with its location within a relatively low gravity region, with generally denser concentrations of seismicity (although sparsely distributed) found further to the west and northwest. Also, the relatively diffuse distribution of earthquakes within the Kawich-Greenwater belt appears to be more extensive south of Yucca Mountain in the Amargosa Desert trough in relatively higher gravity. From the regional gravity, Blakey et al. (1998) have modeled several basin structures with apparent block bounding faults within the sediments in Amargosa Valley. These structures are apparent in the gridded gravity data (Figs. 10-3 and 10-4), and correlate with distributed, limited extent, known and suspected Quaternary faults (Piety, 1996) within Amargosa Valley.

Discussion and Conclusions

The distribution of seismicity in the 1992-present time period is generally consistent with that observed during earlier earthquake monitoring efforts. The 1992 Little Skull Mountain earthquake did occur in an area of relatively high seismicity for the southern Great Basin, and this sequence dominates the 1992-present earthquake catalog in both numbers of events and moment release. The Little Skull Mountain event was followed by an increase in seismicity that is confined to the south-central and southeastern NTS region. Several sequences, not characteristic of the 1978-1992 monitoring period, were observed in this region following the Little Skull Mountain event. The physical source for this increase in seismicity is difficult to isolate. We suggest that this increase in activity is a post-seismic response to the Little Skull Mountain event confined to a particular tectonic environment in the southern NTS. This tectonic setting is characterized by intermediate bouguer gravity values in the transition from the southern to northern Great Basin of Nevada and the presence of several NE oriented faults, unique to the

NTS region. Overall, because the Little Skull Mountain earthquake appears to have been triggered by the 1992 M 7.1 Lander California event, this activity could be attributed to a post Landers response. It is difficult to assess the prospects of potential earthquake activity at Yucca Mountain in light of the Little Skull Mountain sequence, other than to say that there has not been a coincident increase in activity in the Yucca Mountain area or in other areas of NTS. Small earthquakes observed in the Yucca Mountain block in the mid-1990's could have been associated with the relative increase in the post Landers time period, but these were very small events and it would be difficult to draw any particular conclusions.

The following is a summary of conclusions and interpretations of active tectonic processes based on the relocated dataset. Interpretations of the character and distribution of earthquake activity in the southern Great Basin are limited by a lack of understanding of the current state of strain and how this strain is expressed. The following interpretations are developed to be consistent with the distribution of seismicity.

- The lack of any notable seismicity within the Yucca Mountain block makes it difficult to place constraints on site-specific deformation models from the seismicity data alone.

- The distribution and general character of seismicity in the southern Great Basin tends to conform to bouguer gravity anomalies and gradients; and therefore it may represent reactivation of older structures, or deformation dominantly controlled by the properties, strength and current deformation of lower-crust upper-mantle structures. In this interpretation, relatively weaker upper-mantle and lower-crust is assumed to be reflected

in lower gravity values. These low-density upper-mantle lower-crustal features are most likely remnants of Miocence volcanism and tectonism.

- Within the context of this analysis, a significant strike-slip fault through Crater Flat (Amargosa Shear Model) seems unlikely because there appear to be few extensive fault systems within low gravity regions. This may be due to the fact that less dense, potentially weaker, lower-crust upper-mantle would not support continuous strike-slip fault systems. This hypothesis could be tested by assessing the style and extent of fault development in weak versus strong crust-mantle environments in other regions. Right-lateral shear that may be expressed in distributed faulting within Crater Flat is not resolvable from the distribution of seismicity.

- The bouguer gravity and seismicity west of the Kawich-Greenwater gravity low suggests that Bare Mountain is part of a more extensive north-south oriented regional structure. If so, then faults at Yucca Mountain would be considered to be secondary to Bare Mountain and Half-Graben models, with Bare Mountain as the primary fault, would be more likely.

- Recent seismicity in southern and southeastern NTS may be related to a tectonic domain distinct from the Yucca Mountain block. Therefore, increases in seismicity in this region may not impact the potential for short-term increases in seismicity at Yucca Mountain. This hypothesis may or may not be testable.

- Because Yucca Mountain is within the Kawich-Greenwater structure noted by Carr (1984), this would tend to favor less seismically active structures at Yucca Mountain if the current level and character of seismicity can be extrapolated from that observed throughout this feature to the Yucca Mountain block. This observation or model for the behavior of seismicity would tend to favor less seismicity at Yucca Mountain than other areas within the "rift" such as Amargosa Valley, and this general observation holds. It is understood that Yucca Mountain as well as the entire region is characterized by a number of faults with Quaternary offsets, and it would not be surprising to experience another moderate event such as the Little Skull Mountain earthquake anywhere in the NTS region.

- Improved earthquake locations enhance the image of active structures at the regional level and, combined with potential field data, provide a view of regional tectonic processes at small magnitudes in this low strain rate environment. These processes appear to be controlled to a large degree by structures developed during periods of relatively intense tectonism in the Miocene (Fridrich, 1999).

- Earthquake locations and the velocity structure can be better refined applying a full inversion for hypocentral parameters and P-wave and S-wave velocities.

11. Yucca Mountain Area Strong Motion Network

Overview of Network Operations

The non-telemetered Yucca Mountain area strong-motion network consists of nine Terra Tech IDS-3602A 16-bit digital accelerographs (Figure 11-1 and Table 11-1). In 1999 strong-motion sensors were installed at telemetered network stations, but this discussion refers only to the older Terra Tech network. These instruments were installed in 1995 to ensure that large earthquake ground motions, that would clip the regional monitoring network, would be recorded on scale. Also, since the removal of the Blume strong motion network in 1992, there was little to no strong-motion coverage in the region until the Terra Tech instruments were installed. There has been no time since their installation in 1995 when less than 7 instruments have been operating; two units were in repair in 1999. The units are fully programmable and can record three-components of ground motion of up to ±2 g. This is well within the range of earthquake ground motions expected for the largest earthquakes. To ensure uncontaminated ground-motion records, the instruments are bolted to a 3' x 4' x 6" reinforced concrete pad with a secure cover. Power is supplied locally by a lead-acid battery that is trickle-charged during daylight hours by a solar panel mounted on an adjacent aluminum tower; this battery is also bolted to the concrete pad. Therefore the units are standalone and are supported only with their own power source. Also mounted on the tower is a Garmin GPS receiver for acquiring absolute time. Each unit is configured with a 4-Mbyte flash memory card to store recorded time-series data, calibration records, clock/timing information, and instrument recording parameters. During 1999 an upgrade to the units was performed to modernize the GPS

timing systems. The original Trimble GPS receivers were not configured to accommodate the August 1999 overrun in internal buffering experienced by older GPS units throughout the world.

The units are controlled through the IDSMENU v4.03 software supplied by Terra Tech. There are two trigger algorithms that run concurrently when the units are in operation, and each algorithm includes a pre-trigger length parameter setting to ensure that the entire earthquake time-series is recorded. These trigger algorithms are the Threshold (or Energy Trigger) and Short-Term Average (STA) to Long-Term Average (LTA) ratio (STA/LTA). When the STA exceeds a pre-selected multiple of the LTA, the unit begins recording data. The energy-level trigger continuously compares the STA to a selected energy threshold and triggers when this threshold is exceeded. Time-series records submitted to the project include the pre-set instrument operation and triggering parameters. Also recording is set to continue beyond the specified record length in the event of a large earthquake where significant ground motions can continue for many minutes. The recording parameters vary slightly throughout the network, primarily to reduce excessive triggering near buildings and facilities. All time-series data recorded by the instruments, including noise triggers, have been routinely submitted to the YMP Records Processing Center at regular intervals. In 1999, a number of network stations were upgraded to record strong ground motion on separate digitizer channels. The REFTEK instruments operated on the telemetry system can accommodate 6 input channels. Three additional channels, configured with accelerometers, at 10 regional network stations are now included in the real-time telemetry. This is an added benefit to the operation of the Terra Tech instruments because we now have strong-motion data in real-time from the site area; the Terra Tech instruments require site visits to collect recorded data.

Peak Ground Acceleration for Significant Regional Earthquakes

The following is a compilation of the Peak Ground Accelerations (PGA) recorded at Yucca Mountain area strong-motion stations during the 1999 M 4.7 Frenchman Flat, Nevada, M 5.6 Scottys Junction, Nevada, and M 7.1 Hector Mine, California, earthquakes. Key earthquake parameters are summarized below.

Hector Mine:	10/16/99	250 km from Yucca Mtn.
Scottys Junction:	8/01/99	83 km from Yucca Mtn.
Frenchman Flat:	1/27/99	40 km from Yucca Mtn.

M 7.1 Hector Mine, California

Hector Mine Peak Accelerations

Specter Range (Paleozoic Rocks)

Station	%g		
SPRS vertical	.73	PGA 1.29%g	Distance-231 km
n-s	1.29		
e-w	1.29		

Side of Yucca Mountain (Tuffs near Solitario Canyon Fault)

SYMS	.50	PGA 1.21%g	Distance-249 km
	.82		
	1.21		

Bare Mountain (Paleozoics near Bare Mountain Fault)

WCTS	.26	PGA .71%g	Distance-245 km
	.32		
	.71		

Midway Valley (sediments adjacent to Helicopter Pad east of ESF)

MDVS	.58	PGA 1.26%g	Distance-250 km
	.78		
	1.26		

Top of Yucca Mountain (Tuffs at crest of Mountain)

TYMS	.59	PGA 1.46%g	Distance-249 km
	1.14		
	1.46		

M 5.6 Scottys Junction, Nevada

Scotty Junction Peak Accelerations

Station	%g		
SPRS vertical	.25	PGA .60%g	Distance-118 km
n-s	.40		
e-w	.60		
WCTS	.52	PGA .91%g	Distance- 77 km
	.59		
	.91		
MDVS	.48	PGA .91%g	Distacne- 82 km
	.52		
	.91		
TYMS	.45	PGA .74%g	Distance- 81 km
	.68		
	.74		
SYMS	.86	PGA 1.14%g	Distance- 81 km
	1.14		
	1.06		
FOCS	.38	PGA 1.04%g	Distance- 97 km
	1.04		
	.58		
EXHS	.43	PGA .73%g	Distance- 83 km
	.64		
	.73		

M 4.7 Frenchman Flat, Nevada

Frenchman Flat Peak Accelerations

Station	%g		
SPRS vertical	.10	PGA .18%g	Distance- 20 km
n-s	.18		
e-w	.17		
SYMS	.15	PGA .21%g	Distance- 44 km
	.16		
	.21		
MDVS	.14	PGA .20%g	Distance- 40 km
	.20		
	.17		
TYMS	.14	PGA .18%g	Distance- 43 km
	.15		
	.18		
FOCS	.17	PGA .33%g	Distance- 27 km
	.33		
	.23		
EXHS	.14	PGA .18%g	Distance- 40 km
	.18		
	.14		

12. *Kappa* Distance Relations, k_r, for Regional Earthquakes

Kappa estimates and *kappa*-distance long offset relations have been estimated from strong-motion records of the Scottys Junction, Nevada, and Hector Mine, California, earthquakes. A third data set consisting of strong-motion records from the Blume stations of the 1992 Little Skull Mountain (LSM) earthquake were also examined (Lum and Honda, 1992). *Kappa* was measured from the slope of the acceleration spectra of the horizontal components of ground motion from these three events at strong motion sites. Both horizontal components of ground motion from each station were used in the regression. Because of a large scatter in the *kappa*-distance relations for the Blume records, the distance dependence of *kappa* is estimated here from only the Scottys Junction and Hector Mine events. The estimate is based on essentially two distance ranges at common stations of the Yucca Mountain strong-motion network. They provide some basis for estimating ground-motion scaling relations for distant large earthquakes at high frequencies.

The observed spectral decay of an acceleration spectrum at high frequencies can be characterized by its slope parameter k_T or total *kappa*. The total *kappa* is considered to consist of two parts, one deriving from the local site conditions, attenuation and scattering (k_0), and the other reflecting distance dependence of the *kappa* parameter (k_r). As an approximation, the distance-related component of *kappa is* estimated by r^*k_r, where r is the hypocentral distance. This simple model can be written as $k_T = k_0 + rk_r$. From travel paths less than 30 km, Su et al. (1996) estimated k_r = 0.51 msec/km. Biasi and Smith (1998) determined a poorly constrained k_r = 0.26 msec/km for the Yucca Mountain area using small earthquakes recorded to a distance of 70 km.

For the present measurements, S-wave arrivals were picked and acceleration spectra were taken over 15 second windows beginning 2 seconds before the S arrival. Varying the spectral window did not significantly change the *kappa* values. Fifteen second windows were used for both the Scottys Junction and Hector Mine events in order to capture the entire source process times.

Figure 12-1 shows the *kappa* values (symbol 'o' for the Scottys Junction and Hector Mine events) determined from the current YMP strong-motion network. The line shown on the plot is a linear fit for the *kappa* distance dependence to the Scottys Junction and Hector Mine data. Both horizontal components at each site were used in the fit. *Kappa* was also measured from the acceleration spectra of the records from the Blume stations for the 1992 Little Skull Mountain earthquake in an attempt to incorporate *kappa* values over a more complete range of distances. However, because of the large scatter ('x' symbols Figure 12-1), *kappa* values from the Little Skull Mountain earthquake were not useful in constraining *kappa* distance relations. Also, for these relationships to be meaningful for scaling ground motion for distant large earthquakes, it must be assumed that the slopes of the source spectra in the 8-20 Hz band for the Scottys Junction and Hector Mine events are similar. Using the Scottys Junction and Hector Mine total k_T's and distances we find the distance dependence of *kappa* to be: $k_r = 0.24$ msec/km.

The large scatter in the Little Skull Mountain data is most likely due to the variety of site conditions at Blume stations and possibly due to source effects at very close distances. The Little Skull Mountain data was collected over a wide range of distances in the southern Great Basin and many stations were not installed at rock sites. All but three of the current strong motions stations in the Yucca Mountain area are on rock. The *kappa* values in the 100 to 150 km range represent stations

in the Las Vegas basin. Large *kappa* values there may be due to attenuation in the thick sediments of the Las Vegas Valley.

Kappa measurements from the Scottys Junction and Hector Mine events form distinct and fairly consistent clusters. Both events were at distances large compared to the spatial dimensions of the Yucca Mountain array, resulting in a narrow range of source-to-site azimuths. Thus, for each event the path and focal mechanism effects are roughly similar. The fit to the data in Figure 12-1 is limited to two general distant ranges, 75-120 km and 225-250 km, respectively, and its applicability to shorter distances is thus not well constrained. However, the slope (0.24 msec/km) is similar to the 0.26 msec/km value determined from small earthquakes to 70 km distance in Biasi and Smith (1998). Su et al. (1996), in applying M 3-4 Little Skull Mountain aftershocks over short hypocentral distances, found k_r of 0.51 msec/km that contributed to a final k_0 estimate of about 20 msec. The larger estimate of Su et al. (1996) may be due to the shorter travel paths they had from which to make an estimate. Shorter travel paths have a greater fraction of their length in the shallow crust and larger ray parameters (shallower ray-path angles), both of which tend to cause apparent attenuation. Overestimating k_r will tend to decrease k_0 values due to the direct tradeoff between k_0 and rk_r terms in the total *kappa*. For 20 km paths the smaller k_r estimate would increase the average k_0 of Su et al. (1996) by about five msec. A more thorough revaluation of Su et al. data would be required to determine the precise change in k_0. Additional data from other regional moderate-sized earthquakes at a variety distance ranges would be needed to more precisely constrain *kappa*-distance relations.

13. ESF – Yucca Mountain Ground Motion Spectral Ratios

Introduction

This section compares earthquake ground motions in Alcove 5 of the ESF to recordings of the same earthquakes at the surface of Yucca Mountain at station RPY. The goal of the comparison is to estimate how seismic waves may be amplified or de-amplified as they pass from the ESF to the free surface on Yucca Mountain above the ESF. Shear-wave spectral ratios provide the most direct estimate of the seismic response of the ESF overburden. Both waveform data and spectral ratios show clearly that ground motions are significantly lower in the ESF than at the surface of Yucca Mountain.

The sensors at stations RPY and AL5 are quite different in their gains and frequency response, so the effect of the sensing and recording systems had to be removed before spectral estimates could be formed. Station RPY used a CMG-40 broad-band seismometer, the output of which is flat to velocity from 0.033 to 50 Hz. The sensor gain was checked by co-locating a passive L4C-3D 1 Hz geophone (S/N 2088) a few meters away, and calibrating the co-located sensor. Follow-up calibrations of the L4C at the NSL were also conducted. By assuming that the ground motions between co-located CMG-40 and L4C seismometers are the same, a gain of 1740 v/m/s was estimated for the CMG-40. This gain results in approximately 9% smaller ground velocities compared to the manufacturer's estimate of 1600 v/m/s. A similar but independent estimate of the CMG-40 gain was obtained by comparing RPY ground motion for 10-second period teleseismic P waves to the regional average ground motion of calibrated S-13 sensors elsewhere in the network.

Station AL5 uses an L4C-3D seismometer (S/N 2087) for all weak-motion measurements. Analysis of daily system check pulses yielded its gain, free-period, and damping coefficients. The following table shows the gain and damping parameters used for this report:

Station	Channel	Gain (v/m/s)	Free Period (s)	Damping
AL5	Z	146	0.775	0.53
AL5	N	159	0.935	0.69
AL5	E	148	0.990	0.65
RPY	Z	1740	0.033	0.70
RPY	N	1740	0.033	0.70
RPY	E	1740	0.033	0.70

The velocity seismograms were corrected for sensor response beginning from 0.2 Hz, with a fully corrected band of 0.4 to 40 Hz. Ratios between RPY and AL5 include the difference in kappa between the sites and whatever effects may result from the layered structure. In general, absolute estimates of kappa require some knowledge of the earthquake source spectral shape. When the difference in ground motion amplitudes is of interest, the spectral ratio method allows the (unknown) earthquake source term to cancel in division. If layering differences between the stations do not cause frequency-dependent variations, the slope of the ratio should be proportional to the difference in kappa. That is, for D(f) = source spectra, A(f) = kappa model attenuation $\exp(-\pi \kappa f)$, site term S(f), and layering effect L(f) between AL5 and RPY:

$$\text{Ratio RPY/AL5} = [D(f)S_{rpy}(f)A_{rpy}(f)L_{rpy}(f)] / [D(f)S_{al5}(f)A_{al5}(f)]$$

$$= [S_{rpy}L_{rpy}/S_{al5}]\exp[-\pi f (k_{al5} - k_{rpy})]$$

Thus the estimated difference in kappa from ESF Alcove 5 to the surface at RPY depends on estimating site effects $S_{rpy}(f)$ and $S_{al5}(f)$ and on the effect of the intervening layered structure.

Data Analysis

Thirty-seven earthquakes were selected from available recordings in calendar year 1999 for computation of spectral ratios between AL5 and RPY. Events in this group were recorded at distances less than 50 kilometers from RPY (Figure 13-1). Most events were either Little Skull Mountain area aftershocks at a distance of 18-22 km from station RPY or aftershocks from the Frenchman Flat earthquake about 44-48 km distant. Shear-wave arrivals were picked by hand and signal spectra computed from the 0.3 seconds before the S arrival to 1.7 seconds after. The spectral window length was chosen as a compromise intended to capture the direct S wave without including too much scattered energy or induced surface wave energy. Shapes from longer spectral windows show the same major features, and tend to be somewhat smoother. Signal-to-noise ratios were computed by dividing the S-window spectra by an equal length spectrum taken from before the first arrival. Events used for final ratio calculations had a signal-to-noise ratio of 5:1 or greater to at least 25 Hz. Events meeting this criterion at AL5 easily satisfied the criteria at RPY. Event magnitudes ranged from M_L 0.7 to 3.0, with a mean of 1.9, and median of 1.8 (Figure 13-2).

Example waveform pairs in Figures 13-3 to 13-6 show that ground motions in Alcove 5 are markedly smaller than at the surface. Figures 13-3 and 13-4a show waveforms for earthquakes that occurred near Frenchman Flat, about 45 km east of Yucca Mountain. AL5 and RPY components are plotted in pairs, with all traces of a given earthquake plotted at a single common amplitude scale. In every case the AL5 motions are significantly smaller than for the same component at RPY. Noise, especially in the AL5 horizontal components, is visible, but in no way dominates the signal. Filtering from 0.5 to 25 Hz (Figure 13-4b) shows that that the bulk of the noise is at higher frequencies than are interpreted from these data. Figures 13-5 and 13-6 show Ml 2.4 and 0.9 Little Skull Mountain aftershocks, again filtered to pass 0.5 to 25 Hz. These waveforms differ by over an order of magnitude in amplitude, but both yielded good signal-to-noise spectra.

Figures 13-7 shows average signal and noise spectra at AL5 for events used in subsequent stacks. The log-average of the signal is shown to give an indication of the average signal level and the average useable bandwidth of the calculated spectra. Stacking signals from earthquakes with likely corner frequencies in the band should probably not be interpreted beyond this. Over the frequency band of 3 to about 15 Hz the signal exceeds the noise by over 50 to 1. Signal and noise levels averaged across the same earthquakes at RPY are shown in Figure 13-8. At 25 Hz the ratios at RPY average over 100:1. Noise level comparisons for stations RPY and AL5 are shown in Figure 13-9. RPY and AL5 noise spectra are very similar below 13 Hz, with the horizontal components slightly quieter in Alcove 5 below 8 Hz. Above 13 Hz noise at AL5 increases above that at RPY, and exhibits broad peaks centered at 20 and 35 Hz. Shapes among the AL5 vertical and horizontal components are similar, although the vertical component is somewhat less amplified and noise peaks are somewhat shifted in frequency compared to the horizontal components.

In Figure 13-10 the arithmetic averages of the high signal-to-noise spectra used for stacks are compared to the same signal after subtracting the pre-event noise. This plot shows in another way that the noise does not contribute significantly to the average signal spectrum below 25 Hz. Figure 13-10 is important because it shows that "humps" at 19-23 and 26 Hz in the earthquake spectra are apparently not caused by background noise within the ESF. The background noise is small compared to the signal levels. The effect of noise does increase with frequency, and exerts a modest influence above 30 Hz. The individual signal and noise spectra are plotted in Figures 13-11 and 13-12 for the vertical component at Alcove 5. The log-averaged noise from the individual spectra in Figure 13-12 is shown for comparison (bottom-most curve) in Figure 13-11. Similar plots for the AL5 components (north-south component in Figures 13-13 and 13-14 and east-west component in 13-15 and 13-16) confirm that the humps in the stacked signal ratios are reproduced in most individual horizontal component spectra. Noise spectra are, for the most part, very consistent in shape and amplitude. This did not fit the expectation that some earthquakes would occur when the ESF was shut down and thus had low background noise levels and others would show elevated noise of ventilation and other operations. Four noise spectra do diverge from the others in Figure 13-16, but they have a higher, not lower, noise level. Inspection of the original records (top four traces, Figure 13-17) confirm the elevated noise level suggested by the spectra. If these reflect tunnel mechanical noise, then most of the earthquakes in this suite occurred during ESF down-time. Increases in spectral levels in the humps are thus in the observed signal, and are apparently caused by some tunnel analog of a site effect. Ambient noise in the tunnel is apparently amplified selectively by the same process.

Ground-motion ratios are shown in Figure 13-18 in the frequency band from 0.4 to 40 Hz. Vertical ratios generally range from 3:1 to 4:1 in the 3 to 20 Hz band, above which resonance in AL5 causes ratios to decline. A ratio of two above a few Hz would be predicted in recordings at the free surface of a homogeneous half-space compared to those at depth; so it appears that some amplification, probably due to the velocity structure, occurs between the ESF and the surface. Average ratios of 3:1 to 4:1 are estimated for the north-south and east-west components, but tunnel-induced "site effects" cause the ratios to decline rapidly at frequencies of 15 and 13 Hz respectively. Both horizontal components show a modest increase in amplitudes in a narrow band around 3.5 Hz. This could be due to a site amplification at RPY, but could also be some sort of constructive interference with the free surface. The spectral ratios below 13-15 Hz are similar in magnitude to those estimated numerically for the PSHA from seismic velocity and rock density measurements (Figure 13-19). The Yucca 300 m outcrop model assumes competent rock with seismic characteristics of the 300 m depth, but analyzed as a free surface. From that model rock surface to a true free surface on Yucca Mountain, an amplification of approximately 2.2 was estimated for frequencies above about 3 Hz. Thus from a non-free-surface site in Alcove 5 to free-field measurements at RPY, the Yucca 300 m model predicts amplifications of about 4.4, which is greater by 10 to 20% than the observed spectral ratios. There is an interesting correspondence between the minor peak in RPY/AL5 ratios around 3.5 Hz and one predicted by Figure 13-19. A further investigation of the low-frequency portion of the spectral ratios is undertaken below using a suite of teleseisms.

The variability in spectral ratios means that kappa differences cannot be estimated with confidence by the spectral ratio method. In the frequency range below 13 Hz the noise at AL5 and RPY are matched (Figure 13-9), but apparently other frequency dependent differences become important.

Variations might be caused by the layered structure, or by reflections from the free surface or from some internal impedance contrast. In any case their effect is to make the ratios too variable to estimate the difference in kappa. In principle the difference in kappa might be resolved by first isolating the source spectral shapes of all events considered, but such an effort would be better addressed in a more specific report.

RPY-AL5 spectral ratios should approach unity at some low frequency where the seismic wavelength is much larger than the thickness of the overburden. To explore the low (< 2 Hz) spectral region further, a suite of eight teleseisms was analyzed. The average magnitude is Mb 6.3. Because of path attenuation the spectral energy of teleseisms is concentrated to below about 2 Hz. Seismograms were sensor corrected from 0.2 to 40 Hz. Five second spectral windows were taken from 0.5 seconds before the first arrival to 4.5 seconds after. Individual spectra are shown for the eight events in Figure 13-20 and 13-21. While the vertical component shows the greatest spectral levels, as expected, the horizontal components both have significant signal levels as well. Pre-event noise levels are a factor of two to five below the teleseismic signal levels. Spectral ratios (Figure 13-22) for the east-west components are near unity at the lowest sensor-corrected frequencies. The cause of the variability above 0.7 Hz is not known, but could be caused by topographic and surface-wave conversion of the incident P arrival. The north-south ratios do not converge to a low-frequency estimate, at least to 0.2 Hz, and average about 2.5 at 0.2 Hz. Elevated ratios may be caused by suppression of the AL5 level or enhancement of the RPY level. The north-south topographic trend of Yucca Mountain may play some role in elevating RPY spectral levels. The vertical component ratios are more consistent among themselves, and average somewhat less than unity at low frequencies. Figure 13-23 shows the mean of spectral ratios from Figure 13-22 (solid lines) and the

local earthquake ratios (dotted lines) repeated from Figure 13-19. The shapes compare favorably between earthquake sets, but there is only a general correspondence between amplification levels. Horizontal ratios from teleseisms reach about 3:1, compared to 3.5:1 or more from local events. The minor peak in both horizontal component ratios around 3.5 Hz is identified in both earthquake sets. Differences in spectral ratios might have a couple of possible explanations. First, the first few seconds of the teleseismic P-wave signal cannot be scattered by the same degree as shear-waves having a long crustal travel path. Scattered energy tends to have a wider variety of ray parameters and back-azimuths than does a simple upwardly traveling wave, so to a greater degree than for teleseisms, energy can reach one station without necessarily reaching the other. Second, teleseisms have a steeper angle of incidence and thus cross the layering of Yucca Mountain at higher angles than do local earthquakes. Theoretically the spectral ratios should vary with back-azimuth in the presence of dipping stratigraphy. The data analyzed here are too few in number to establish a back-azimuth dependence in the spectral ratios, but a comparison of a South American event to one from Japan suggested that the differences could be large.

14. Summary

In its third and fourth years of operation, the SGBDSN comprised 26 digital sites (as of the end of FY98) and performed at a highly reliable level during the two years, with over 99.6% uptime in data collection at the central recording site. We have continued to use data-processing applications associated with the Datascope database to pick arrival times and make preliminary locations. The Datascope database has enabled us to control the quality of the earthquake data better, to easily manipulate it, and to efficiently analyze many facets of it. We now have all the SGBDSN catalog data in this database since 10/01/1995.

A total of 1,077,610 triggers were recorded by the network stations in FY98-99; from this pool, triggers were associated by arrival time into roughly 41,858 events. Of these, 7,812 events were classified as local earthquakes, and 5,733 earthquakes were well enough located within or near the edge of the network to be included in the FY98-99 seismicity catalog (Appendix 3). Roughly 40% of the FY98-99 catalog events are within the aftershock zone of the 1992 Little Skull Mountain earthquake. Although this aftershock sequence has been persistent, the decay constant determined for the modified Omori's law is not low compared to other known sequences and is similar to that of the recent Eureka Valley, California, sequence nearby. The low network threshold (roughly M_L = -0.3) for complete detection of events in this area guarantees that LSM aftershocks will be a significant portion of the catalog for several years hence.

The linear fit to the FY98-99 seismicity data within the perimeter of the SGBDSN gives a *b*-value

of 0.86 and a recurrence rate of approximately 1000 events with $M_L > 0$ per year. Extrapolated to beyond the observed seismicity, this suggests that the recurrence interval is approximately 100 years for a magnitude 6.3 earthquake within approximately 65 km of the proposed repository at Yucca Mountain.

Aside from the earthquakes detected with the network, 282 presumed manmade events were identified in FY98-99 (Appendix 4). Most of these were blasts from known mining sites in the Bare Mountains and toward Beatty, Nevada. Numerous events of surface blast character were recorded near the station STC and are presumed to be associated with military training. The most interesting of the manmade seismic events were a series of collapse-like events, with four known to have occurred, detected in eastern Yucca Flat where known shot cavities exist. The waveform data strongly suggest a negative monopole mechanism such as theoretically associated with a cavity collapse.

For FY98-99 a total of 93 events in the SGBDSN catalog were large enough to have focal mechanisms reliably determined. Generally, the tension axes of the mechanisms cluster closely at low dip angles around 60° west of north (or its opposite at 60° east of south). The pressure axes are more scattered, showing a broader range of dips, but aligning generally along 30° east of north. This result agrees fairly well, with perhaps a 15° counterclockwise rotation, with the general trend of axes in mechanisms for 1978-1992 events detected by the former analog monitoring network, which covers a larger area in the southern Great Basin. A diagram showing the pressure and tension axes in a proper spatial view shows that anomalous focal mechanisms for FY98-99 are mostly toward the west and southwest fringe of the network. When the focal mechanism data is subsetted for LSM

earthquakes only, the resulting composite pressure and tension axes plot indicates even more consistency, reflecting a uniform stress field over the area encompassing those aftershocks.

For FY98-99 we examined two sequences of earthquakes in detail. A swarm of earthquakes occurred near Thirsty Canyon off the northwest corner of NTS, starting in October 1997 and lasting through about August of 1998. Although a portable station was installed nearly over the hypocentral source area, location accuracy was poor throughout this period due to the closest permanent station TYM being down. With TYM back up, location of roughly 80 residual events in 1999 shows a NNW alignment, which agrees fairly well with the focal mechanism of the largest shock of the swarm, a $M_L = 3.6$ event. A second sequence of earthquakes occurred in January 1999 in Frenchman Flat. The mainshock, with M_w 4.7, was the largest event within NTS since the 1992 Little Skull Mountain earthquake. This event had a normal-to-oblique slip mechanism on a NE trending fault.

In FY98-99 four more earthquakes were located within 10 km of the proposed repository. The largest of this group had an $M_L = 0.07$. A recurrence curve for earthquakes within 10 km of the proposed repository was formed using all such events detected since SGBDSN stations were routinely analyzed. This limited sample (18) shows a much lower threshold (roughly 1/2 unit lower) for complete detection of Yucca Mountain earthquakes than that for the analog network operating from 1978 to 1995. It is concluded that the current threshold lies in the range of -0.3 to -0.5 M_L for complete detection of earthquakes near Yucca Mountain. When normalized for their respective recording periods, the recurrence curves determined by the analog network and the SGBDSN nearly overlay at magnitudes above the analog threshold. When the recurrence curve for Yucca Mountain events is compared to that for the southern Great Basin as a whole (normalized to a comparably

small area), the absolute rate of Yucca Mountain earthquakes is seen to be at least 20 times less than for a typical area of similar size within the southern Great Basin. Reasonable adjustments to the assumptions in this analysis change this result by a factor of two or less.

Spectral ratios between RPY and AL5 indicate that horizontal component ground motion on Yucca Mountain is 3 to 4 times greater than in the ESF at Alcove 5 up to frequencies of 13 to 15 Hz. Narrow-band variations around this average may be due to localized amplifications or deamplifications in the AL5 measurements caused by interaction with the free-surface and underside reflections from strong impedance contrasts. Estimates above to 13 to 15 Hz are complicated by a strong, apparently tunnel-induced "site effect" in the Alcove 5 measurements. Frequency-dependent amplifications cause horizontal ground motions in AL5 to exceed those at the surface above about 20 Hz. This may be a peculiarity of the Alcove 5 site, but recordings from other ESF locations would be required to evaluate this. Results from teleseismic spectral ratios suggest that the spectral ratios between RPY and AL5 could vary significantly with back-azimuth.

References

Aki, K., 1965. Maximum–liklihood estimate of b in the formula logÃ = a –bM and its confidence limits, Bull. Earthquake Res. Inst., Tokyo Univ., 43, 237-239.

Aki, K., and P. G. Richards, 1980. *Quantitative Seismology: Theory and Methods*, W. H. Freeman & Co.

Anderson, J. G., J. N. Brune, D. dePolo, J. Gomberg, S. C. Harmsen, M. K. Savage, A. F. Sheehan, and K. D. Smith, 1992. Preliminary report: The Little Skull Mountain Earthquake, June 29, 1992, in Dynamic Analysis and Design Considerations for High-Level Nuclear Waste Repositories, Structural Division of Amer. Soc. Civil Eng.

Biasi, G. P. and K. D. Smith, 1998. Project report: Site effects for seismic monitoring stations in the vicinity of Yucca Mountain, Nevada, W.B.S 1.2.3.2.8.4.1, Deliverable SPT38BM4, Yucca Mountain Project, Dept. of Energy, Las Vegas NV.

Blakely, R. J., R. L. Morin, E. H. McKee, K. M. Schmidt, V. E. Langenheim and G. L. Dixon, 1998. Three-dimensional model of Paleozoic basement beneath Amargosa Desert and Pahrump Valley, California and Nevada: Implications for tectonic evolution and water resources, USGS Open-File Report 98-496.

Carr, W. J, 1984. Regional structural setting of Yucca Mountain, southwestern Nevada, and late Cenozoic rates of tectonic activity in part of the southwestern Great Basin, Nevada and California, U. S. Geological Survey, Open-File Report 84-854.

Carr, W. J., 1990. Styles of extension in the Nevada Test Site region, Southern Walker Lane Belt: An integration of volcano-tectonic and detachment fault models, in Wernicke, B. P., ed., Basin and Range extensional tectonics near the latitude of Las Vegas, Nevada, Geological Society of America, Geological Society of America Memoir 176, p. 283-303.

Crowe, B., C. Fridrich, G. Thompson, K. D. Smith, G. Biasi, and L. Bowker, 1996. Tectonic and volcanic setting of the Yucca Mountain area, Volcanic Hazard Synthesis Report prepared for the *DOE/Yucca Mountain Project.*

Ferrill, D.A., J. A. Stamatakos, S. M. Jones, B. Rahe, H. L. McKague, R. H. Martin, and A. P. Morris, 1996. Quaternary slip history of the Bare Mountain fault (Nevada) from the morphology and distribution of alluvial fan deposits, Geology, 24, 559-562. Boulder, Colorado: Geological Society of America.

Fisher, F., P. Papanek, and R. Hamilton, 1972. The Massachusetts Mountain earthquake of 5 August 1971 and its aftershocks, Nevada Test Site, U. S. Geological Survey Report No. 474-149.

Flesch, L. M., W. E. Holt, A. J. Haines, and B. Shen-Tu, 2000. Dynamics of the Pacific-North American plate boundary in the western United States, Science, 287, 835-836.

Fridrich, C.J., 1999. Tectonic evolution of the Crater Flat Basin, Yucca Mountain region, Nevada, Cenozoic Basins of the Death Valley Region. Wright, L.A. and Troxel, B.W., eds. Special Paper 333, 169-195. Boulder, Colorado: Geological Society of America.

Gardner, J., and L. Knopoff, 1974. Is the sequence of earthquakes in southern California, with aftershocks removed, Poissonian?, Bull. Seism. Soc. Am., 64, 1363-1367.

Grauch, V. J. S., D. A. Sawyer, C. J. Fridrich, and M. R. Hudson, 1997. Geophysical interpretations west of and within the northwestern part of the Nevada Test Site, U. S. Geological Survey Open-File Report 97-476.

Gross, S., 1996. Aftershocks of nuclear explosions compared to natural aftershocks, Bull. Seism. Soc. Am., 86, 1054-1060.

Haimson, B. C., 1982. A comparative study of deep hydrofracturing and overcoring stress measurements at six locations with particular interest to the Nevada Test Site, in U. S. Geological Survey Open-File Report 82-1075, pp. 276-304.

Hamilton, R. M., and J. H. Healy, 1969. Aftershocks of the Benham nuclear explosion, Bull. Seism. Soc. Am., 59, 2271-2281.

Hamilton, R. M., B. E. Smith, F. G. Fisher, and P. J. Papanek, 1971. Seismicity of the Pahute Mesa area, Nevada Test Site, 8 December 1968 through 31 December 1970, U. S. Geological Survey, Special Studies-89.

Hanks, T. C., and H. Kanamori, 1979. A moment magnitude scale, J. Geophys. Res., 84, 2348-2350.

Harmsen, S. C., 1991. Seismicity and focal mechanisms for the southern Great Basin of Nevada and California in 1990, U. S. Geological Survey Open-File Report 91-367.

Harmsen, S. C., 1992. Seismicity and focal mechanisms for the southern Great Basin of Nevada and California in 1991, U. S. Geological Survey Open-File Report 92-340.

Harmsen, S. C., 1993. Preliminary seismicity and focal mechanisms for the southern Great Basin of Nevada and California: January 1992 through September 1992, U. S. Geological Survey Open-File Report 93-369.

Harmsen, S. C., 1994. The Little Skull Mountain, Nevada, Earthquake of 29 June 1992: Aftershock focal mechanisms and tectonic stress field implications, Bull. Seism. Soc. Am., 84,1484-1505.

Harmsen, S. C., and A. M. Rogers, 1986. Inferences about the local stress field from focal mechanisms: applications to earthquakes in the southern Great Basin of Nevada, Bull. Seism. Soc. Am., 76, 1560-1572.

Harmsen, S. C., and C. G. Bufe, 1991. Seismicity and focal mechanisms for the southern Great Basin of Nevada and California – 1987 through 1989, U. S. Geological Survey Open-File Report 91-572.

Hill, D. P., P. A. Reasenberg, A. Michael, W. J. Arabasz, G. Beroza, D. Brumbaugh, J. N. Brune, R. Castro, S. Davis, D. dePolo, W. L. Ellsworth, J. Gomberg, S. Harmsen, L House, S. M. Jackson, M. J. S. Johnston, L. Jones, R. Keller, S. Malone, L. Munguia, S. Nava, J. C. Pechmann, A. Sanford, R. W. Simpson, R. B Smith, M. Stark, M. Stickney, A. Vidal, S. Walter, V. Wong, and J. Zollweg, 1993. Seismicity remotely triggered by the magnitude 7.3 Landers, California, earthquake, Science, 260, 1617-1623.

Hittleman, A.M., R.E. Habermann, D.T. Dater and L. Di, 1992. Gravity earth system data, United Stated Department of Commerce and NOAA, National Geophysical Data Center.

Hoffman, L. R., and Mooney, W. D., 1984. A seismic study of Yucca Mountain and vicinity, southern Nevada — Data report and preliminary results, U. S. Geological Survey, Open-File Report 83-588.

Kisslinger, C., 1993. The stretched exponential function as an alternative model for decay rate, J. Geophys. Res.,98, 1913-1922.

Klein, F. W., 1989. Users guide to HYPOINVERSE, a program for VAX computers to solve for earthquake locations and magnitudes, U. S. Geological Survey Open-File Report, 89-314.

Lee, M. Y., 1996. Hydraulic fracturing stress measurements in Test Hole ESF-AOD-HDFR#1, Thermal Test Facility, Exploratory Studies Facility at Yucca Mountain, report by Sandia National Laboratories to the Yucca Mountain Project, Las Vegas, Nevada.

Lum, P. K., and K. K. Honda, 1992. Processed seismic motion records from Little Skull Mountain, Nevada, earthquake of June 29, 1992, recorded at stations in southern Nevada, Report # JAB-10733-TM6 UC-703 National Technical Information Service.

Meremonte, M. E., and Rogers, A. M., 1987. Historical catalog of southern Great Basin earthquakes 1868-1978, U. S. Geological Survey, Open-File Report 87-80.

Meremonte, M. E., J. Gomberg, and E. Cranswick, 1995. Constraints on the 29 June 1992 Little Skull Mountain sequence provided by robust hypocentral estimates: Bull. Seism. Soc. Am., 85, 1039-1049.

O'Leary, D. W., 2000. Tectonic significance of the Rock Valley fault zone, Nevada Test Site; in USGS Digital Data Series 058, Geologic and Geophysical Characterization Studies of Yucca Mountain, Nevada, A Potential High-Level Radioactive-Waste Repository.

Piety, L. A., 1996. Compilation of known and suspected Quaternary faults within 100 km of Yucca Mountain, U. S. Geological Survey Open-File Report 94-112.

Quinlan, D., 1995. A tutorial for Datascope: the ASIS relational database system, Boulder Real Time Technologies, Inc., Boulder, Colorado.

Reasenberg, P. A., and Oppenheimer, D., 1985. FPFIT, FPPLOT, and FPPAGE: fortran computer programs for calculating and displaying earthquake fault–plane solutions, U. S. Geological Survey, Open-File Report 85-739.

Richter, C. F., 1935. An instrumental earthquake magnitude scale, Bull. Seism. Soc. Am., 25, 1-32.

Rogers, A. M., S. C. Harmsen, and M. E. Meremonte, 1987. Evaluation of the seismicity of the southern Great Basin and its relationship to the tectonic framework of the region, U. S. Geological Survey Open-File Report 87-408.

Rogers, A. M., S. C. Harmsen, E. J. Corbett, K. F. Priestly and D. dePolo, 1991. The seismicity of Nevada and some adjacent parts of the Great Basin, in Slemmons, D. B., E. R. Engdahl, M. D. Zoback, and D. D. Blackwell, eds., Neotectonics of North America, Geological Society of America, Decade Map Volume 1, 153-184.

Savage, M. K., and D. M. dePolo, 1993. Foreshock probabilities in the western Great–Basin and eastern Sierra Nevada, Bull. Seism. Soc. Am., 83, 1910-1938.

Savage, J. C., J. L. Svarc, and W. H. Prescott, 1999. Strain accumulation at Yucca Mountain, Nevada, J. Geophys. Res., 104, 17,627-17,631.

Schneider, J. F., N. A. Abrahamson, and T. C. Hanks, 1996. Ground motion modeling of scenario earthquakes at Yucca Mountain: Provisional draft final report for Activity 8.3.1.17..3.3, Feb 6.

Schweickert, R. A., and M. M. Lahren, 1997. Strike-slip fault system in Amargosa Valley and Yucca Mountain, Nevada, Tectonophysics, 272, 25-41.

Shields, G., K. Smith, and J. Brune, 1995. Source parameters of a sequence of very small earthquakes in the Rock Valley Fault Zone, southern Nevada Test Site, abstract for 1995 annual fall meeting, EOS Supplement, American Geophysical Union, p. F426.

Smith, K. D., D. von Seggern, G. P. Biasi, C. L. Middlebrooks, and J. N. Brune, 1996, Performance of the Southern Great Basin Digital Seismic Network, proceedings of

Methods of Seismic Hazard Evaluation Focus '95, *American Nuclear Society*, Chicago, Illinois.

Smith, K. D., D. H. von Seggern, K. Meyeda, and W. R. Walter, 1997. Seismic observations from the August 28, 1997, ML=2.6, suspected underground cavity collapse at the Nevada Test Site, abstract for the 1997 annual fall meeting, EOS Supplement, American Geophysical Union, p. 345.

Smith, K. D., J. N. Brune, D. dePolo, M. K. Savage, R. Anooshehpoor, and A. F. Sheehan, 2000. The 1992 Little Skull Mountain earthquake sequence, Southern Nevada Test Site, in USGS Digital Data Series 058, Geologic and Geophysical Characterization Studies of Yucca Mountain, Nevada, A Potential High-Level Radioactive-Waste Repository.

Smith, K. D., G. Shields, and J. N. Brune, 2000. A sequence of very shallow earthquakes in the Rock Valley Fault Zone, Southern Nevada Test Site, in USGS Digital Data Series 058, Geologic and Geophysical Characterization Studies of Yucca Mountain, Nevada, A Potential High-Level Radioactive-Waste Repository.

Snoke, J. A., J. W. Munsey, A. G. Teague, and G. A. Bollinger, 1984. A program for focal mechanism determination by combined use of polarity and SV-P amplitude ratio data. Earthquake Notes, v. 55, n. 3, p. 15.

Snyder, D. B., and W. J. Carr, 1984. Interpretation of gravity data in a complex volcano-tectonic setting, southwestern Nevada, J. Geophys. Res. 89, 10,193-10,206.

Stock, J. M., J. H. Healy, S. H. Hickman, and M. D. Zoback, 1985. Hydraulic fracturing stress measurements at Yucca Mountain, Nevada, and relationship to the regional stress field, J. Geophys. Res., 90, 8691-8706.

Su, F., J. G. Anderson, J. N. Brune, and Y. Zeng, 1996. A comparison of direct S-wave and coda-wave site amplification determined from aftershocks of the Little Skull Mountain earthquake, Bull. Seism. Soc. Am., 86, 1006-1018.

Von Seggern, D., and D. DePolo, 1994. Seismicity for the southern Great Basin of Nevada and California in 1993, report to the Yucca Mountain Project, DOE–YMSCO, Las Vegas NV

Von Seggern, D., D. DePolo, and K. Smith, 1995. Seismicity for the southern Great Basin of Nevada and California in 1994, report to the Yucca Mountain Project, DOE–YMSCO, Las Vegas NV (DTN #GS950383117412.003).

Von Seggern, D. H., and K. D. Smith, 1997. Seismicity in the vicinity of Yucca Mountain, Nevada, for the period October 1, 1995, to September 30, 1996, report to the Yucca Mountain Project, DOE–YMSCO, Las Vegas NV (DTN #MO970483117412.002).

Von Seggern, D. H., and D. M. dePolo, 1998. Seismicity in the vicinity of Yucca Mountain, Nevada, for the period October 1, 1996, to September 30, 1997, report to the Yucca Mountain Project, DOE–YMSCO, Las Vegas NV (DTN #MO980683117412.000)

Von Seggern, D. H., and J. N. Brune, 2000. Seismicity in the southern Great Basin, 1868–1992, in USGS Digital Data Series 058, Geologic and Geophysical Characterization Studies of Yucca Mountain, Nevada, A Potential High-Level Radioactive-Waste Repository.

Young, S.R., A. P. Morris, and G. L. Stirewalt, 1993. Geometric analyses of alternative models of faulting at Yucca Mountain, Nevada. High Level Radioactive Waste Management, Proceedings of the Fourth Annual International Conference, Las Vegas, Nevada, April 26-30, 1993. 2, 1818-1825. La Grange Park, Illinois: American Nuclear Society.

Wallace, T. C., D. V. Helmberger, and G. R. Engen,1983. Evidence of tectonic release from underground nuclear explosions, Bull. Seism. Soc. Am., 73, 593-613.

Table 3-1
Comparison of SGBDSN and NEIC ML Estimates

date yy/mm/dd	time hh:mm:sec	latitude deg	latitude min	longitude deg	longitude min	depth (km)	SGBDSN ML	NEIC ML*	difference SGBDSN-NEIC
97/11/12	08:41:33.37	36	50.35	116	15.71	11.26	3.02	---	-----
98/03/10	14:21:04.86	37	10.05	116	36.00	5.46	3.19	---	-----
98/03/23	00:10:21.89	37	10.35	116	36.32	6.38	3.05	---	-----
98/03/25	12:55:53.34	36	57.62	116	43.67	2.46	3.04	3.3	-0.26
98/04/02	19:20:16.45	37	10.45	116	36.29	5.91	3.57	---	-----
99/01/05	10:57:27.51	36	48.01	115	57.69	1.00	3.40	3.5	-0.10
99/01/22	14:41:56.61	36	48.01	115	55.32	14.21	3.19	3.1	0.09
99/01/23	03:00:32.61	36	48.25	115	57.51	0.01	3.85	3.7	0.15
99/01/23	07:11:20.27	36	48.23	115	57.65	0.70	3.42	3.3	0.12
99/01/25	18:52:05.15	36	47.48	115	58.53	0.04	4.03	4.5+	-----
99/01/25	19:51:54.06	36	48.42	115	57.70	5.33	3.59	3.5	0.09
99/01/27	10:44:21.78	36	46.98	115	58.67	9.36	4.14	4.8+	-----
99/01/27	13:18:29.32	36	48.85	115	57.24	12.52	3.15	---	-----
99/01/28	12:39:02.64	36	47.24	115	58.76	4.80	3.22	3.4	-0.18
99/05/11	05:34:25.02	36	45.42	115	58.95	10.79	3.01	---	-----
99/06/23	07:03:15.09	37	12.20	116	49.40	6.40	3.33	3.2	0.13
average difference of SGBDSN ML - NEIC ML									= 0.01

Notes:

* NEIC ML reported only to nearest tenth

+ These earthquakes were at Frenchman Lake and were known to have low SGBDSN ML estimates.

Table 5-1
Location and Magnitude Parameters for Yucca Flat "Collapse" Events

date	time UTC	latitude	longitude	depth (km)	ML
07/19/1998	14:46:50.52	37.0683	116.0057	0.00	1.68
02/27/1999	12:35:25.01	37.0713	116.0162	0.00	1.43
04/04/1999	17:42:35.14	37.0688	116.0052	0.00	1.15
04/04/2000	09:17:59.04	37.0793	115.9847	0.00	0.52

Table 6-1
Focal Mechanisms for FY98-99

date	origin time hhmm	sec	latitude deg	min	longitude deg	min	depth (km)	mag ML							dip+dip#rake* dir	ang	Fj	nobs	avwt	stdr		delta^ strdiprak			
971013	444	20.84	36	42.23	116	18.33	11.56	2.20	0	0	0.0	0.00	0.0	0.0	A	260 20-140	0.00	27	0.04	0.72	0.00	5	5	0	0
971017	1756	54.26	36	35.63	116	39.96	11.96	2.50	0	0	0.0	0.00	0.0	0.0	A	130 70 -30	0.01	41	0.05	0.62	0.00	0	8	25	0
971020	317	33.77	37	1.47	115	55.17	11.76	3.00	0	0	0.0	0.00	0.0	0.0	A	90 70-120	0.06	43	0.12	0.52	0.00	5	5	0	0
971020	519	37.40	37	1.64	115	54.33	11.36	1.70	0	0	0.0	0.00	0.0	0.0	A	235 50-130	0.15	16	0.25	0.70	0.00	8	10	5	0
971020	530	27.05	37	1.70	115	54.99	10.71	2.00	0	0	0.0	0.00	0.0	0.0	A	135 60 -70	0.19	26	0.25	0.55	0.00	5	18	15	0
971022	1108	58.05	36	38.56	116	14.16	6.63	2.10	0	0	0.0	0.00	0.0	0.0	A	145 75 0	0.04	30	0.09	0.61	0.00	8	20	10	0
971023	747	11.16	37	1.38	115	54.26	10.14	2.50	0	0	0.0	0.00	0.0	0.0	A	135 70-100	0.10	36	0.17	0.34	0.00	8	3	10	0
971025	243	25.08	37	9.84	116	36.20	10.10	1.90	0	0	0.0	0.00	0.0	0.0	A	90 85 170	0.10	24	0.16	0.77	0.00	3	23	60	0
971025	2350	10.65	37	9.71	116	35.91	7.67	2.20	0	0	0.0	0.00	0.0	0.0	A	160 50 -40	0.07	29	0.12	0.66	0.00	5	10	5	0
971025	2357	51.82	37	10.37	116	35.73	8.45	2.40	0	0	0.0	0.00	0.0	0.0	A	90 80 170	0.04	41	0.08	0.77	0.00	3	35	40	0
971026	919	20.99	37	9.60	116	35.96	8.71	2.30	0	0	0.0	0.00	0.0	0.0	A	180 70 0	0.13	32	0.18	0.75	0.00	5	20	10	0
971027	933	14.90	36	42.00	116	16.63	9.08	1.90	0	0	0.0	0.00	0.0	0.0	A	135 70 -50	0.03	30	0.07	0.65	0.00	10	3	5	0
971027	1130	39.79	37	9.85	116	35.87	6.22	2.00	0	0	0.0	0.00	0.0	0.0	A	170 85 10	0.04	22	0.11	0.73	0.00	8	53	40	0
971031	2109	41.65	37	11.07	116	35.46	3.08	1.80	0	0	0.0	0.00	0.0	0.0	A	90 60-170	0.18	31	0.24	0.73	0.00	3	10	5	0
971103	1406	19.23	36	44.60	116	15.46	8.27	2.20	0	0	0.0	0.00	0.0	0.0	A	95 50-170	0.01	27	0.08	0.52	0.00	8	10	5.	0
971107	830	22.71	37	1.42	115	54.60	6.57	2.20	0	0	0.0	0.00	0.0	0.0	A	140 50 -90	0.02	20	0.12	0.30	0.00	5	8	5	0
971107	2312	25.25	37	10.34	116	36.14	7.55	1.70	0	0	0.0	0.00	0.0	0.0	A	245 20 60	0.14	21	0.20	0.34	0.00	18	28	45	0
971109	1505	25.58	37	1.78	115	55.46	10.33	3.00	0	0	0.0	0.00	0.0	0.0	A	85 60-140	0.10	39	0.16	0.52	0.00	3	10	0	0
971109	1558	7.79	37	1.62	115	55.01	10.63	2.60	0	0	0.0	0.00	0.0	0.0	A	85 65-140	0.06	41	0.10	0.48	0.00	3	8	0	0
971110	0806	25.48	37	10.98	116	35.08	7.31	2.20	0	0	0.0	0.00	0.0	0.0	A	165 50 -30	0.17	28	0.22	0.67	0.00	8	10	5	0
971111	747	28.96	37	10.11	115	56.96	4.29	1.90	0	0	0.0	0.00	0.0	0.0	A	230 70 170	0.13	19	0.23	0.68	0.00	13	40	155	0
971112	841	33.49	36	50.66	116	15.53	13.02	3.40	0	0	0.0	0.00	0.0	0.0	A	345 80 10	0.01	27	0.06	0.59	0.00	8	18	5	0
971114	222	41.32	36	42.17	116	18.47	10.96	2.10	0	0	0.0	0.00	0.0	0.0	A	140 55 -70	0.00	30	0.03	0.70	0.00	8	3	10	0
971120	1106	57.61	36	51.80	115	58.22	5.74	1.70	0	0	0.0	0.00	0.0	0.0	A	250 65 120	0.09	21	0.16	0.45	0.00	10	3	10	0
971121	649	21.70	36	43.49	116	17.83	9.64	1.80	0	0	0.0	0.00	0.0	0.0	A	145 60 -40	0.04	28	0.08	0.67	0.00	20	8	10	0
971123	1026	16.65	36	43.54	116	17.92	9.32	1.70	0	0	0.0	0.00	0.0	0.0	A	170 75 -30	0.04	28	0.07	0.69	0.00	5	5	10	0
971204	1331	44.03	37	10.25	116	36.07	9.31	2.30	0	0	0.0	0.00	0.0	0.0	A	170 85 10	0.11	27	0.16	0.71	0.00	0	25	20	0
971207	1755	34.31	37	10.36	116	35.83	7.59	1.70	0	0	0.0	0.00	0.0	0.0	A	195 50 40	0.12	21	0.17	0.52	0.00	8	13	10	0
971211	1202	43.14	36	41.99	116	17.67	10.43	2.00	0	0	0.0	0.00	0.0	0.0	A	80 80-170	0.01	29	0.05	0.60	0.00	5	5	15	0
971214	1605	55.85	36	45.54	116	16.78	8.53	2.40	0	0	0.0	0.00	0.0	0.0	A	270 65-170	0.06	34	0.09	0.71	0.00	3	23	10	0
971214	1820	59.54	37	10.02	116	36.19	8.20	2.30	0	0	0.0	0.00	0.0	0.0	A	80 70-160	0.06	32	0.12	0.66	0.00	5	30	15	0
971215	1826	11.52	37	10.52	116	35.51	11.05	2.90	0	0	0.0	0.00	0.0	0.0	A	170 45 -10	0.06	48	0.10	0.64	0.00	0	20	10	0
971215	2114	18.43	36	49.26	116	45.31	4.23	2.50	0	0	0.0	0.00	0.0	0.0	A	120 35 -80	0.02	41	0.07	0.81	0.00	13	20	30	0
971219	2236	31.03	36	41.83	116	18.62	11.01	1.30	0	0	0.0	0.00	0.0	0.0	A	280 25-100	0.06	23	0.12	0.71	0.00	25	8	20	0
971219	2237	48.75	36	42.07	116	18.49	11.44	2.40	0	0	0.0	0.00	0.0	0.0	A	110 70-120	0.02	34	0.06	0.77	0.00	3	5	30	0
971224	1407	48.28	36	43.14	116	17.20	12.83	2.20	0	0	0.0	0.00	0.0	0.0	A	170 75 -30	0.01	26	0.04	0.65	0.00	10	3	5	0
971224	2153	9.93	37	9.87	116	35.82	6.65	1.90	0	0	0.0	0.00	0.0	0.0	A	140 60 -30	0.07	21	0.13	0.60	0.00	8	10	10	0
980101	1842	10.00	36	51.23	116	3.81	7.92	1.70	0	0	0.0	0.00	0.0	0.0	A	195 40 -70	0.15	15	0.24	0.45	0.00	5	10	10	0
980101	2037	14.53	36	29.31	116	35.34	9.39	1.60	0	0	0.0	0.00	0.0	0.0	A	235 75 140	0.12	38	0.16	0.79	0.00	15	10	45	0
980102	721	0.84	36	29.90	116	35.21	7.15	2.00	0	0	0.0	0.00	0.0	0.0	A	245 85 170	0.03	27	0.09	0.81	0.00	5	45	60	0
980105	14	55.78	36	45.62	116	13.30	7.54	2.30	0	0	0.0	0.00	0.0	0.0	A	355 85 0	0.02	31	0.06	0.69	0.00	5	15	5	0
980106	1558	6.37	36	42.83	116	18.27	10.58	1.80	0	0	0.0	0.00	0.0	0.0	A	165 70 -40	0.02	33	0.05	0.69	0.00	8	5	10	0
980119	0104	15.58	36	42.96	116	18.32	9.29	2.20	0	0	0.0	0.00	0.0	0.0	A	110 45-100	0.02	33	0.06	0.70	0.00	18	5	15	0
980210	1921	38.03	37	10.23	116	35.77	6.65	2.30	0	0	0.0	0.00	0.0	0.0	A	155 50 -40	0.10	28	0.15	0.57	0.00	10	10	10	0
980210	1926	38.77	37	10.09	116	35.75	5.53	2.30	0	0	0.0	0.00	0.0	0.0	A	110 45-140	0.02	28	0.08	0.82	0.00	25	23	10	0
980221	1038	45.44	37	10.72	116	35.93	8.12	2.10	0	0	0.0	0.00	0.0	0.0	A	145 65 -20	0.03	22	0.09	0.58	0.00	10	13	10	0

Table 6-1 (cont'd)

date	origin time hhmm	sec	latitude deg	min	longitude deg	min	depth (km)	mag ML						dip+dip# dir	rake* ang	Fj	nobs	avwt	stdr		delta^ strdiprak				
980301	923	48.06	36-	42.85	116-	18.68	10.13	1.90	0	0	0.0	0.00	0.0	0.0	A 145	70 -70	0.00	24	0.04	0.75	0.00	10	3	5		0
980310	1421	4.91	37-	9.77	116-	35.58	10.64	3.10	0	0	0.0	0.00	0.0	0.0	A 175	60 0	0.02	32	0.08	0.71	0.00	5	15	10		0
980313	153	52.01	37-	10.07	116-	36.16	9.03	2.00	0	0	0.0	0.00	0.0	0.0	A 170	70 30	0.06	23	0.14	0.62	0.00	3	5	25		0
980323	10	22.10	37-	10.41	116-	36.08	7.31	3.20	0	0	0.0	0.00	0.0	0.0	A 155	80 -20	0.01	46	0.06	0.56	0.00	3	8	5		0
980325	1255	53.66	36-	57.09	116-	42.07	8.14	3.00	0	0	0.0	0.00	0.0	0.0	A 175	90 20	0.01	37	0.07	0.85	0.00	13	33	40		0
980328	1513	53.85	36-	44.37	116-	16.73	12.51	1.60	0	0	0.0	0.00	0.0	0.0	A 130	50 -60	0.01	27	0.05	0.64	0.00	0	0	5		0
980331	1458	46.10	37-	10.30	116-	36.42	6.81	1.70	0	0	0.0	0.00	0.0	0.0	A 320	75 10	0.05	23	0.13	0.65	0.00	5	18	20		0
980402	1920	16.56	37-	10.65	116-	35.97	9.25	3.30	0	0	0.0	0.00	0.0	0.0	A 145	40 0	0.04	45	0.08	0.59	0.00	8	18	10		0
980403	1704	29.65	37-	10.14	116-	36.04	8.60	2.60	0	0	0.0	0.00	0.0	0.0	A 155	75 -30	0.12	35	0.18	0.58	0.00	3	3	20		0
980413	1750	25.75	36-	42.08	116-	18.48	11.94	1.50	0	0	0.0	0.00	0.0	0.0	A 130	70-110	0.04	24	0.08	0.85	0.00	30	13	40		0
980414	0105	52.43	36-	42.36	116-	18.27	11.95	2.70	0	0	0.0	0.00	0.0	0.0	A 115	70-110	0.05	37	0.08	0.75	0.00	10	3	20		0
980425	0202	1.34	37-	2.02	116-	30.23	6.86	2.40	0	0	0.0	0.00	0.0	0.0	A 345	85 -60	0.05	33	0.11	0.65	0.00	10	5	5		0
980425	1517	12.26	36-	54.86	116-	12.04	9.63	1.80	0	0	0.0	0.00	0.0	0.0	A 235	60-170	0.08	25	0.12	0.71	0.00	8	20	15		0
980428	342	47.18	36-	42.08	116-	18.49	12.10	1.90	0	0	0.0	0.00	0.0	0.0	A 355	80 30	0.01	24	0.05	0.74	0.00	8	5	15		0
980601	1633	0.41	36-	59.60	116-	17.88	6.46	2.00	0	0	0.0	0.00	0.0	0.0	A 170	85 40	0.16	24	0.21	0.61	0.00	13	10	25		0
980611	156	50.12	36-	40.90	116-	17.16	2.40	2.60	0	0	0.0	0.00	0.0	0.0	A 95	85-170	0.00	23	0.09	0.80	0.00	10	38	70		0
980613	2205	27.50	37-	10.15	116-	35.99	7.69	2.80	0	0	0.0	0.00	0.0	0.0	A 140	65 -20	0.04	26	0.11	0.61	0.00	8	10	10		0
980616	954	20.02	36-	42.67	116-	18.59	10.92	2.00	0	0	0.0	0.00	0.0	0.0	A 155	65 -70	0.01	27	0.06	0.72	0.00	15	8	35		0
980620	1044	19.58	36-	42.43	116-	18.39	11.23	1.90	0	0	0.0	0.00	0.0	0.0	A 120	55 -90	0.00	22	0.05	0.72	0.00	10	13	25		0
980625	148	32.04	37-	10.07	116-	36.34	8.30	3.00	0	0	0.0	0.00	0.0	0.0	A 145	80 -20	0.05	33	0.11	0.64	0.00	3	10	30		0
980629	433	22.70	36-	42.52	116-	18.21	11.72	2.10	0	0	0.0	0.00	0.0	0.0	A 155	60 -70	0.02	27	0.07	0.70	0.00	5	18	30		0
980704	1146	58.90	36-	43.01	116-	18.40	9.10	1.80	0	0	0.0	0.00	0.0	0.0	A 170	70 -40	0.04	23	0.10	0.74	0.00	10	13	40		0
980718	534	22.54	36-	44.15	116-	17.53	9.87	2.20	0	0	0.0	0.00	0.0	0.0	A 160	70 -40	0.05	21	0.11	0.73	0.00	28	15	40		0
980805	818	53.64	36-	44.81	116-	16.82	9.10	2.00	0	0	0.0	0.00	0.0	0.0	A 350	75 -30	0.10	21	0.16	0.66	0.00	8	13	30		0
981024	1453	4.77	36-	36.99	116-	16.73	7.69	2.10	0	0	0.0	0.00	0.0	0.0	A 185	35 20	0.12	25	0.17	0.45	0.00	5	3	10	*	0
981031	1436	56.63	36-	43.03	116-	17.89	11.85	1.00	0	0	0.0	0.00	0.0	0.0	A 80	70-150	0.04	19	0.12	0.66	0.00	8	10	50		0
981116	1731	56.96	36-	50.86	116-	15.33	12.02	1.30	0	0	0.0	0.00	0.0	0.0	A 105	60-110	0.09	16	0.18	0.63	0.00	18	10	15		0
981130	129	20.37	36-	58.56	116-	10.92	7.34	2.30	0	0	0.0	0.00	0.0	0.0	A 75	85-160	0.00	26	0.09	0.65	0.00	10	13	10		0
981208	506	13.74	36-	44.22	116-	17.35	10.88	2.10	0	0	0.0	0.00	0.0	0.0	A 135	65 -70	0.04	24	0.10	0.77	0.00	18	15	20		0
981223	1623	39.48	36-	42.83	116-	18.74	10.18	1.10	0	0	0.0	0.00	0.0	0.0	A 95	60-140	0.06	17	0.12	0.69	0.00	8	13	25		0
981227	400	13.04	36-	43.02	116-	18.54	10.14	1.80	0	0	0.0	0.00	0.0	0.0	A 155	65 -50	0.06	24	0.12	0.72	0.00	15	18	25		0
990122	1441	57.20	36-	47.76	115-	55.52	10.22	3.10	0	0	0.0	0.00	0.0	0.0	A 150	50-110	0.01	28	0.08	0.49	0.00	10	10	5	*	0
990127	1044	22.18	36-	46.38	115-	58.82	6.86	0.00	0	0	0.0	0.00	0.0	0.0		120	40-100	0.03	48	0.08	0.74	0.00	25	10	25		0
990128	244	30.08	36-	41.74	116-	18.54	11.99	1.10	0	0	0.0	0.00	0.0	0.0	A 155	70 -60	0.00	19	0.04	0.79	0.00	30	10	10		0
990205	342	21.38	36-	42.27	116-	18.89	11.80	1.50	0	0	0.0	0.00	0.0	0.0	A 170	70 -60	0.01	28	0.05	0.71	0.00	3	5	5		0
990206	1819	47.76	37-	9.15	116-	10.58	10.91	1.50	0	0	0.0	0.00	0.0	0.0	A 170	85 -10	0.17	19	0.22	0.80	0.00	8	23	30		0
990210	317	58.01	36-	42.08	116-	18.49	12.26	1.60	0	0	0.0	0.00	0.0	0.0	A 140	55 -80	0.00	20	0.05	0.73	0.00	8	3	15		0
990212	818	25.78	36-	47.38	116-	13.69	6.66	1.60	0	0	0.0	0.00	0.0	0.0	A 120	55-110	0.00	21	0.04	0.74	0.00	18	8	10		0
990324	622	5.08	36-	43.46	116-	18.35	10.24	1.30	0	0	0.0	0.00	0.0	0.0	A 170	75 -40	0.00	18	0.08	0.75	0.00	15	15	30		0
990401	1914	43.19	36-	43.08	116-	18.40	10.54	1.30	0	0	0.0	0.00	0.0	0.0	A 125	70 -50	0.00	18	0.07	0.60	0.00	18	10	10		0
990401	2340	58.59	36-	42.45	116-	18.24	12.07	1.20	0	0	0.0	0.00	0.0	0.0	A 350	85 30	0.07	16	0.15	0.76	0.00	8	13	15		0
990402	111	48.86	37-	10.63	116-	35.88	7.66	1.00	0	0	0.0	0.00	0.0	0.0	A 130	85 20	0.08	16	0.15	0.73	0.00	0	5	15		0
990402	814	43.86	37-	10.71	116-	35.88	8.18	1.20	0	0	0.0	0.00	0.0	0.0	A 130	45 -20	0.06	18	0.13	0.57	0.00	10	13	10		0
990423	1124	43.15	36-	47.40	116-	13.74	6.98	1.90	0	0	0.0	0.00	0.0	0.0	A 355	85 0	0.00	23	0.04	0.75	0.00	8	35	10		0
990512	1925	1.59	36-	43.86	116-	17.39	10.22	1.10	0	0	0.0	0.00	0.0	0.0	A 265	60 170	0.07	15	0.19	0.73	0.00	10	33	10	*	0
990706	327	33.84	36-	47.45	116-	13.95	6.59	1.30	0	0	0.0	0.00	0.0	0.0	A 280	55-150	0.06	23	0.15	0.68	0.00	18	10	20	*	0
990814	26	2.59	37-	24.91	117-	3.99	5.14	2.30	0	0	0.0	0.00	0.0	0.0	A 140	40 -50	0.14	15	0.20	0.73	0.00	8	10	10	*	0

Table 6-1 continued

+ dip dir = direction of the fault plane dip (90° from the strike angle of fault plane)
# dip ang = dip of the fault plane from horizontal
* rake = angle at which the hanging wall moves relative to foot wall, counterclockwise from horizontal
^delta strdiprak = 95% confidence region for strike angle (str), dip angle (dip), and rake (rak)

Table 8-1
Earthquakes Recorded by the SGBDSN Near Yucca Mountain – 1995-1999

Date	Time (UTC)	latitude deg	latitude min	longitude deg	longitude min	depth (km)	magnitude (ML)	
95/05/05	13:21:33.13	36	50.65	116	24.01	6.08	0.58	
95/07/01	15:26:56.69	36	40.84	116	30.88	8.65	-0.96	^
95/07/07	07:58:59.68	36	49.74	116	24.75	6.06	-0.27	
95/07/28	06:18:51.42	36	54.12	116	30.51	4.79	-0.48	
95/09/04	12:39:47.12	36	44.46	116	29.98	4.44	0.72	^
95/11/19	22:16:24.90	36	50.79	116	23.66	6.52	-0.25	
95/11/20	02:26:57.39	36	50.83	116	23.74	6.44	-0.43	
95/12/06	23:27:15.85	36	43.58	116	28.83	8.12	0.29	^
96/01/29	10:20:32.32	36	44.23	116	29.44	9.90	-0.35	^
96/03/30	19:57:28.63	36	48.60	116	27.98	7.24	-0.59	
96/04/08	07:14:49.64	36	49.94	116	25.19	8.26	-0.58	
96/06/02	10:15:33.29	36	49.25	116	29.43	9.81	0.01	
96/06/02	16:46:15.29	36	49.09	116	29.15	8.79	-0.69	
96/08/12	04:22:50.68	36	48.48	116	23.09	5.02	-0.62	
96/10/26	02:11:34.17	36	54.89	116	27.59	5.49	-0.39	
97/02/25	06:04:11.76	36	53.03	116	26.17	2.86	-0.32	
97/06/14	20:26:46.94	36	50.05	116	24.60	4.27	0.18	
97/06/16	22:03:31.89	36	49.86	116	24.18	3.89	-0.64	
97/07/07	15:36:53.26	36	42.18	116	28.68	5.22	0.07	^
97/07/31	17:54:50.68	36	42.29	116	26.98	9.53	1.18	^
98/07/25	06:35:50.65	36	51.44	116	32.28	6.54	-0.75	&
98/07/27	02:23:45.03	36	44.54	116	24.86	5.86	-0.72	^
98/08/12	19:44:31.67	36	50.87	116	32.72	4.66	0.07	&
99/03/29	16:02:57.20	36	49.10	116	22.94	6.17	-0.09	
99/04/03	11:07:33.01	36	54.05	116	32.63	6.88	-0.11	

& Crater Flat area (outside YM block but still < 10 km)
^ > 10 km from RPY but in southern part of mountain block

Table 11-1
Strong-Motion Station Name and Location Reference

Station	Serial#	Latitude-Longitude		Station Location
SPRS	564	36.6880	-116.1781	Specter Range
LWLS	565	36.6440	-116.3980	Lathrop Wells
BYMS	566	36.8393	-116.4776	Solitario Canyon
SYMS	567	36.8377	-116.4732	Upper Solitario Canyon
WCTS	568	36.7927	-116.6257	Wildcat Canyon
MDVS	569	36.8519	-116.4223	Midway Valley
TYMS	570	36.8393	-116.4684	Top of Yucca Mountain
EXHS	572	36.8495	-116.4303	Exile Hill
FOCS	571	36.7840	-116.2860	Field Operations Center

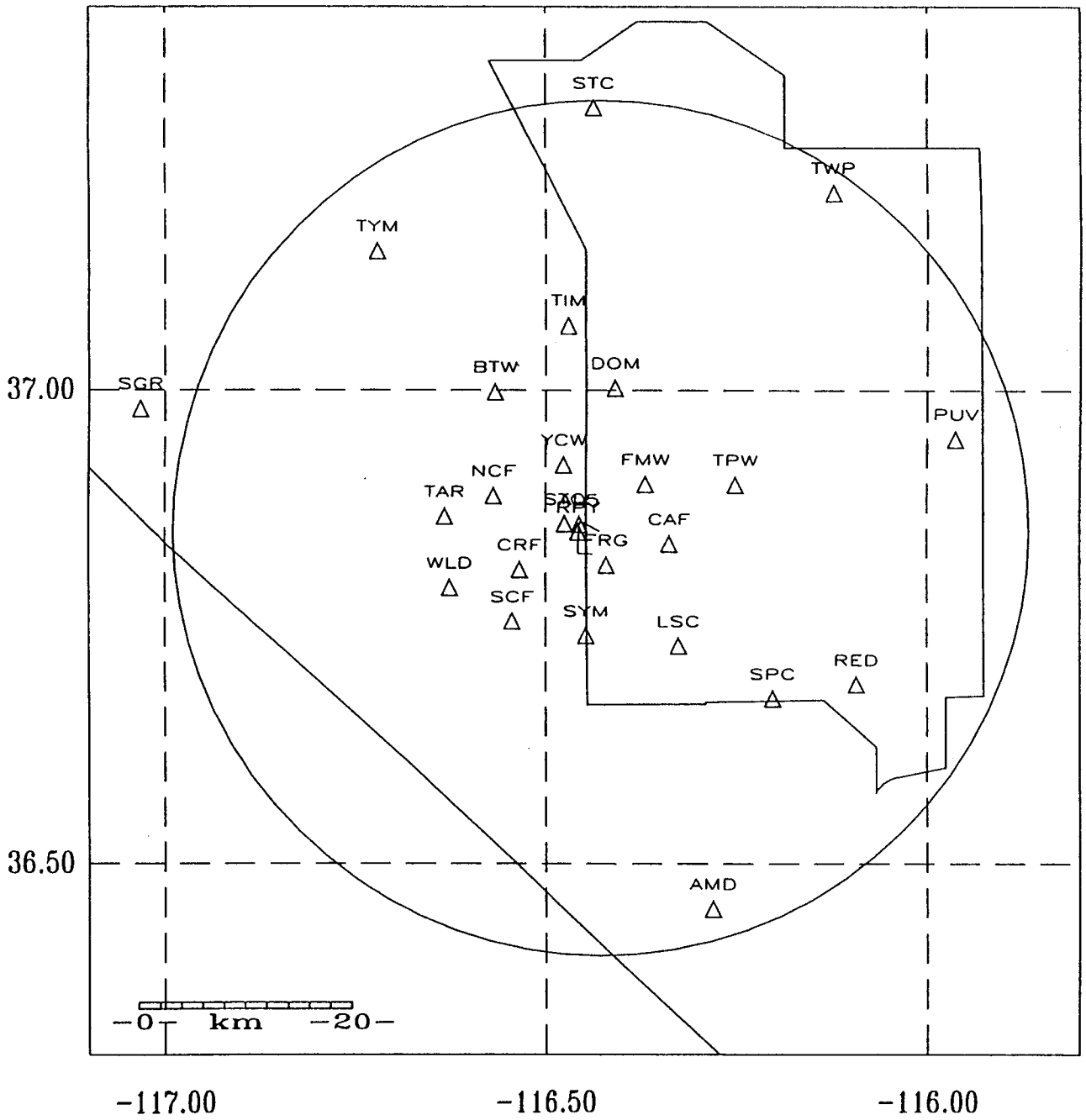

Figure 2-1. Stations of the Southern Great Basin Digital Seismic Network.

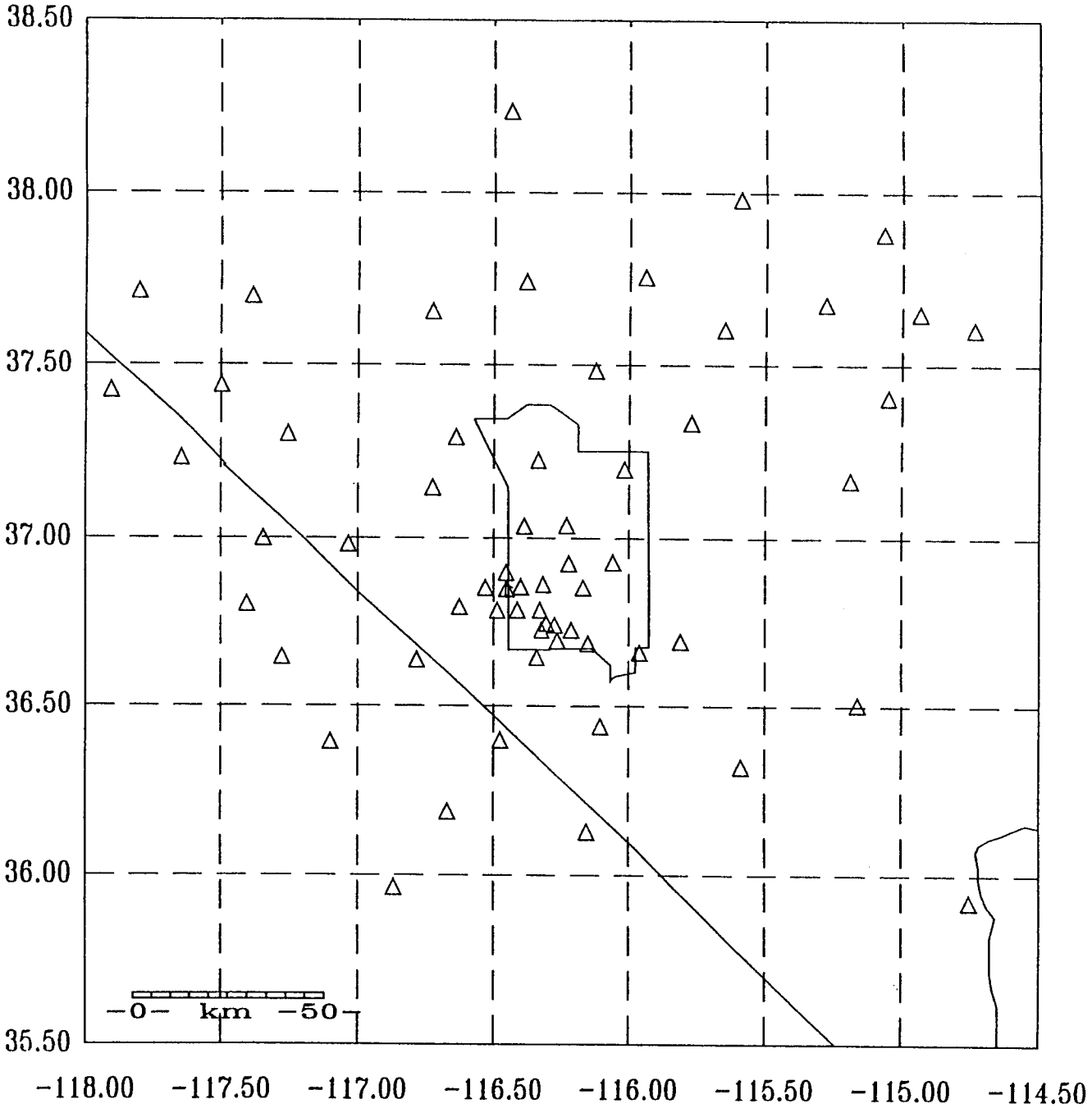

Figure 2-2. Stations of the Southern Great Basin Seismic Network (analog).

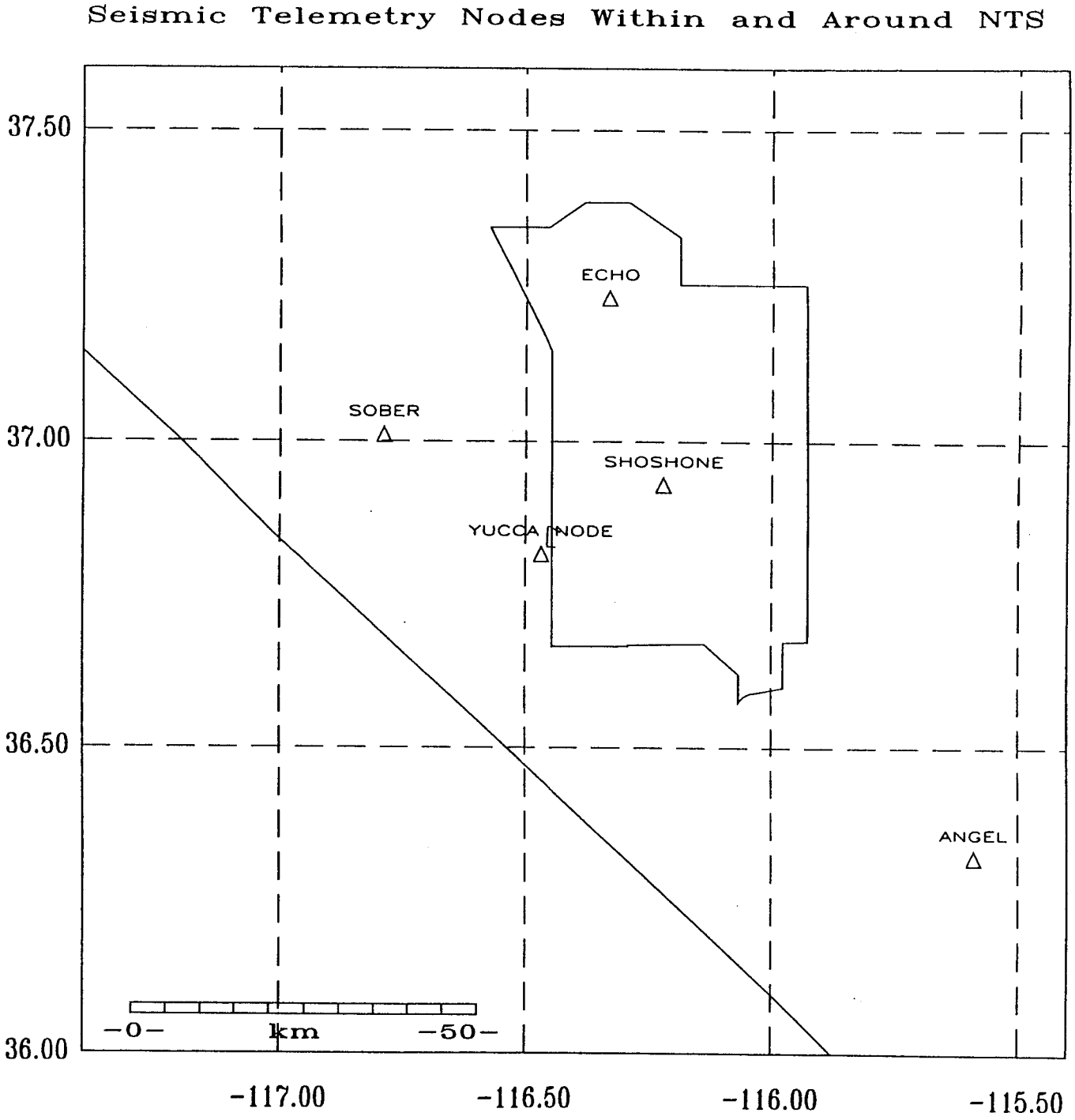

Figure 2-3. Seismic telemetry nodes for the SGBDSN.

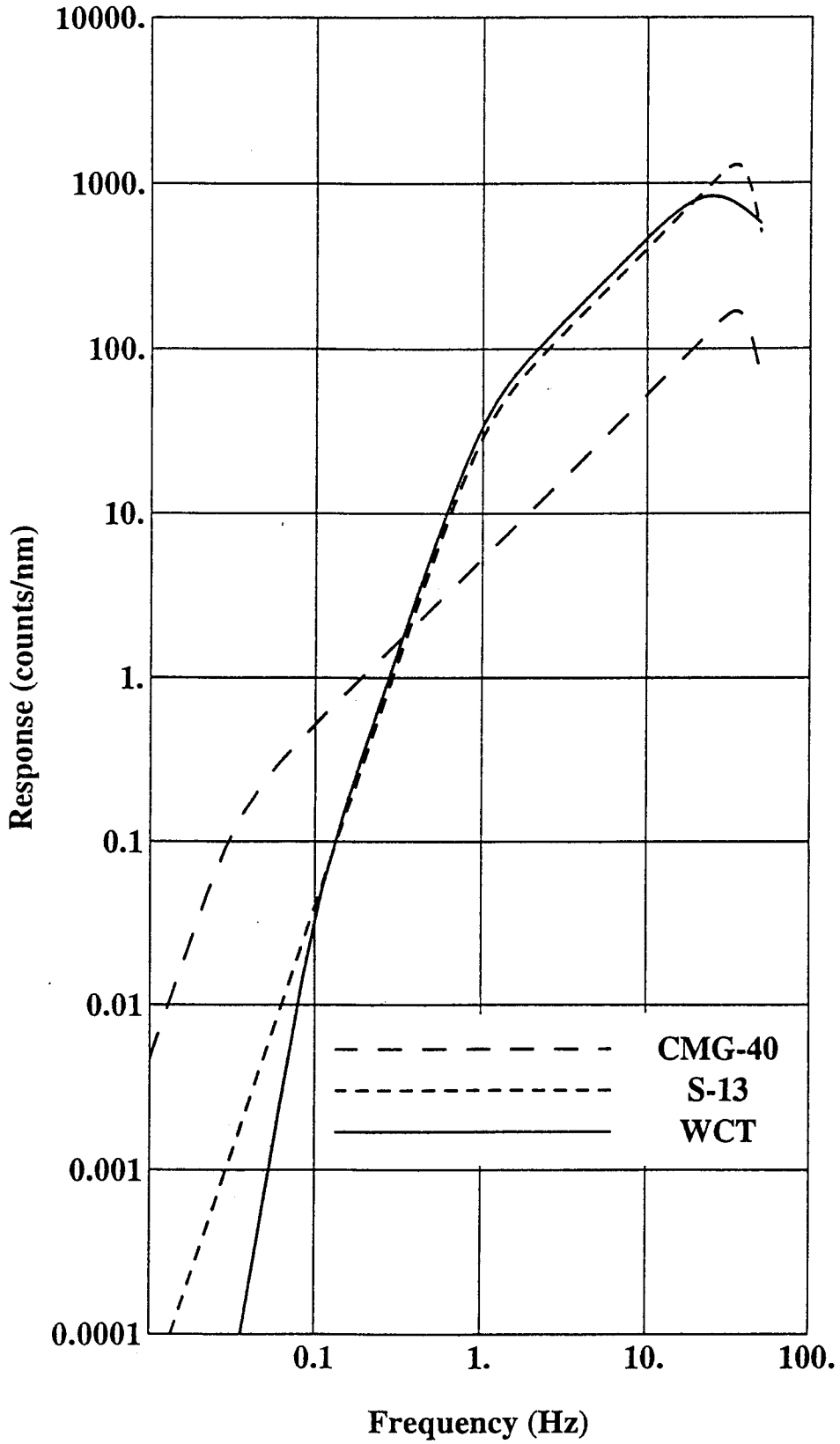

Figure 2-4. Displacement response of the SGBDSN S-13 and CMG-40 stations and of a typical analog SGBSN station (WCT).

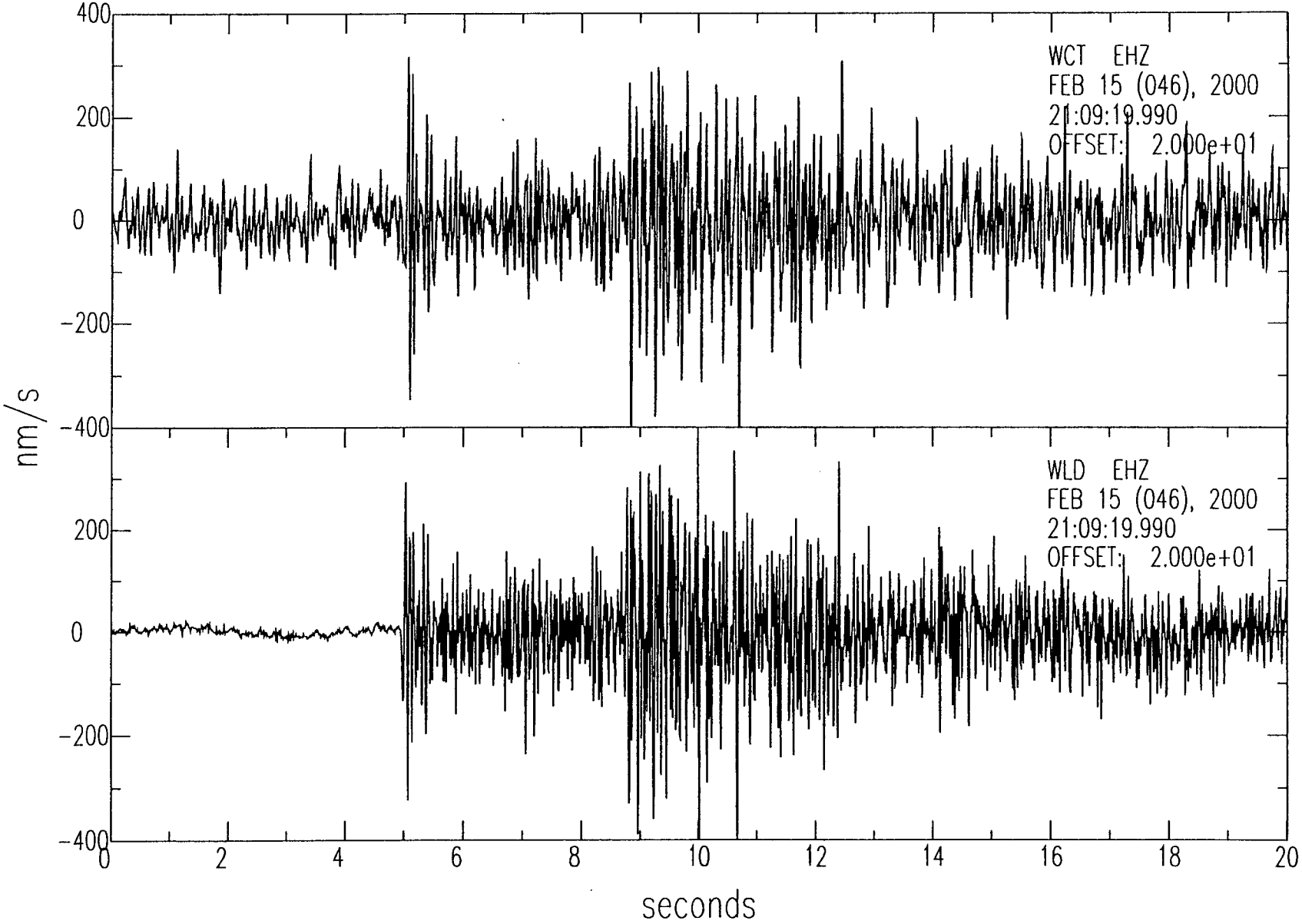

Figure 2-5. Comparison of local earthquake recordings made at collocated analog (WCT) and digital (WLD) stations.

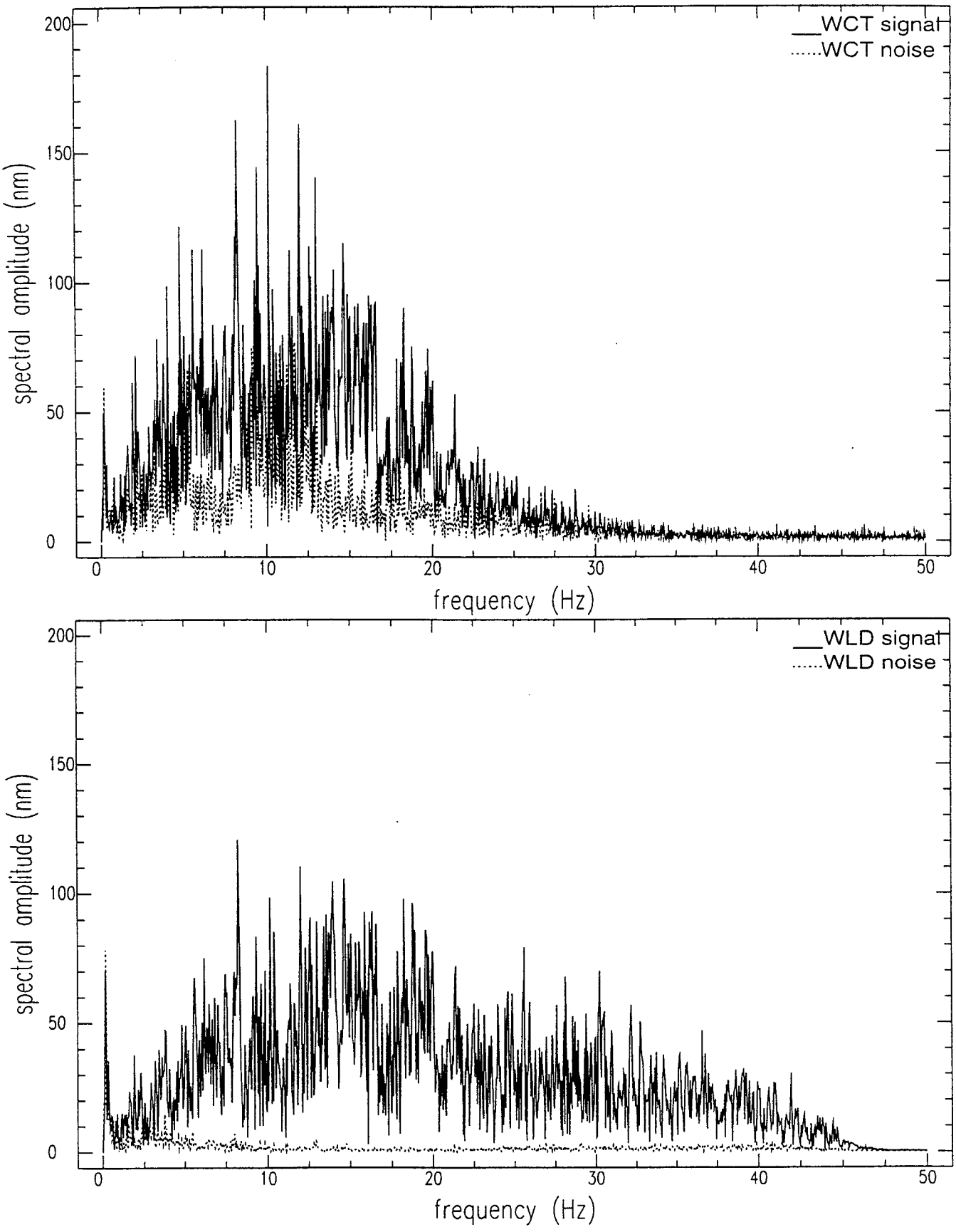

Figure 2-6. Comparison of spectra of a local earthquake recorded at collocated analog (WCT) and digital (WLD) stations.

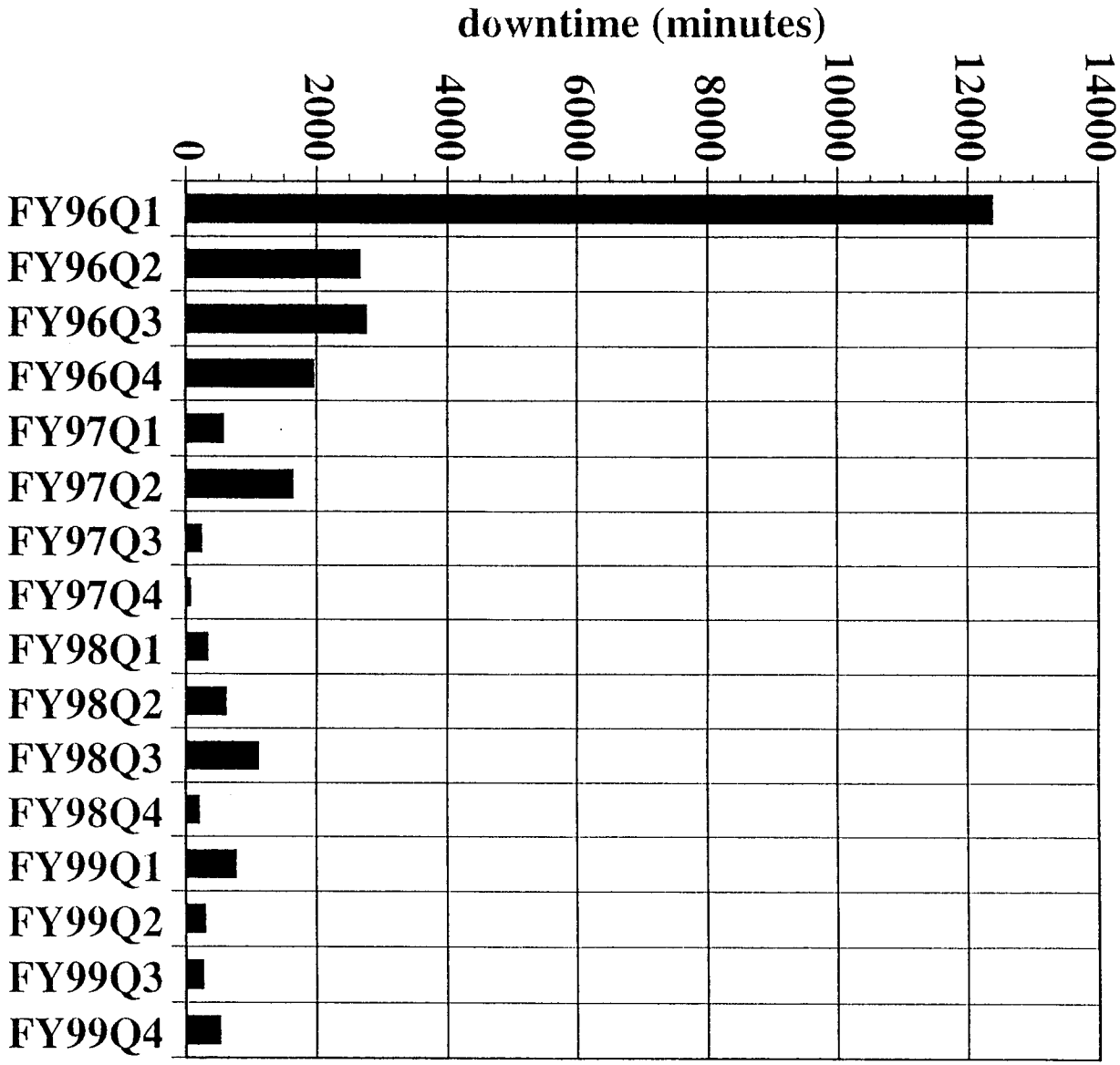

Figure 2-7. Downtime of the SGBDSN network for FY96 through FY99.

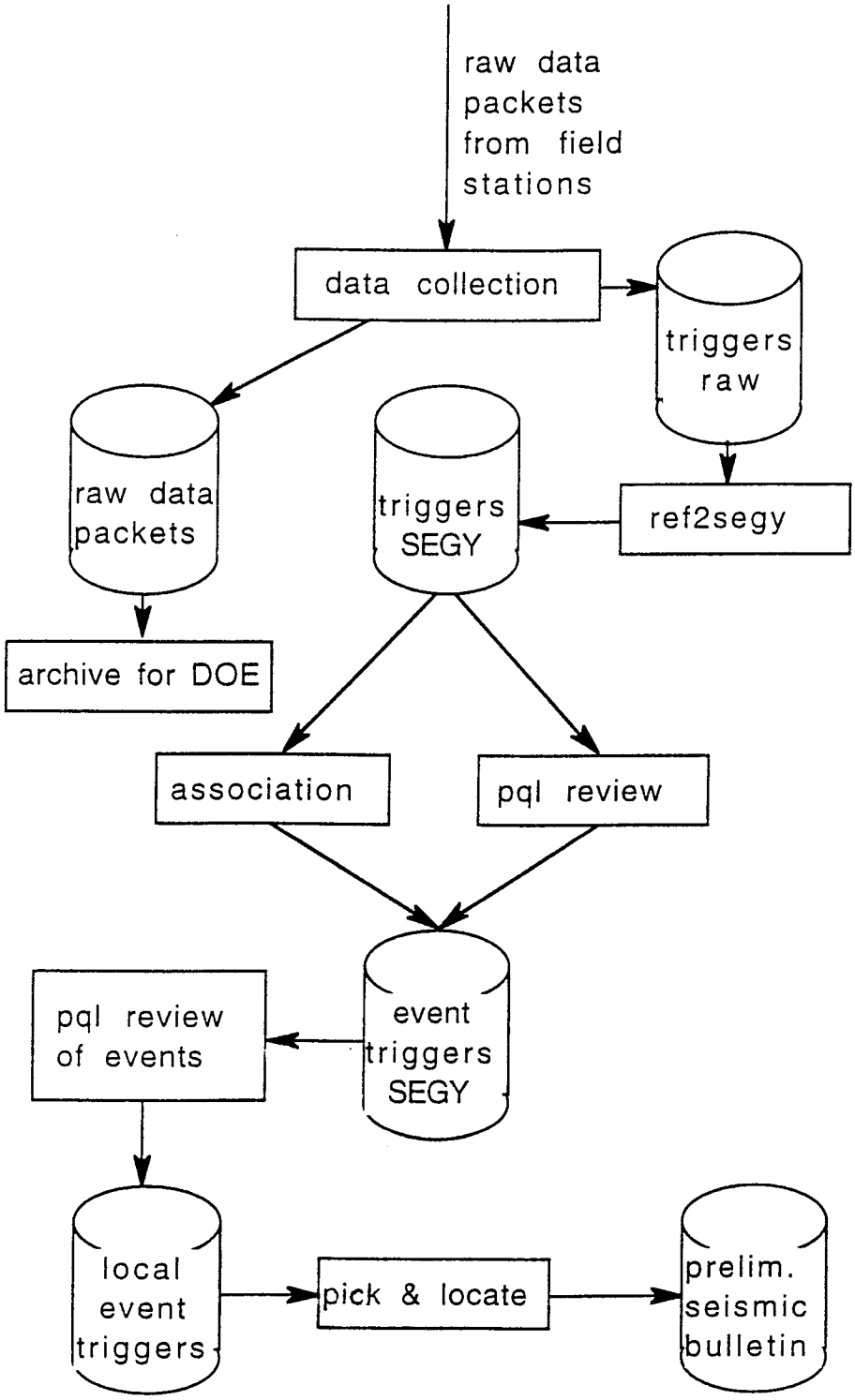

Figure 2-8. Data Flow for the SGBDSN seismic recording.

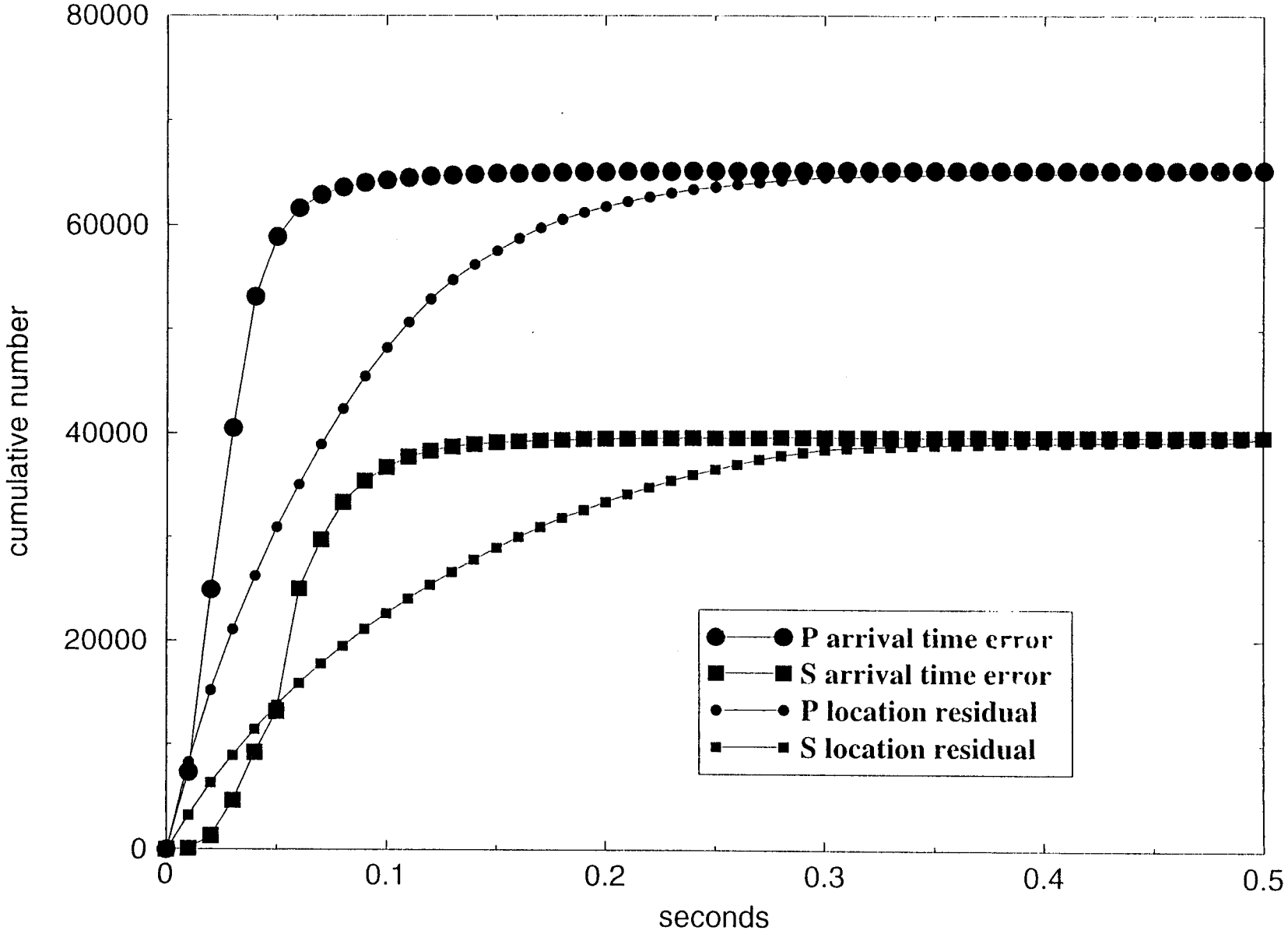

Figure 2-9. Timing errors and location residuals for the SGBDSN network.

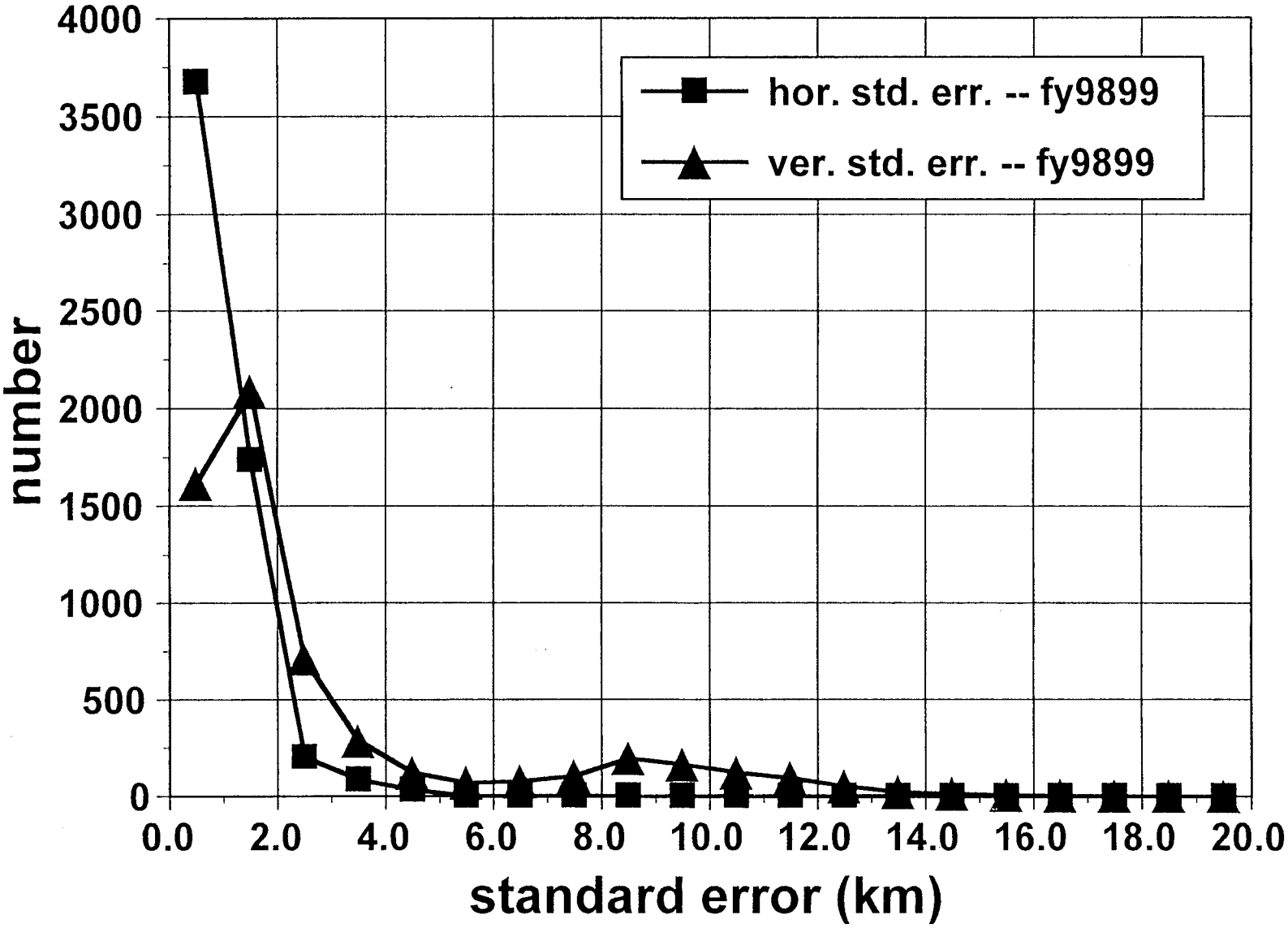

Figure 2-10. Histogram of one standard error values for horizontal and vertical location precision of all FY98-99 earthquakes.

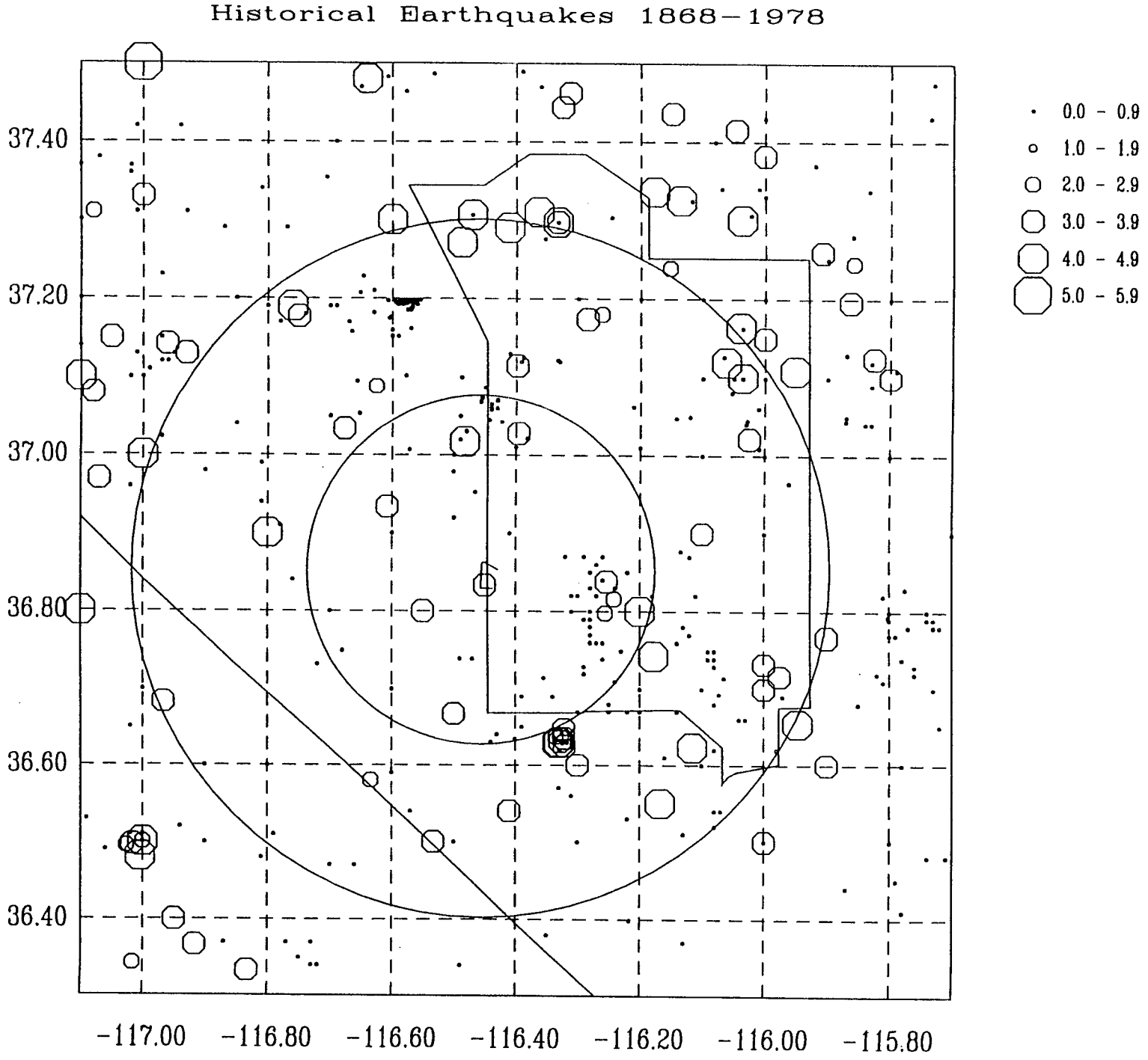

Figure 3-1. Historical seismicity (1868 to 1978) of the Yucca Mountain area.

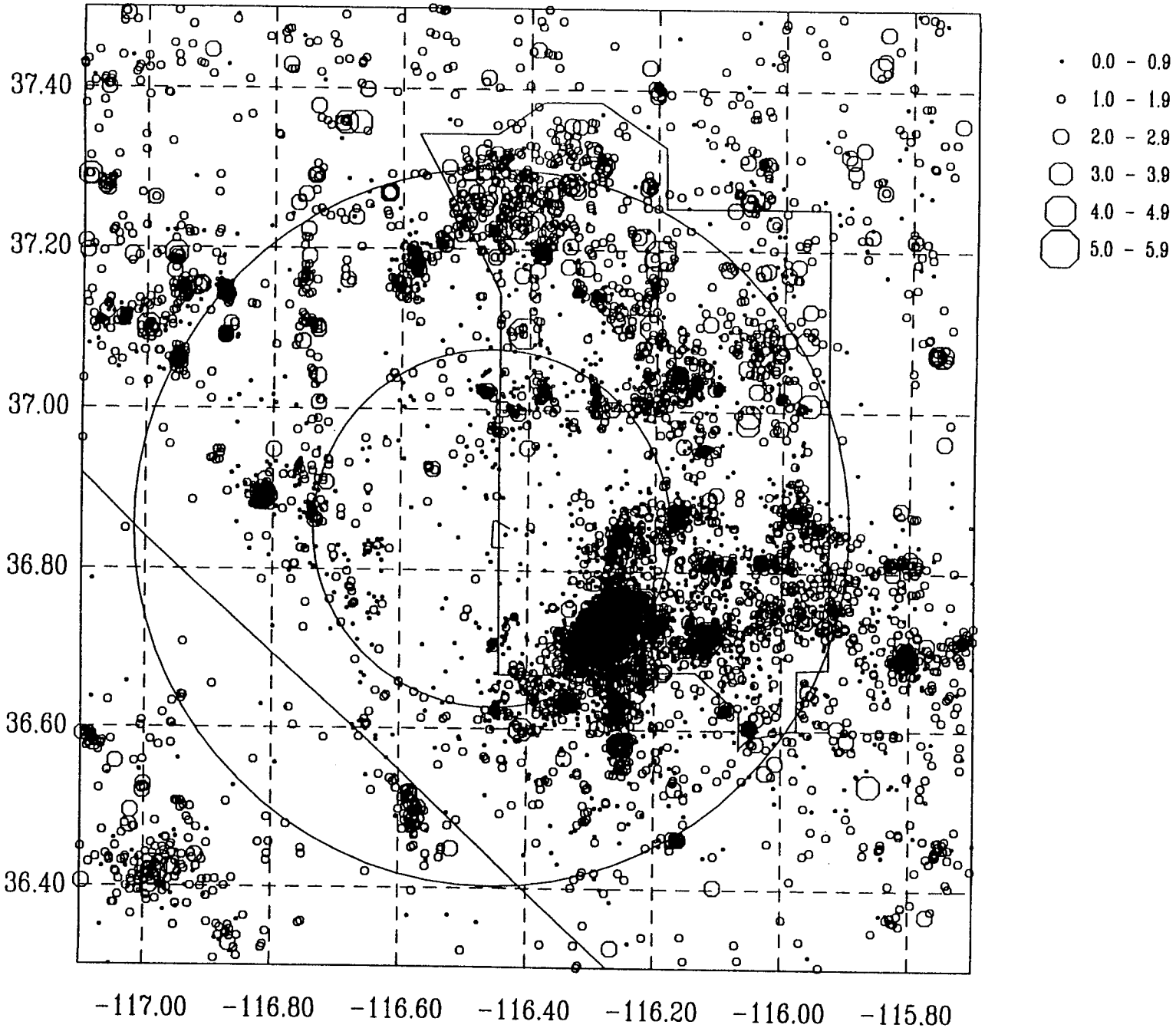

Figure 3-2. Seismicity (1978-1995) of the Yucca Mountain area from the analog SGBSN.

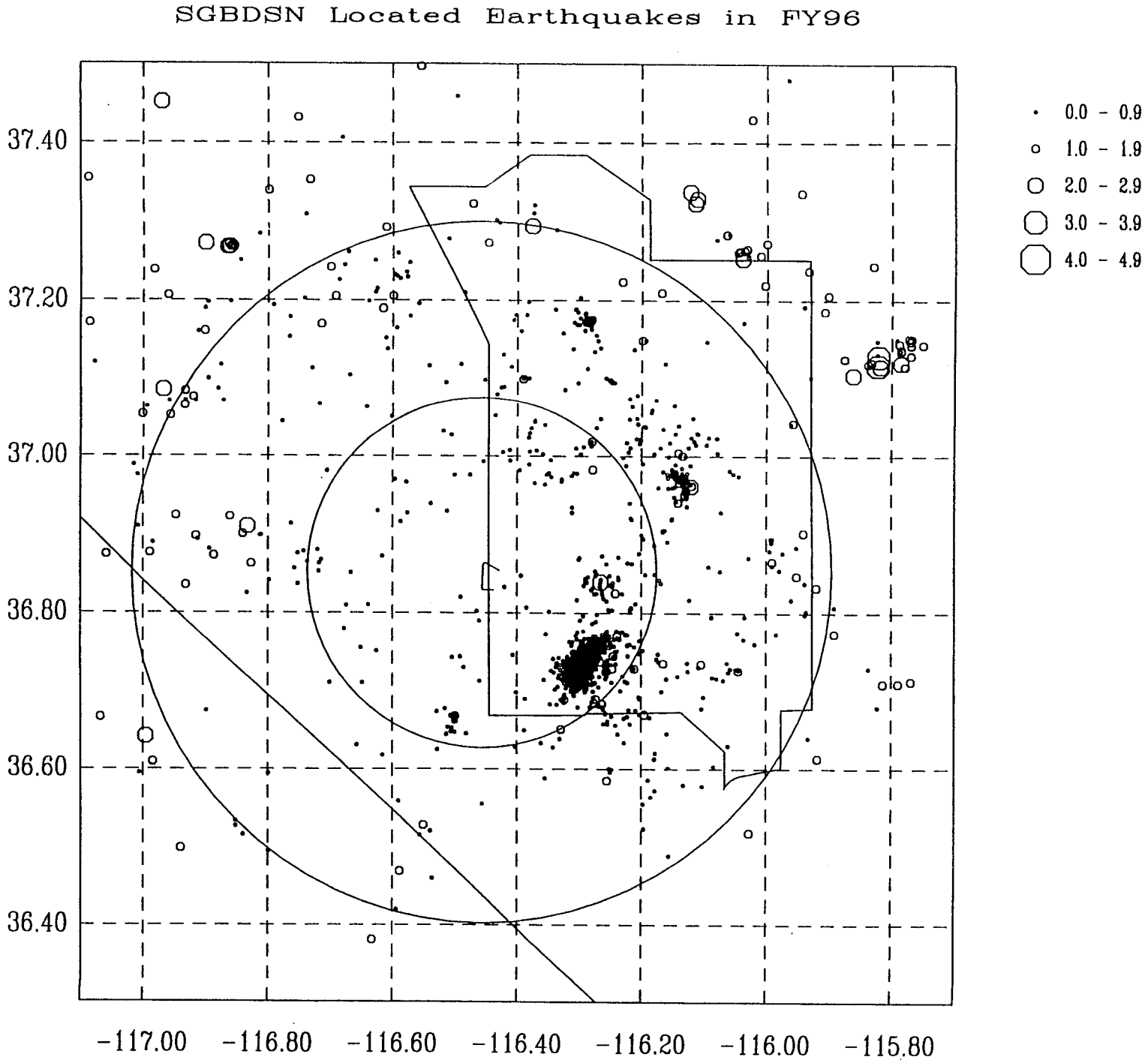

Figure 3-3. Seismicity of the Yucca Mountain area from the digital SGBDSN in FY96.

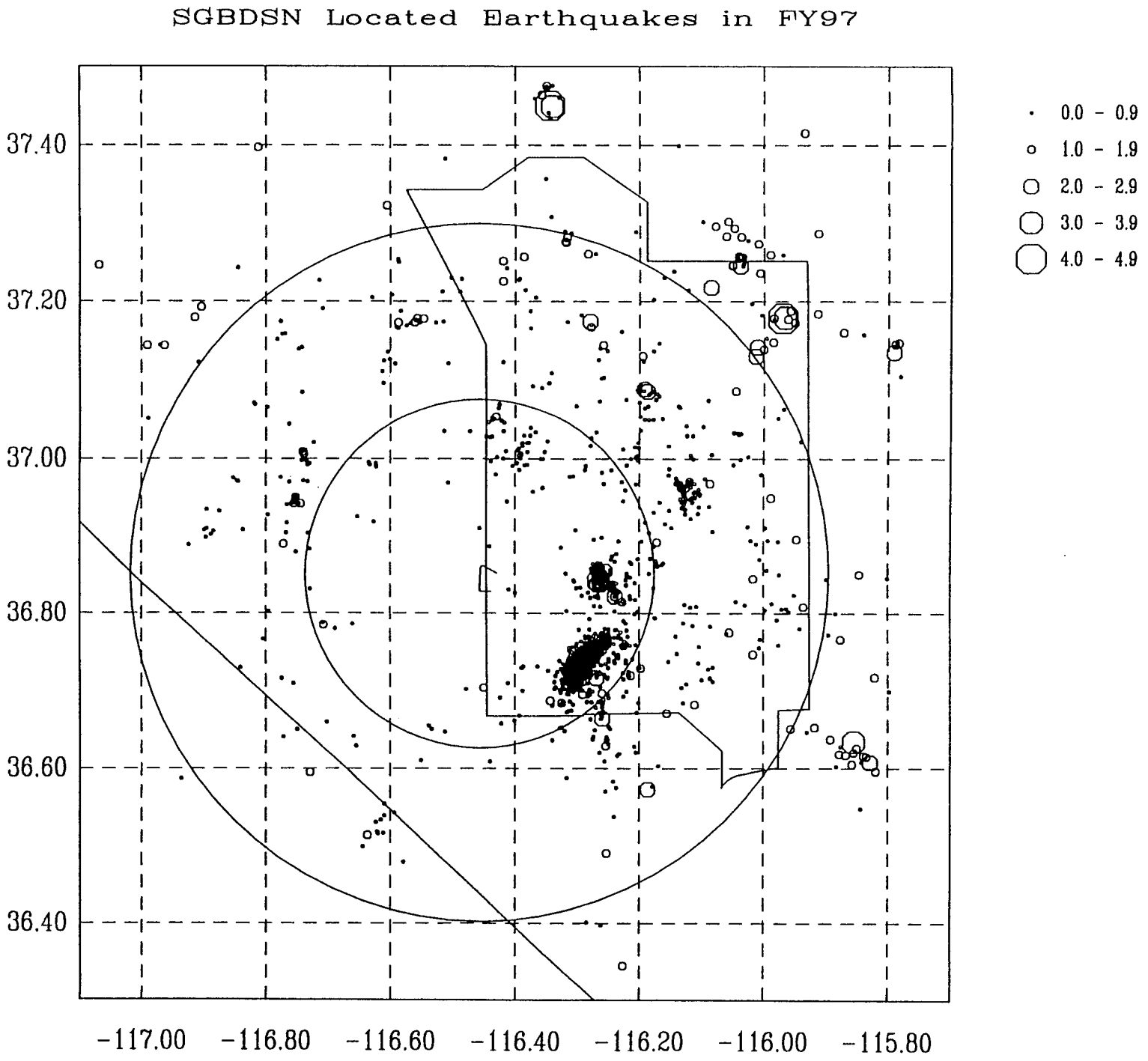

Figure 3-4. Seismicity of the Yucca Mountain area from the digital SGBDSN in FY97.

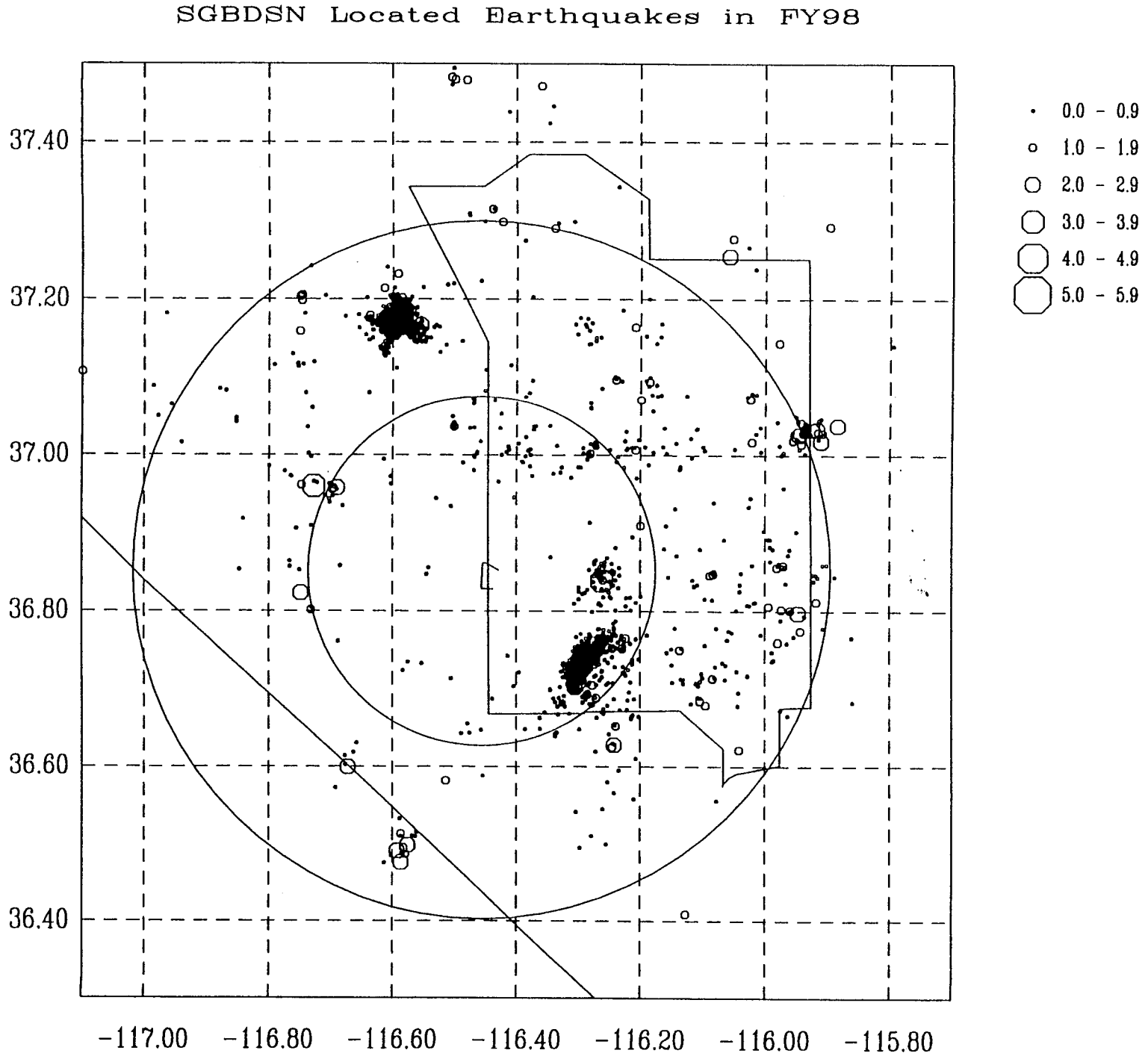

Figure 3-5. Seismicity of the Yucca Mountain area from the digital SGBDSN in FY98.

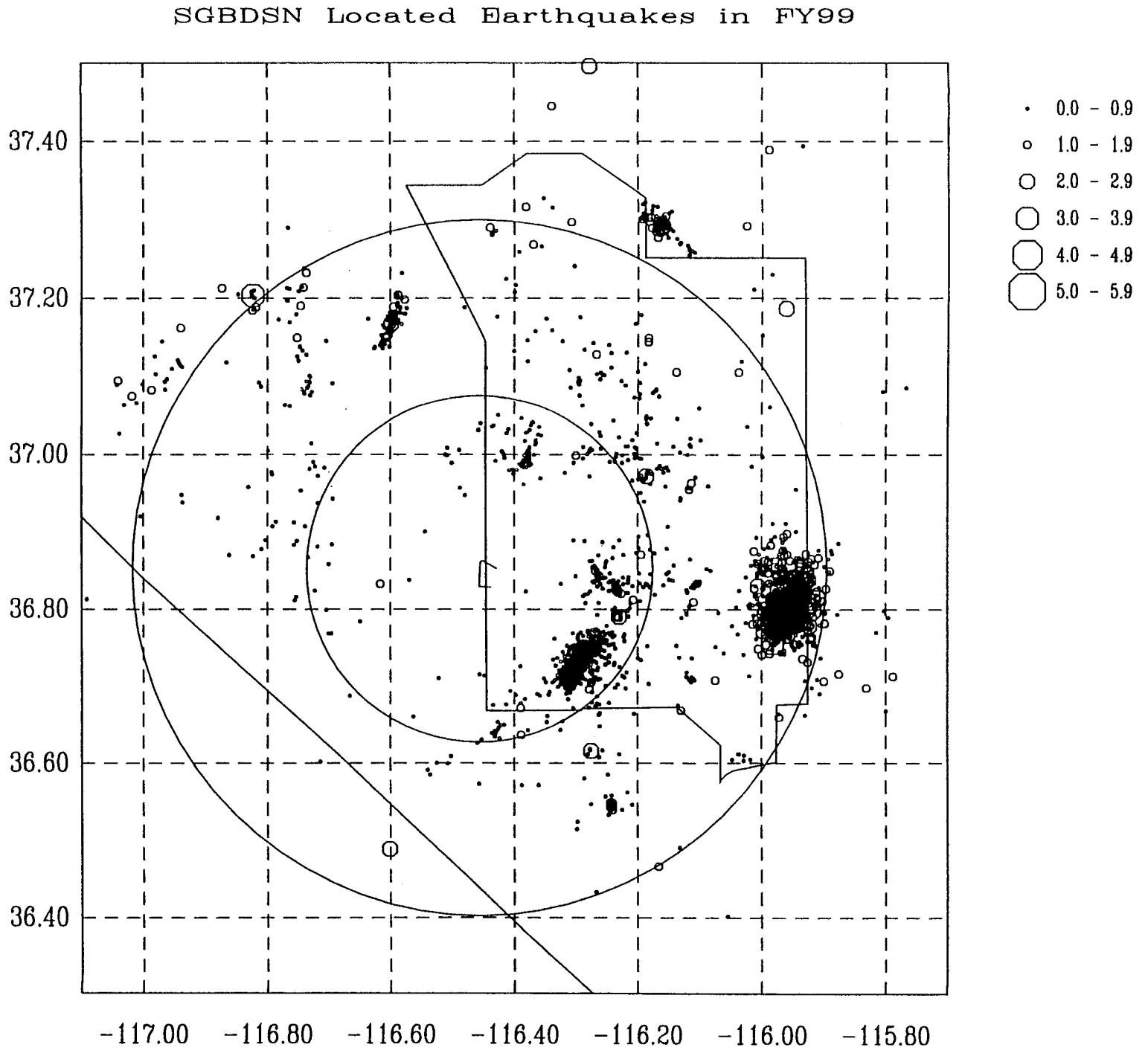

Figure 3-6. Seismicity of the Yucca Mountain area from the digital SGBDSN in FY99.

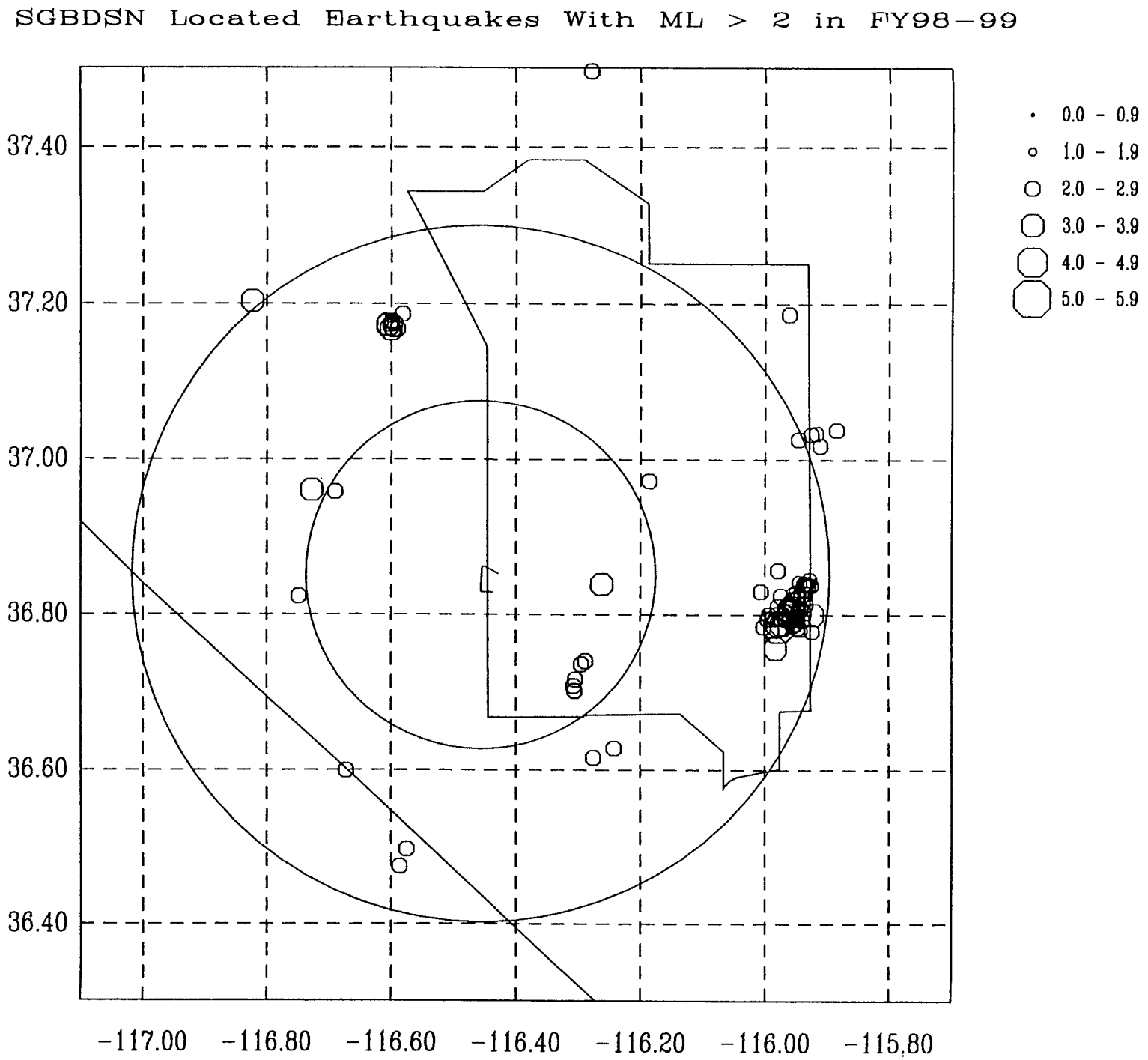

Figure 3-7. Earthquakes with $M_L > 2$ in FY98-99.

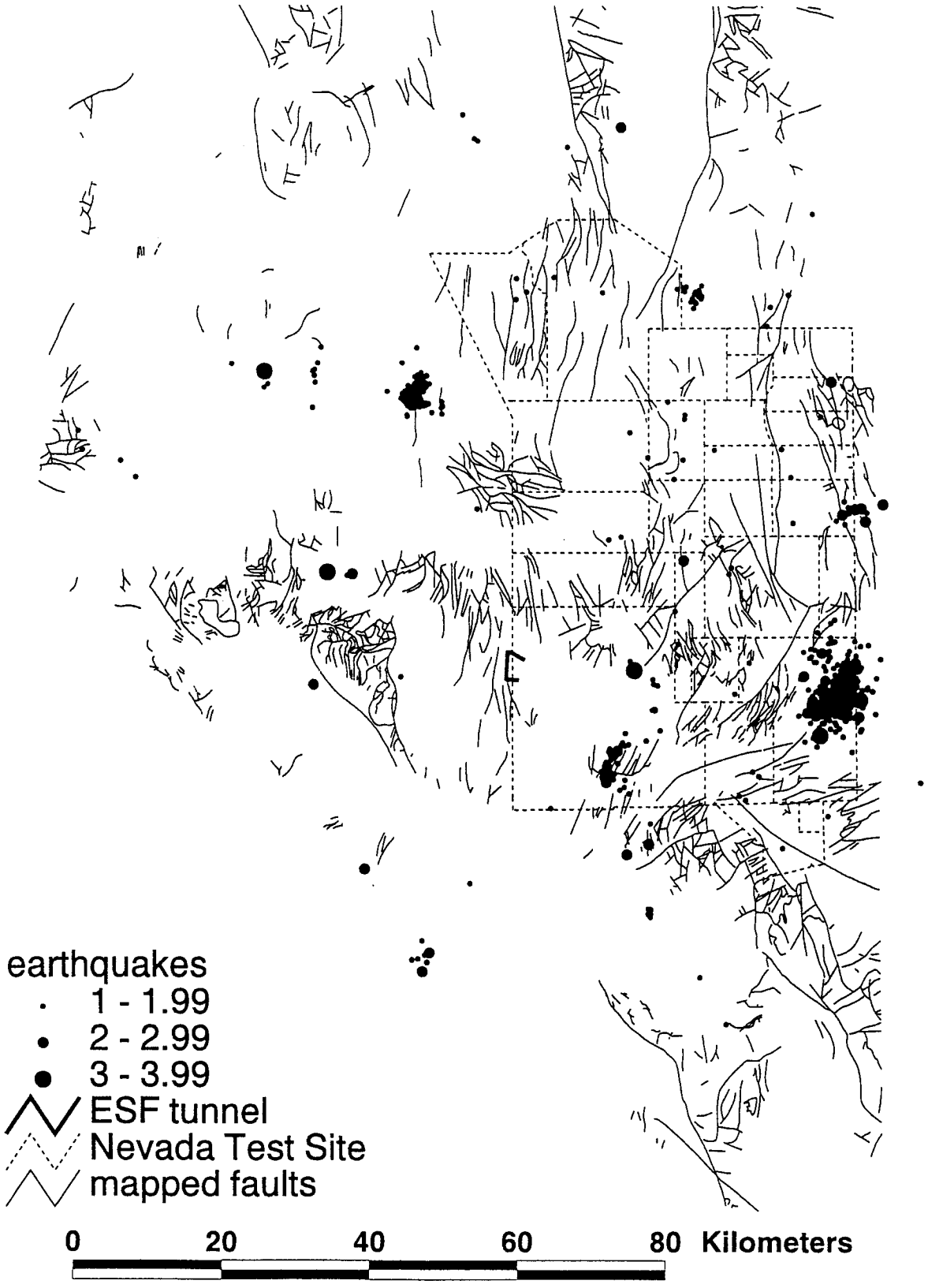

Figure 3-8. Seismicity in FY98-99 ($M_L > 1$) superimposed on known faults of the Yucca Mountain area.

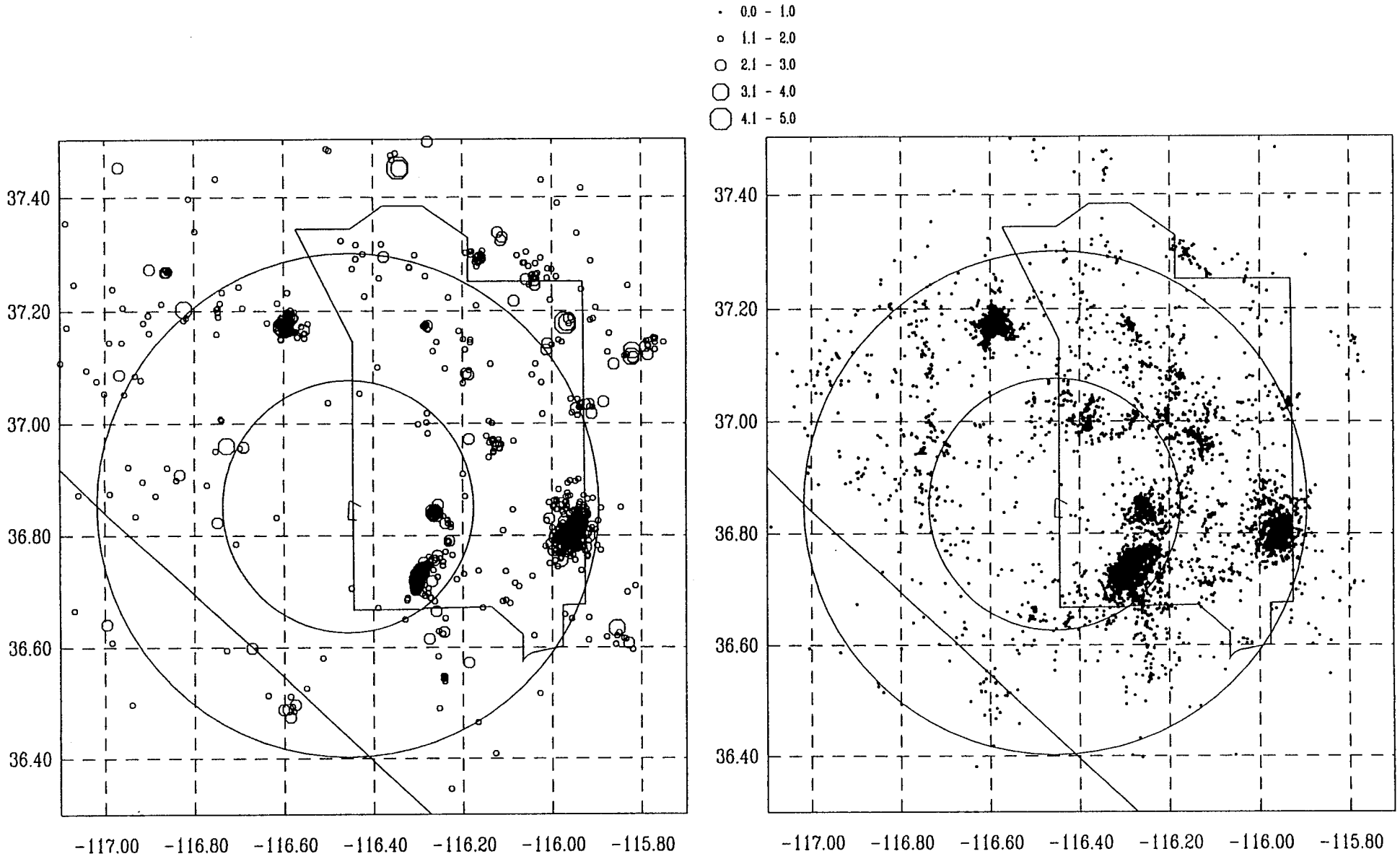

Figure 3-9. Epicenters of the M ≥ 1 (left) and M < 1 (right) earthquakes in the FY96-99 SGBDSN catalog.

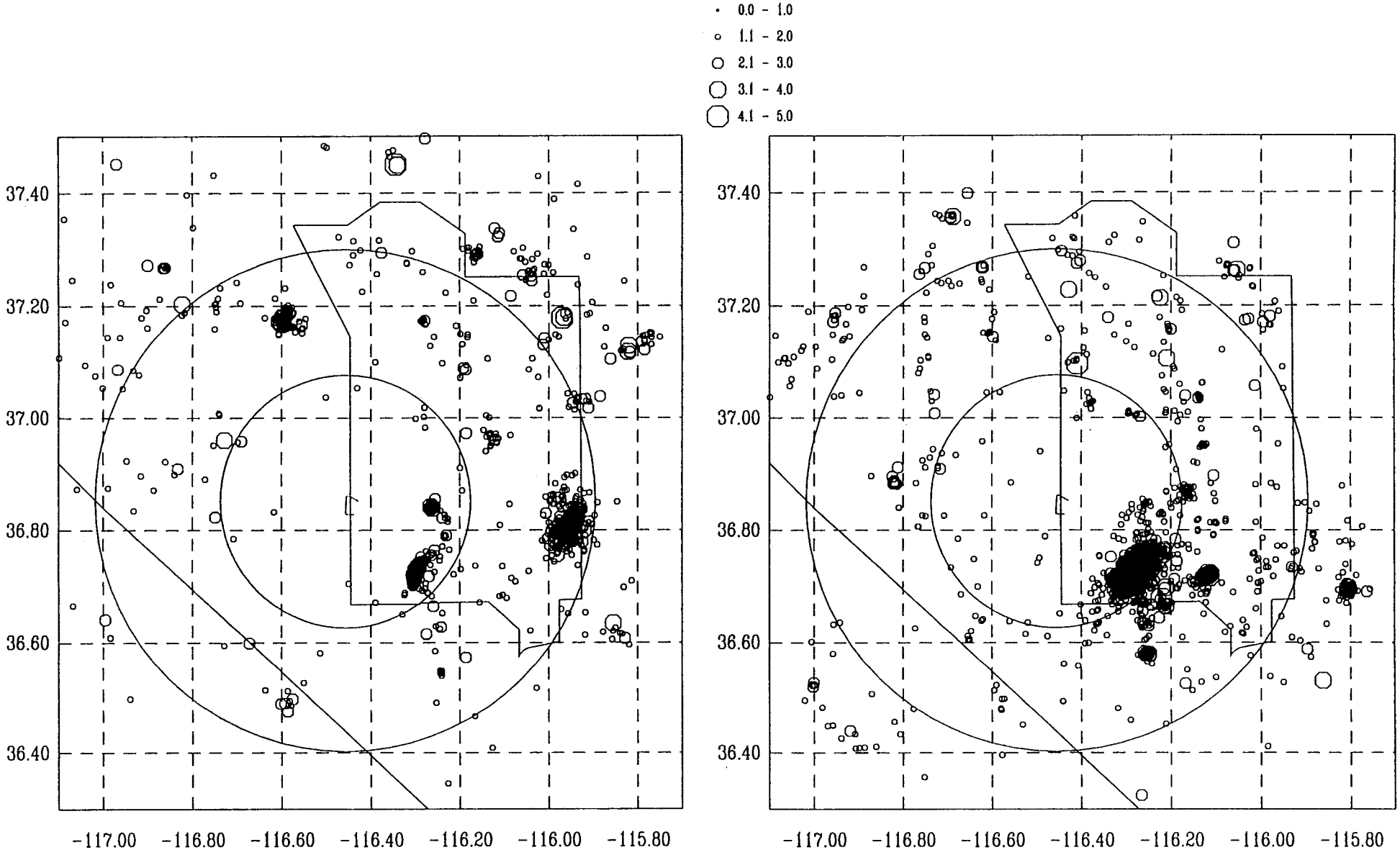

Figure 3-10. Epicenters of M ≥ 1 FY96-99 SGBDSN earthquakes (left) and M ≥ 1 post-LSM SGBSN earthquakes (right).

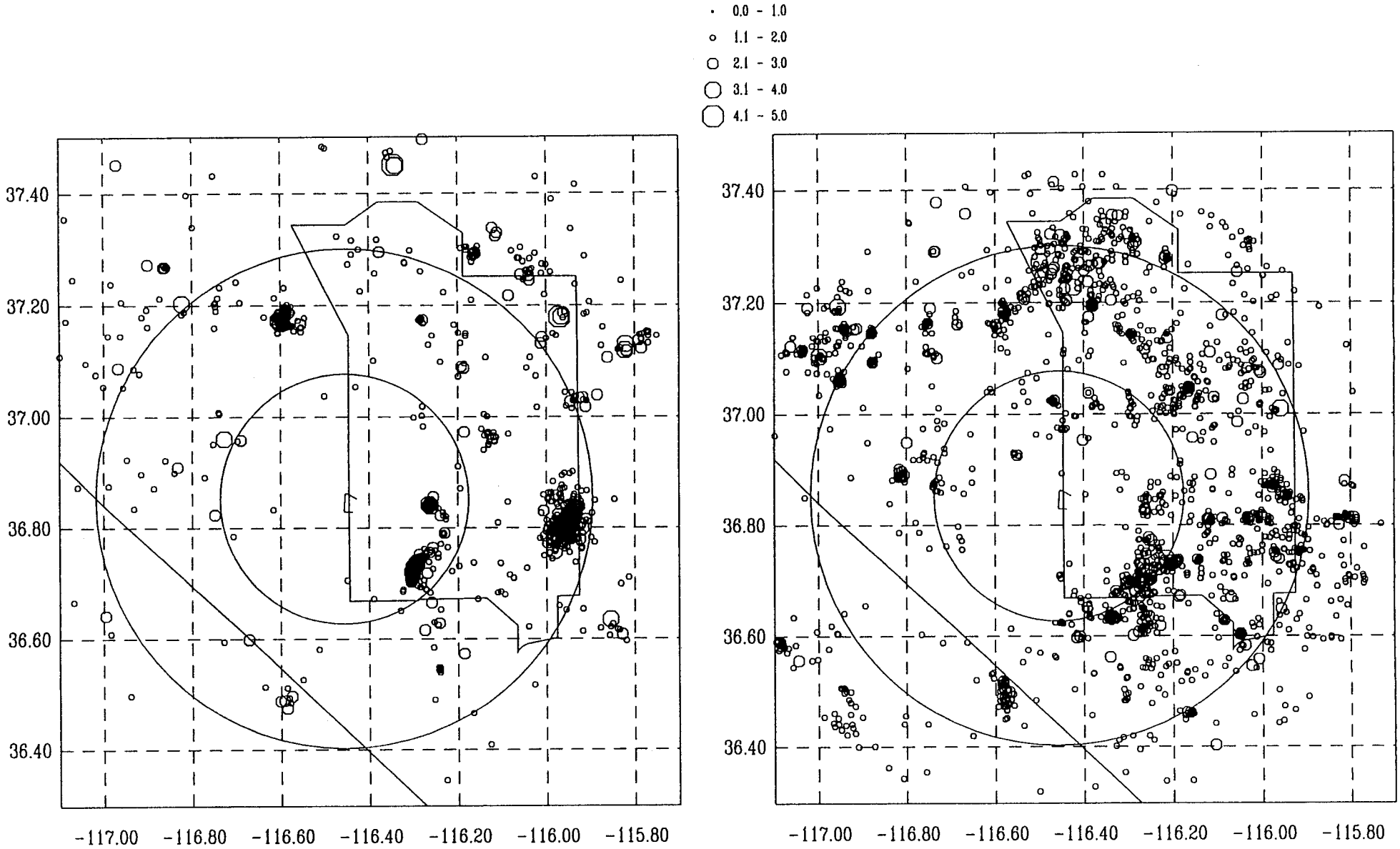

Figure 3-11. Epicenters of M ≥ 1 FY96-99 SGBDSN earthquakes (left) and M ≥ 1 pre-LSM SGBSN earthquakes (right).

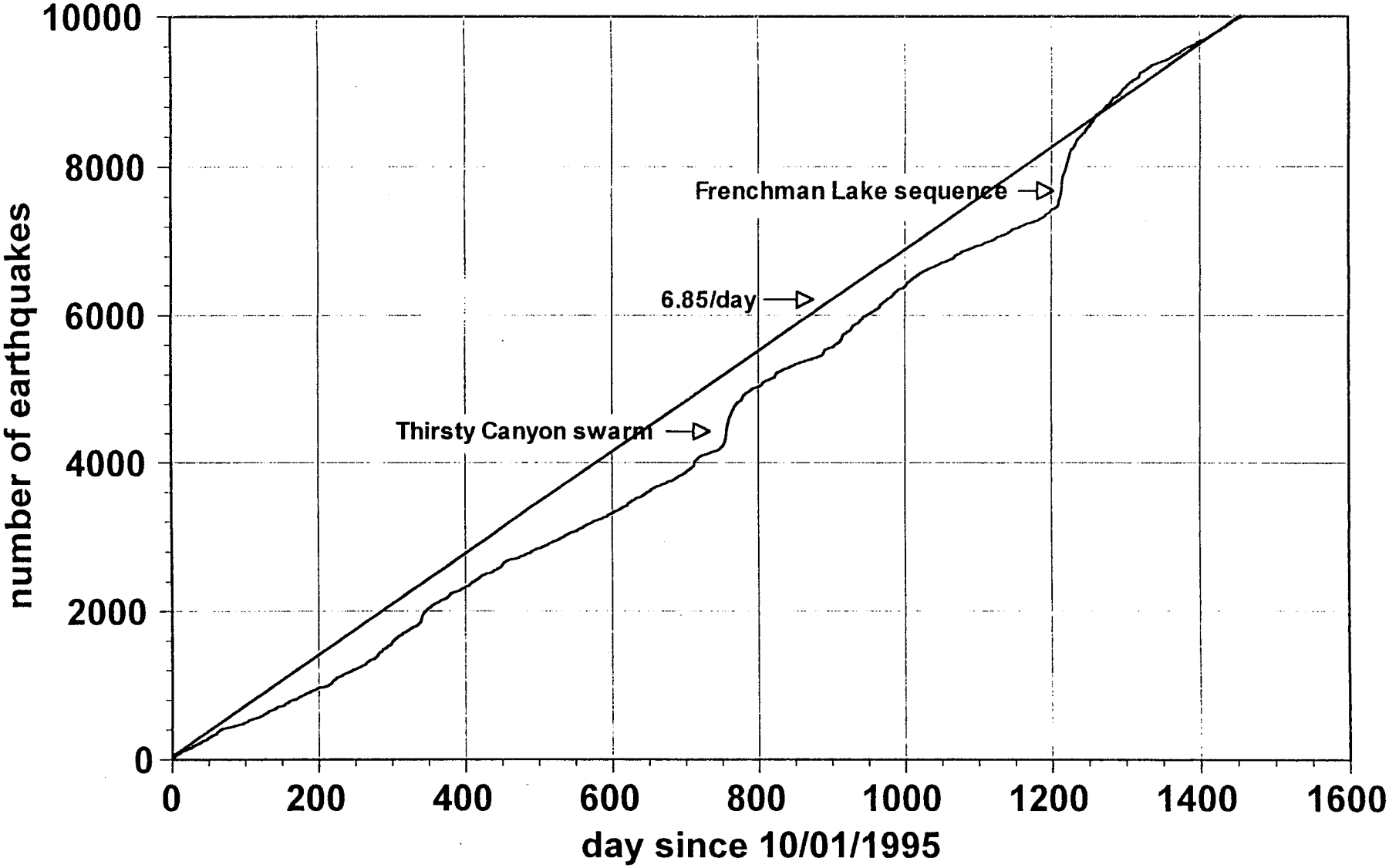

Figure 3-12. Number of reported earthquakes per day from the SGBDSN catalog for FY96-99.

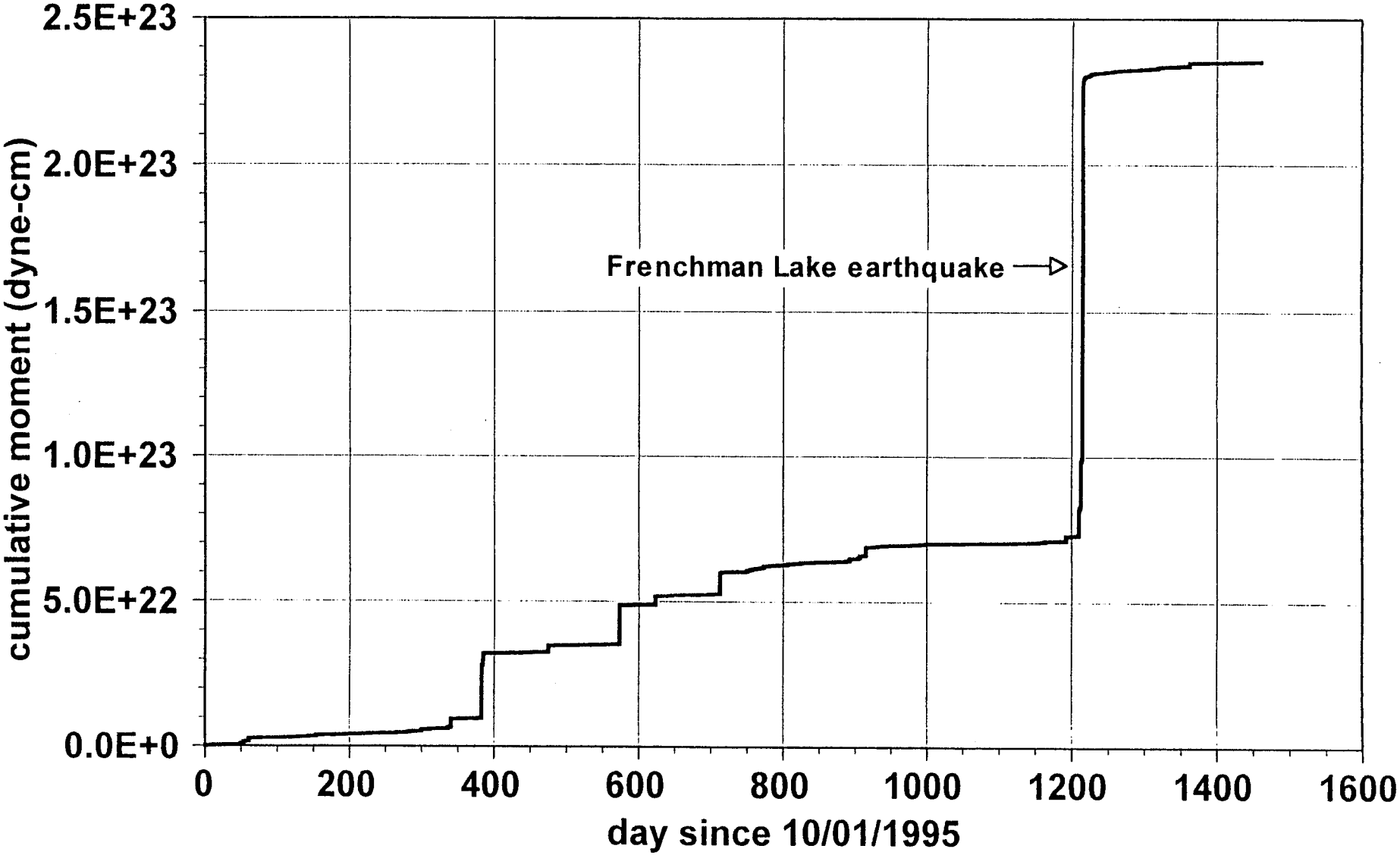

Figure 3-13. Cumulative moment of reported earthquakes from the SGBDSN catalog for FY96-99.

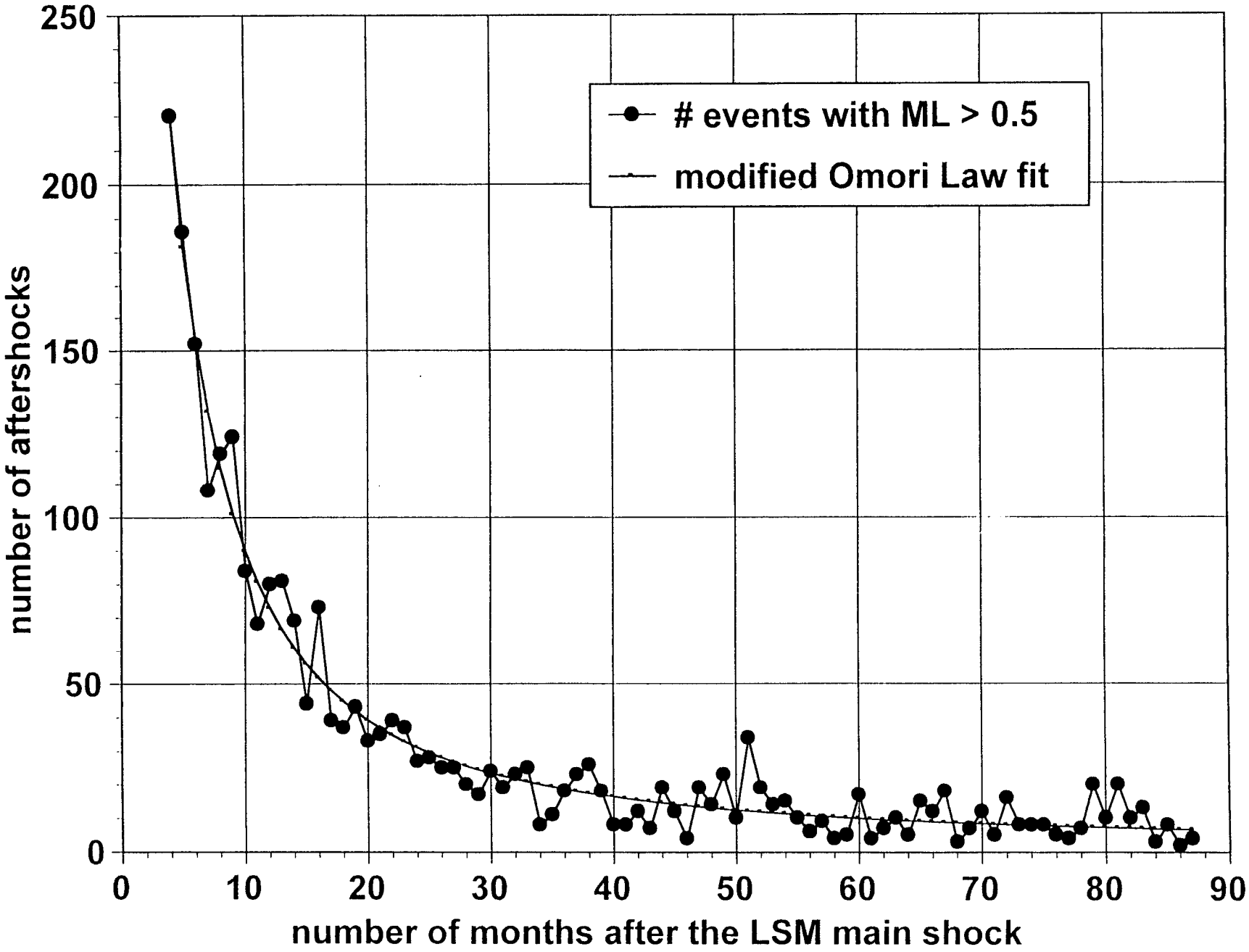

Figure 3-14. Aftershocks per month ($M_L > 0.5$) for the Little Skull Mountain sequence since October 1992.

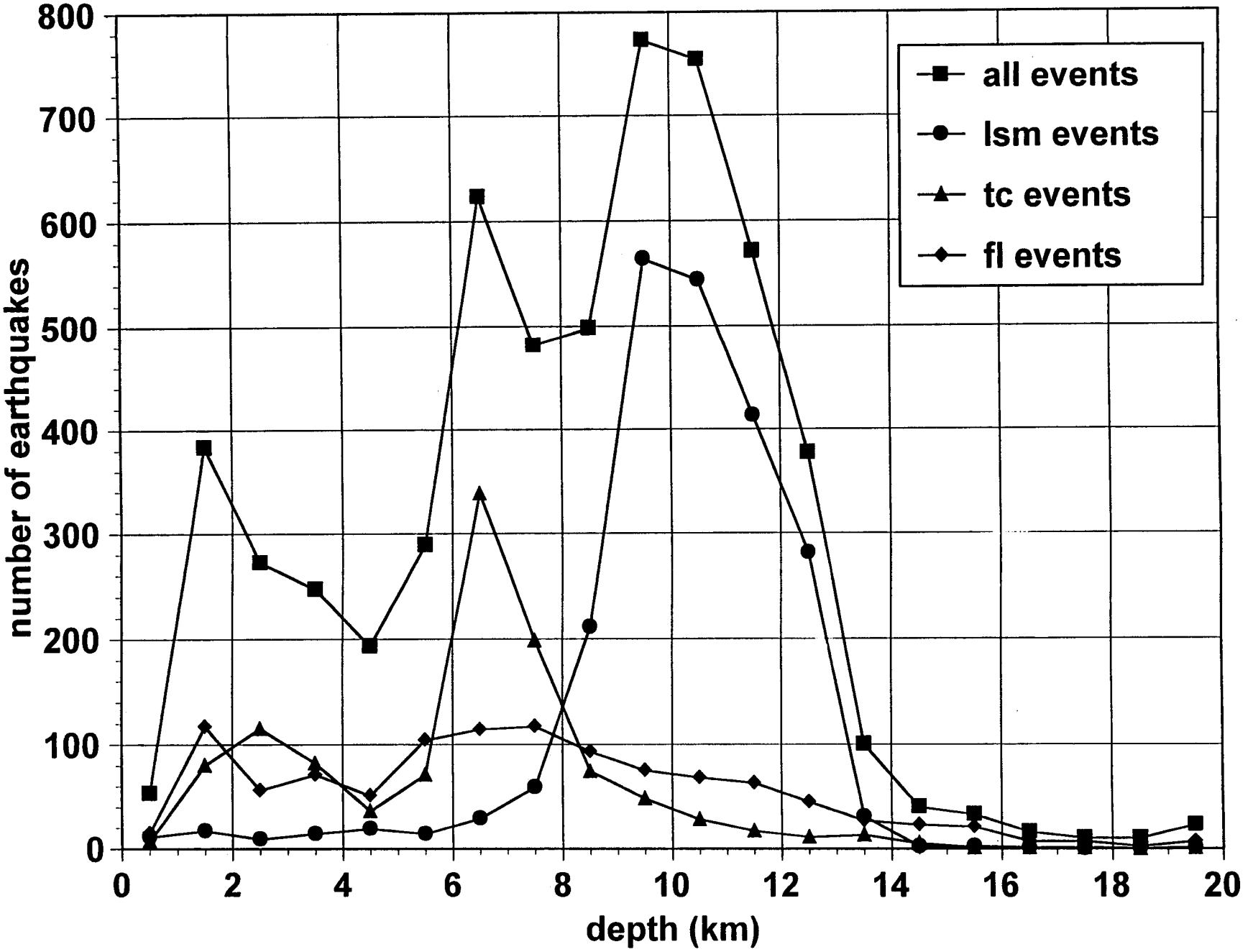

Figure 3-15. Density of reported depths in the FY98-99 SGBDSN catalog. The density has been also computed for 1) "lsm" = Little Skull Mountain, 2) "tc" = Thirsty Canyon, 3) "fl" = Frenchman Lake.

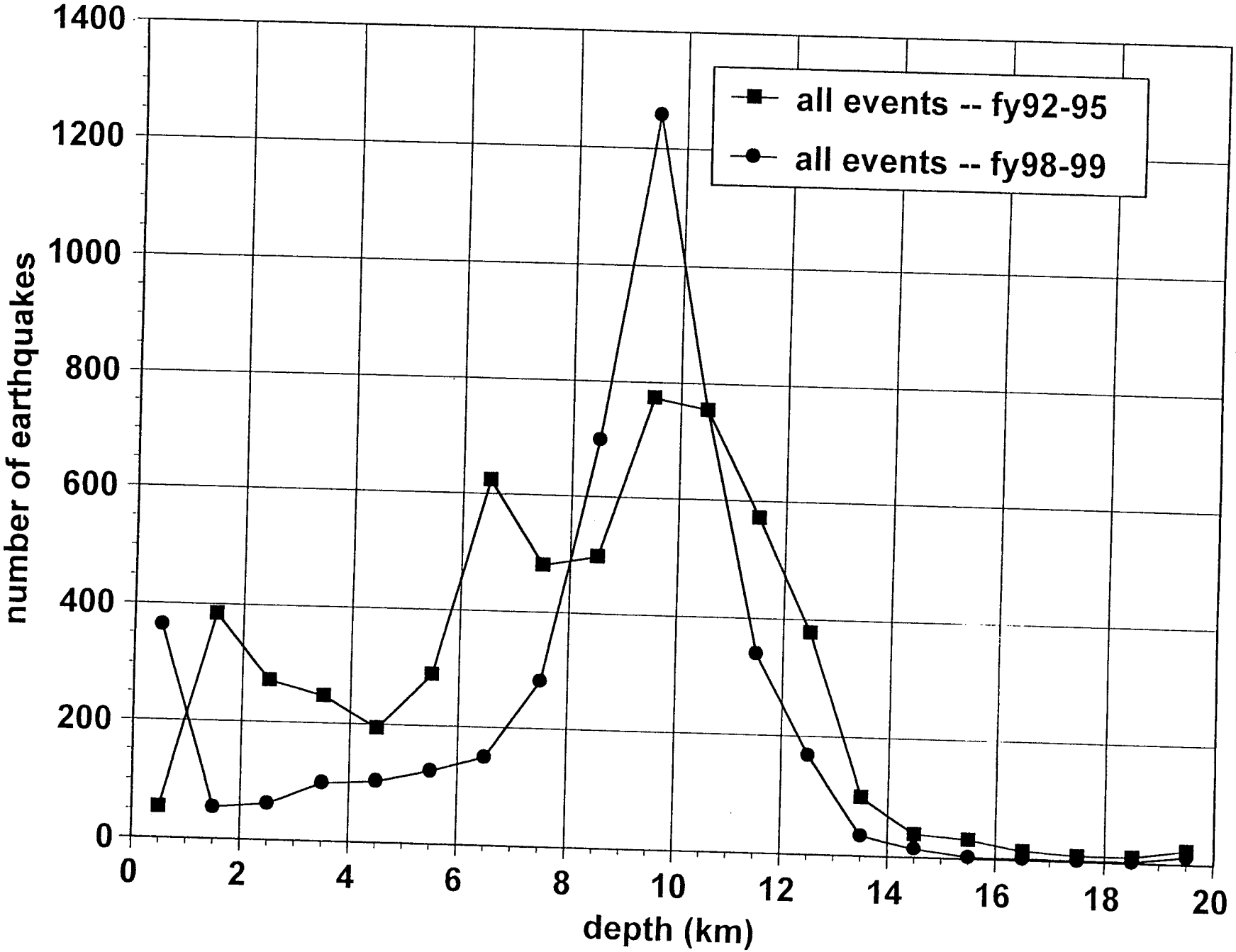

Figure 3-16. Density of reported depths in the FY98-99 SGBDSN catalog in comparison with that for the FY92-95 analog SGBSN catalog.

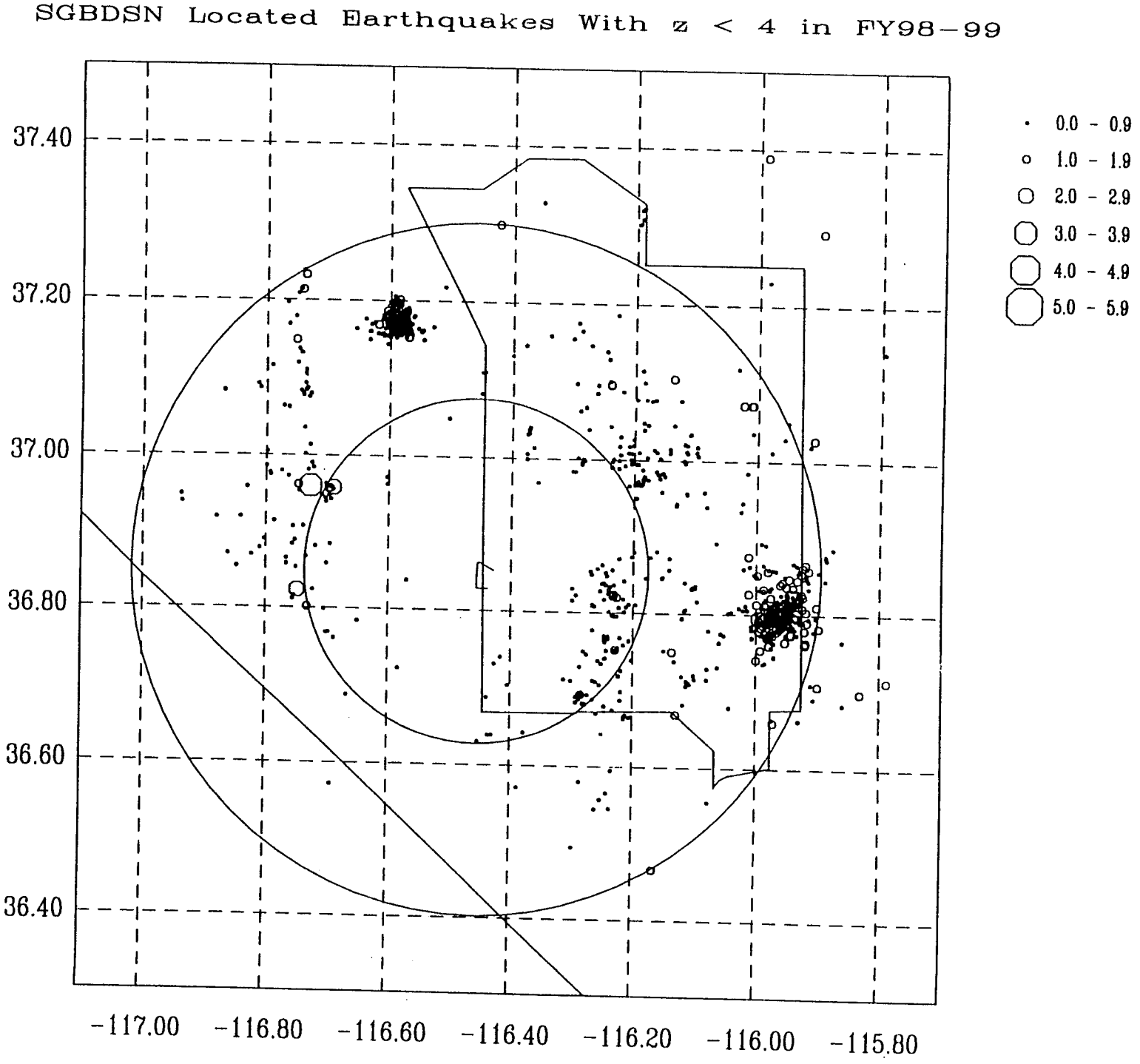

Figure 3-17. Shallow (z < 4 km) earthquakes reported in the FY98-99 SGBDSN catalog.

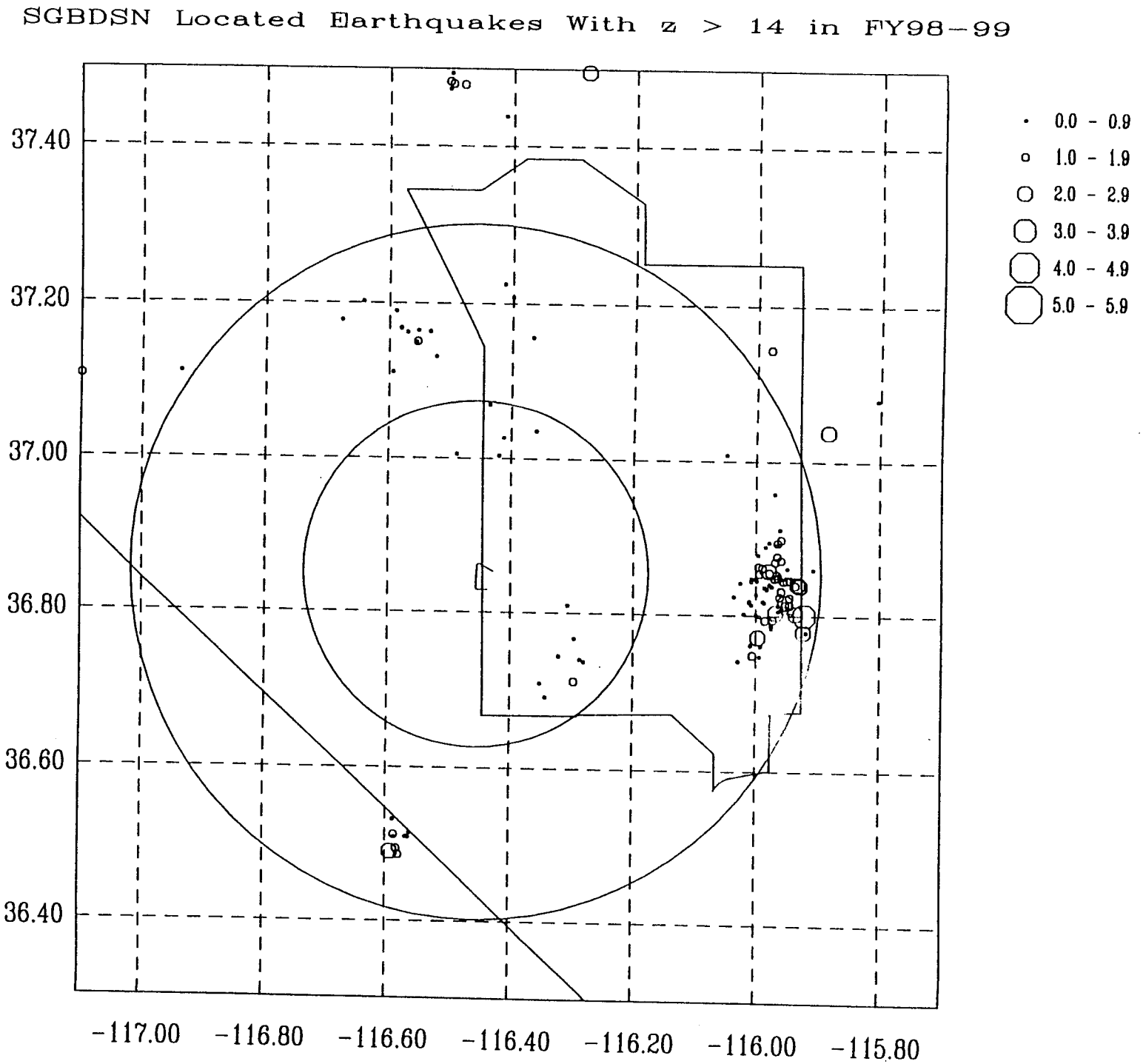

Figure 3-18. Deep (z > 14 km) earthquakes reported in the FY98-99 SGBDSN catalog.

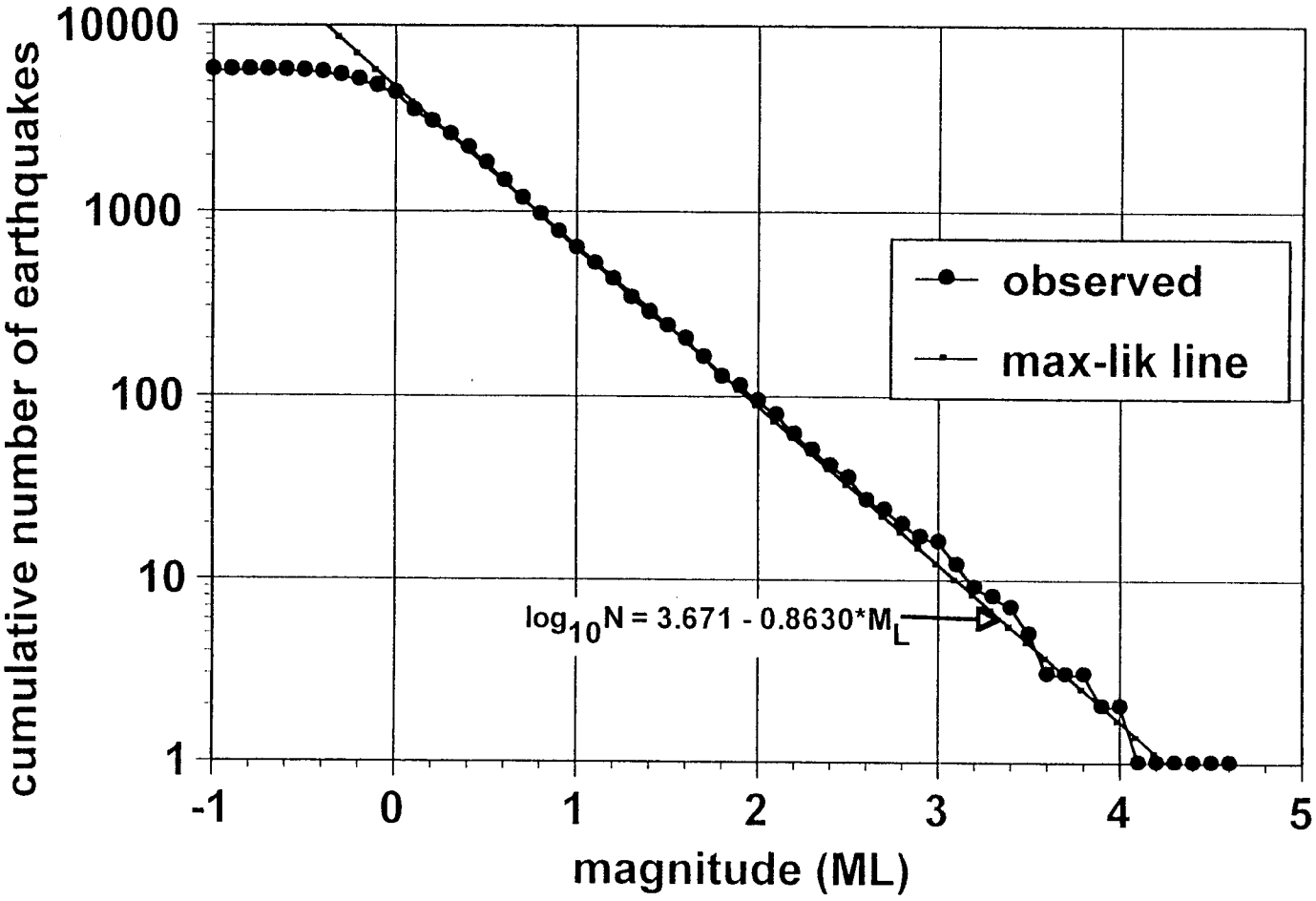

Figure 3-19. Recurrence curve for the FY98-99 SGBDSN catalog. The line is a maximum-likelihood fit according to Aki (1965).

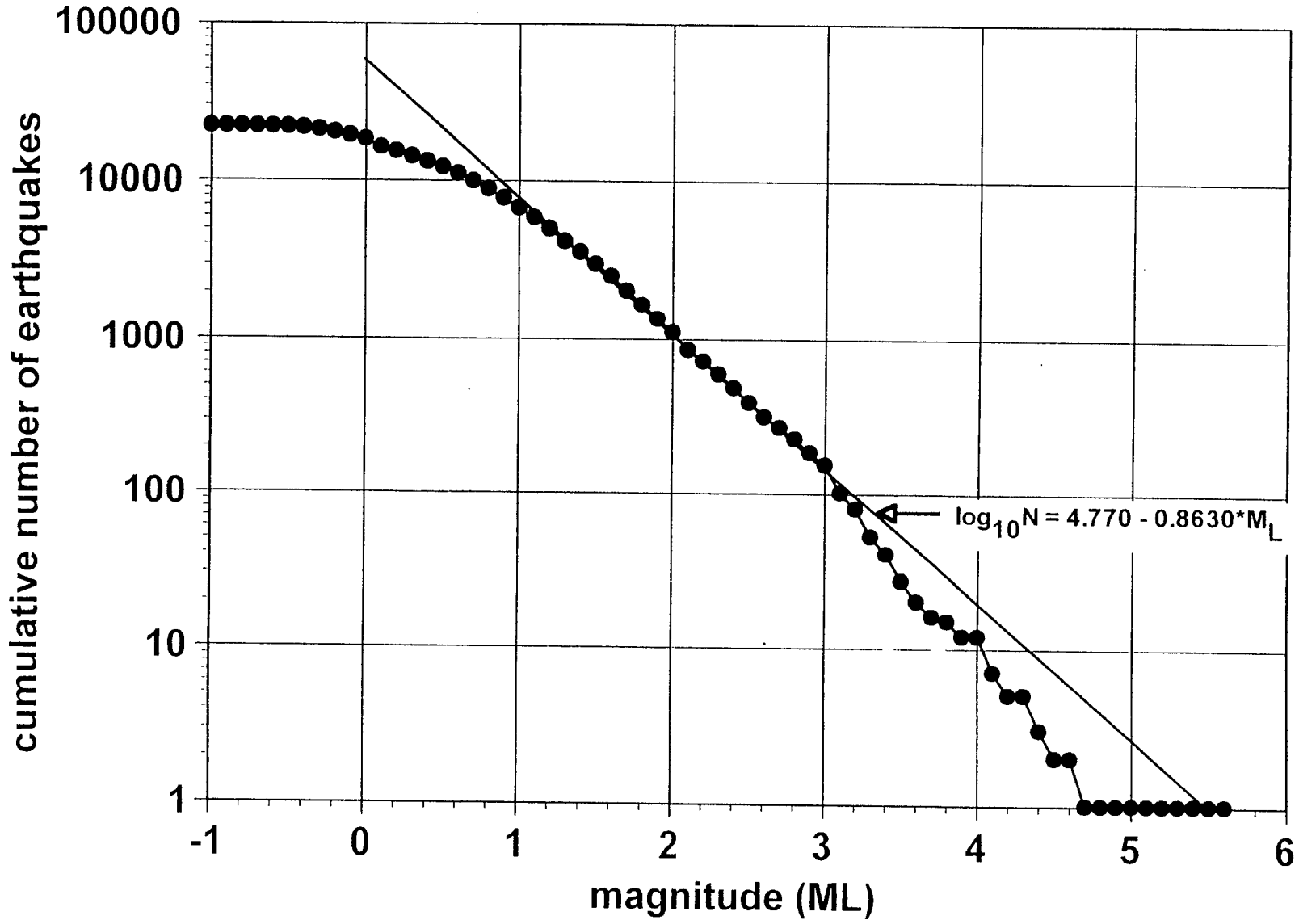

Figure 3-20. Recurrence curve for the 1978-1995 analog SGBSN catalog. The line is identical to that in Figure 3-16, except of a change in the intercept.

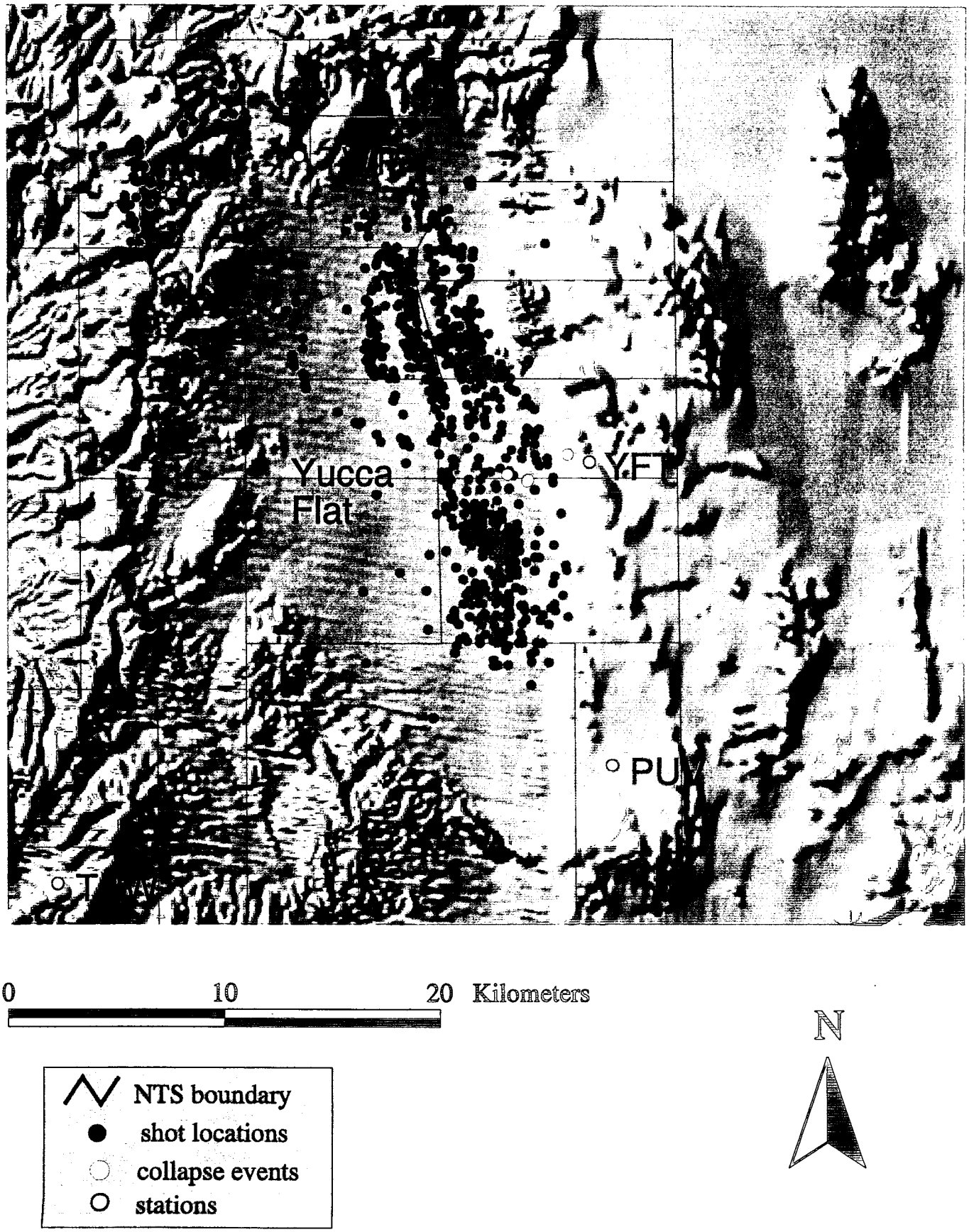

Figure 5-1. Location of presumed collapse events on DEM data.

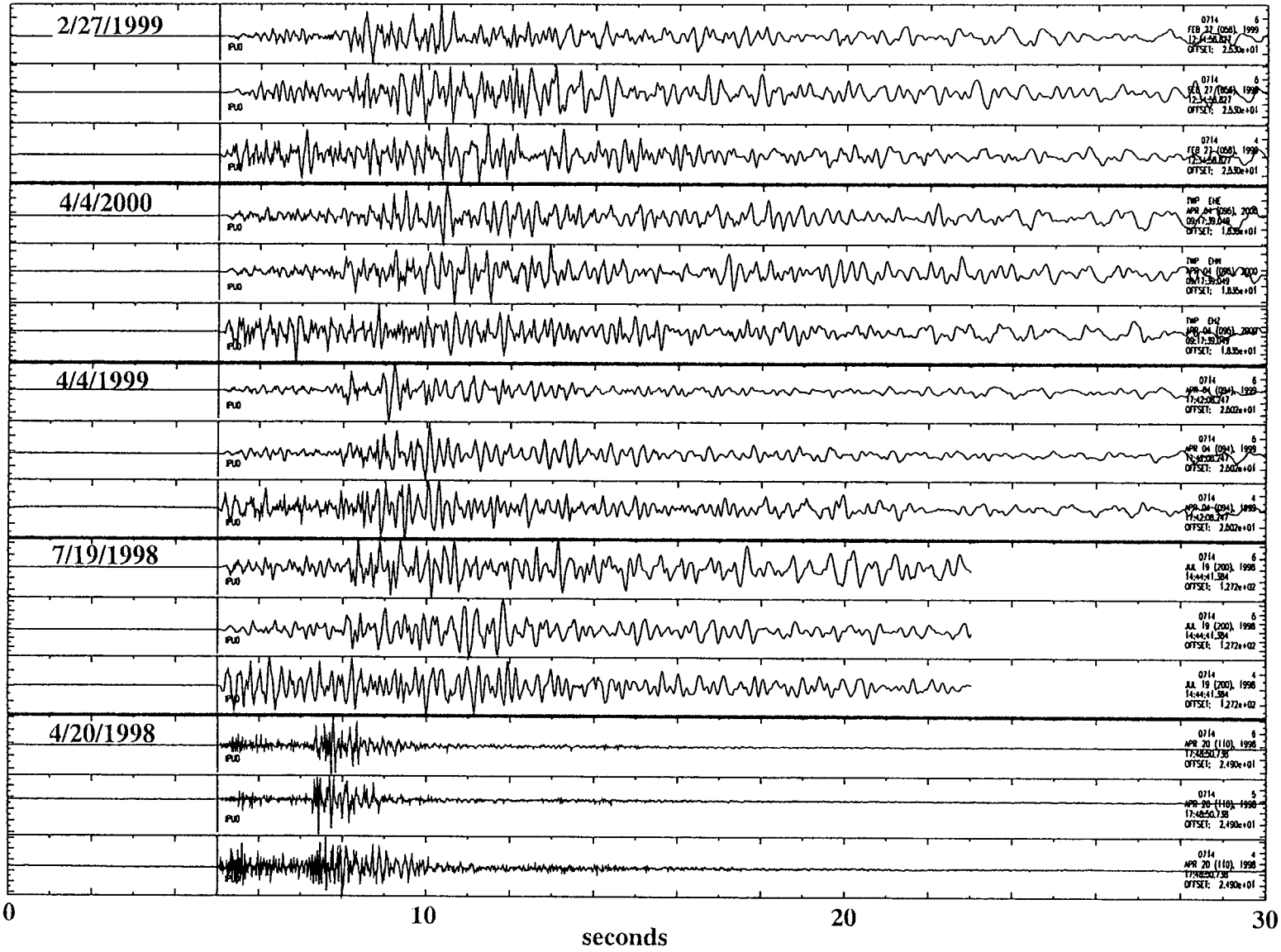

Figure 5-2. TWP recordings. Sequence is E,N,Z from top to bottom for each event.

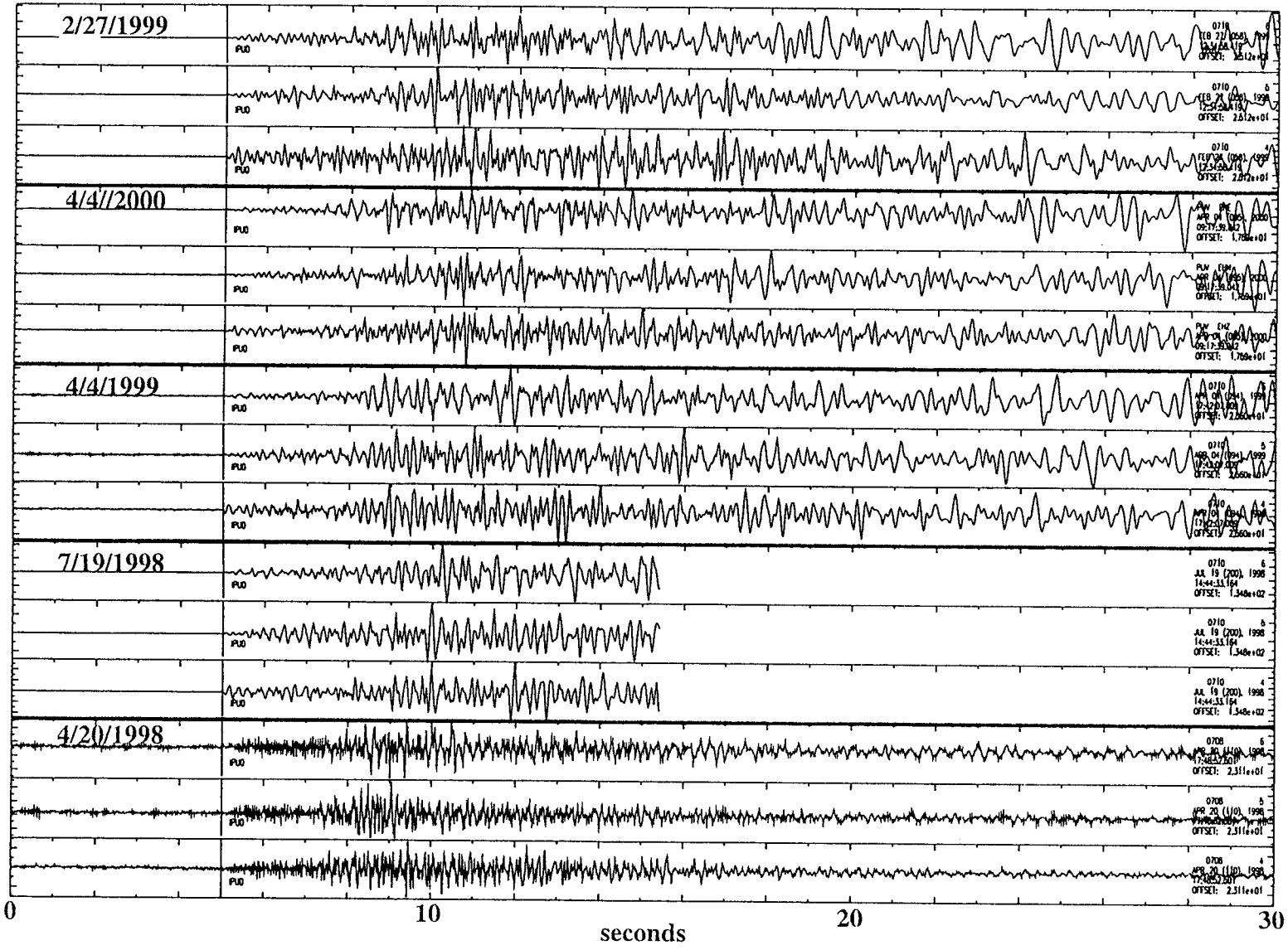

Figure 5-3. PUV recordings. Sequence is E,N,Z from top to bottom for each event.

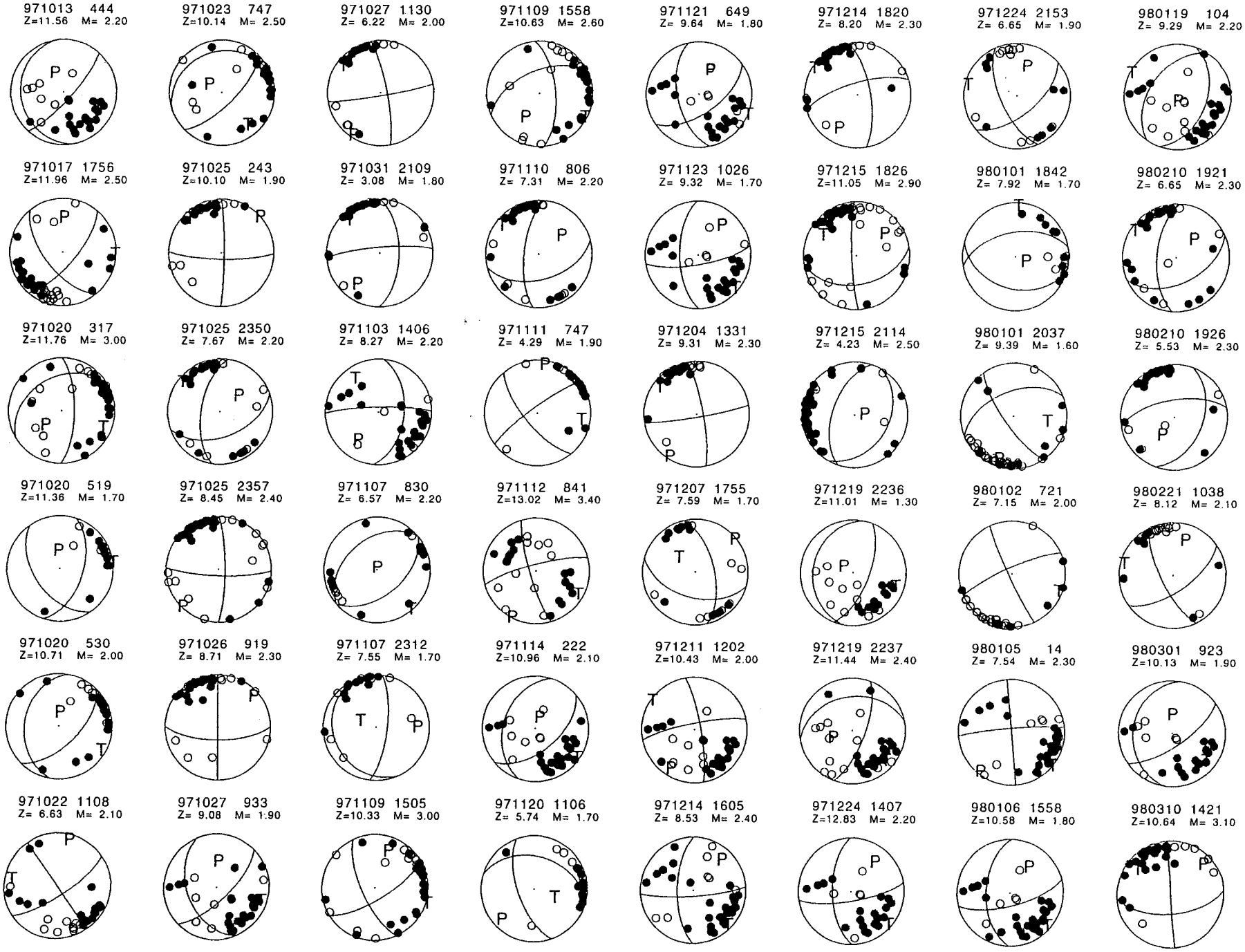

Figure 6-1. Focal mechanisms for selected FY98-99 earthquakes in the SGBDSN catalog.

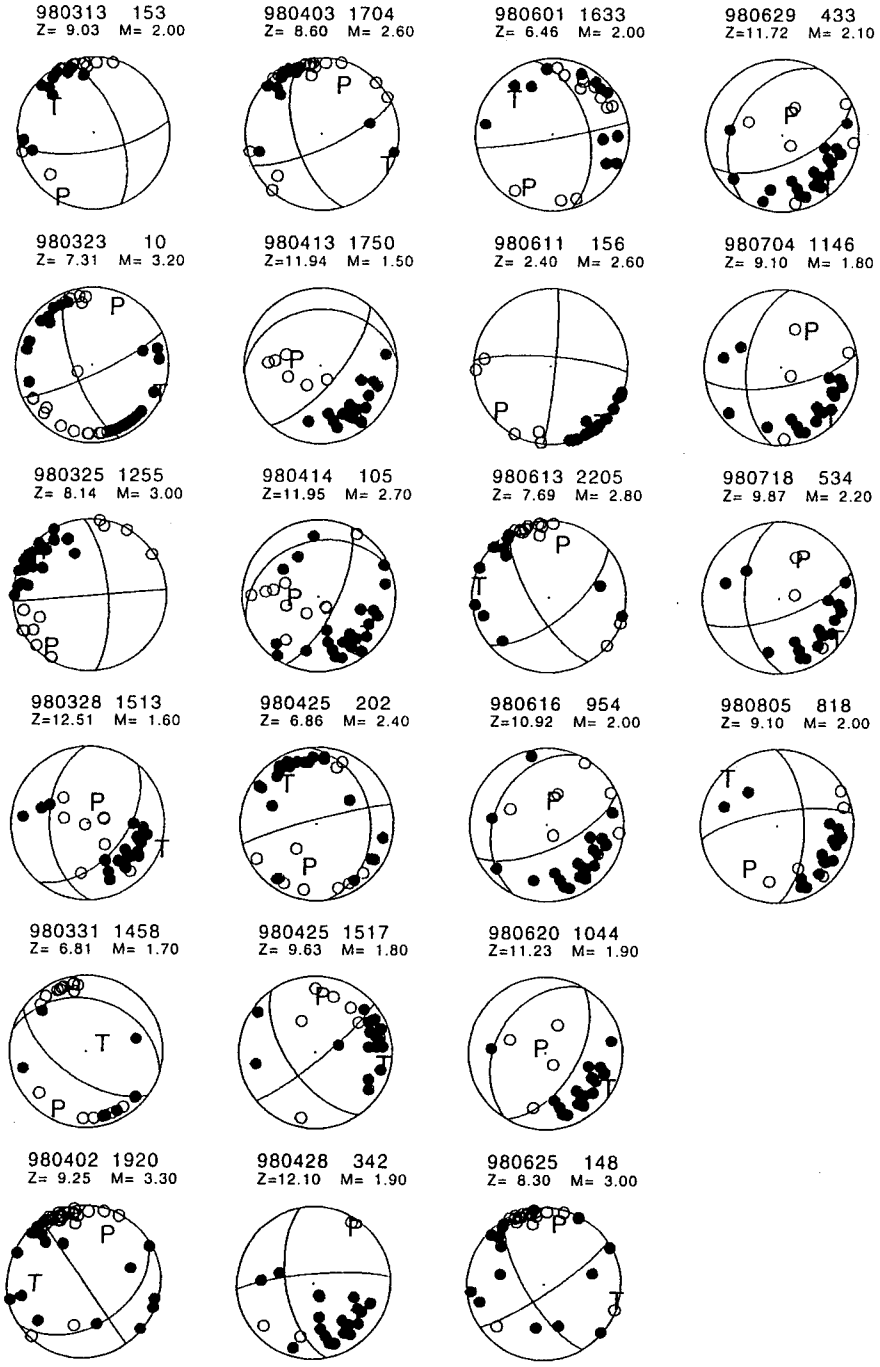

Figure 6-1. Focal mechanisms for selected FY98-99 earthquakes in the SGBDSN catalog.

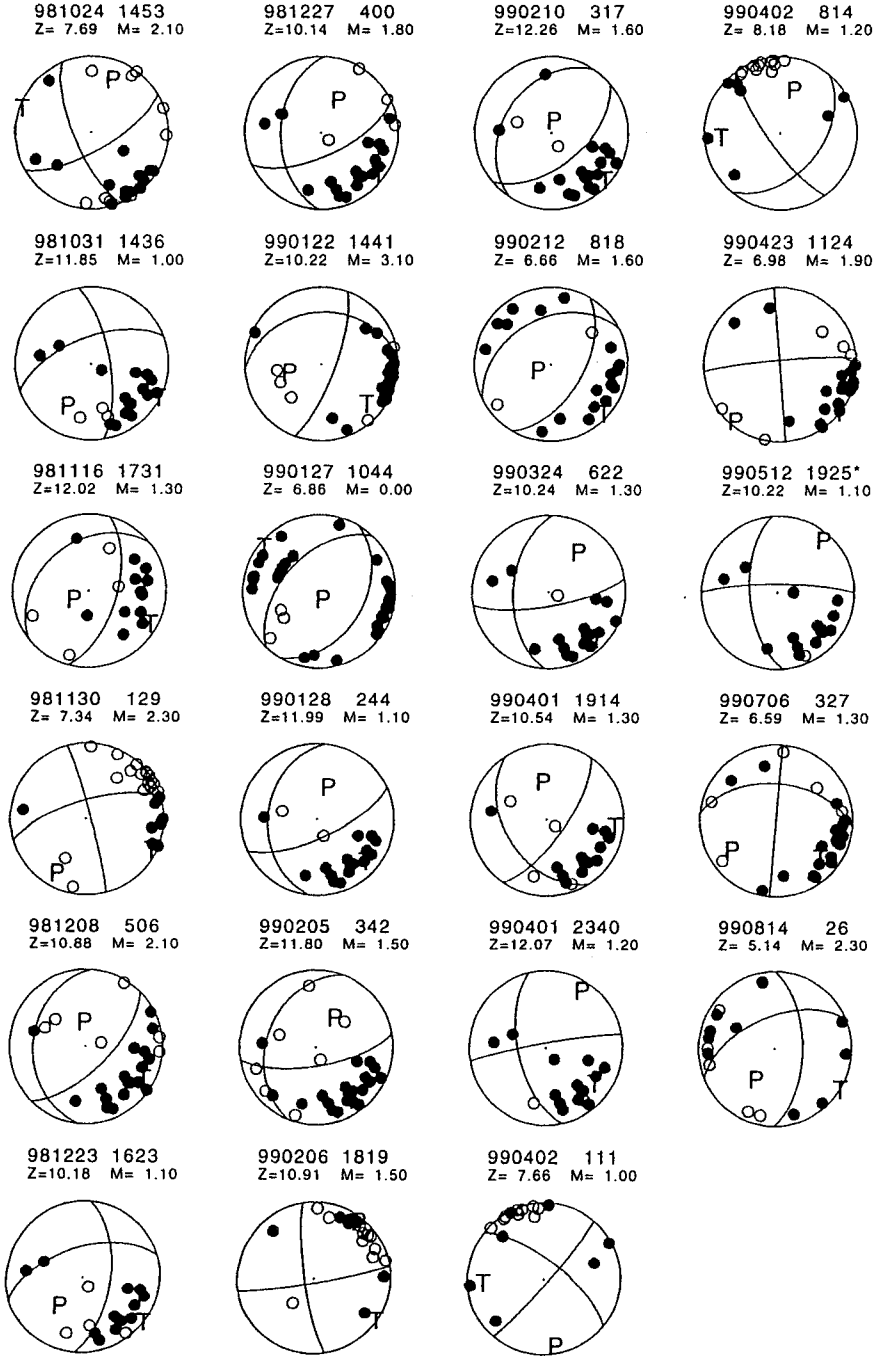

Figure 6-1. Focal mechanisms for selected FY98-99 earthquakes in the SGBDSN catalog.

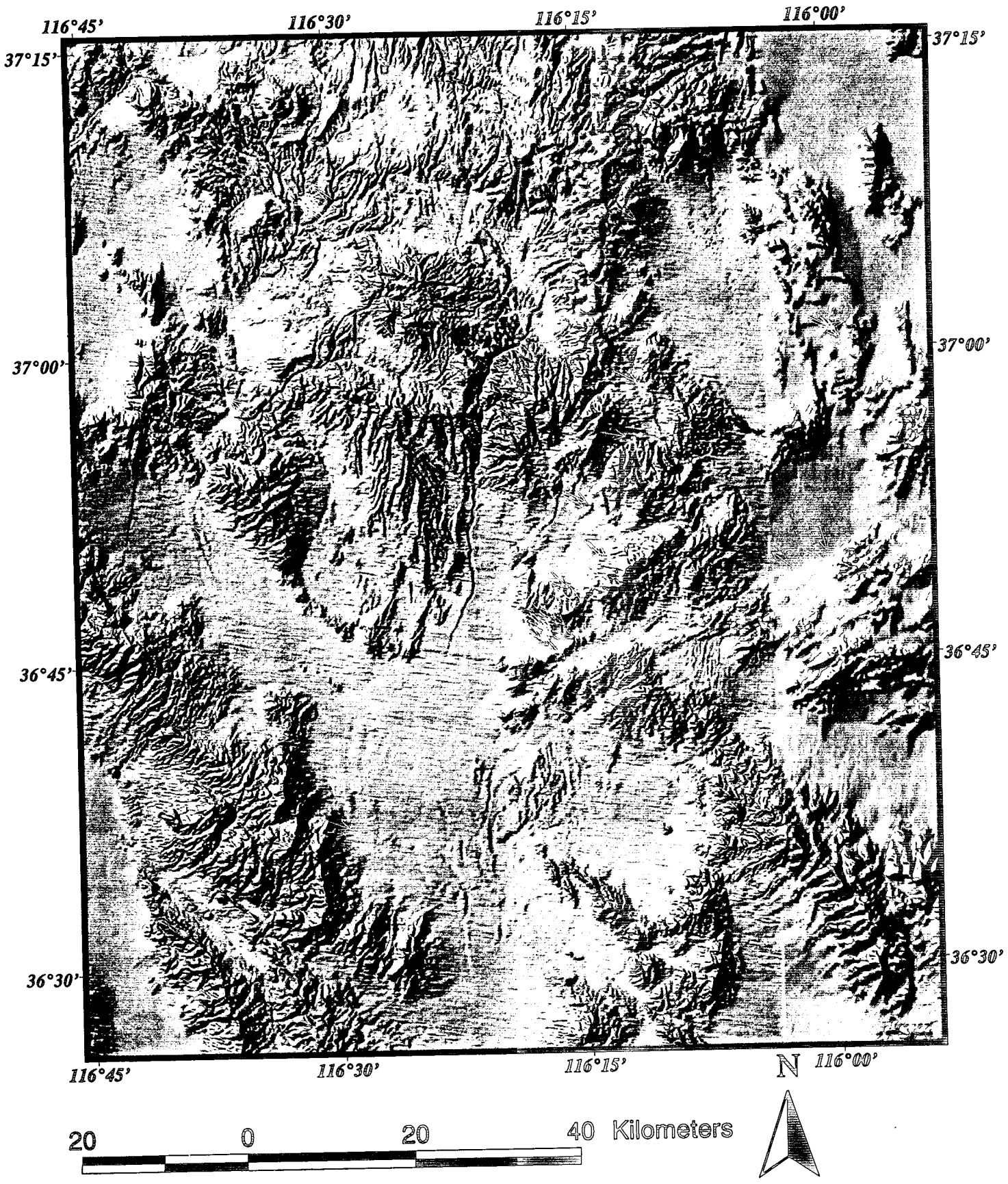

Figure 6-2. Tension axes of the focal mechanisms of Table 6-1, projected to the horizontal plane and plotted at the earthquake epicenter.

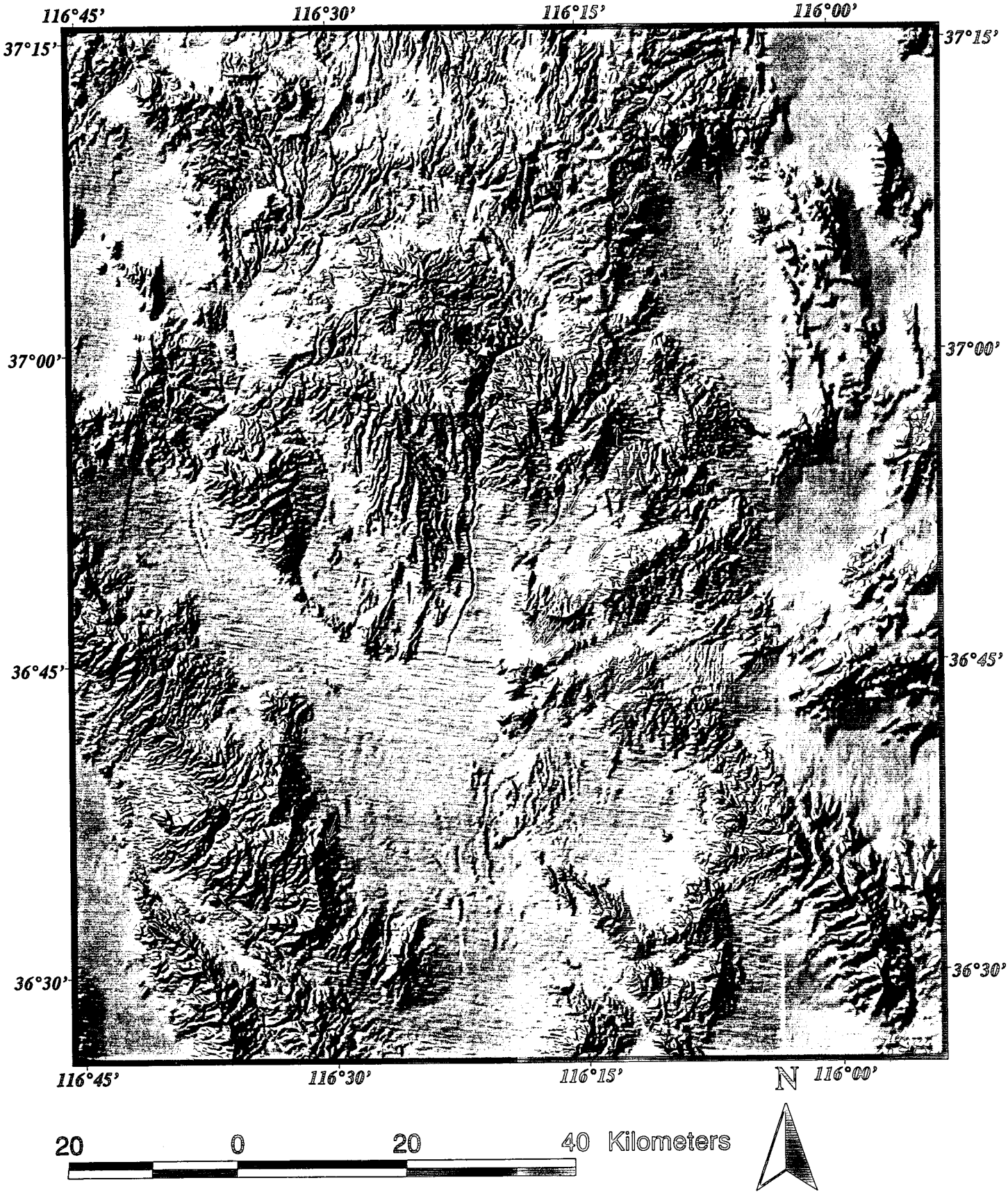

Figure 6-3. Pressure axes of the focal mechanisms of Table 6-1, projected to the horizontal plane and plotted at the earthquake epicenter.

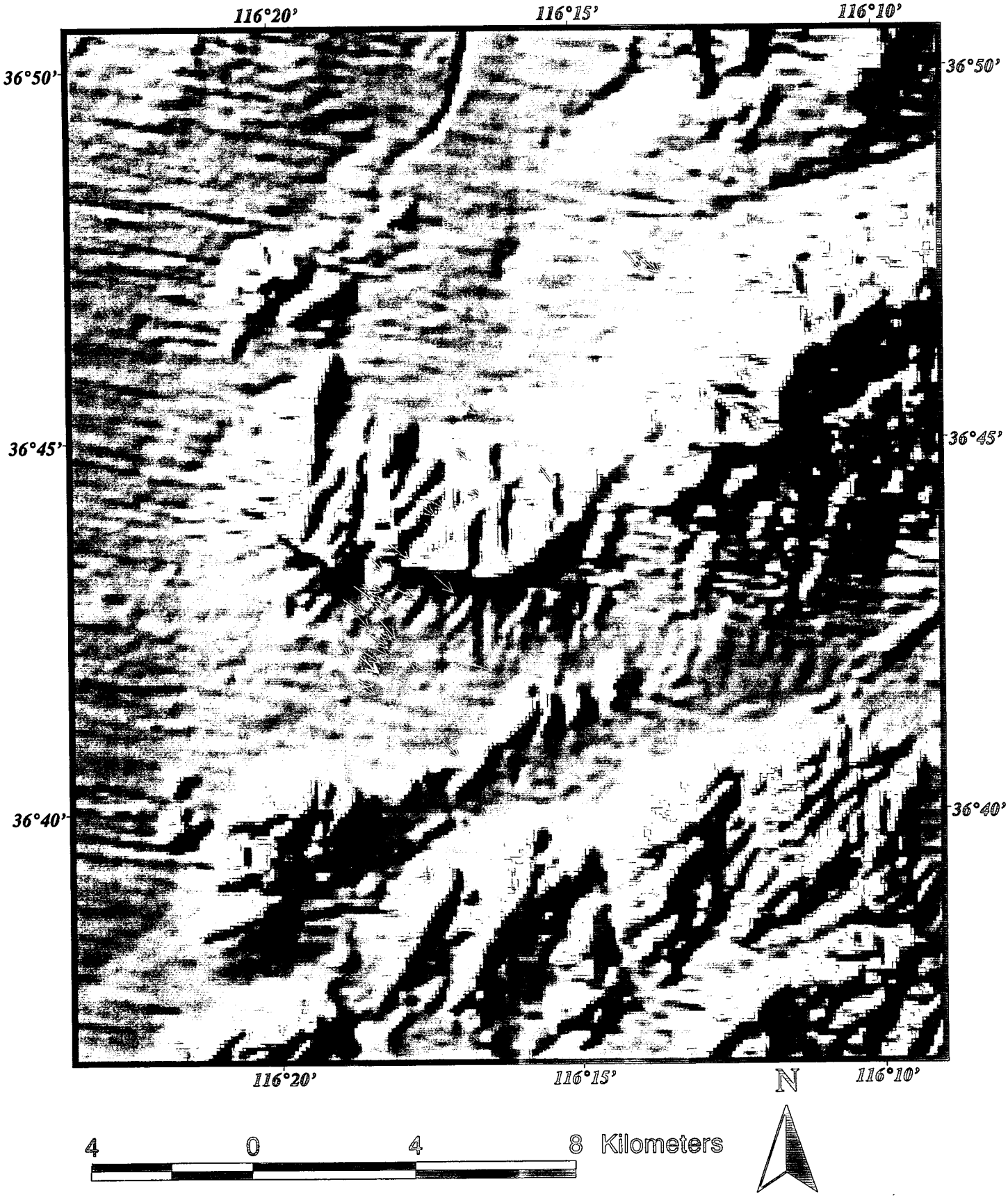

Figure 6-4. Tension axes of Little Skull Mountain focal mechanisms of Table 6-1, projected to the horizontal plane and plotted at the earthquake epicenter.

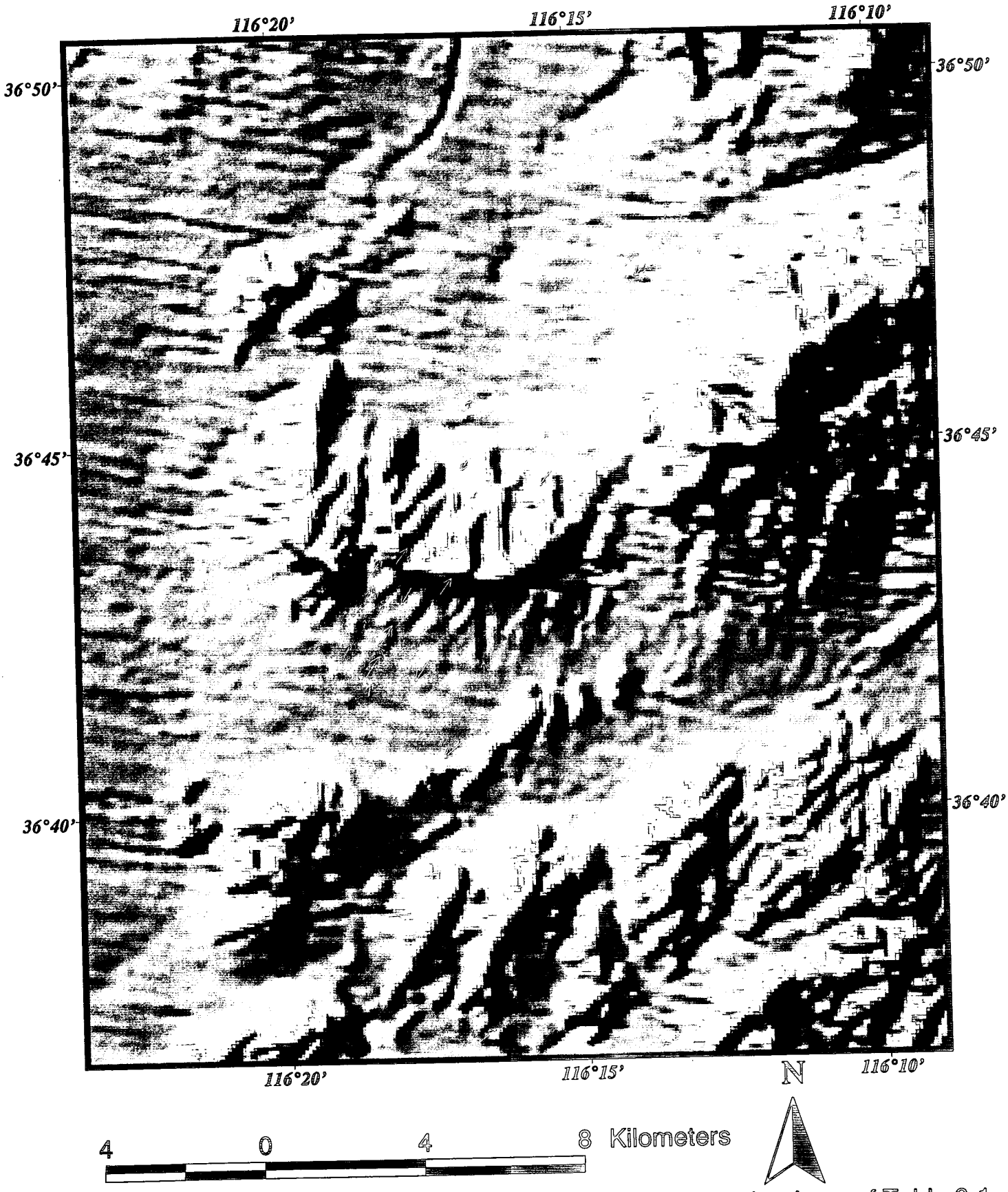

Figure 6-5. Pressure axes of Little Skull Mountain focal mechanisms of Table 6-1, projected to the horizontal plane and plotted at the earthquake epicenter.

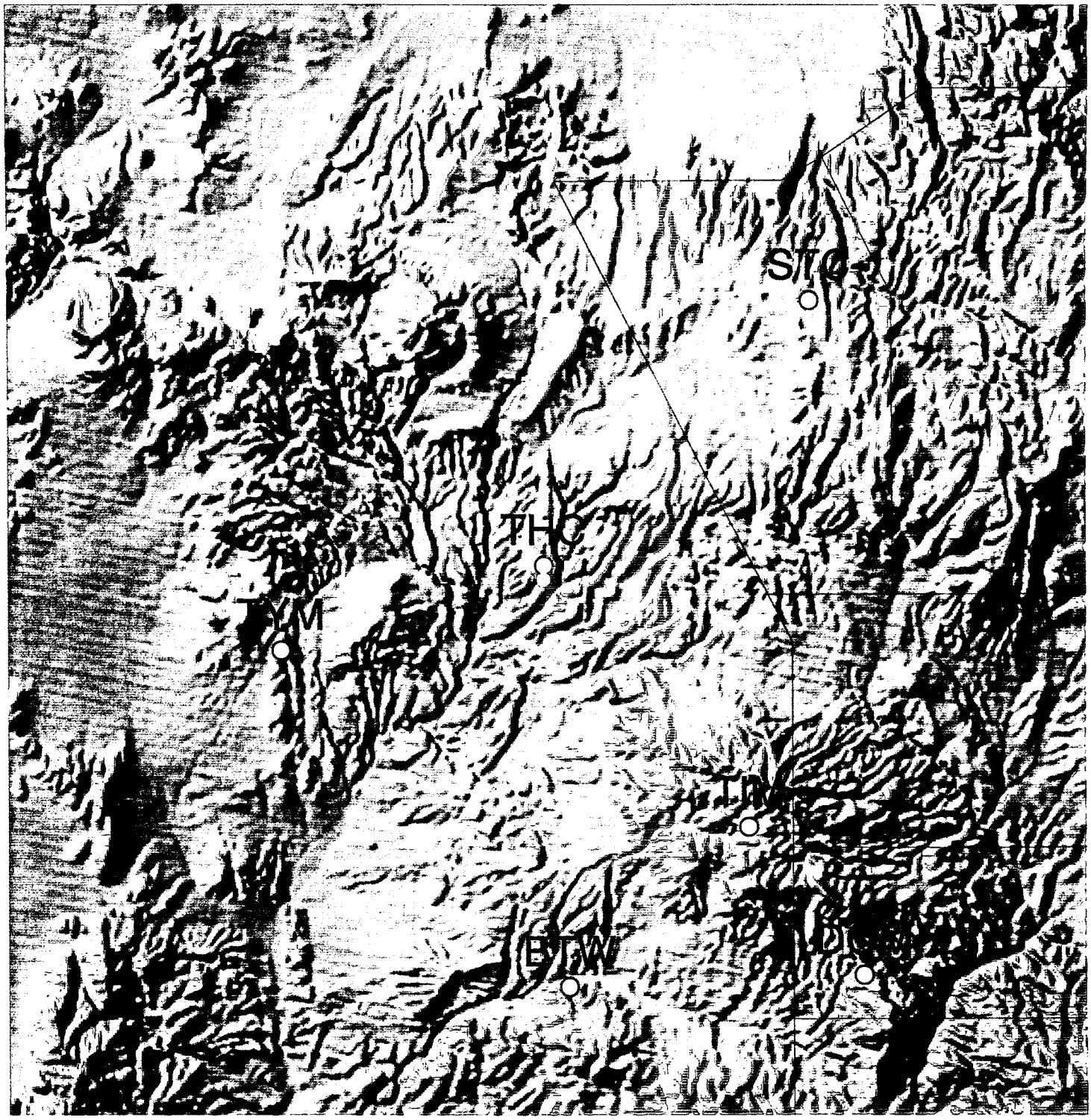

Figure 7-1. Location of main shock and seismic stations.

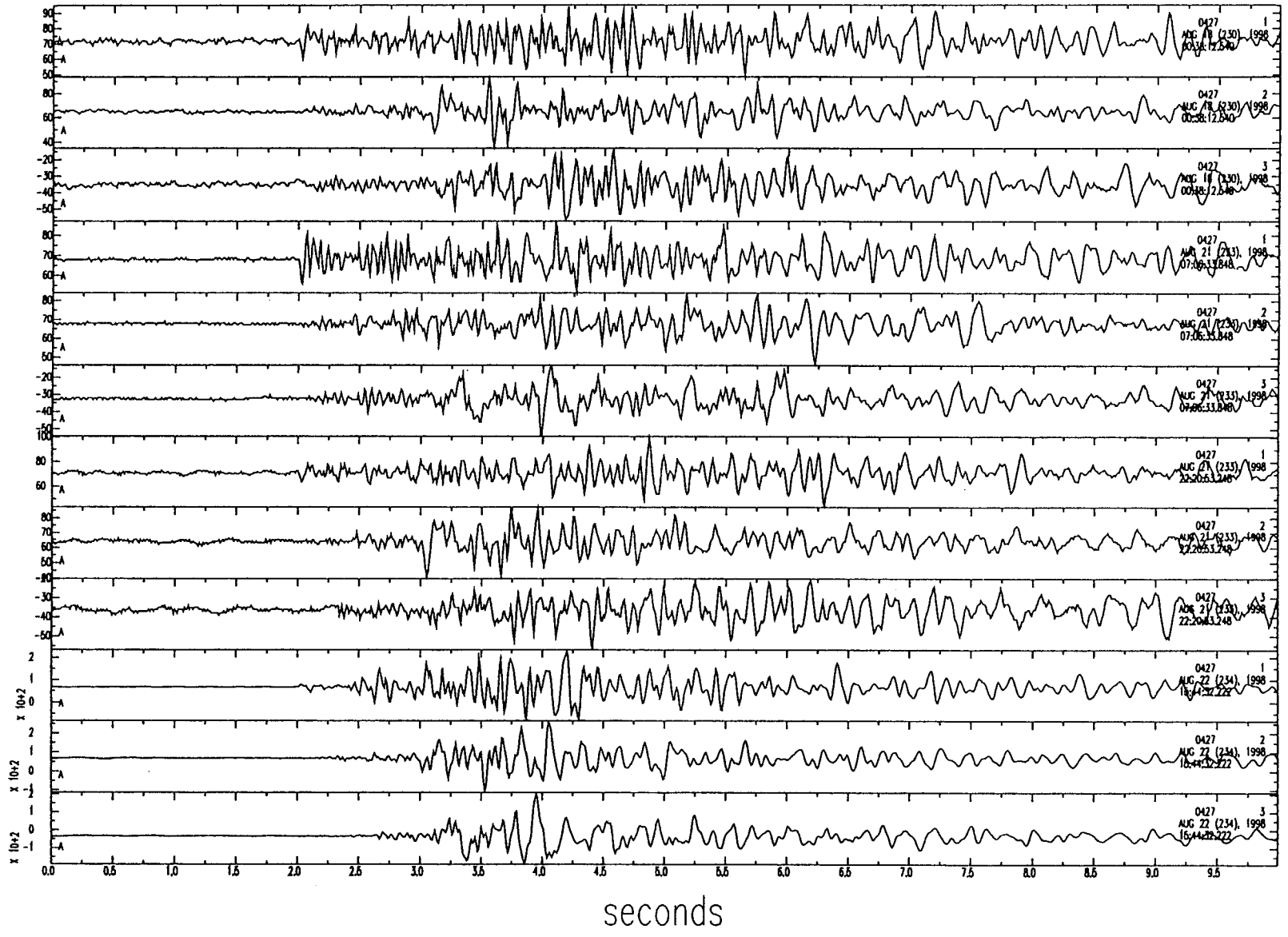

Figure 7-2. Recordings of typical Thirsty Canyon earthquakes at the portable station THC.

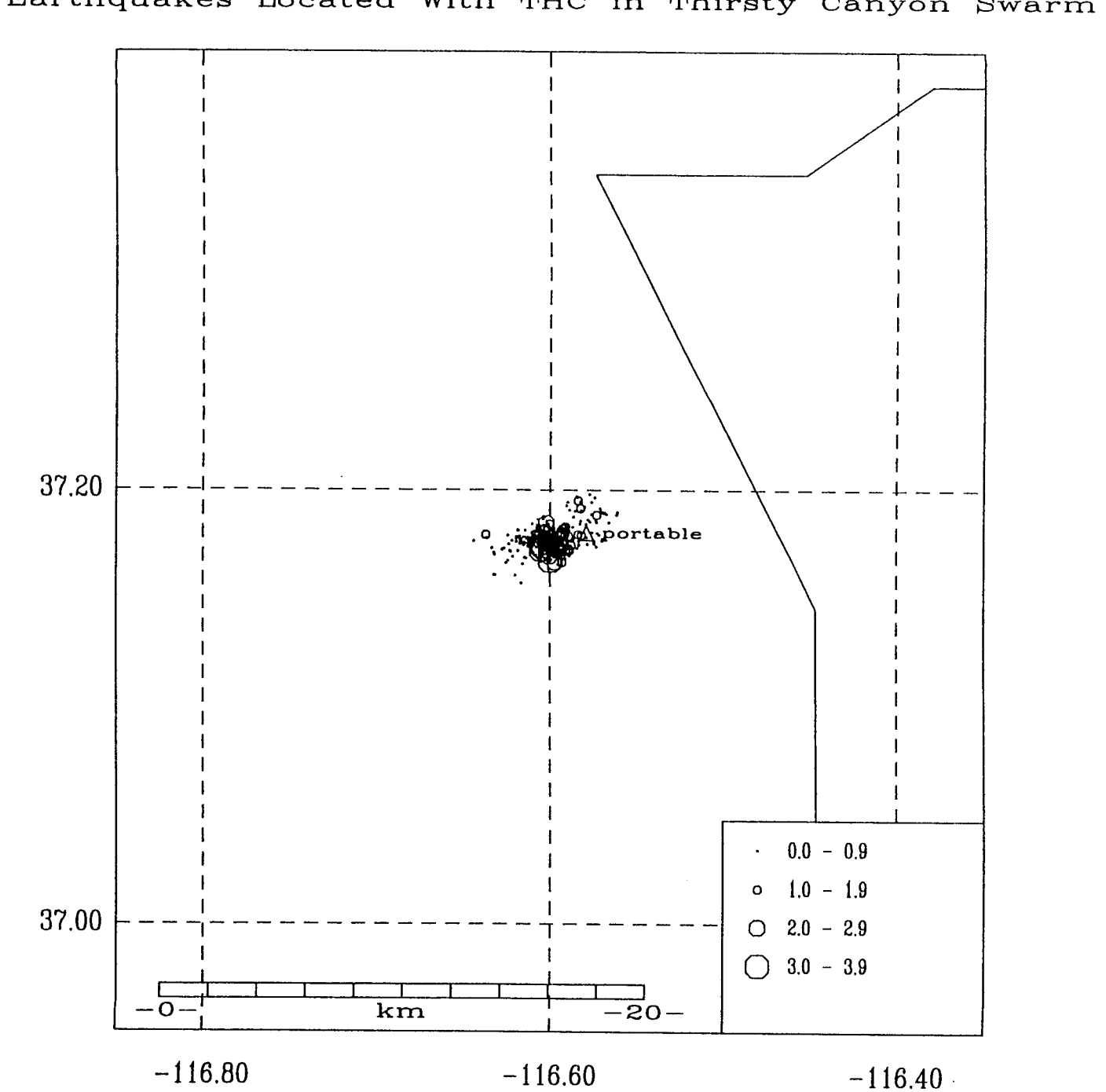

Figure 7-3. Earthquakes of the Thirsty Canyon swarm located with THC arrivals included.

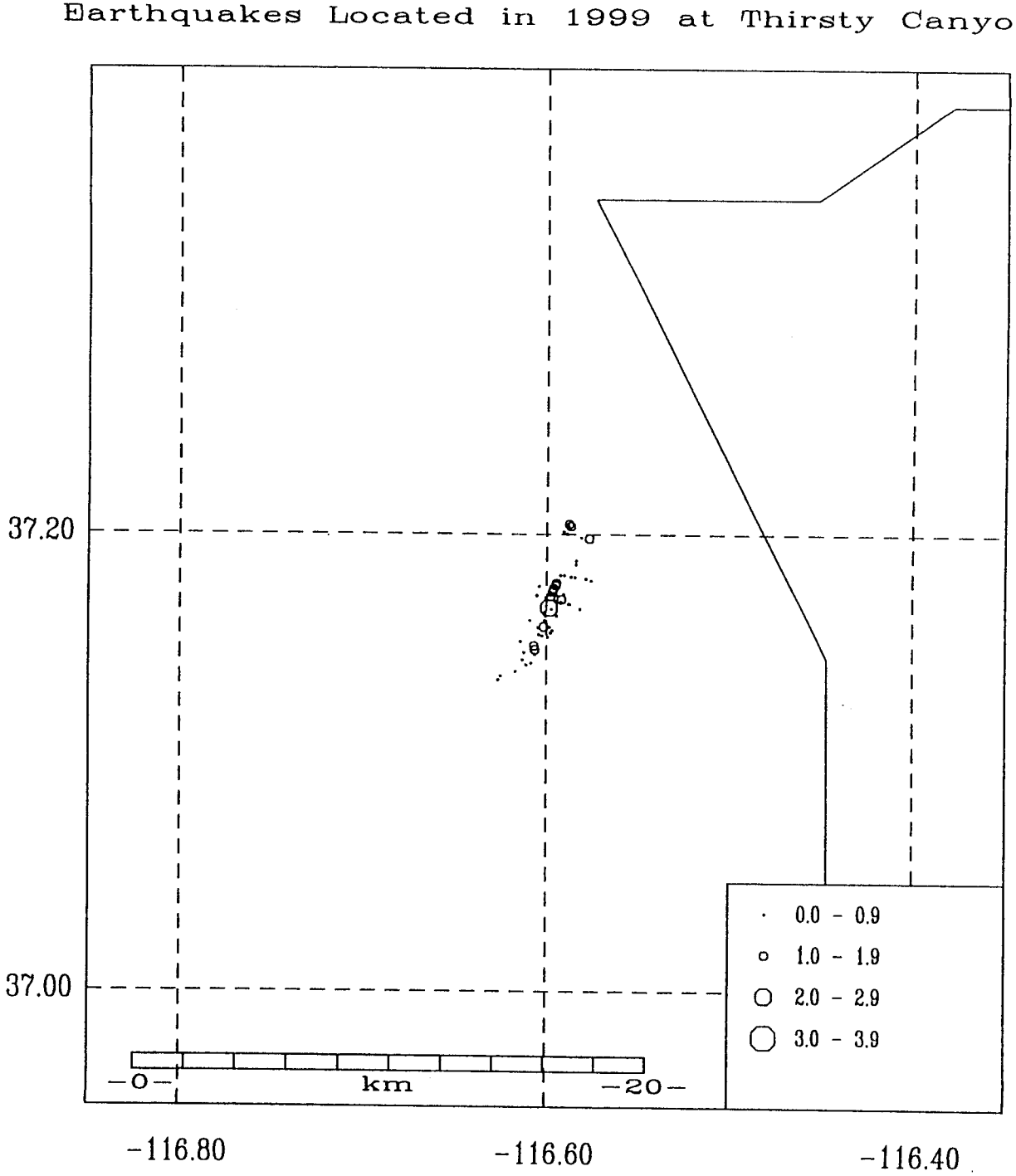

Figure 7-4. Earthquakes of the Thirsty Canyon swarm located with TYM arrivals included.

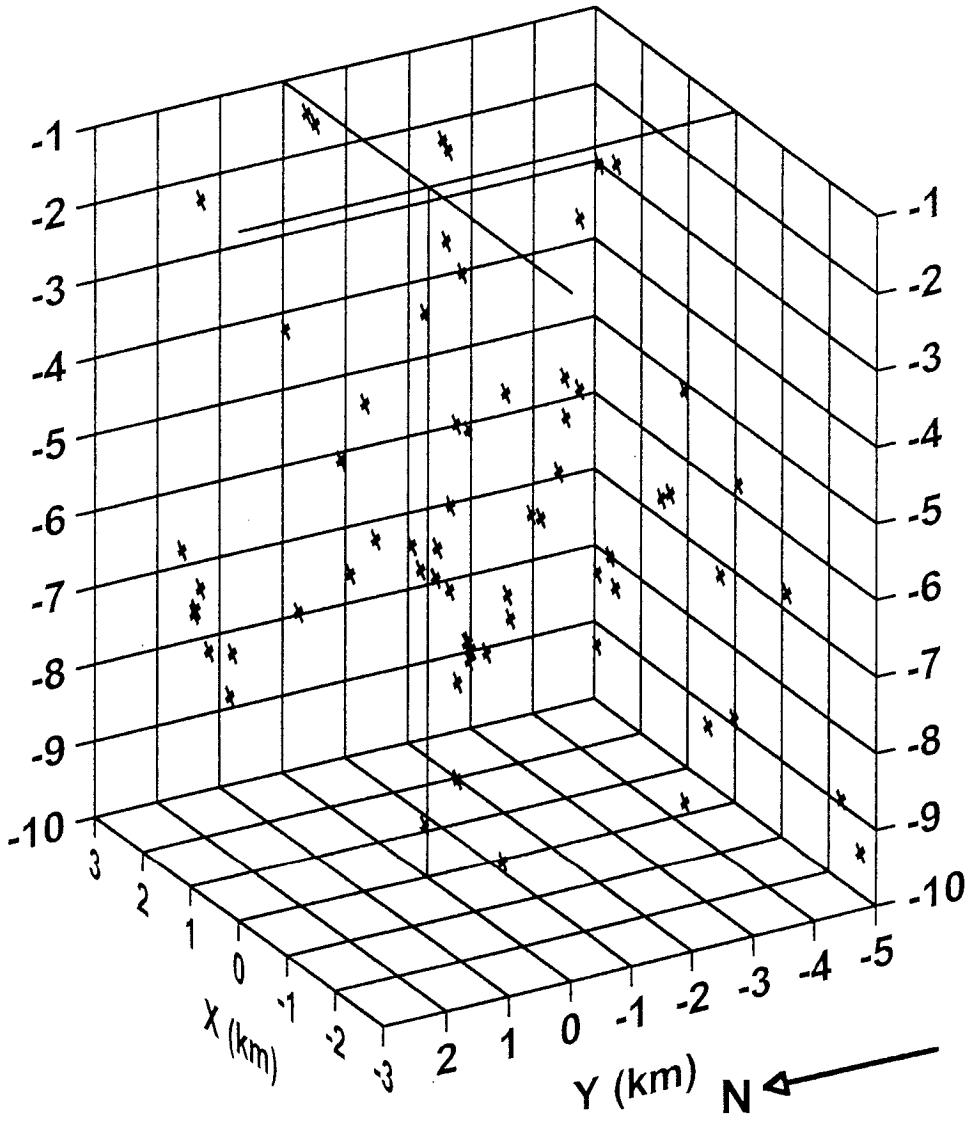

Figure 7-5a. Projection of Thirsty Canyon earthquakes located with TYM, as viewed from 300° azimuth (WNW) and at an inclination of 25°.

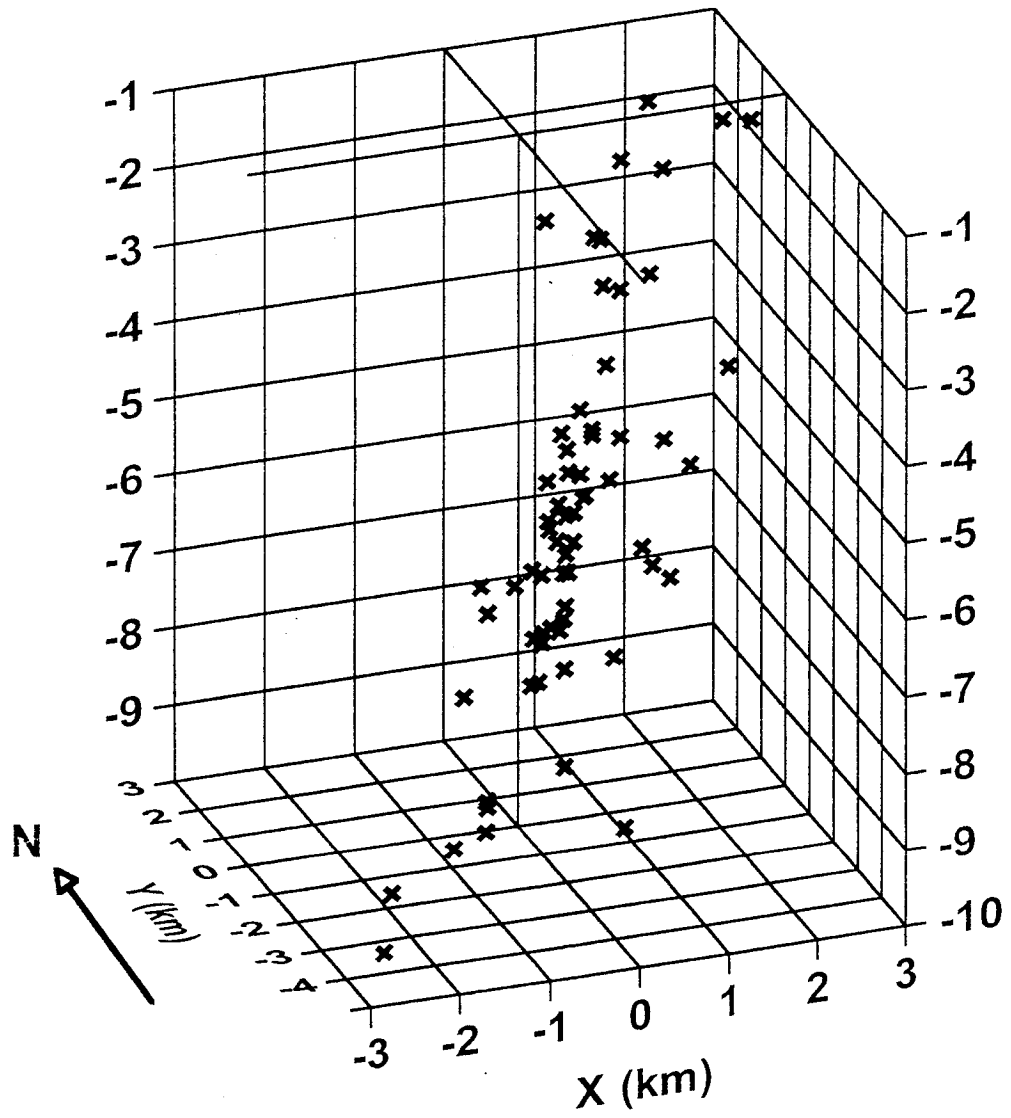

Figure 7-5b. Projection of Thirsty Canyon earthquakes located with TYM, as viewed from 210° azimuth (SSW) and at an inclination of 25°.

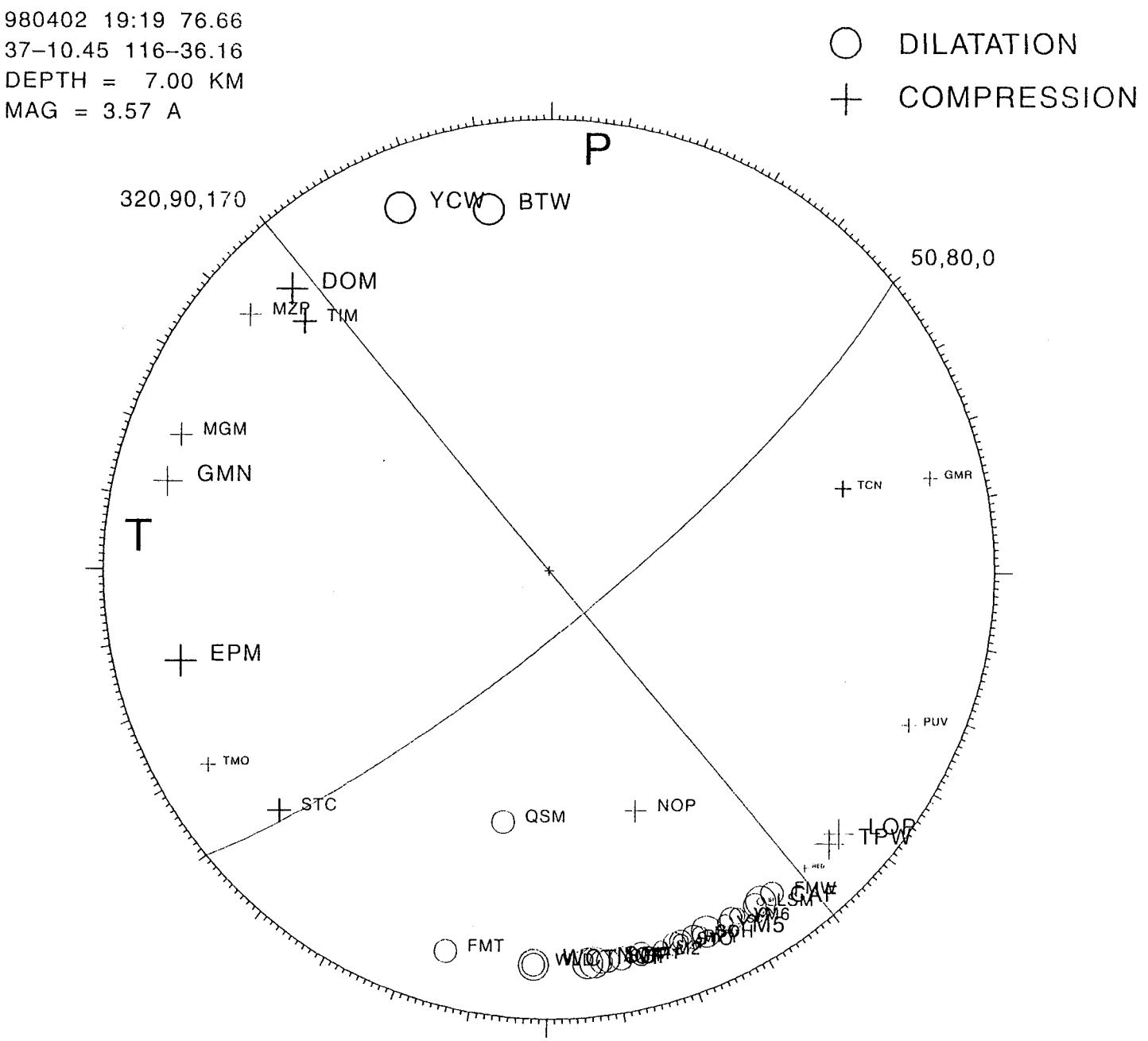

Figure 7-6. Focal mechanism of the largest of the Thirsty Canyon swarm (M_L = 3.57).

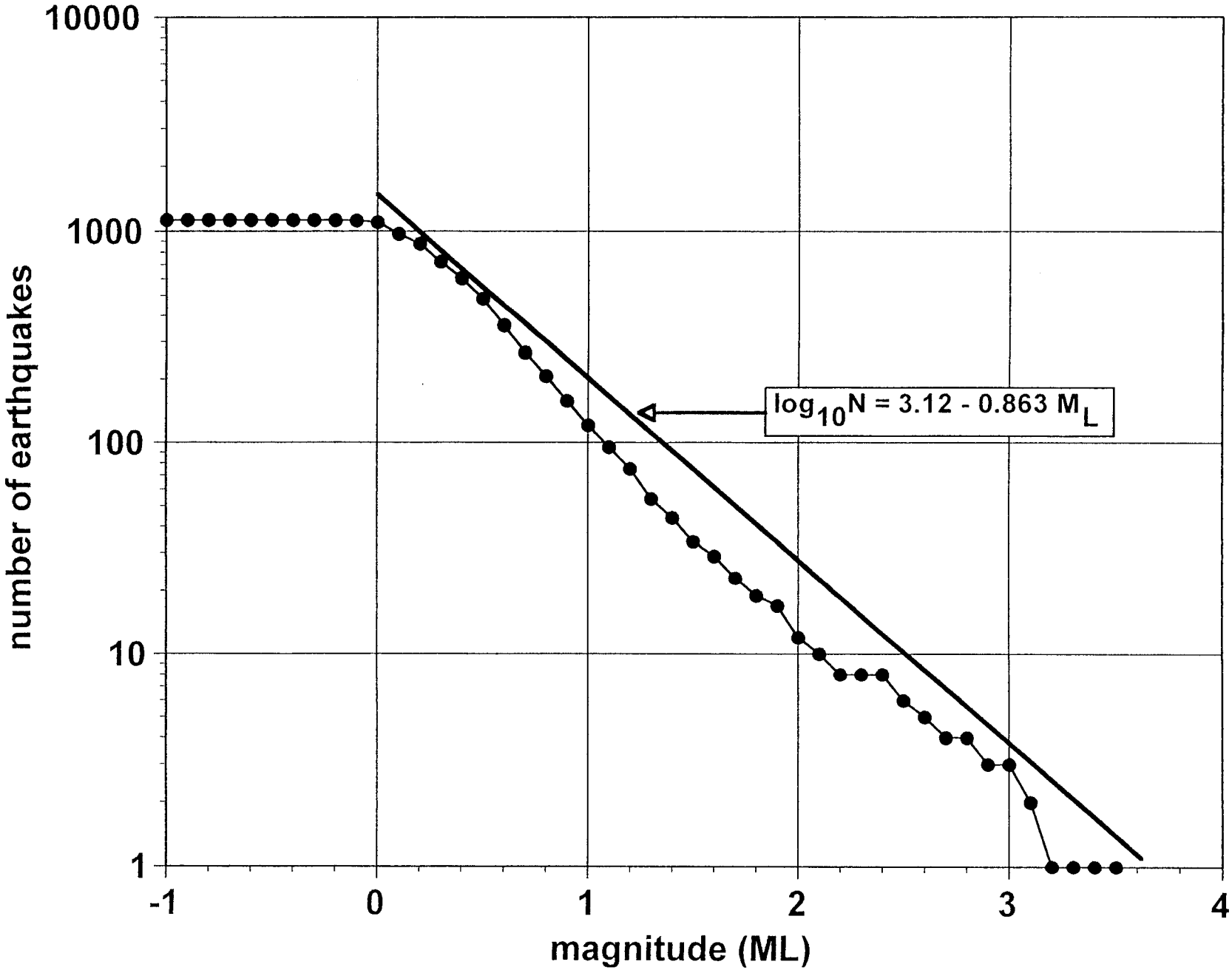

Figure 7-7. Recurrence curve for the Thirsty Canyon earthquake swarm. Line has a slope identical to that for the entire FY98-99 SGBDSN catalog but a change in the intercept.

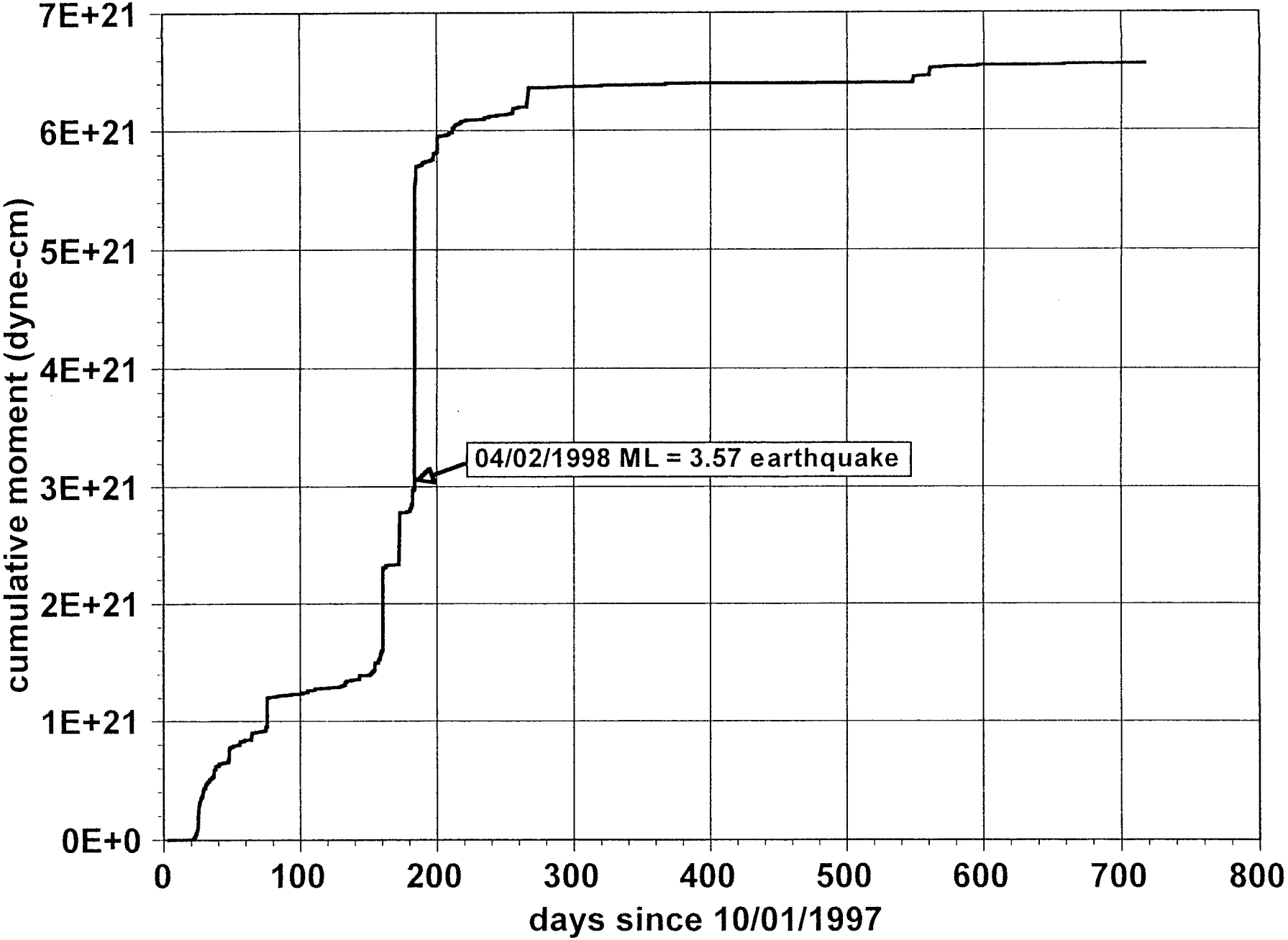

Figure 7-8. Cumulative moment release of the Thirsty Canyon earthquake swarm.

Figure 7-9. Aftershocks of the Scotty's Junction earthquake of August 1, 1999.

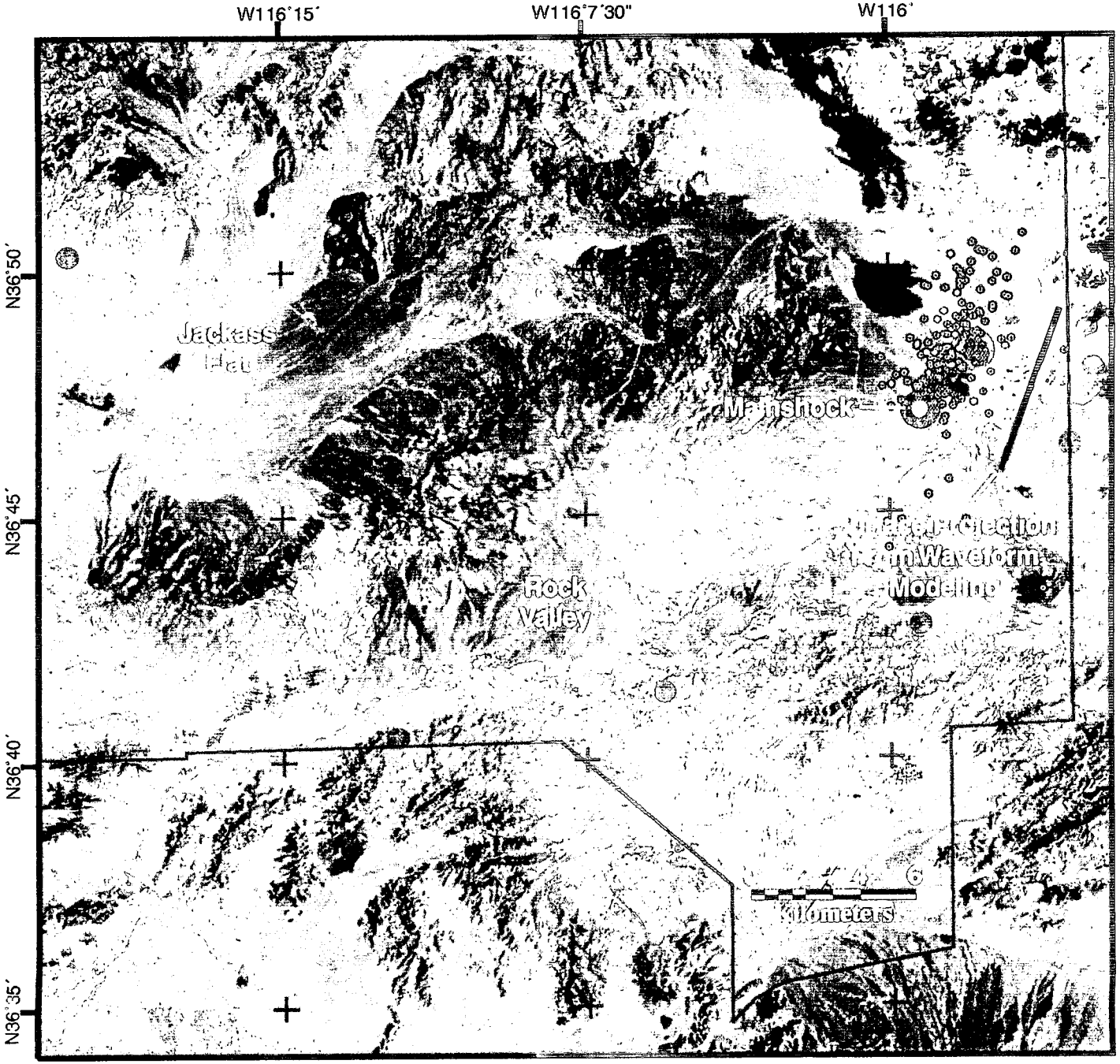

Figure 7-10. Aftershocks of the Frenchman Flat earthquake of January 27, 1999.

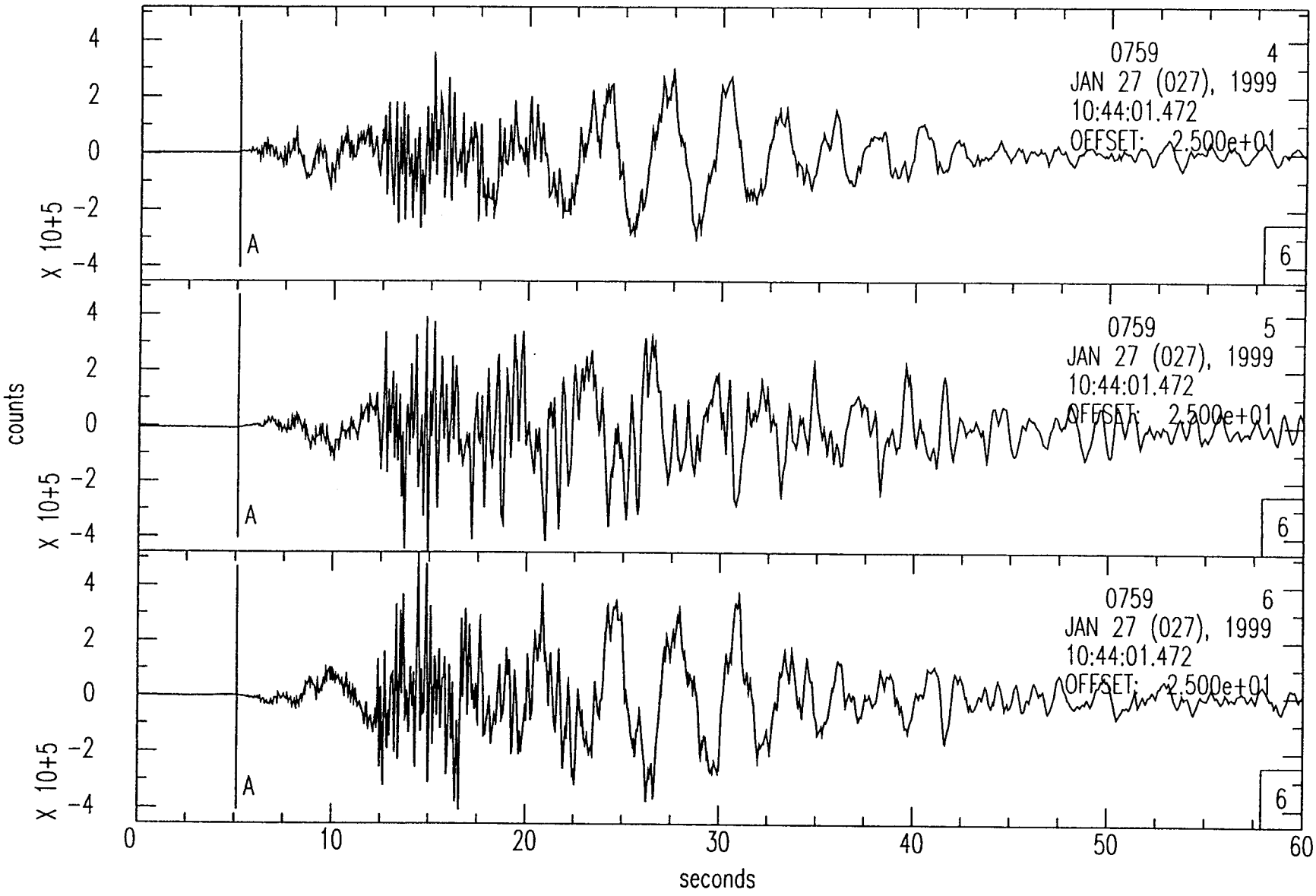

Figure 7-11. Recordings of the Frenchman Flat earthquake of January 27, 1999 at the broadband station TIM.

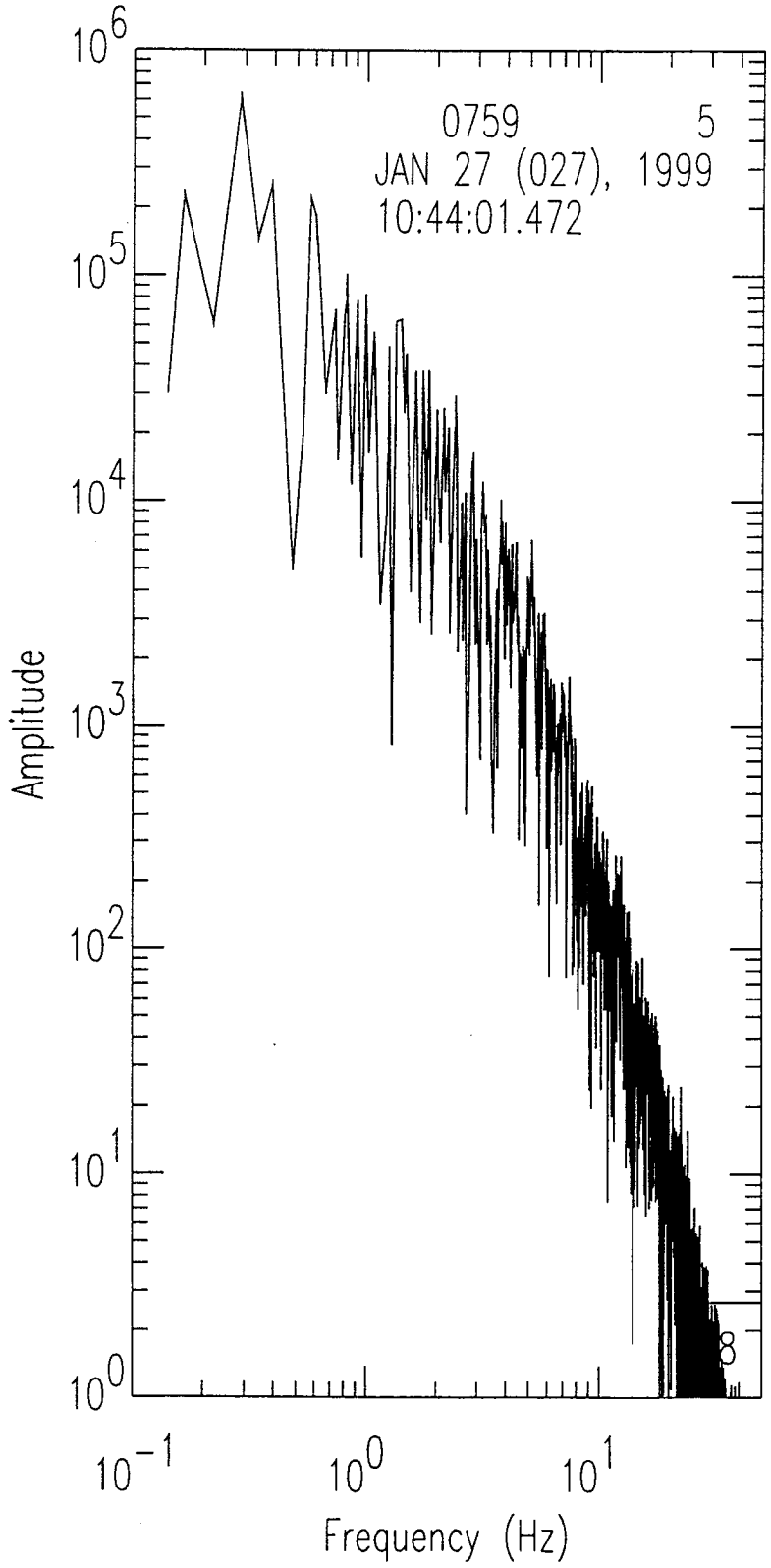

Figure 7-12. Spectrum of the N-S component of the TIM recordings of the Frenchman Flat earthquake. Spectrum has been integrated to represent pseudo displacement.

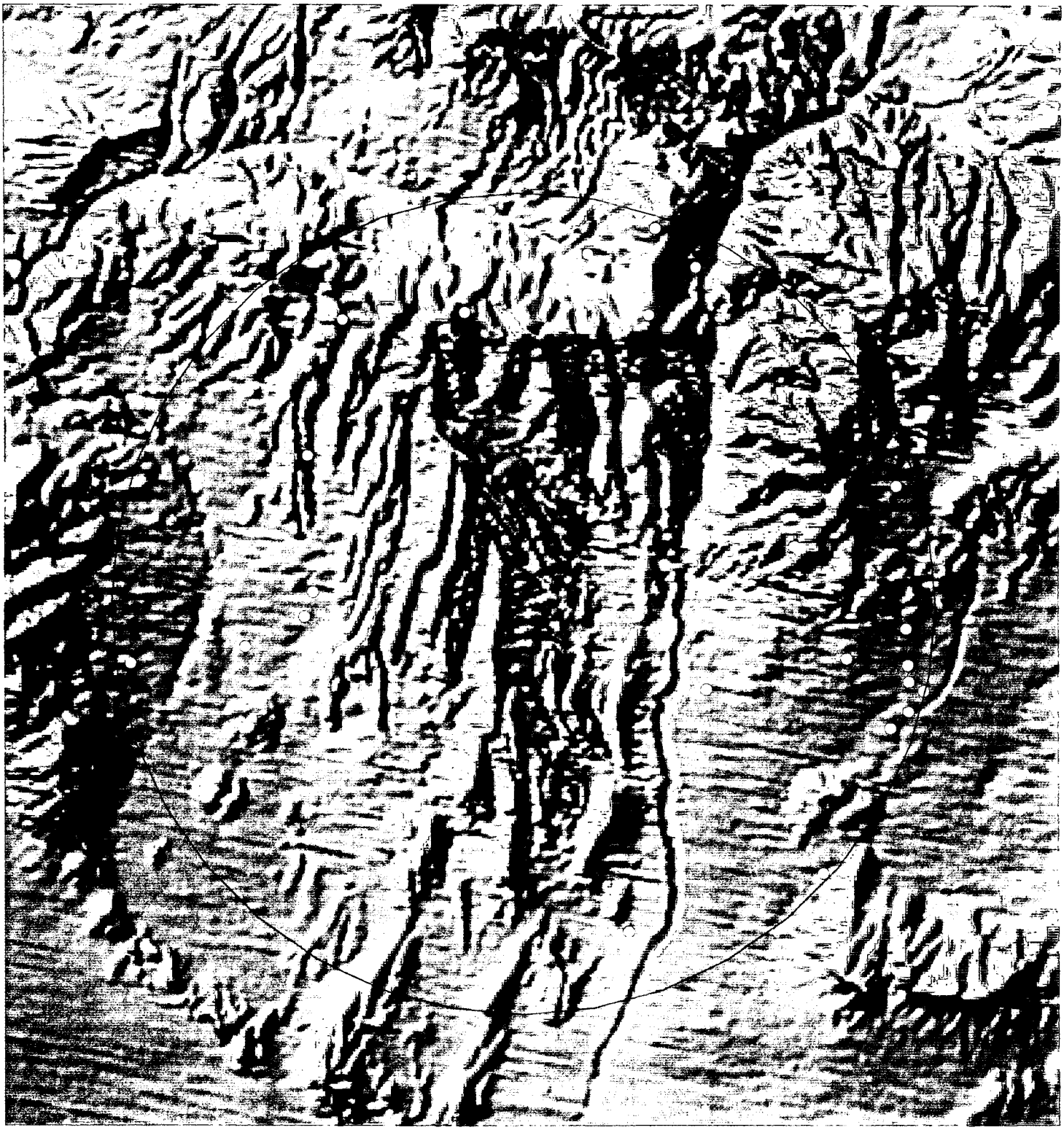

Figure 8-1. Earthquakes in FY98-99 within 15 km of RPY.

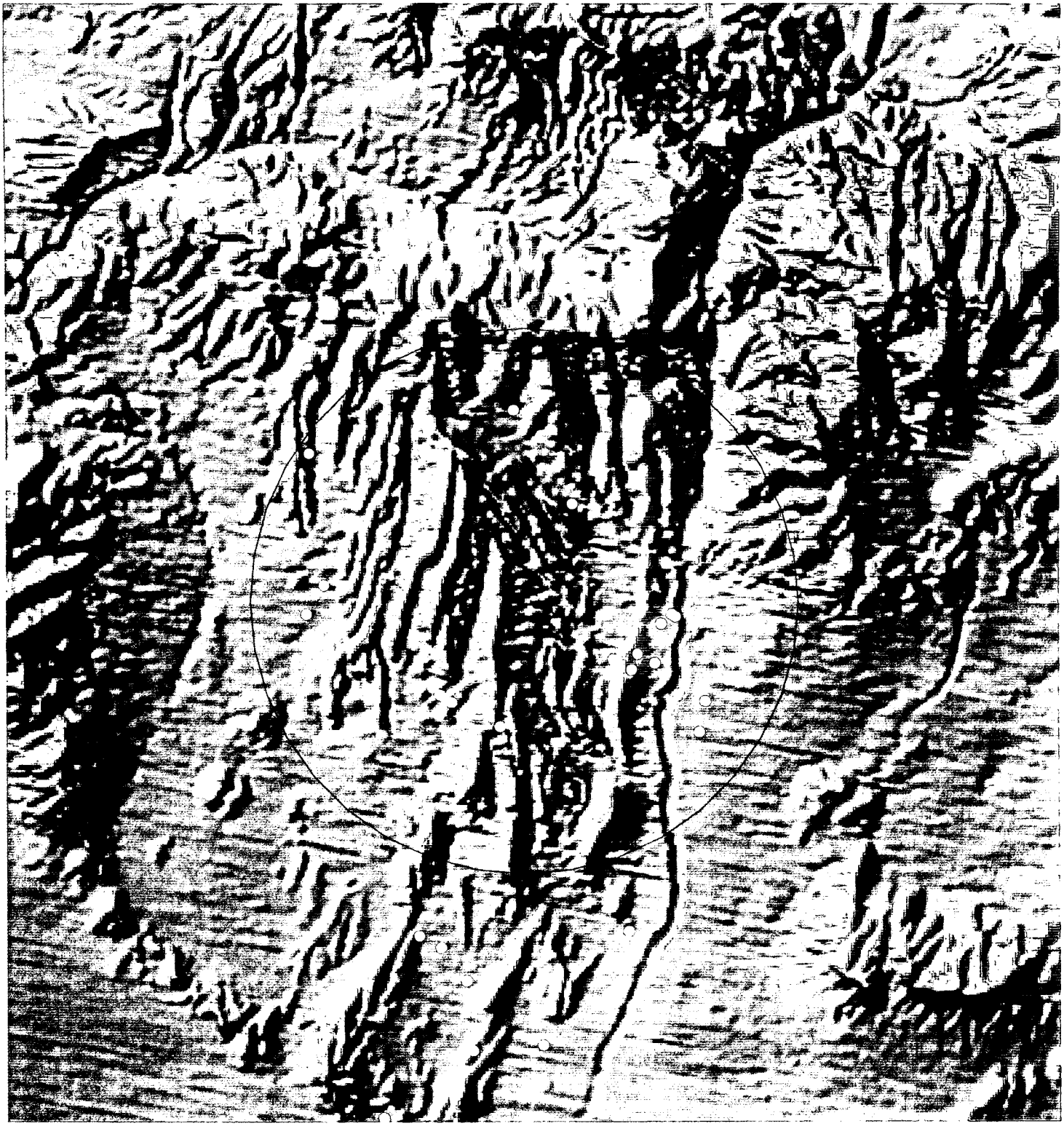

Figure 8-2. Eighteen earthquakes since 5/5/95 within 10 km of RPY plus seven more in the southern Yucca Mountain block.

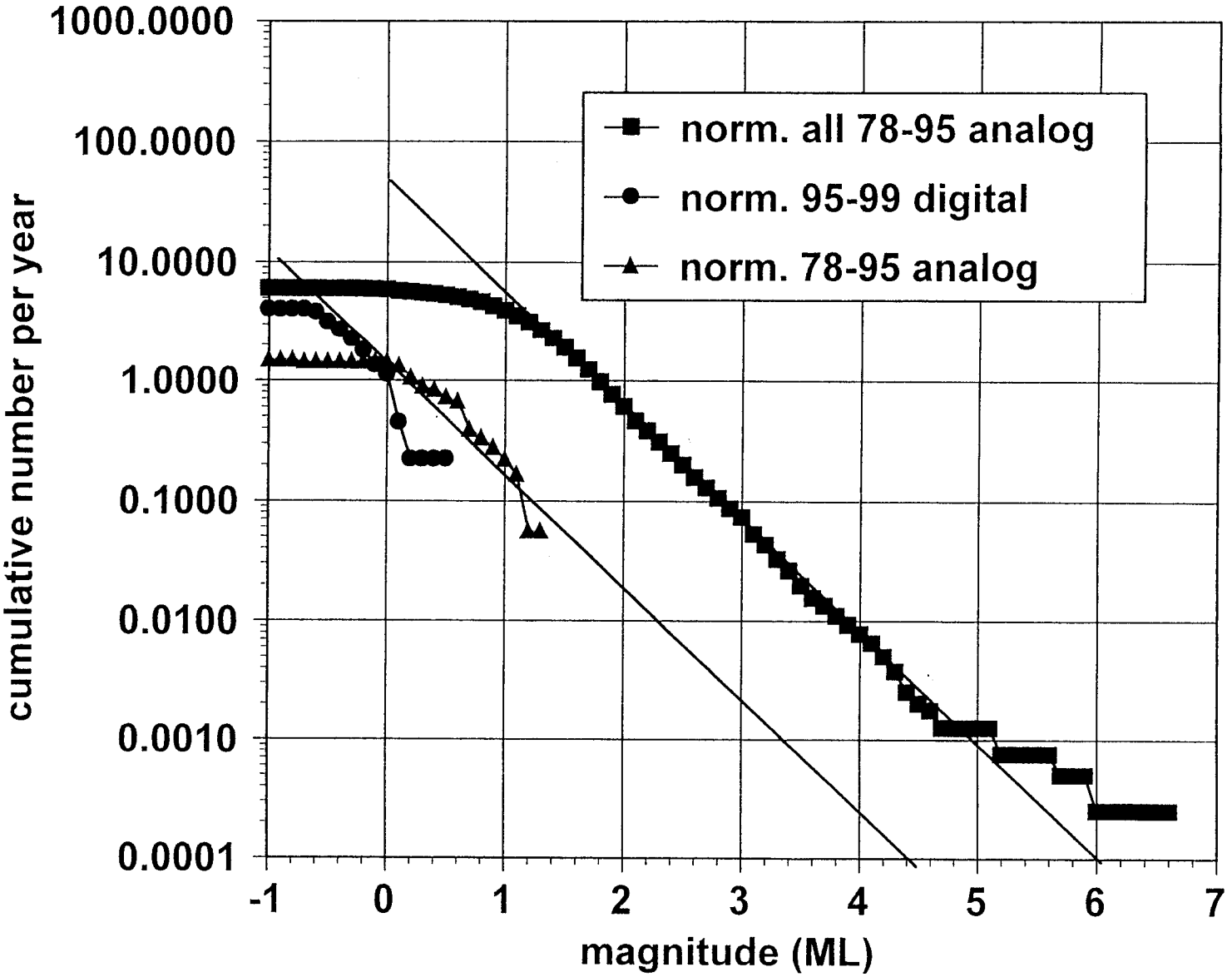

Figure 8-3. Recurrence curve for the 10-km area around RPY from SGBDSN monitoring plus comparative curves from previous analog network monitoring.

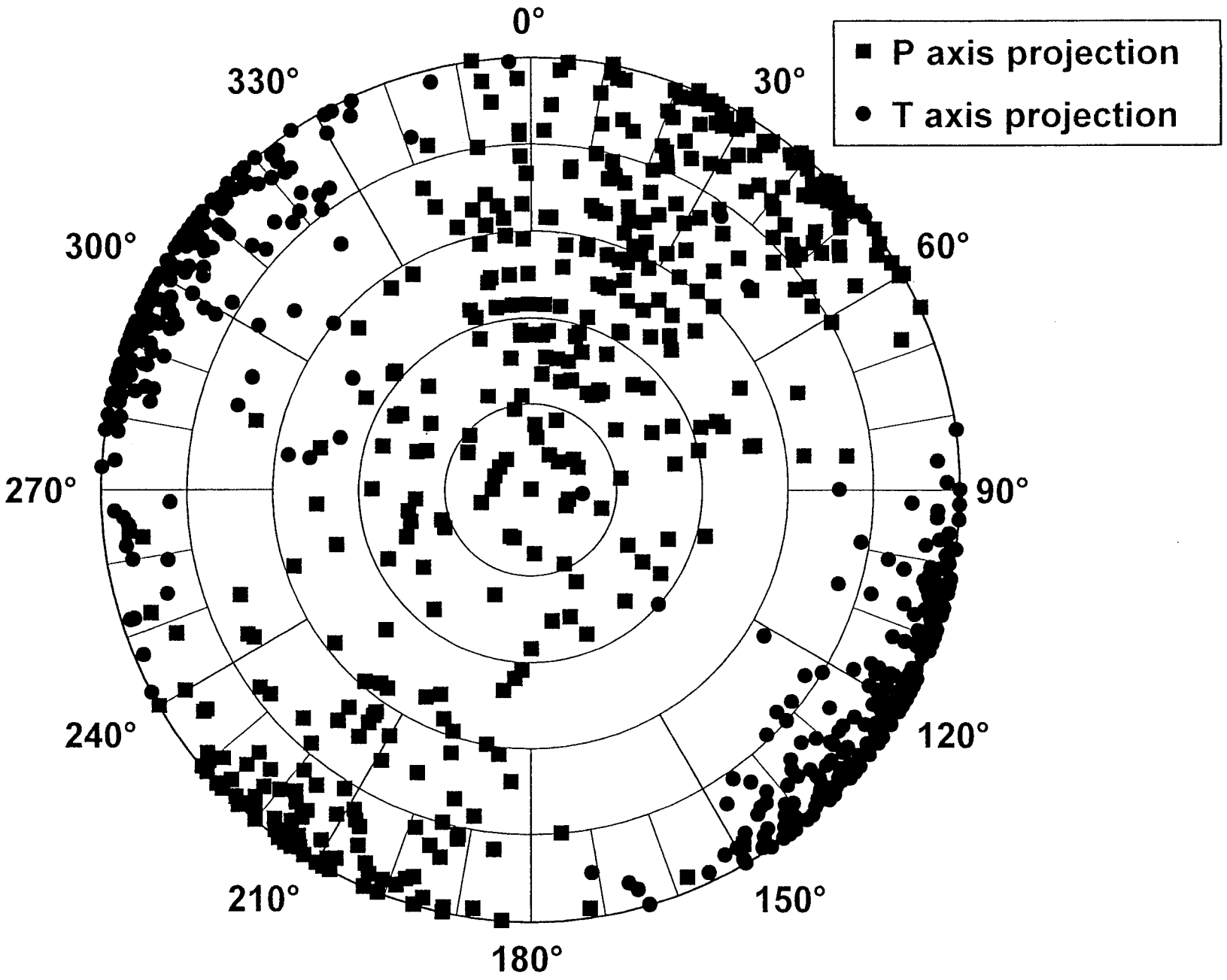

Figure 9-1. Pressure and tension axes from all focal mechanisms in the vicinity of Yucca Mountain (approximately 65 km from RPY).

Figure 9-2. Tension axes projected to the horizontal plane.

Figure 9-3. Pressure axes projected to the horizontal plane.

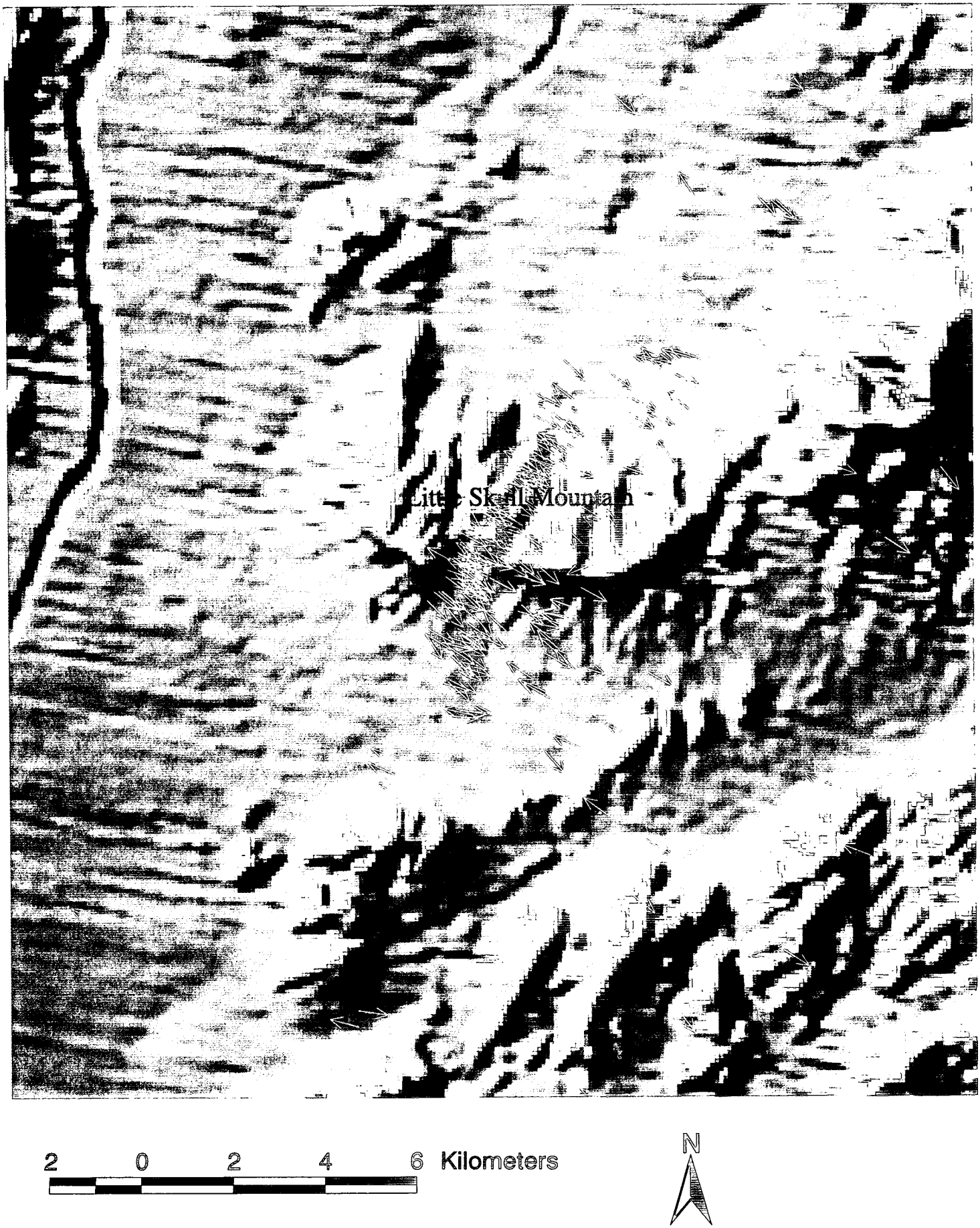

Figure 9-4. Tension axes projected to the horizontal plane --LSM area.

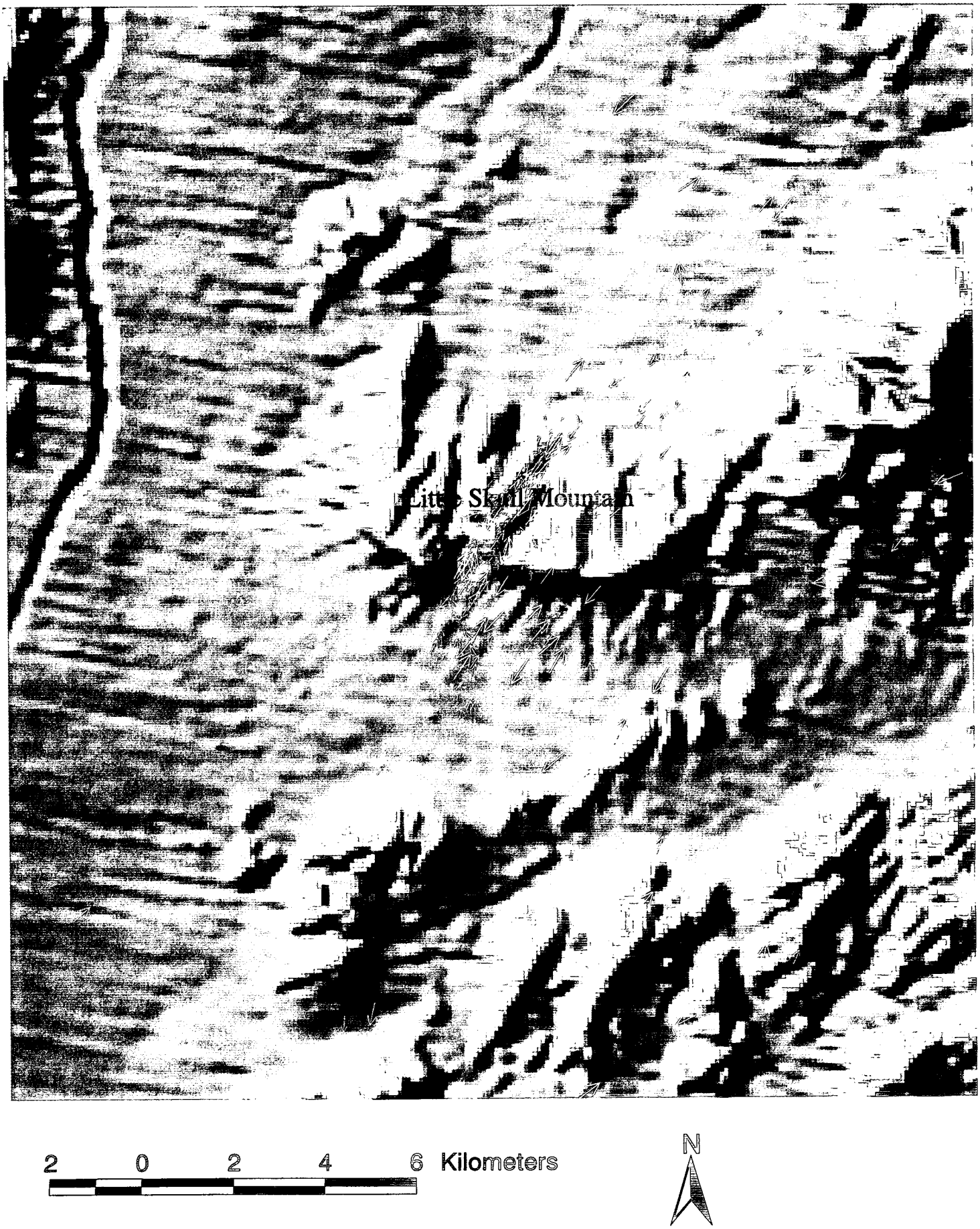

Figure 9-5. Pressure axes projected to the horizontal plane --LSM area.

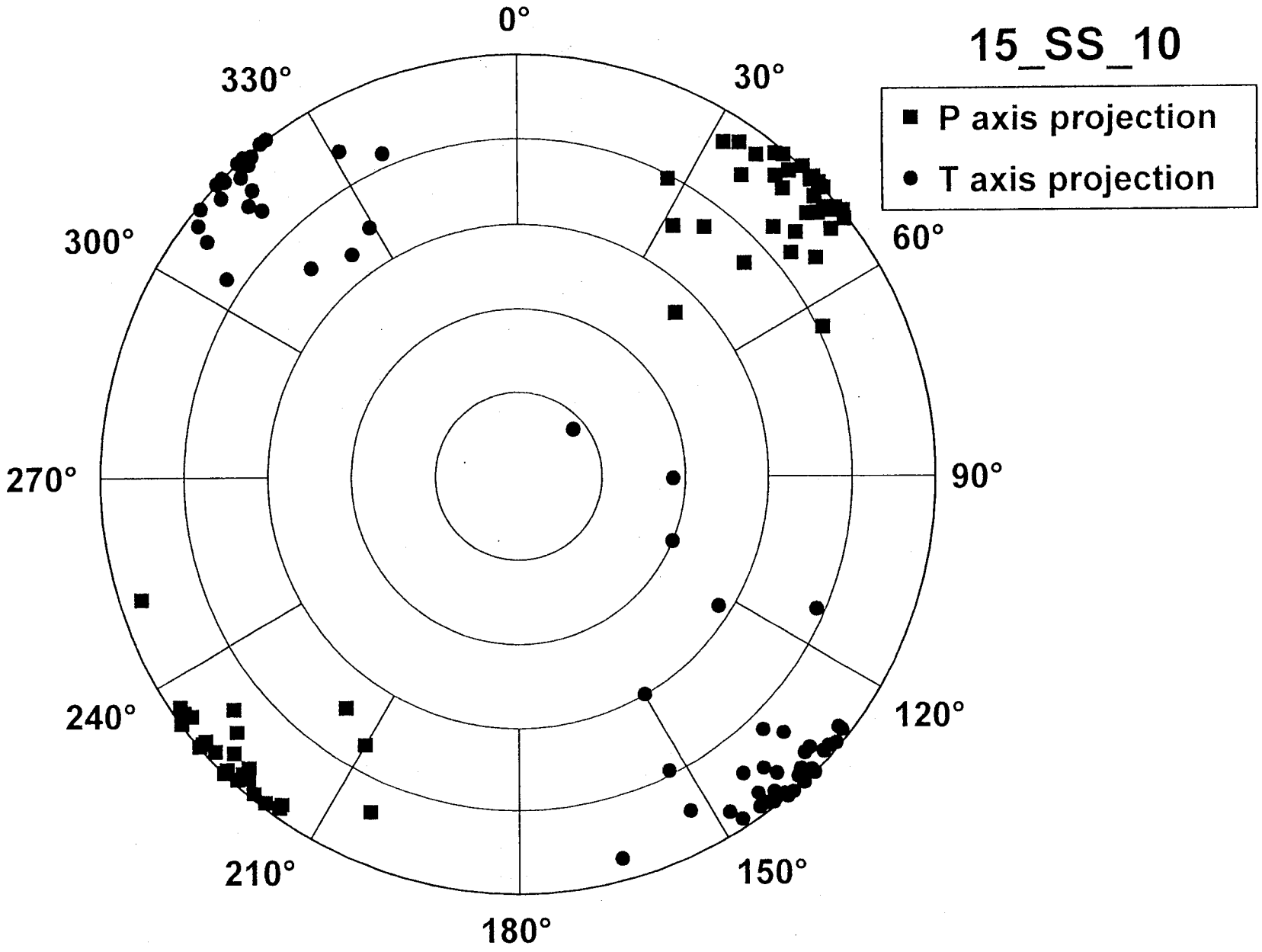

Figure 9-6. Pressure and tension axes from focal mechanisms of 50 simulated earthquakes at 10 km depth with strike-slip mechanism as recorded by 15 stations.

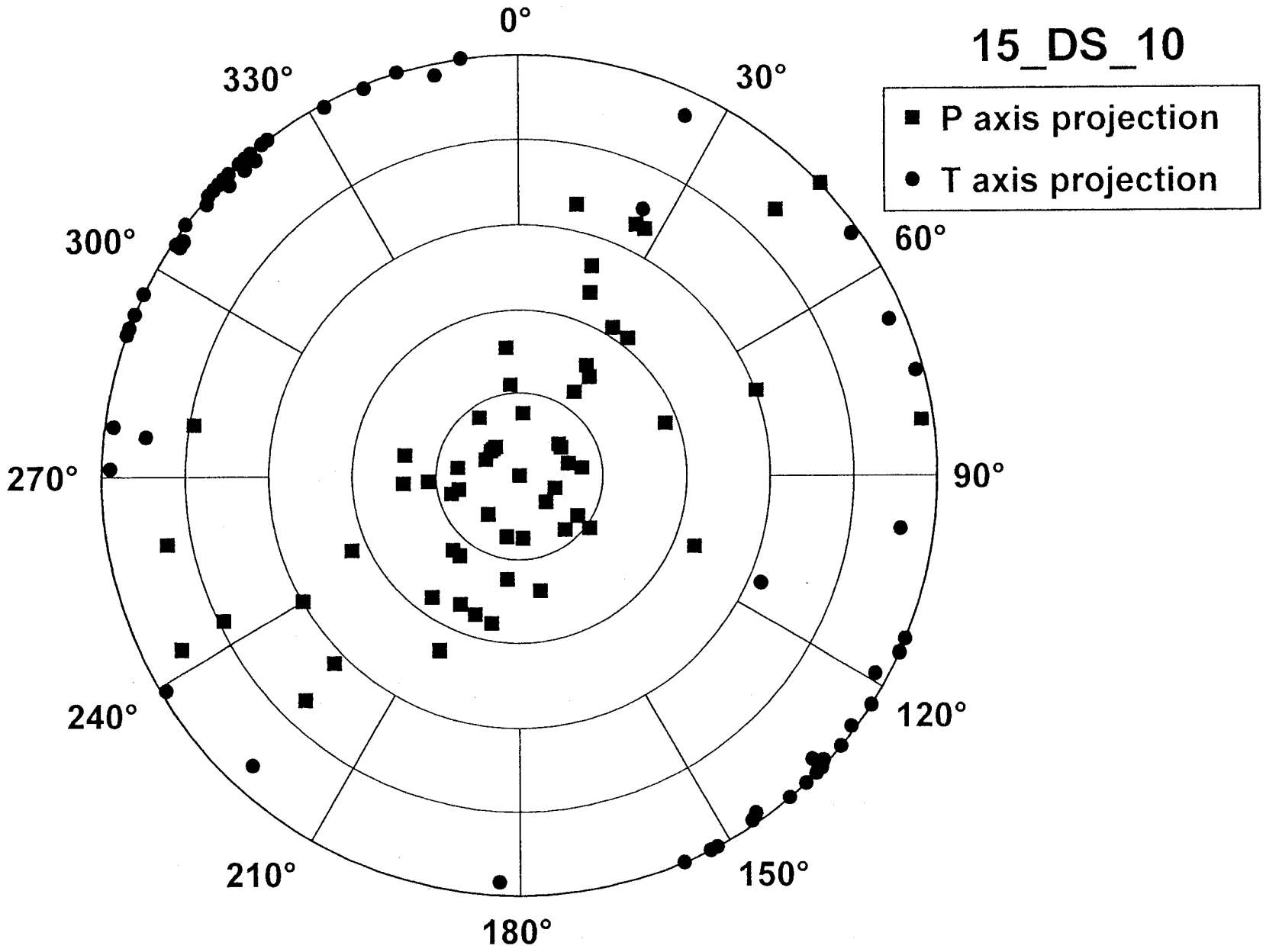

Figure 9-7. Pressure and tension axes from focal mechanisms of 50 simulated earthquakes at 10 km depth with dip-slip mechanism as recorded by 15 stations.

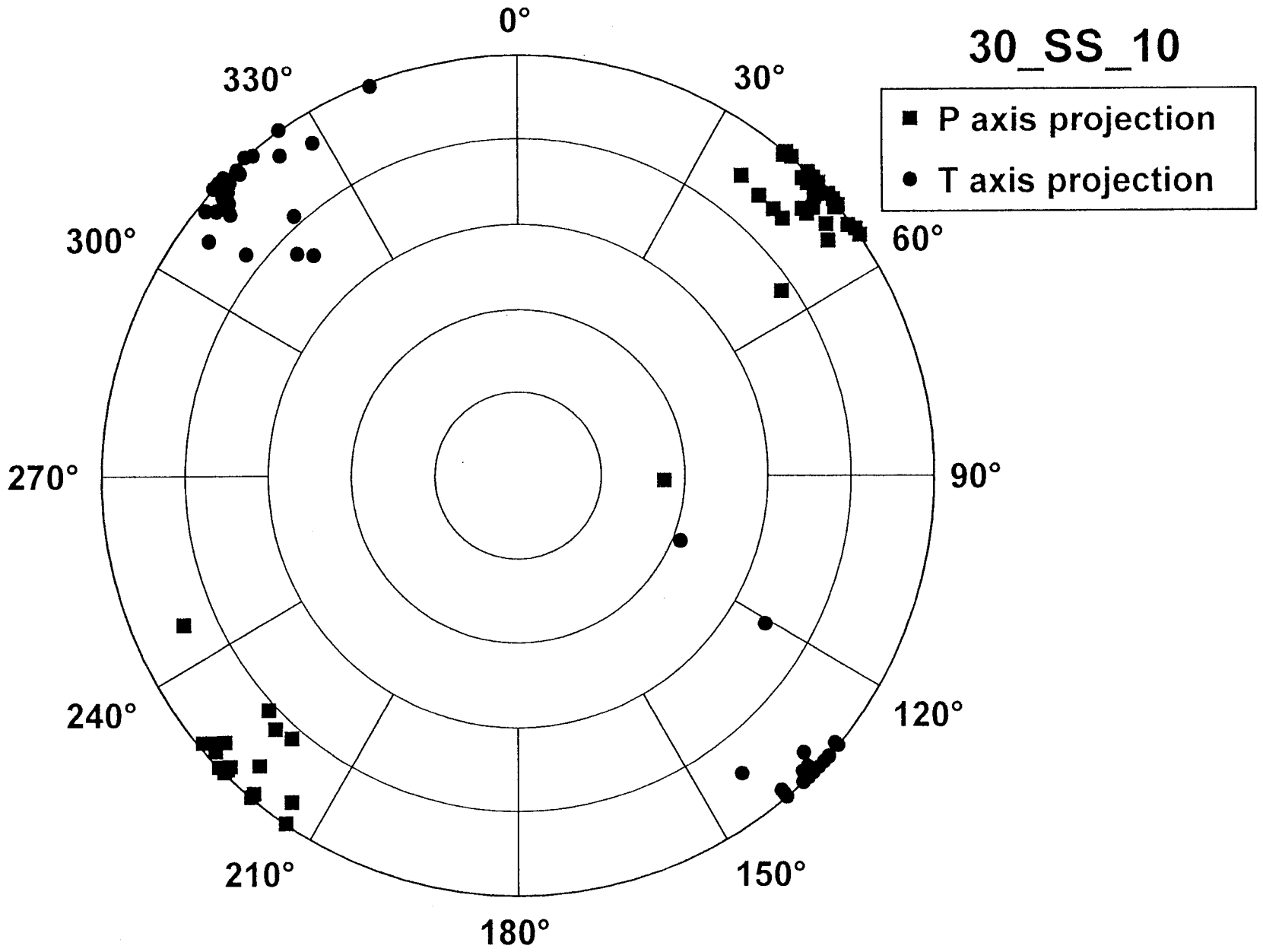

Figure 9-8. Pressure and tension axes from focal mechanisms of 50 simulated earthquakes at 10 km depth with strike-slip mechanism as recorded by 30 stations.

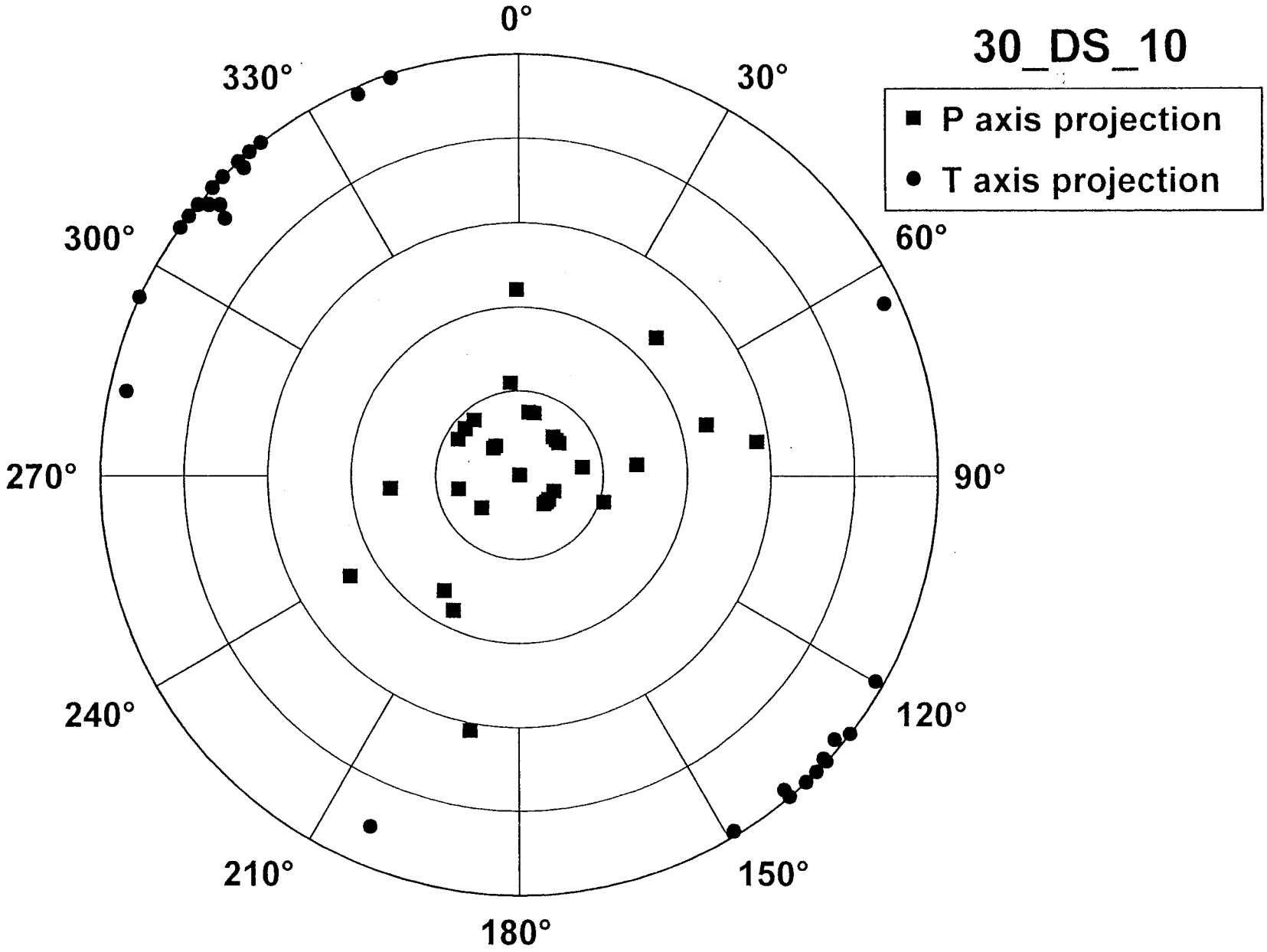

Figure 9-9. Pressure and tension axes from focal mechanisms of 50 simulated earthquakes at 10 km depth with dip-slip mechanism as recorded by 30 stations.

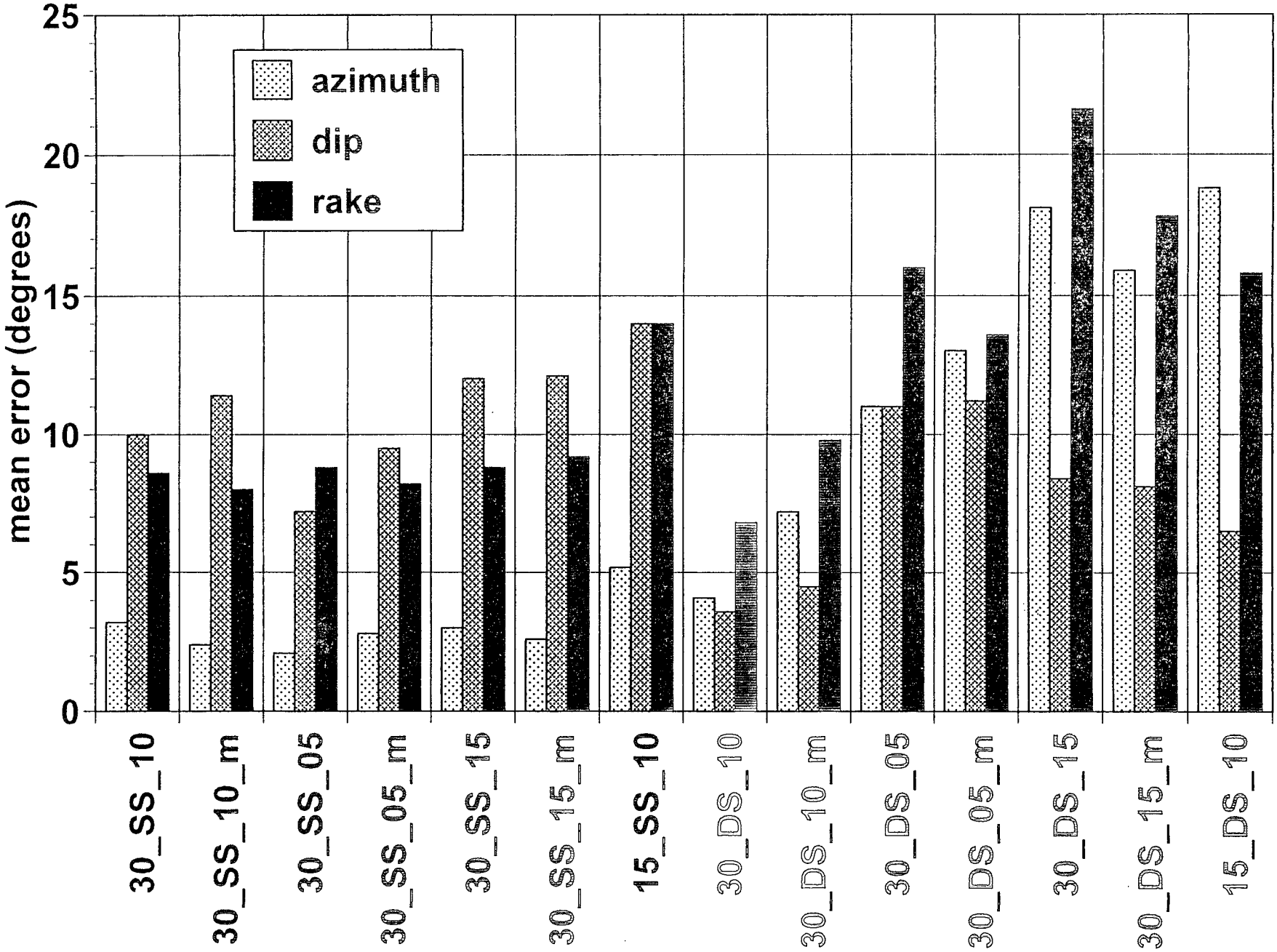

Figure 9-10. Mean errors in the estimated focal mechanism parameters for 14 simulated suites of 50 earthquakes with various constraints (see text).

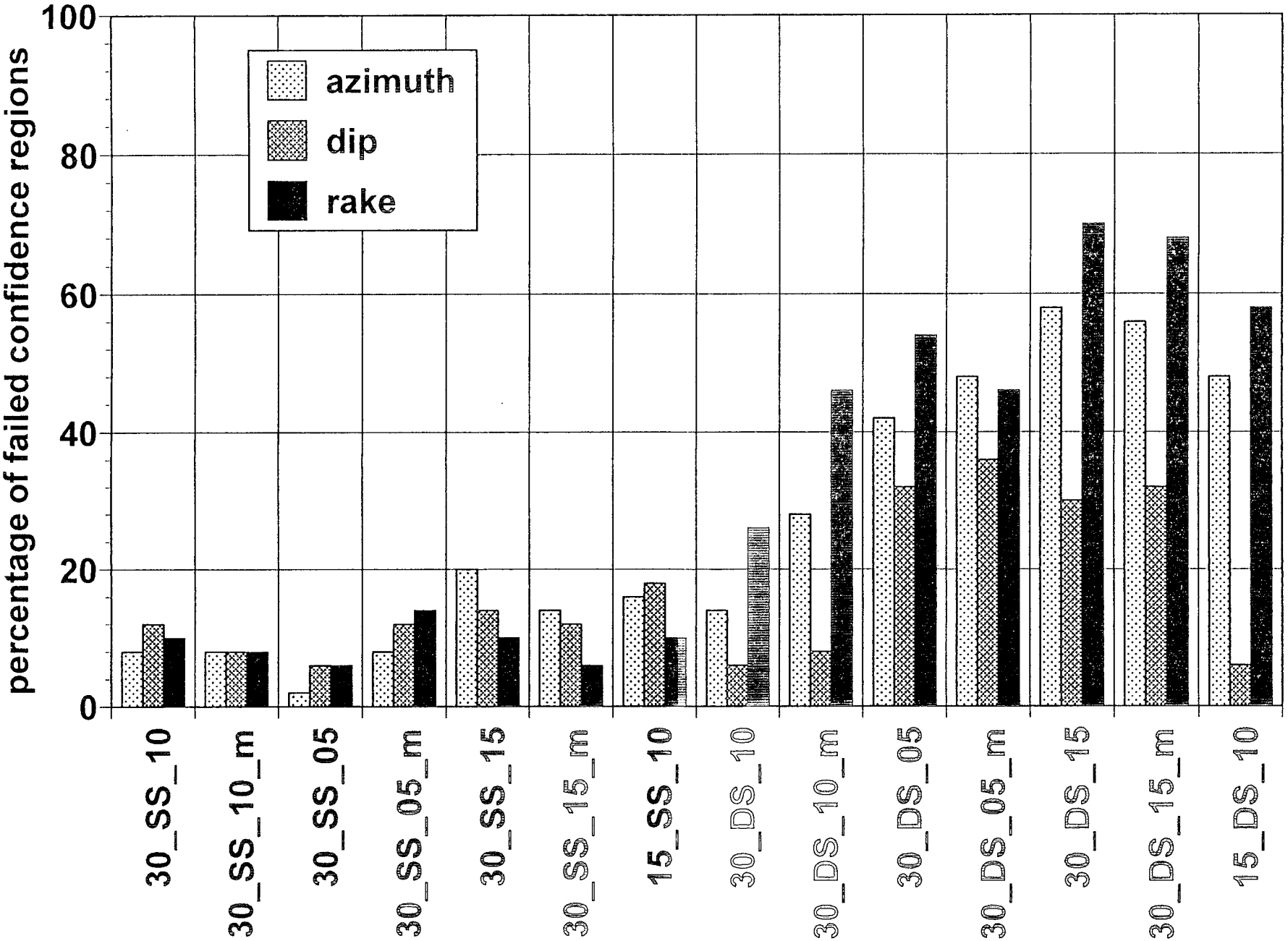

Figure 9-11. Percentage of cases in which the confidence bars failed to cover the true parameter for 14 simulated suites of 50 earthquakes with various constraints (see text).

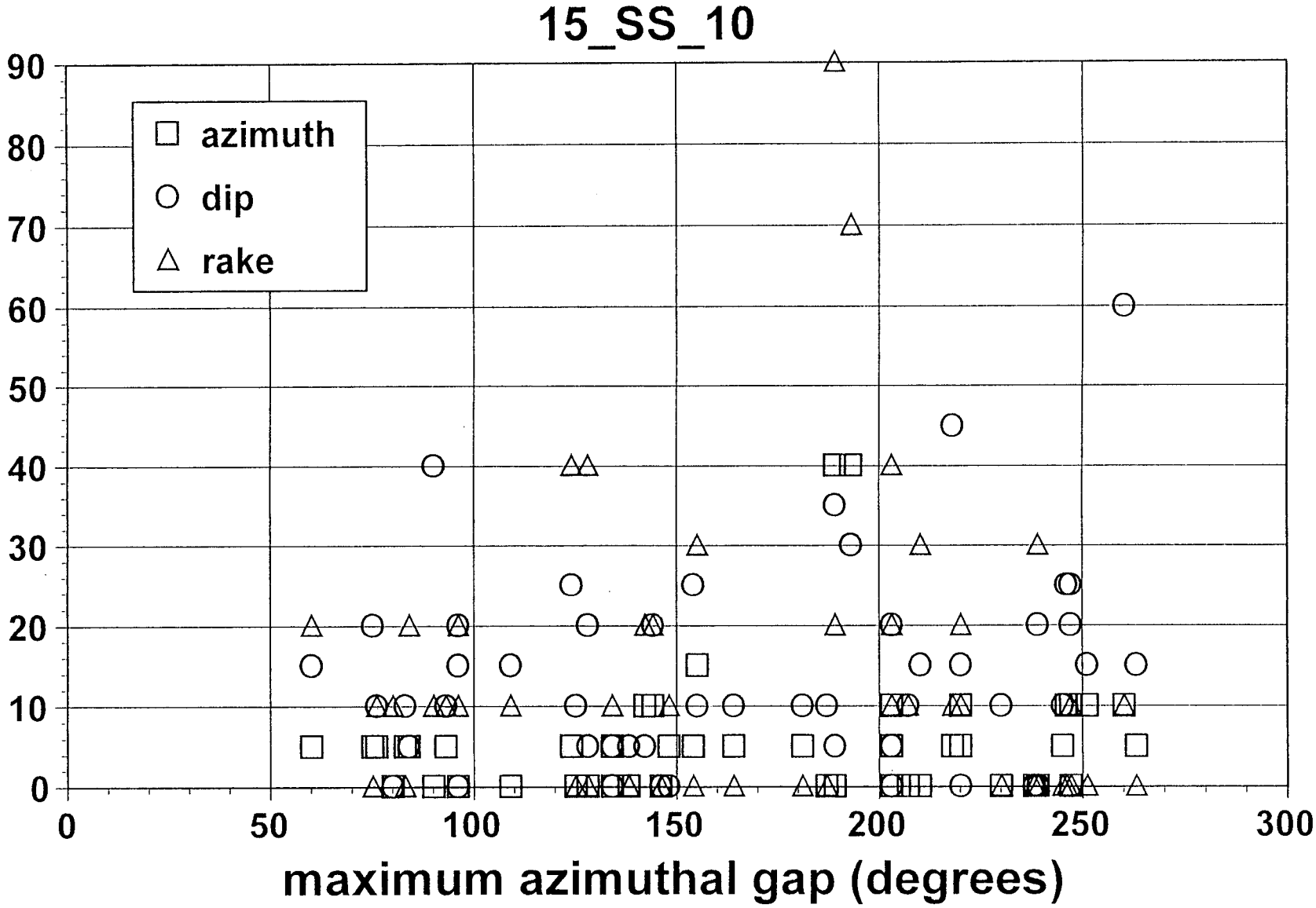

Figure 9-12. Mean errors in the estimated focal mechanism parameters versus maximum azimuthal gap in the station configuration around the epicenter for 50 simulated earthquakes at 10 km depth with strike-slip mechanism as recorded by 15 stations.

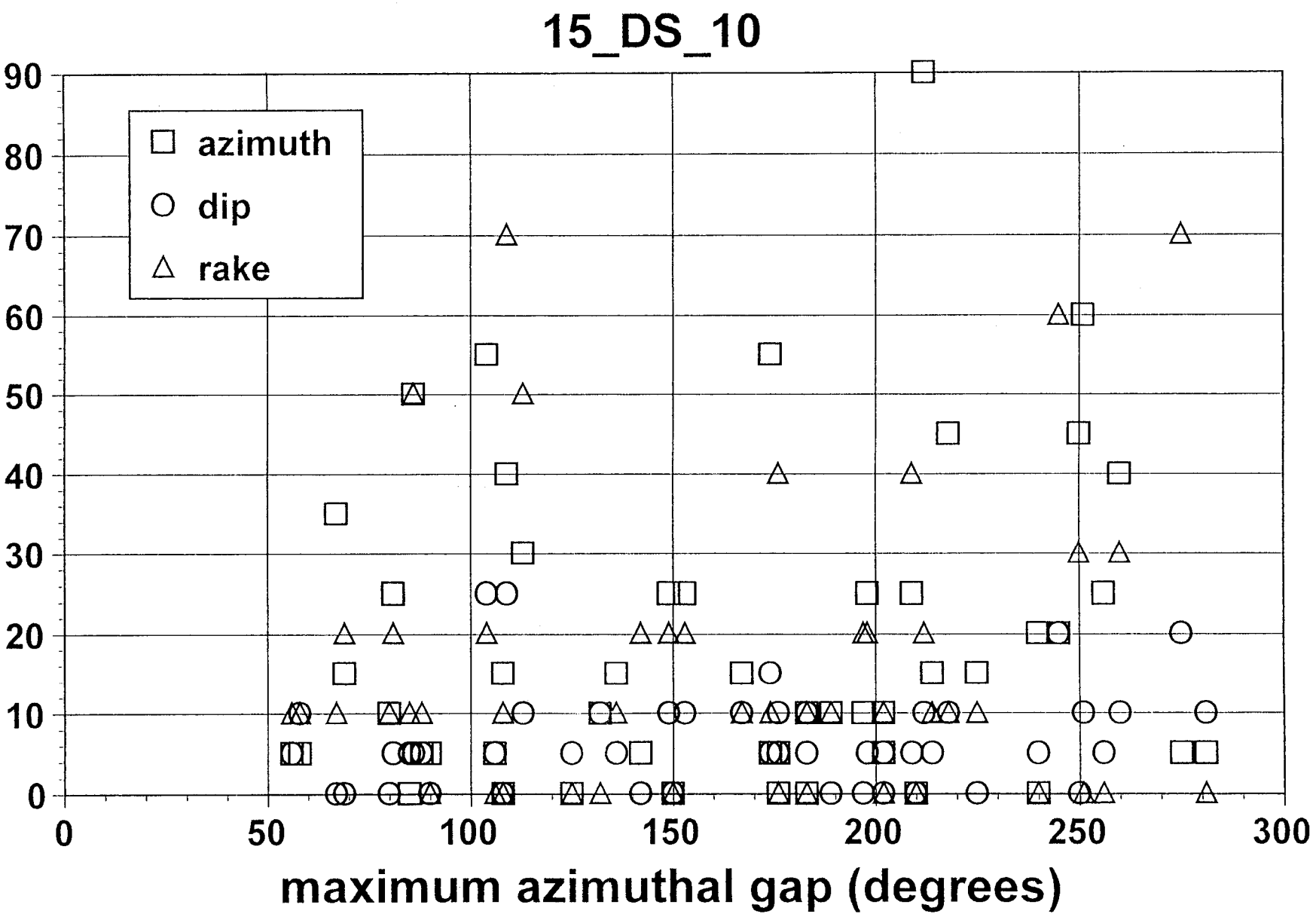

Figure 9-13. Mean errors in the estimated focal mechanism parameters versus maximum azimuthal gap in the station configuration around the epicenter for 50 simulated earthquakes at 10 km depth with dip-slip mechanism as recorded by 15 stations.

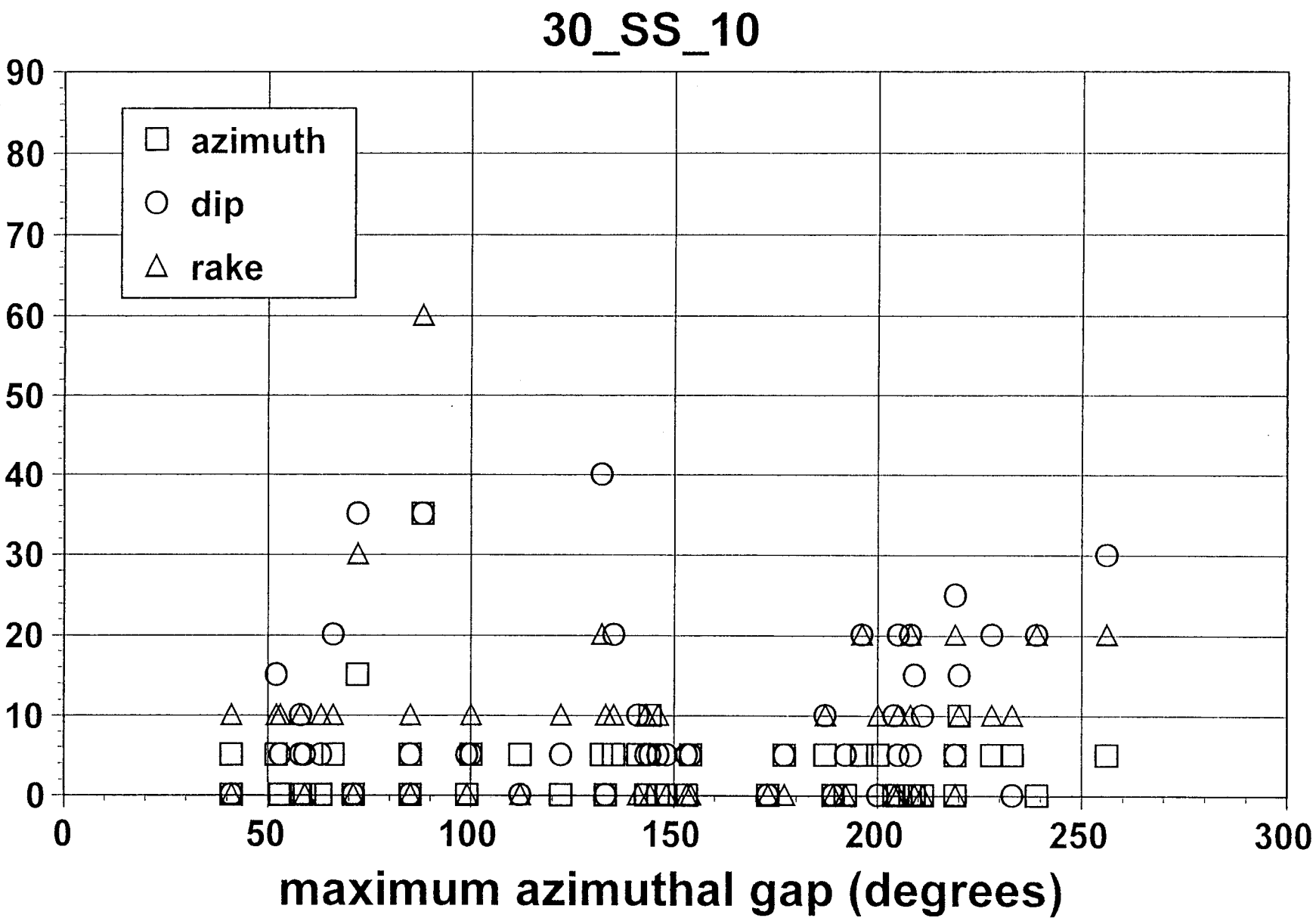

Figure 9-14. Mean errors in the estimated focal mechanism parameters versus maximum azimuthal gap in the station configuration around the epicenter for 50 simulated earthquakes at 10 km depth with strike-slip mechanism as recorded by 30 stations.

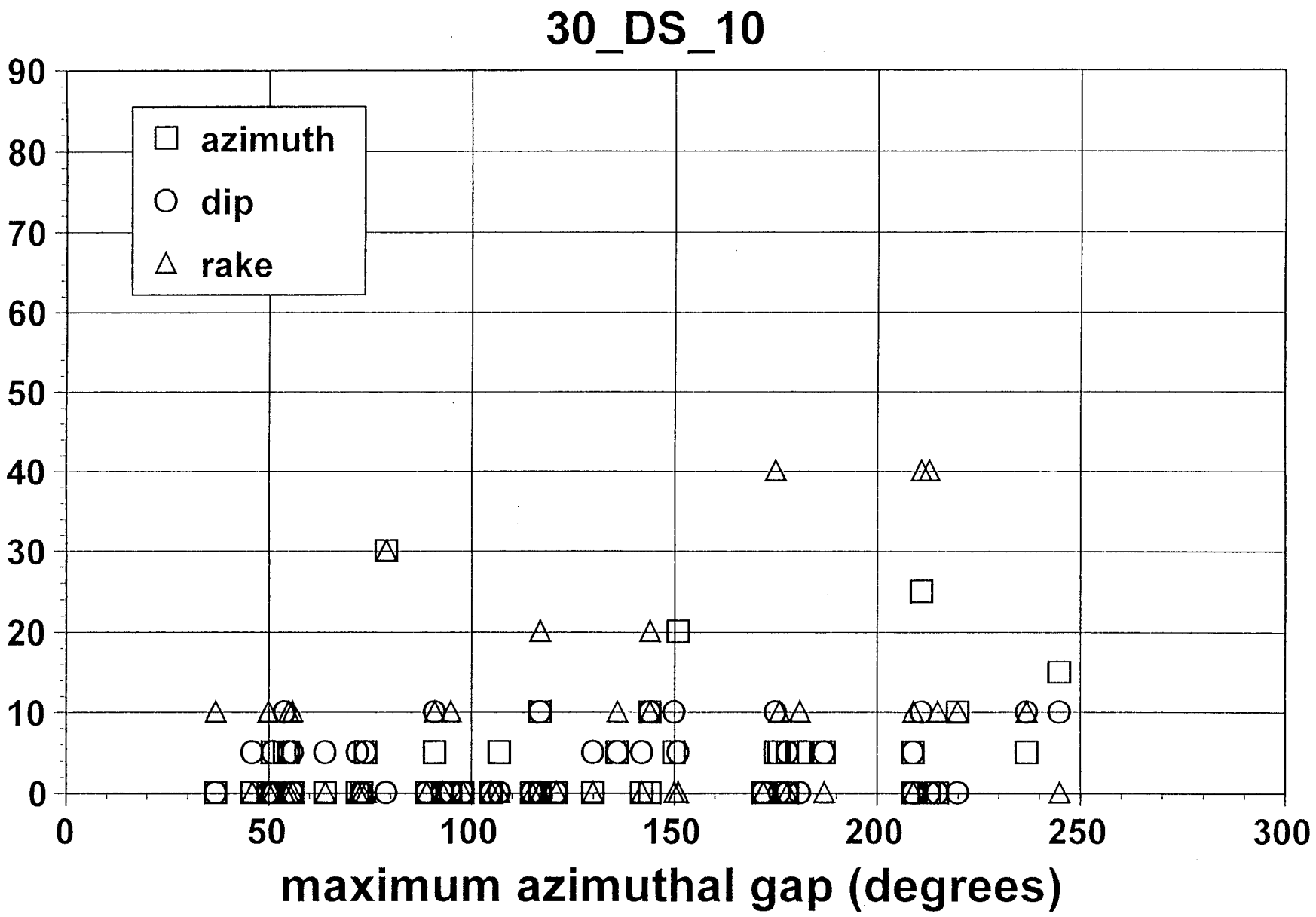

Figure 9-15. Mean errors in the estimated focal mechanism parameters versus maximum azimuthal gap in the station configuration around the epicenter for 50 simulated earthquakes at 10 km depth with dip-slip mechanism as recorded by 30 stations.

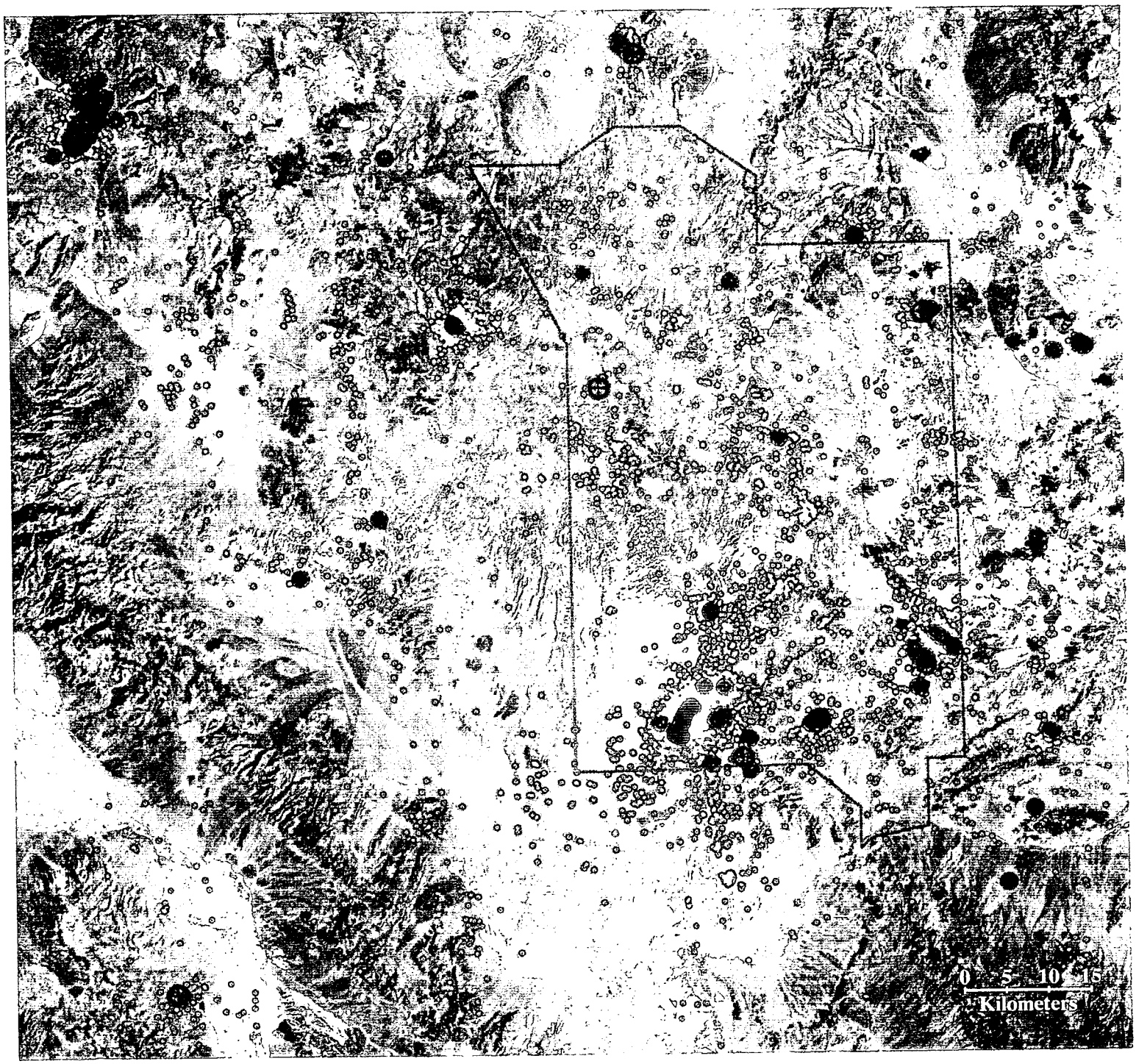

Figure 10-1. Relocated earthquakes 1992-1999.

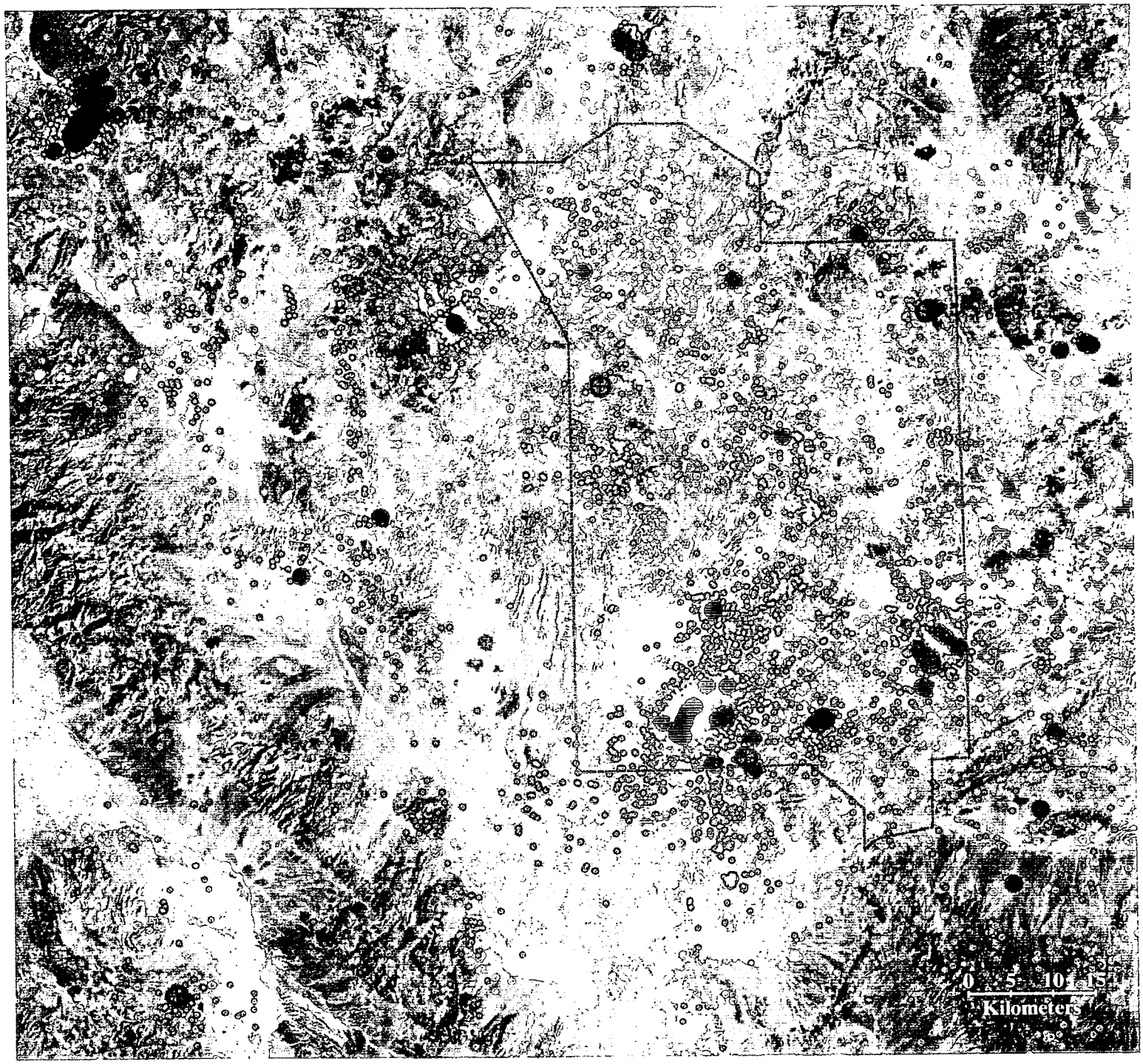

Figure 10-2. Relocated earthquakes 1992-1999 (red) and historical earthquakes 1868-1992 (yellow).

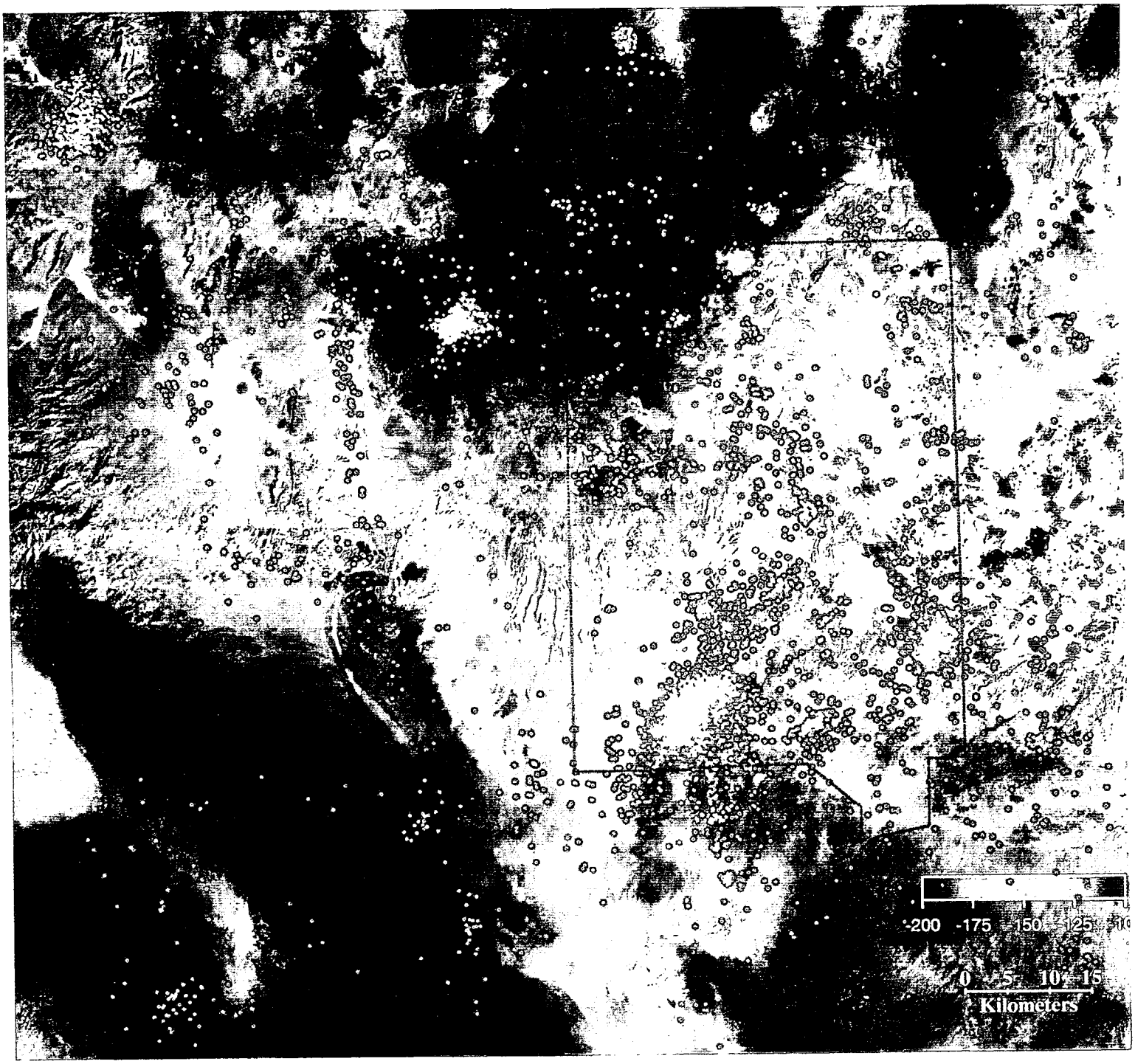

Figure 10-3. Relocated earthquakes 1992-1999 on color-shaded Bouguer gravity field.

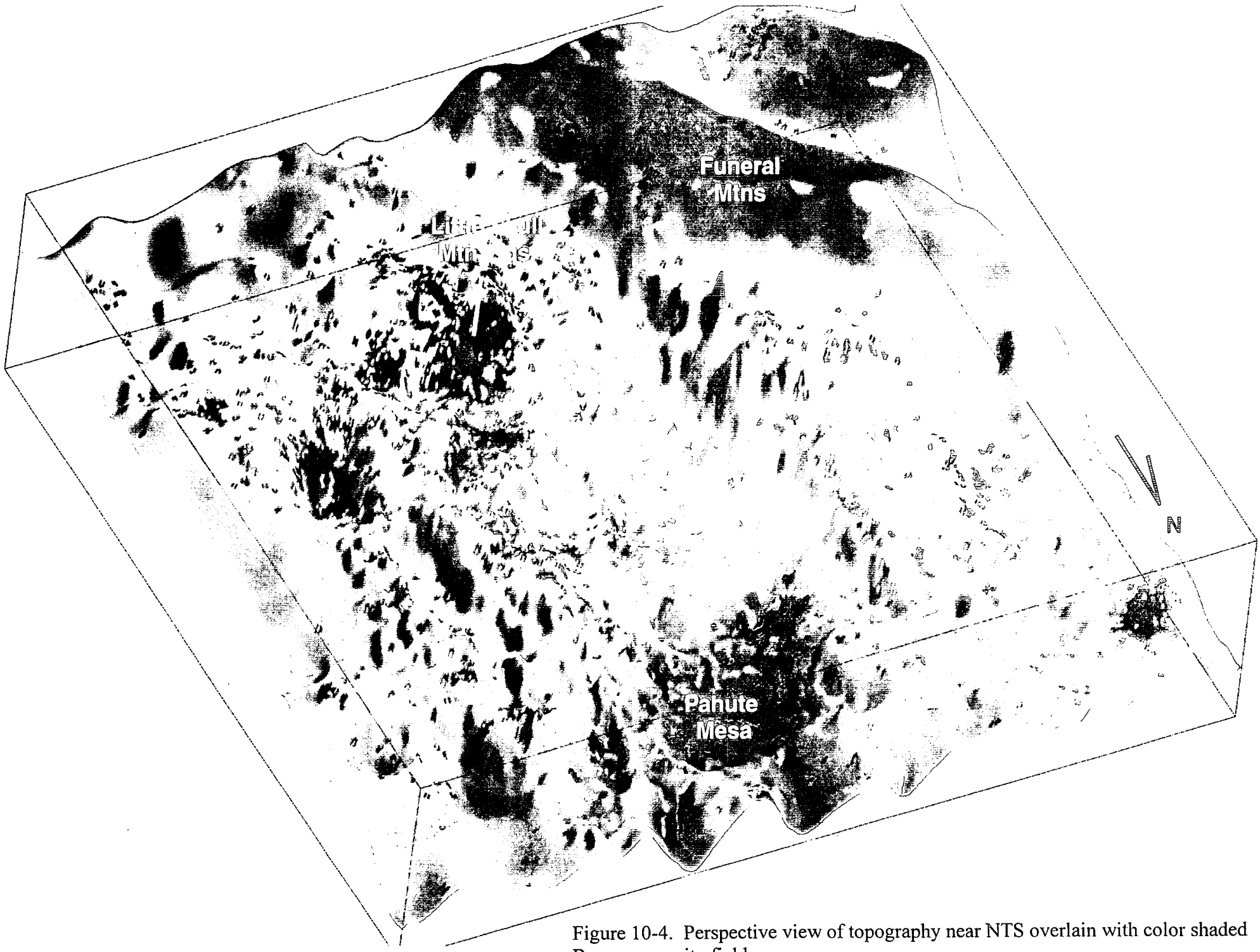

Figure 10-4. Perspective view of topography near NTS overlain with color shaded Bouguer gravity field.

Yucca Mountain Strong Motion Network
Non-Telemetered Stations
In Operation Since 1993

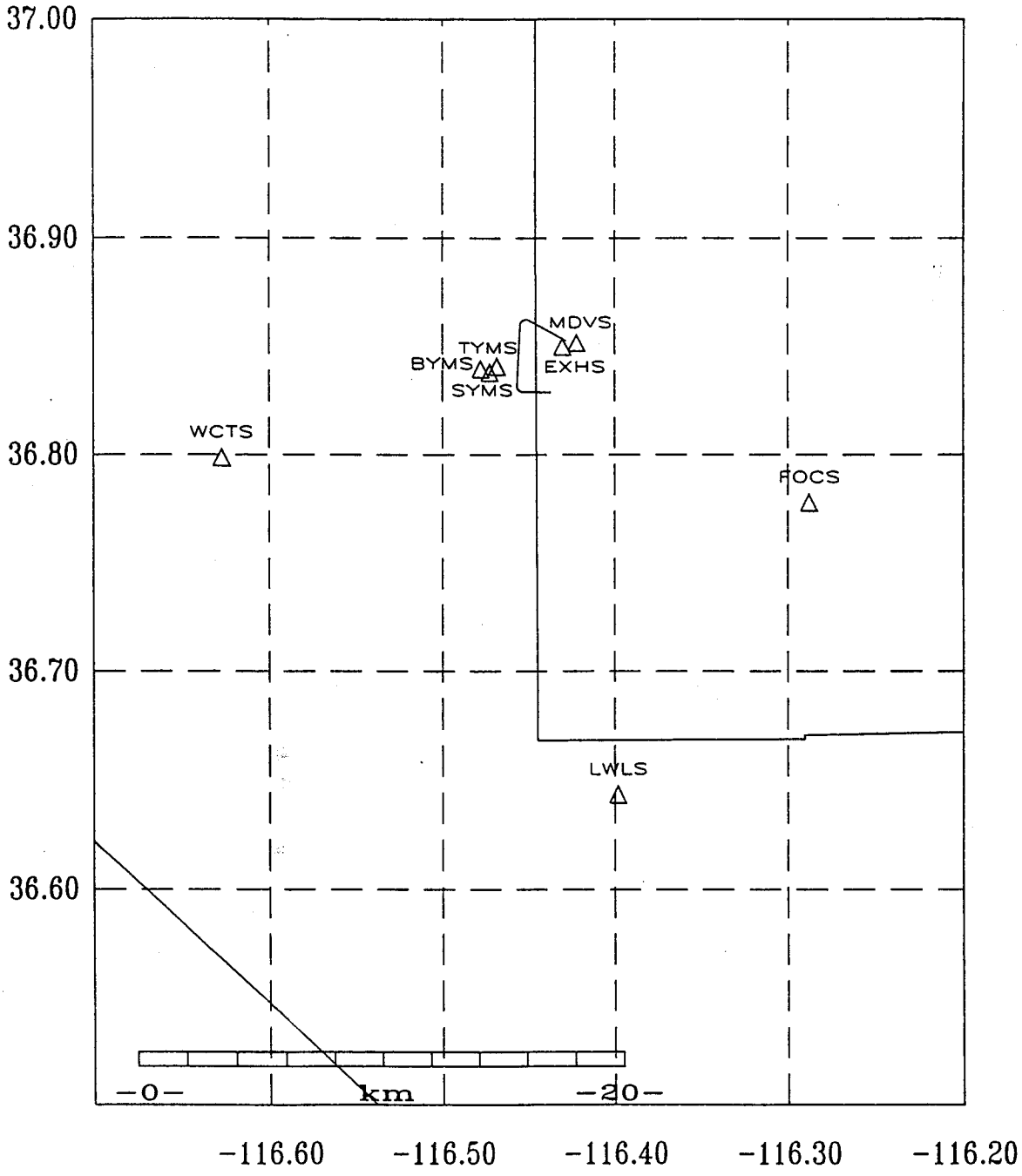

Figure 11-1

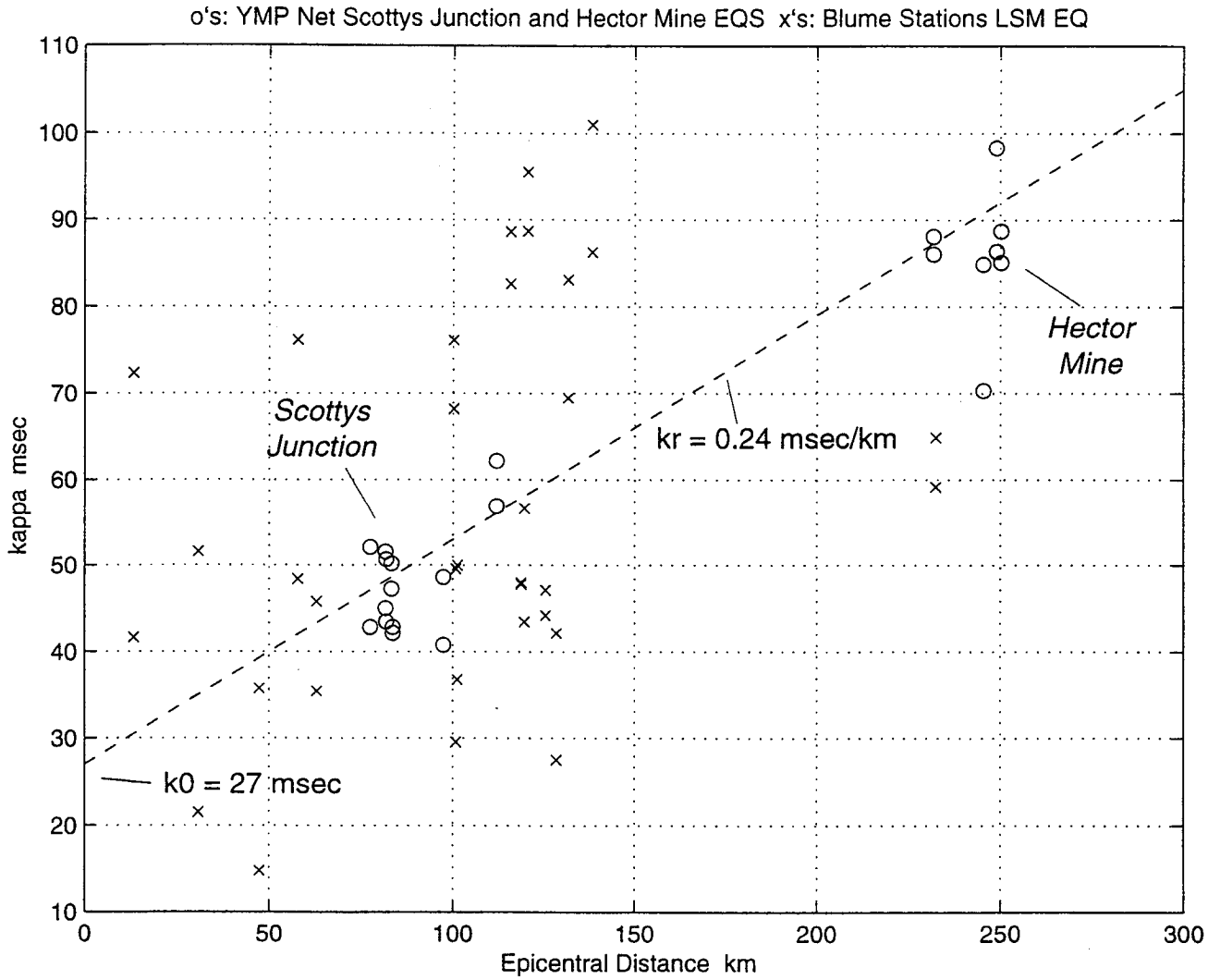

Linear fit to only the Hector Mine and Scottys Junction earthquake data recorded at YMP Strong Motion Stations. Blume stations shown for reference to the scatter in kappa for that data set.

Figure 12-1. Kappa values (k_T) determined from strong-motion stations.

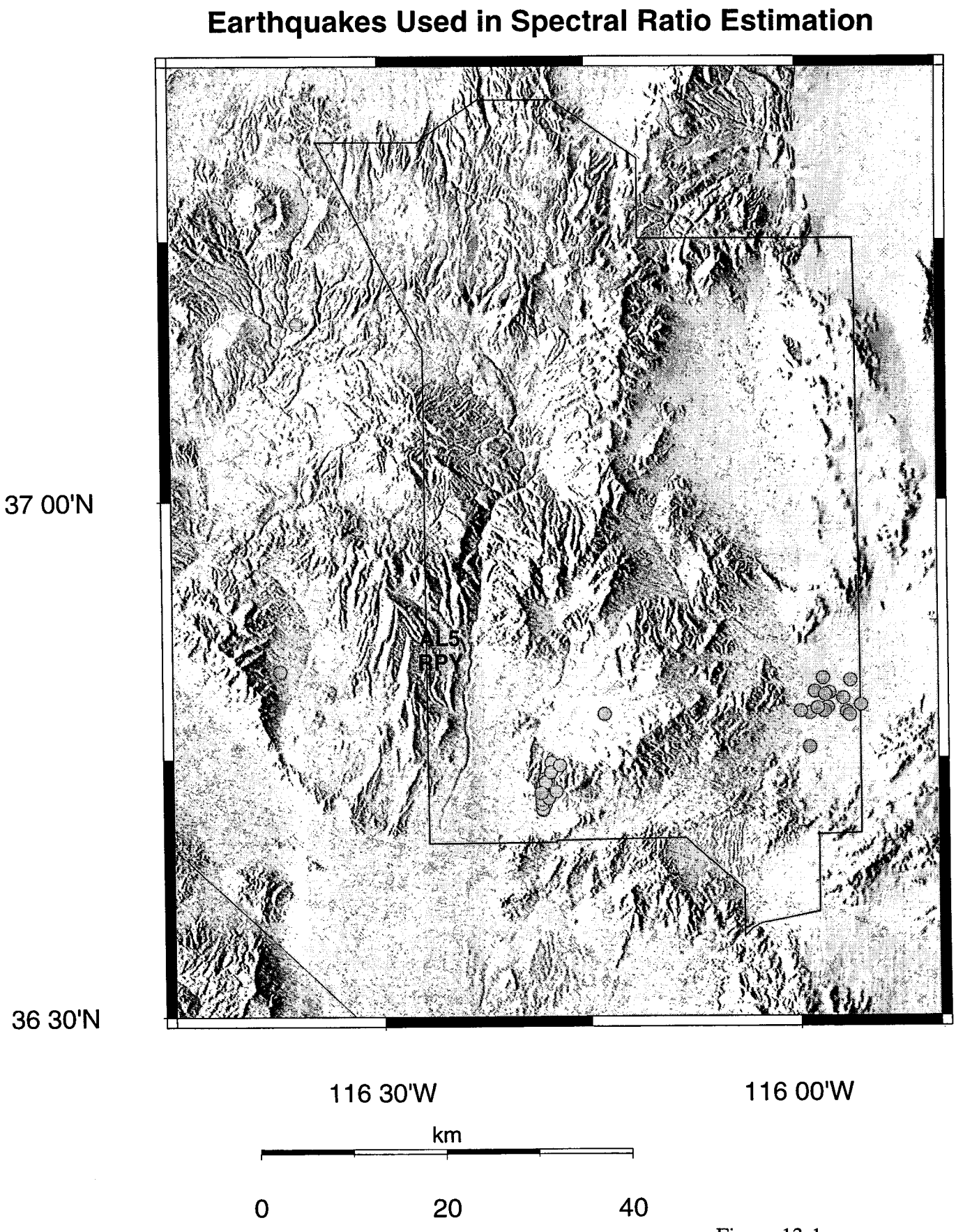
Earthquakes Used in Spectral Ratio Estimation
37 00'N
AL5
RPY
36 30'N
116 30'W
116 00'W
km
0
20
40

Figure 13-1

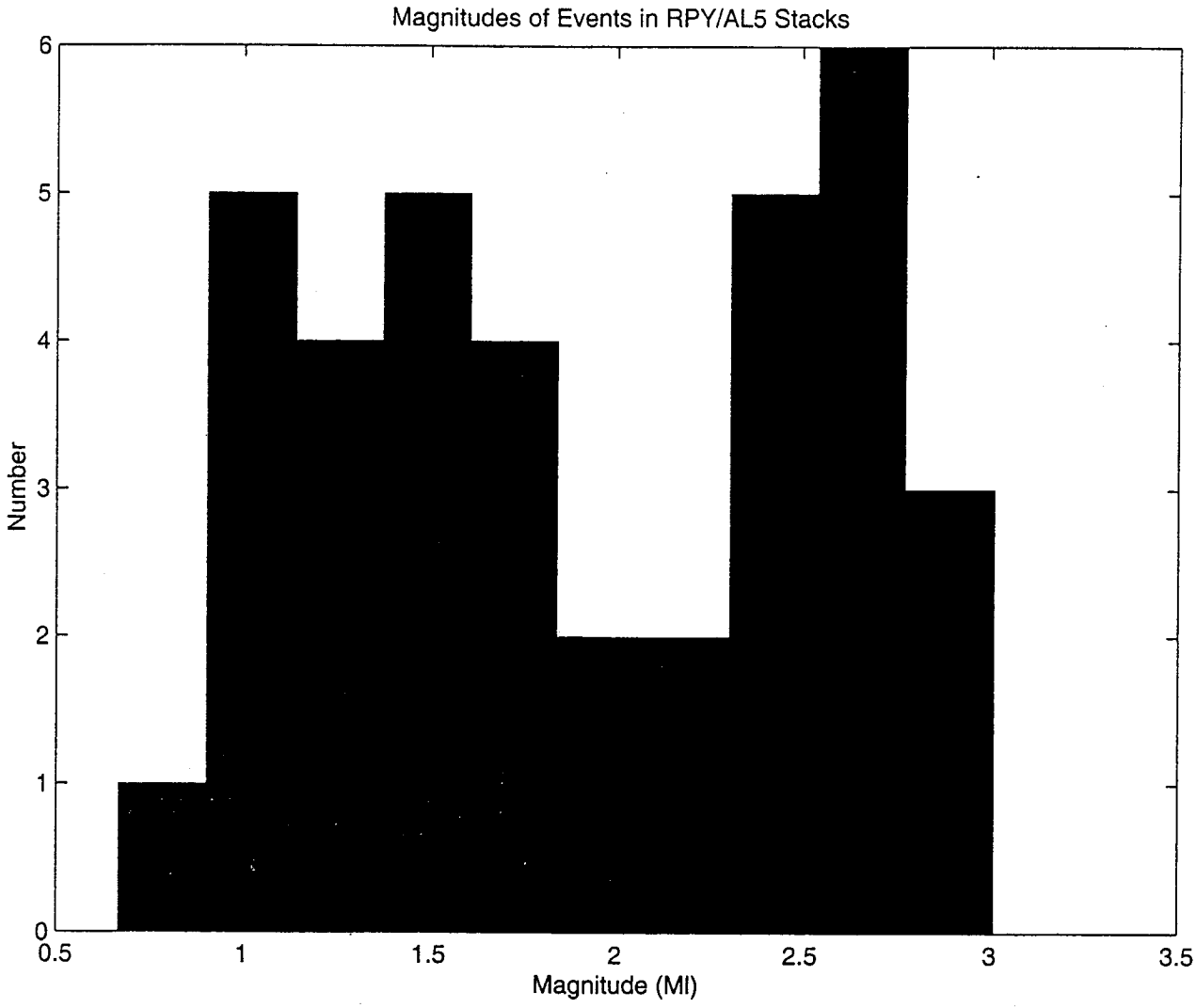
Magnitudes of Events in RPY/AL5 Stacks
Number
Magnitude (Ml)
0
1
2
3
4
5
6
0.5
1
1.5
2
2.5
3
3.5

Figure 13-2

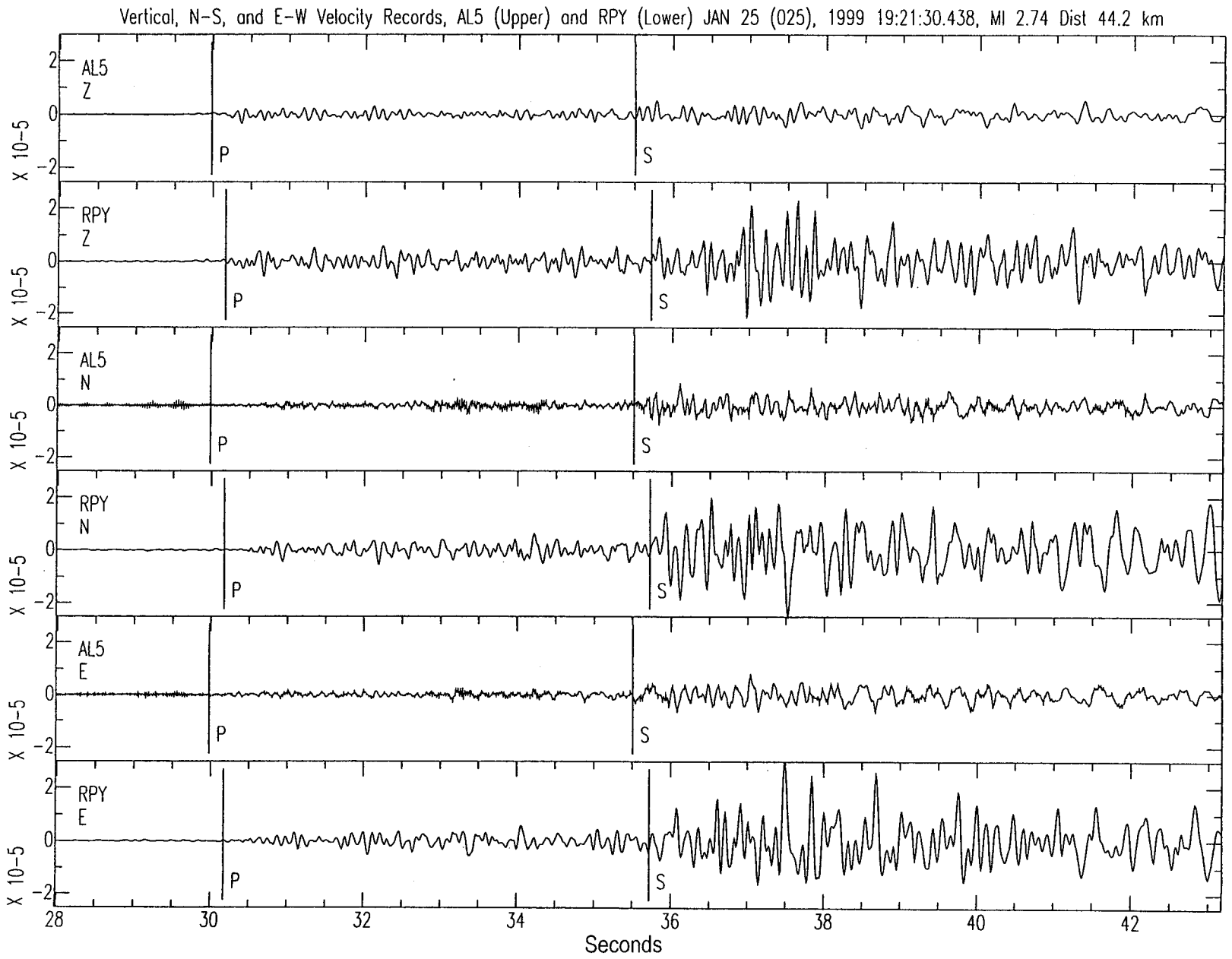
Vertical, N-S, and E-W Velocity Records, AL5 (Upper) and RPY (Lower) JAN 25 (025), 1999 19:21:30.438, MI 2.74 Dist 44.2 km
AL5
Z
RPY
Z
AL5
N
RPY
N
AL5
E
RPY
E
P
S
X 10-5
2
0
-2
28
30
32
34
36
38
40
42
Seconds

Figure 13-3

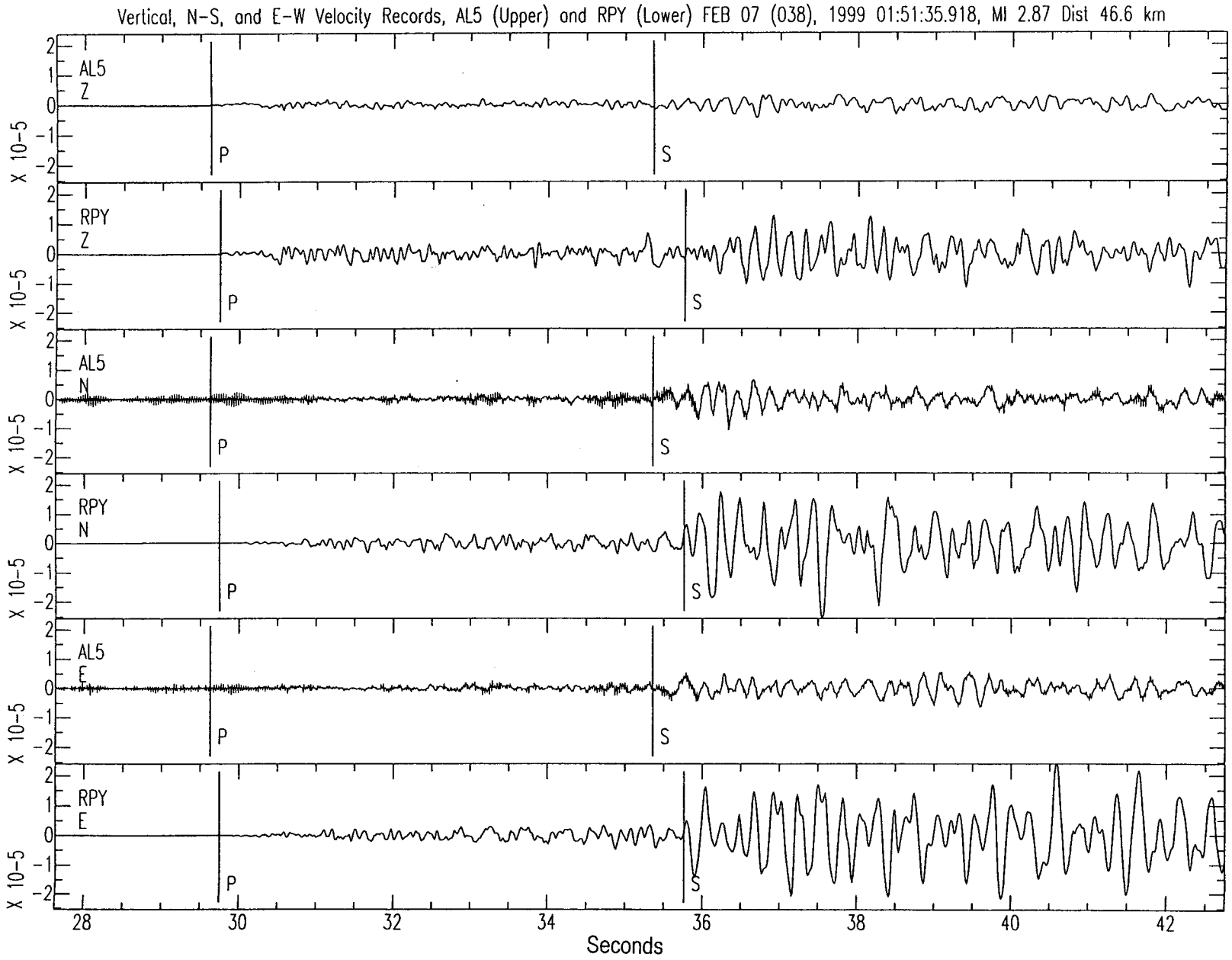
Vertical, N-S, and E-W Velocity Records, AL5 (Upper) and RPY (Lower) FEB 07 (038), 1999 01:51:35.918, MI 2.87 Dist 46.6 km
AL5
Z
RPY
Z
AL5
N
RPY
N
AL5
E
RPY
E
P
S
X 10-5
2
1
0
-1
-2
28
30
32
34
36
38
40
42
Seconds

Figure 13-4a

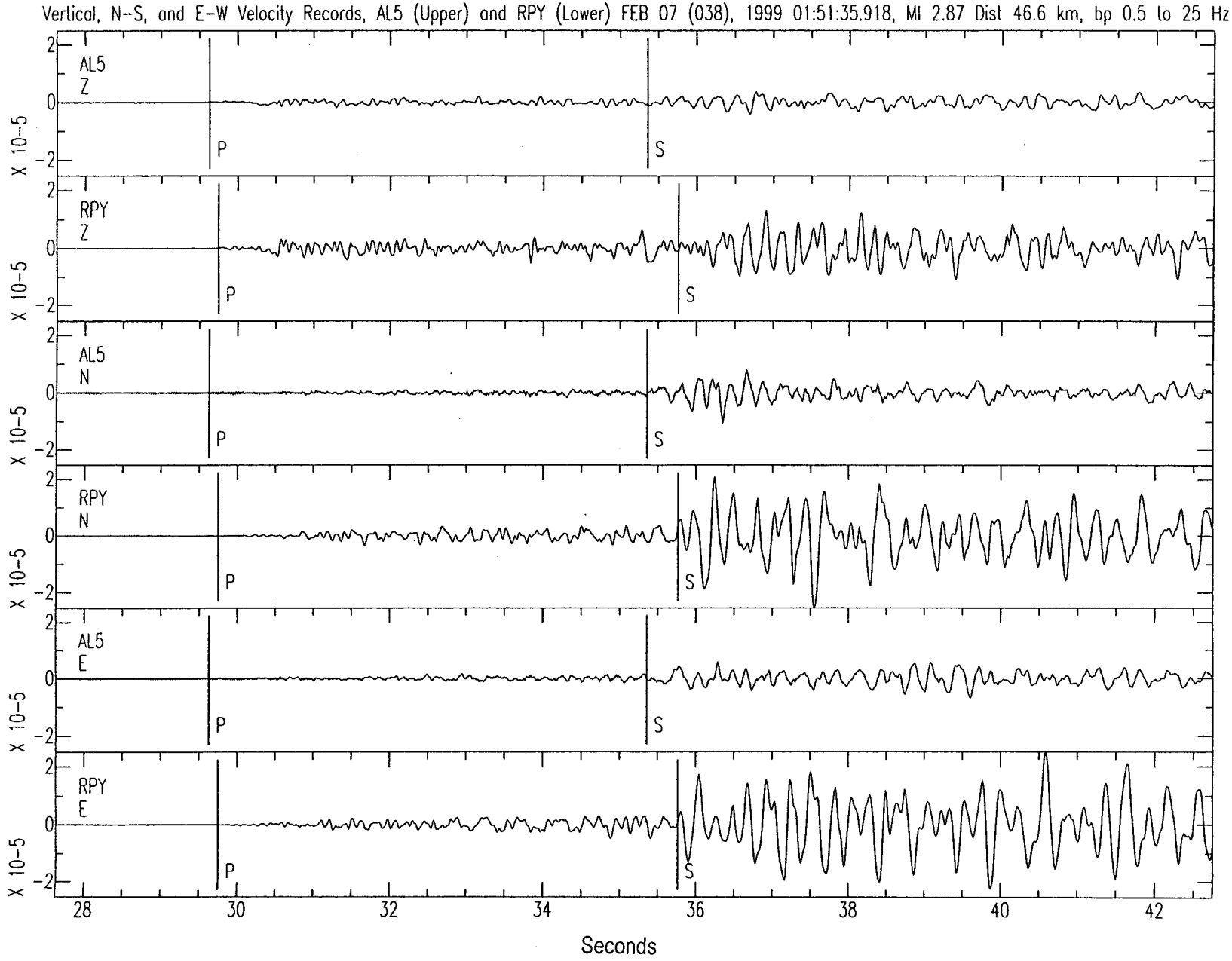
Vertical, N-S, and E-W Velocity Records, AL5 (Upper) and RPY (Lower) FEB 07 (038), 1999 01:51:35.918, MI 2.87 Dist 46.6 km, bp 0.5 to 25 Hz
AL5 Z
RPY Z
AL5 N
RPY N
AL5 E
RPY E
P
S
X 10-5
2
0
-2
28
30
32
34
36
38
40
42
Seconds

Figure 13-4b

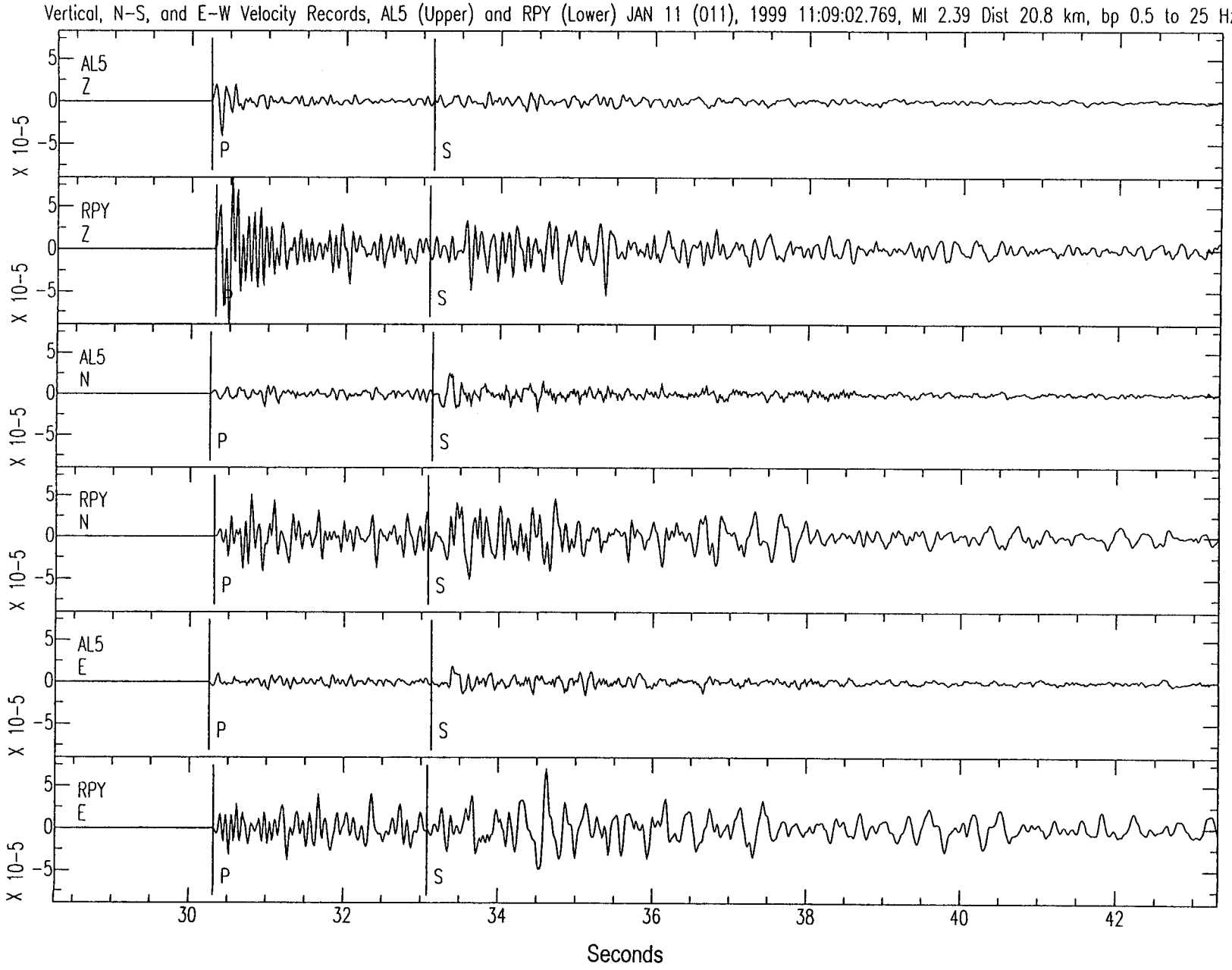
Vertical, N-S, and E-W Velocity Records, AL5 (Upper) and RPY (Lower) JAN 11 (011), 1999 11:09:02.769, MI 2.39 Dist 20.8 km, bp 0.5 to 25 Hz
AL5
Z
RPY
Z
AL5
N
RPY
N
AL5
E
RPY
E
P
S
X 10-5
5
0
-5
30
32
34
36
38
40
42
Seconds

Figure 13-5

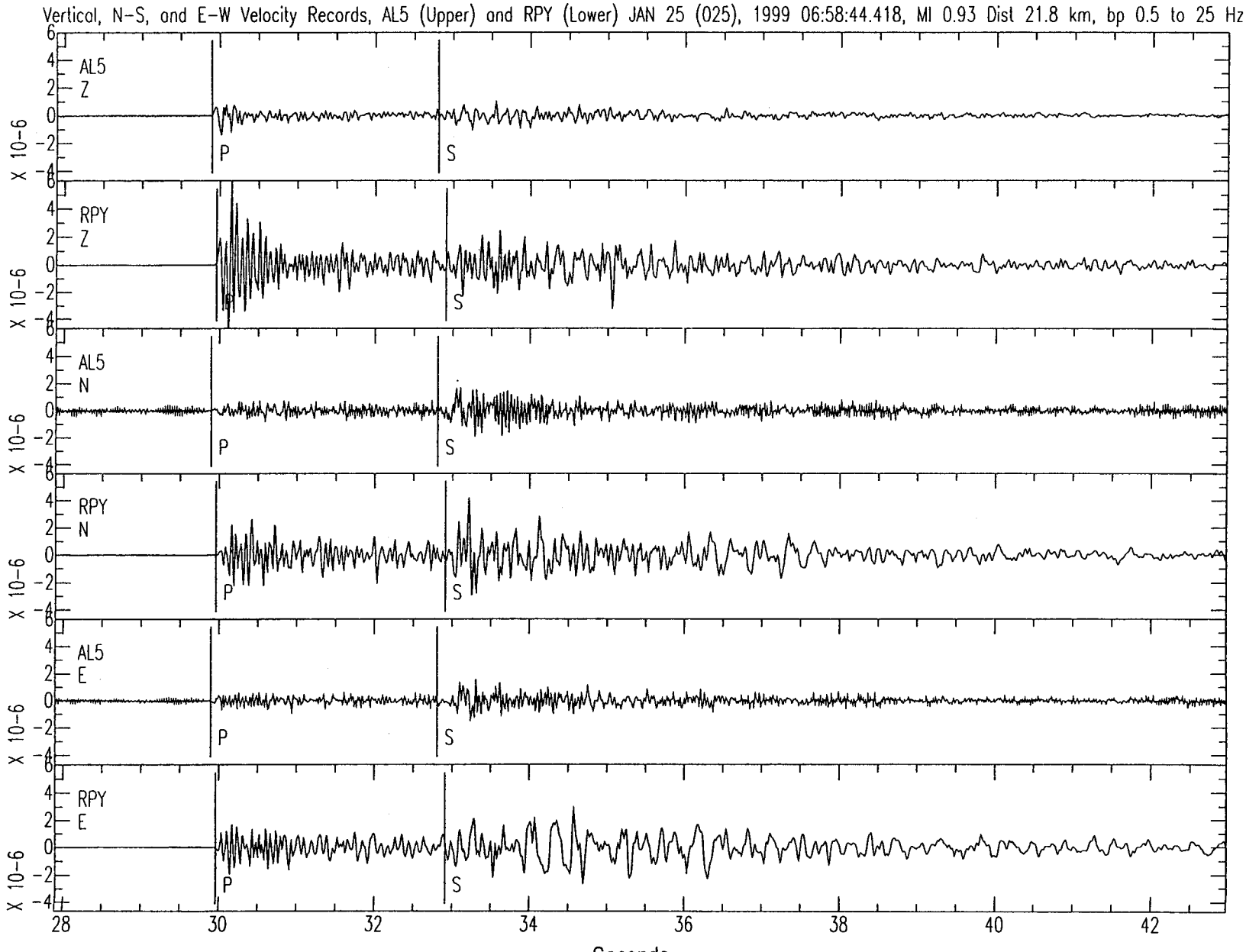
Vertical, N-S, and E-W Velocity Records, AL5 (Upper) and RPY (Lower) JAN 25 (025), 1999 06:58:44.418, MI 0.93 Dist 21.8 km, bp 0.5 to 25 Hz
AL5 Z
RPY Z
AL5 N
RPY N
AL5 E
RPY E
P
S
X 10-6
6
4
2
0
-2
-4
28
30
32
34
36
38
40
42
Seconds

Figure 13-6

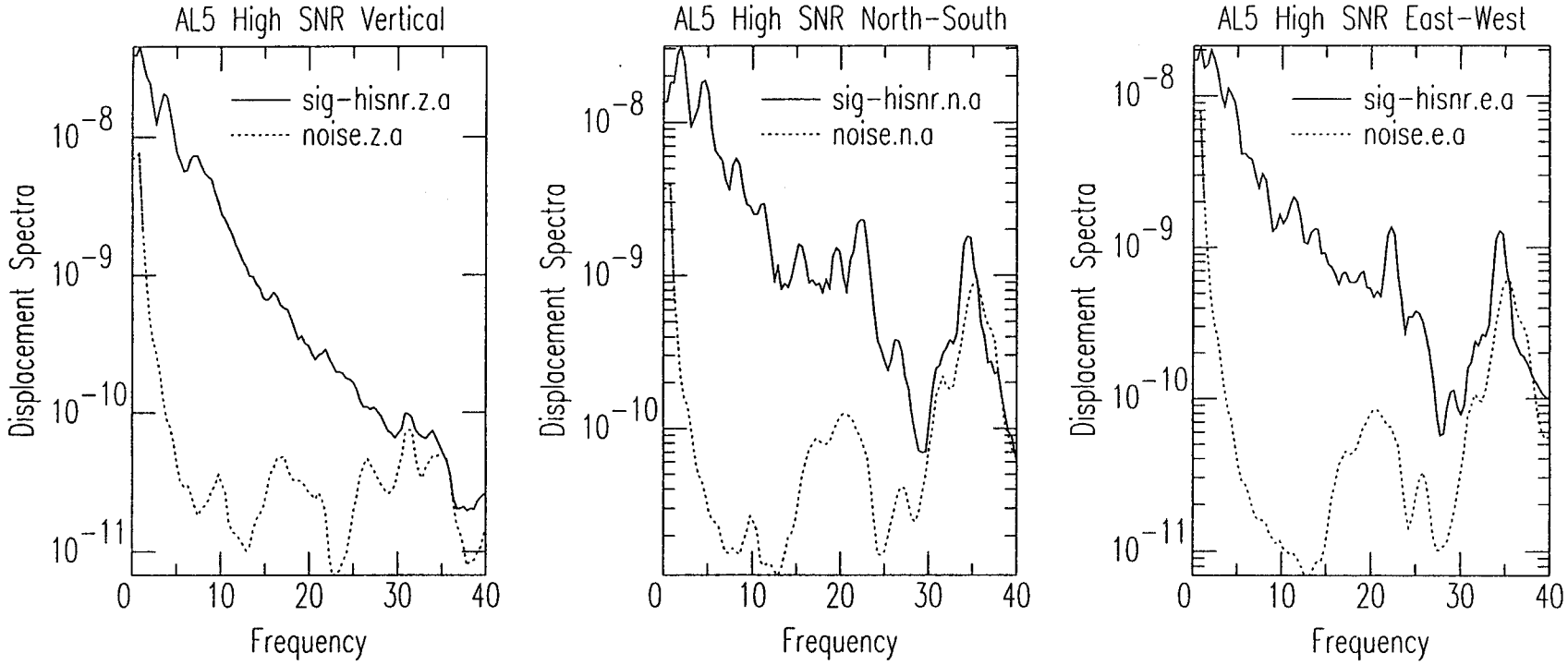
AL5 High SNR Vertical
sig-hisnr.z.a
noise.z.a
Displacement Spectra
10^{-8}
10^{-9}
10^{-10}
10^{-11}
0
10
20
30
40
Frequency
AL5 High SNR North-South
sig-hisnr.n.a
noise.n.a
Displacement Spectra
10^{-8}
10^{-9}
10^{-10}
0
10
20
30
40
Frequency
AL5 High SNR East-West
sig-hisnr.e.a
noise.e.a
Displacement Spectra
10^{-8}
10^{-9}
10^{-10}
10^{-11}
0
10
20
30
40
Frequency

Figure 13-7

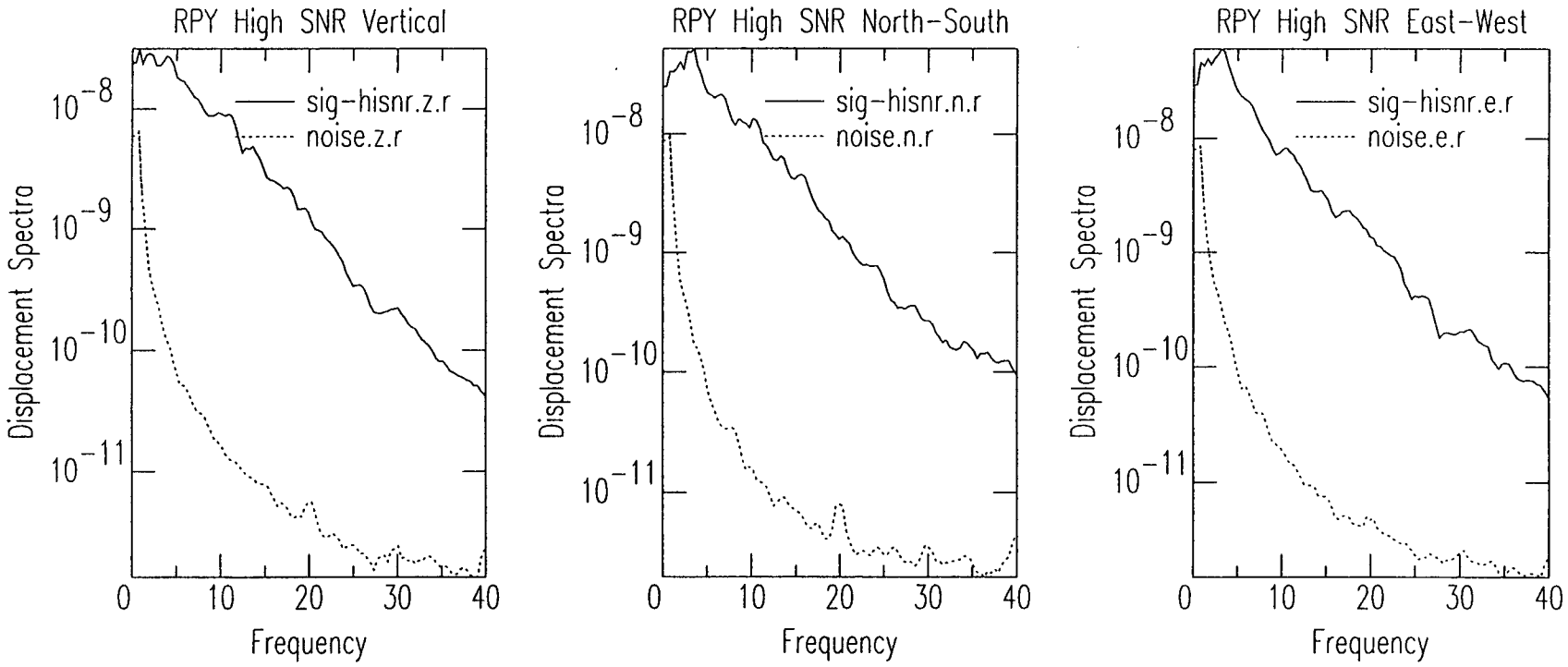
RPY High SNR Vertical
sig-hisnr.z.r
noise.z.r
Displacement Spectra
10^{-8}
10^{-9}
10^{-10}
10^{-11}
0
10
20
30
40
Frequency
RPY High SNR North-South
sig-hisnr.n.r
noise.n.r
Displacement Spectra
10^{-8}
10^{-9}
10^{-10}
10^{-11}
0
10
20
30
40
Frequency
RPY High SNR East-West
sig-hisnr.e.r
noise.e.r
Displacement Spectra
10^{-8}
10^{-9}
10^{-10}
10^{-11}
0
10
20
30
40
Frequency

Figure 13-8

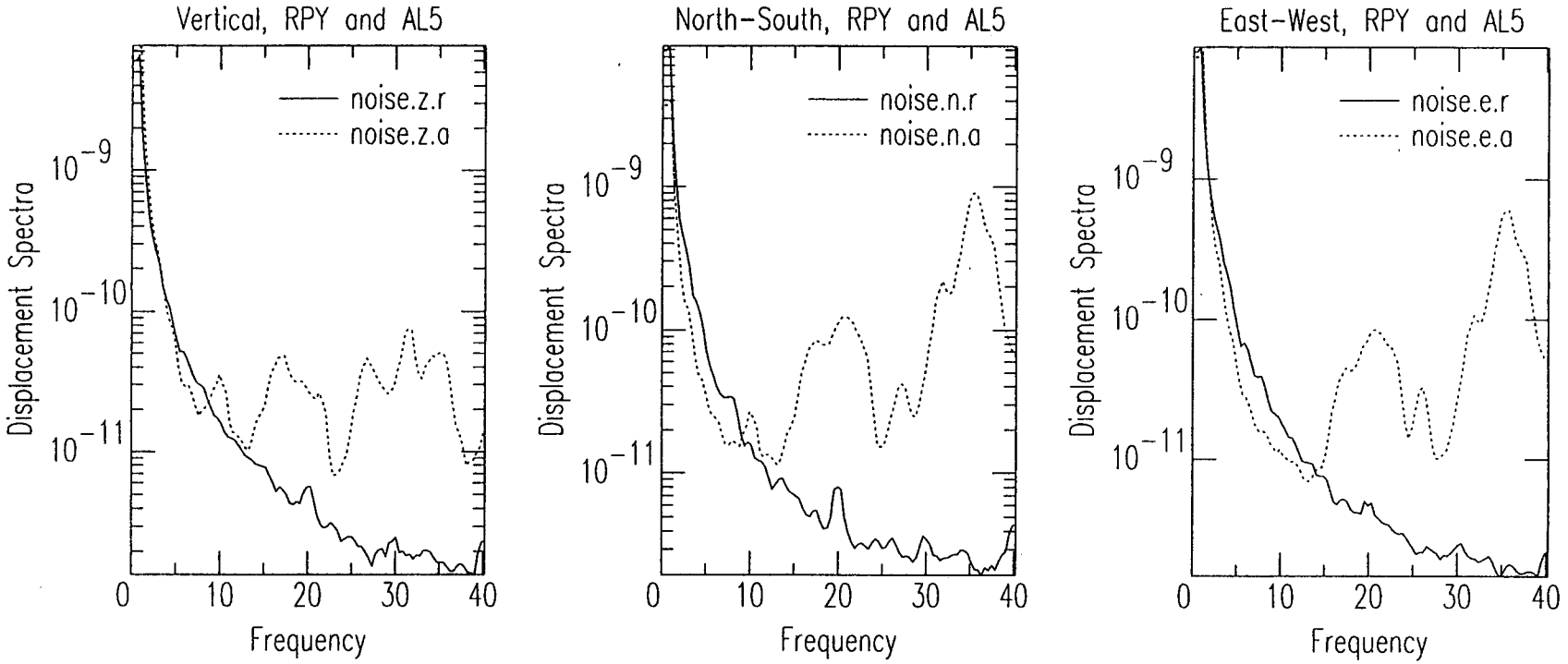
Vertical, RPY and AL5
noise.z.r
noise.z.a
Displacement Spectra
10^{-9}
10^{-10}
10^{-11}
0
10
20
30
40
Frequency
North-South, RPY and AL5
noise.n.r
noise.n.a
Displacement Spectra
10^{-9}
10^{-10}
10^{-11}
0
10
20
30
40
Frequency
East-West, RPY and AL5
noise.e.r
noise.e.a
Displacement Spectra
10^{-9}
10^{-10}
10^{-11}
0
10
20
30
40
Frequency

Figure 13-9

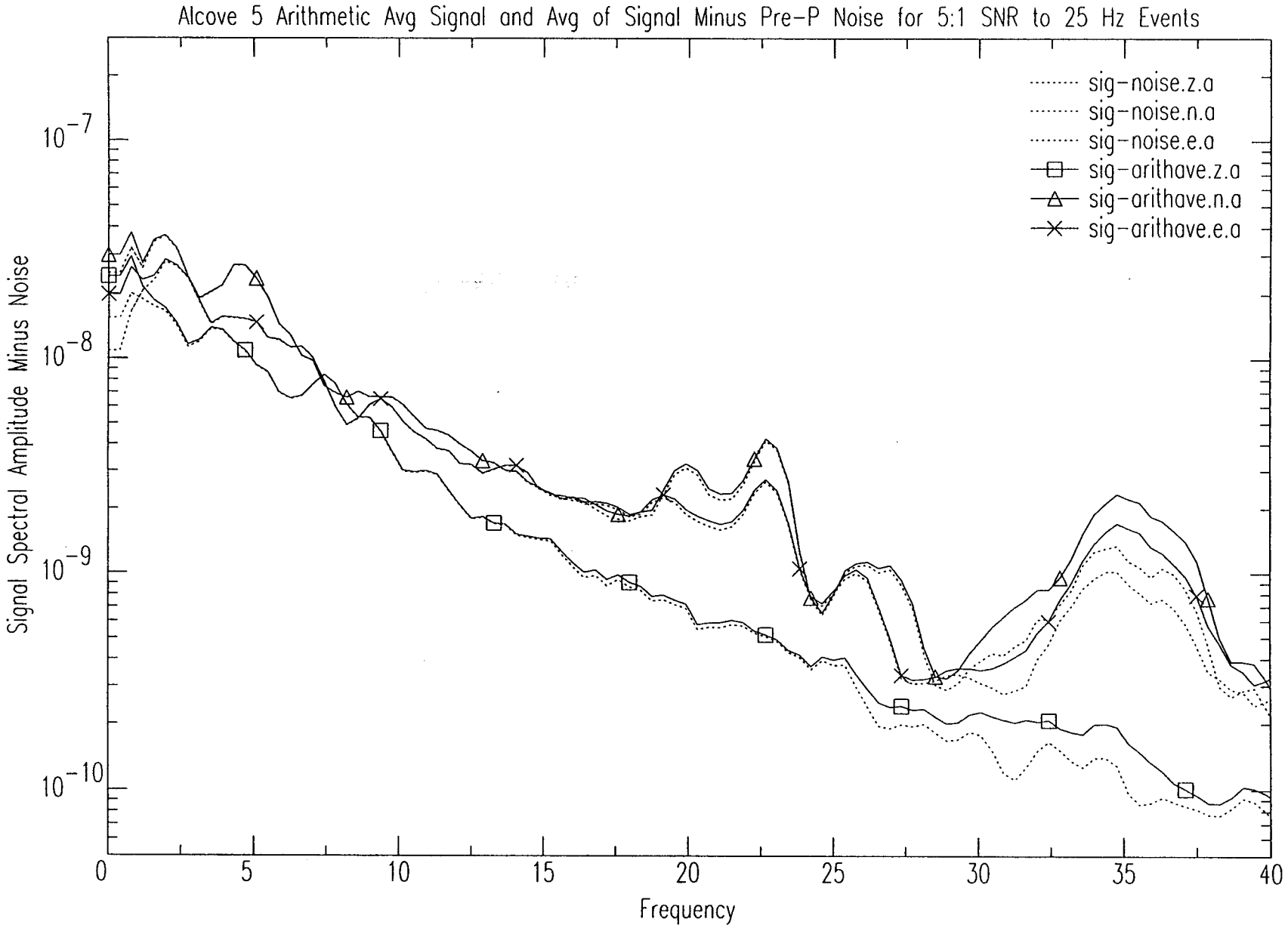
Alcove 5 Arithmetic Avg Signal and Avg of Signal Minus Pre-P Noise for 5:1 SNR to 25 Hz Events
sig-noise.z.a
sig-noise.n.a
sig-noise.e.a
sig-arithave.z.a
sig-arithave.n.a
sig-arithave.e.a
Signal Spectral Amplitude Minus Noise
10^{-7}
10^{-8}
10^{-9}
10^{-10}
0
5
10
15
20
25
30
35
40
Frequency

Figure 13-10

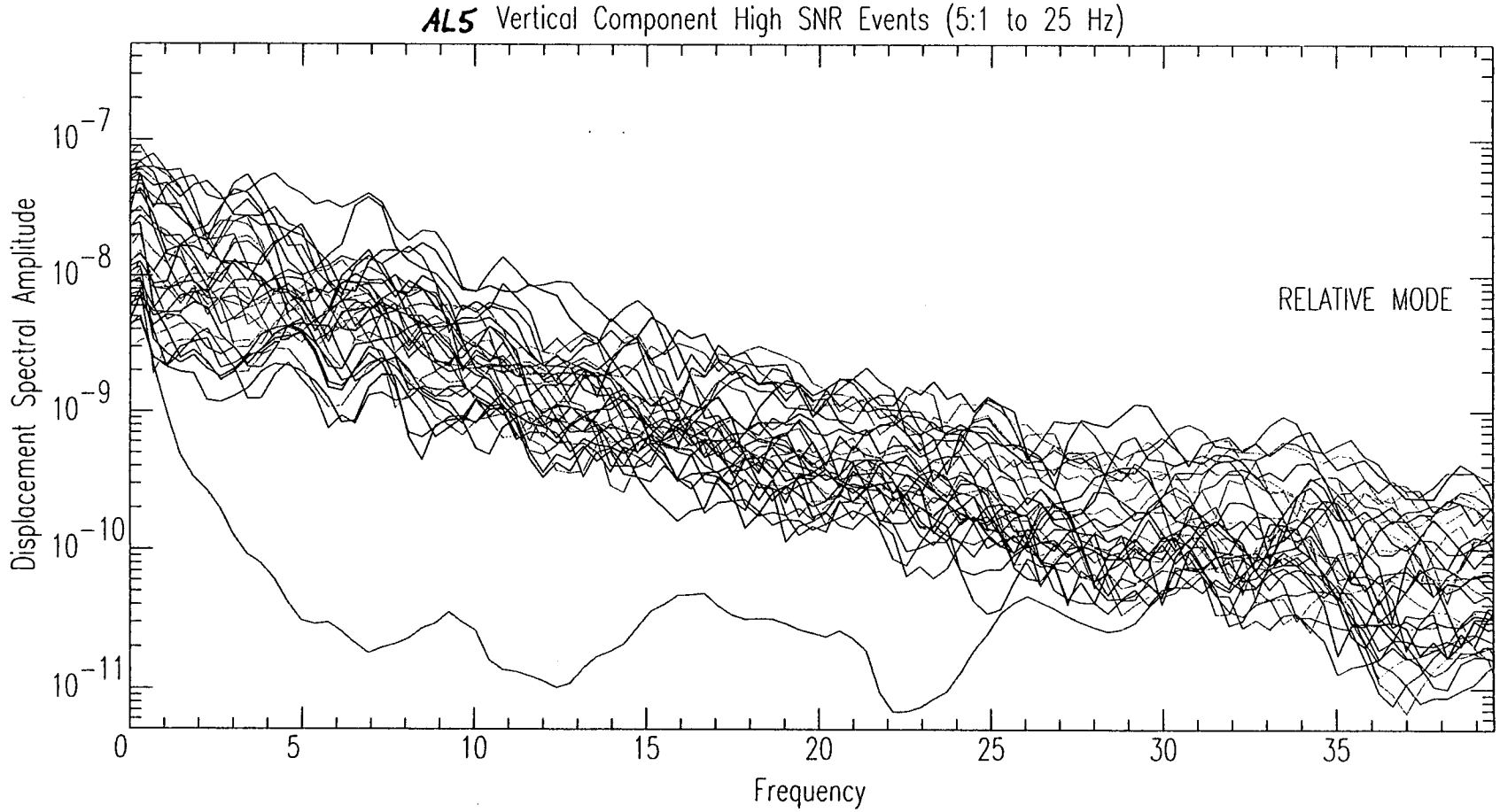
AL5 Vertical Component High SNR Events (5:1 to 25 Hz)
Displacement Spectral Amplitude
10^{-7}
10^{-8}
10^{-9}
10^{-10}
10^{-11}
RELATIVE MODE
0
5
10
15
20
25
30
35
Frequency

Figure 13-11

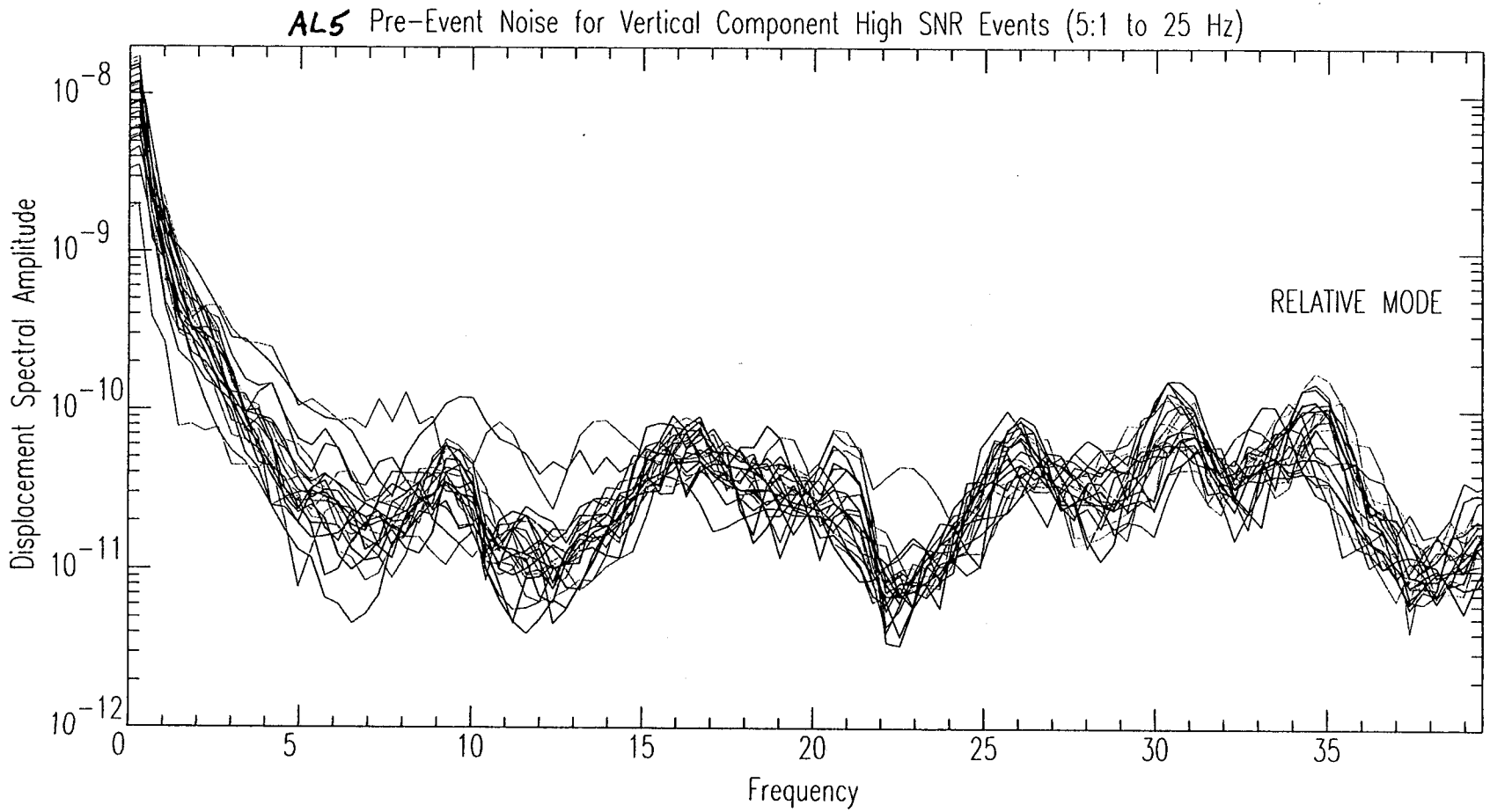
ALS Pre-Event Noise for Vertical Component High SNR Events (5:1 to 25 Hz)
Displacement Spectral Amplitude
10^{-8}
10^{-9}
10^{-10}
10^{-11}
10^{-12}
RELATIVE MODE
0
5
10
15
20
25
30
35
Frequency

Figure 13-12

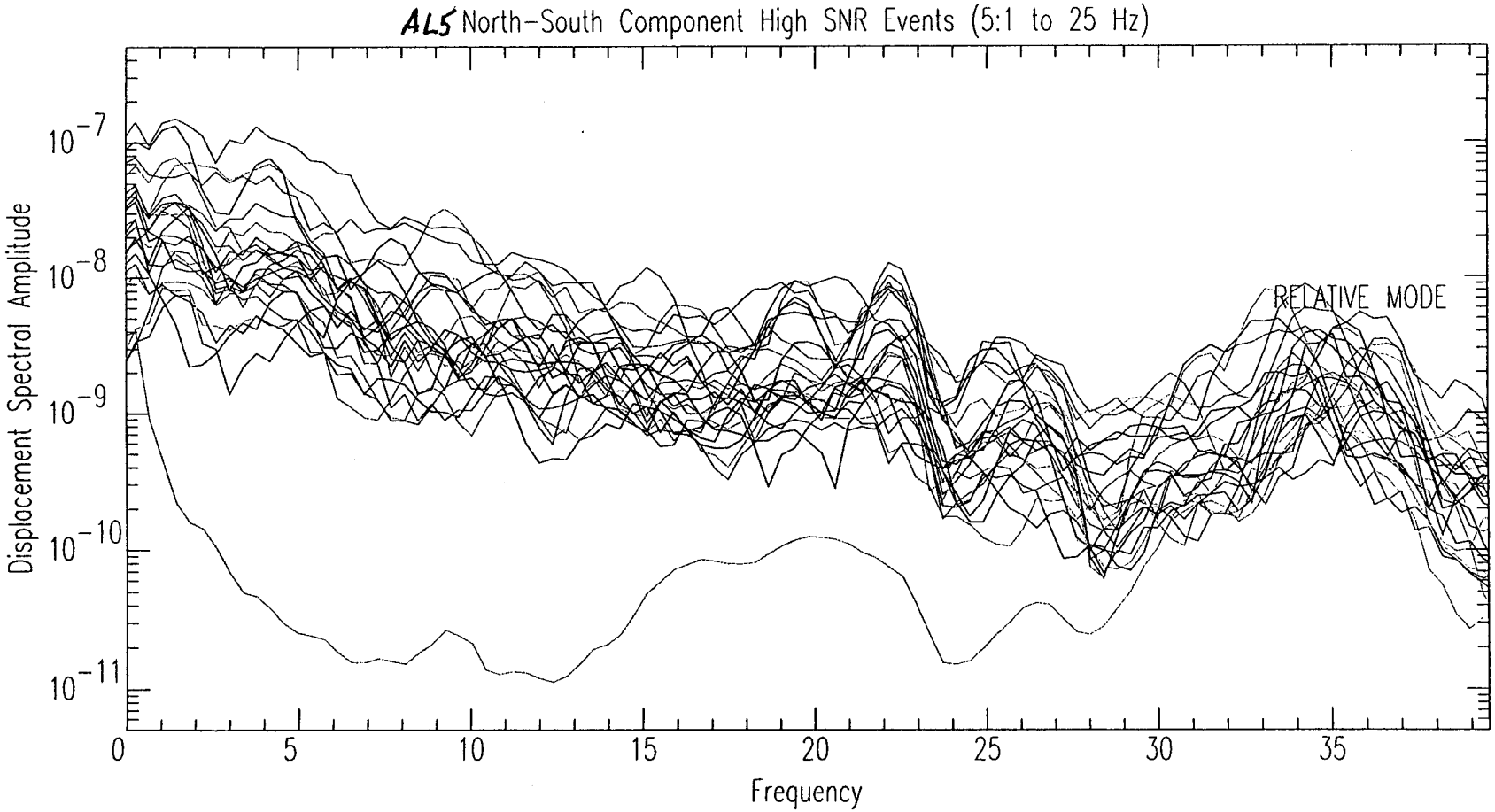
ALS North-South Component High SNR Events (5:1 to 25 Hz)
Displacement Spectral Amplitude
10^{-7}
10^{-8}
10^{-9}
10^{-10}
10^{-11}
RELATIVE MODE
0
5
10
15
20
25
30
35
Frequency

Figure 13-13

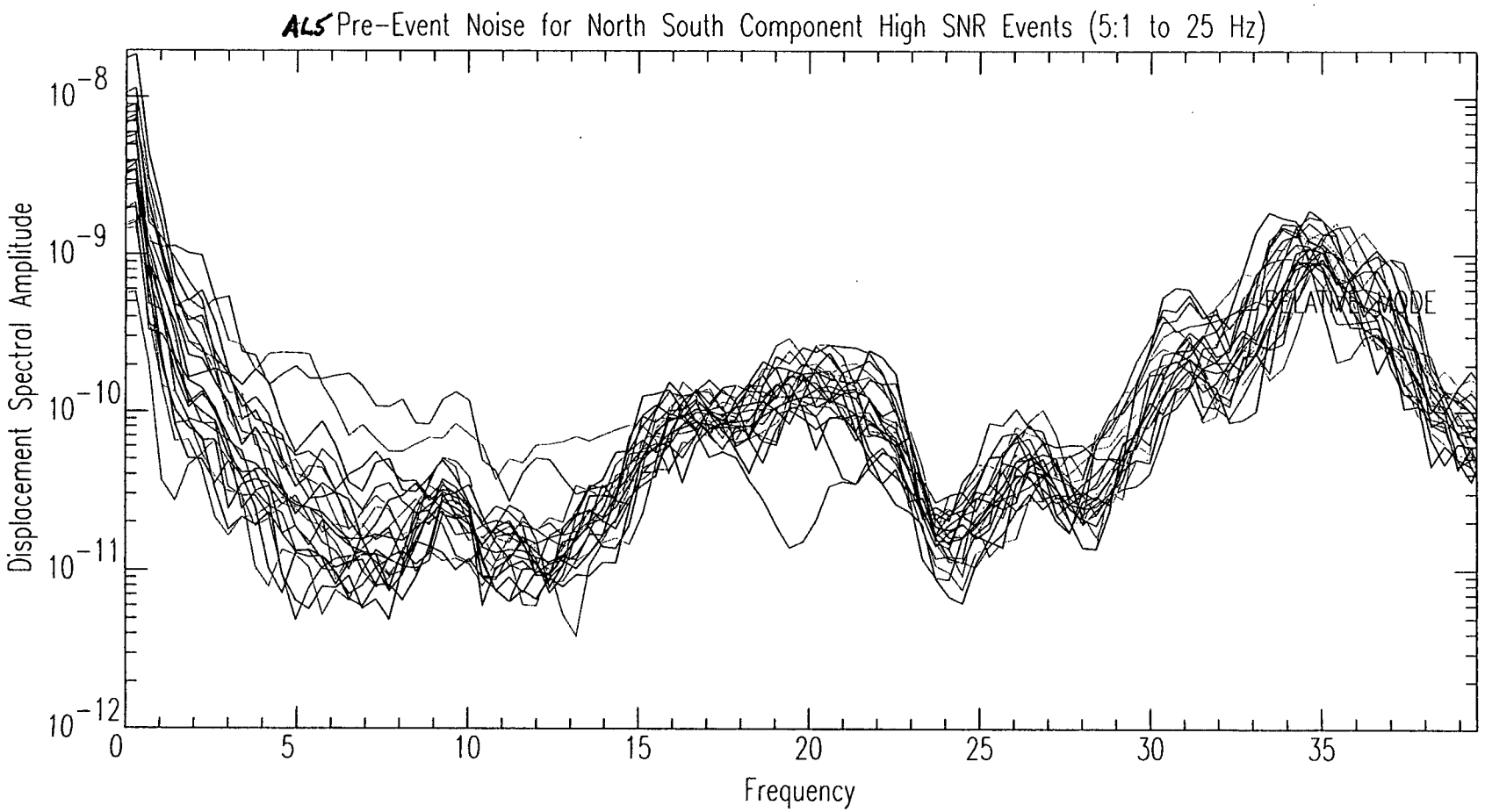
ALS Pre-Event Noise for North South Component High SNR Events (5:1 to 25 Hz)
Displacement Spectral Amplitude
10^{-8}
10^{-9}
10^{-10}
10^{-11}
10^{-12}
0
5
10
15
20
25
30
35
Frequency
RELATIVE MODE

Figure 13-14

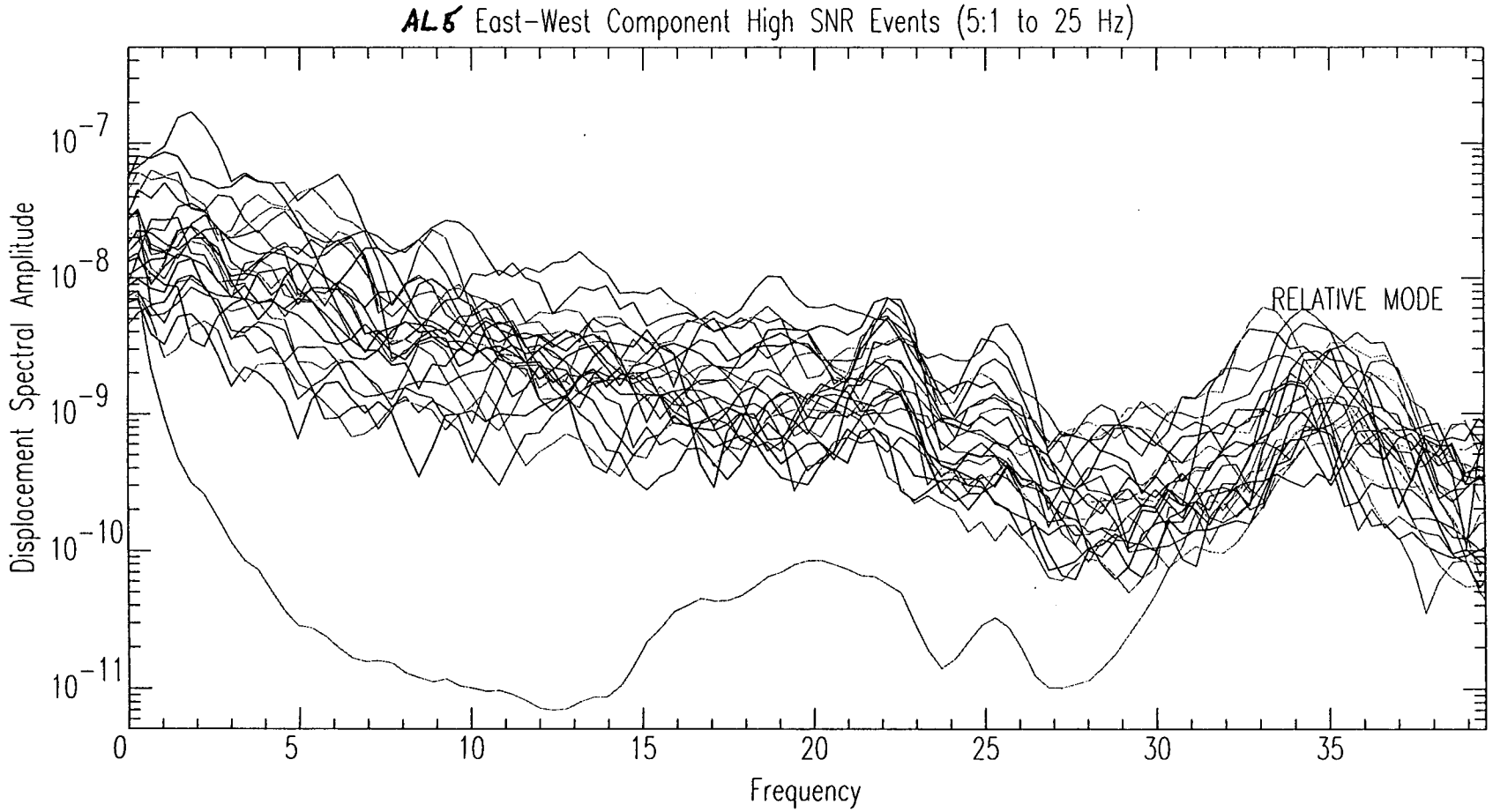
ALE East-West Component High SNR Events (5:1 to 25 Hz)
Displacement Spectral Amplitude
10^{-7}
10^{-8}
10^{-9}
10^{-10}
10^{-11}
RELATIVE MODE
0
5
10
15
20
25
30
35
Frequency

Figure 13-15

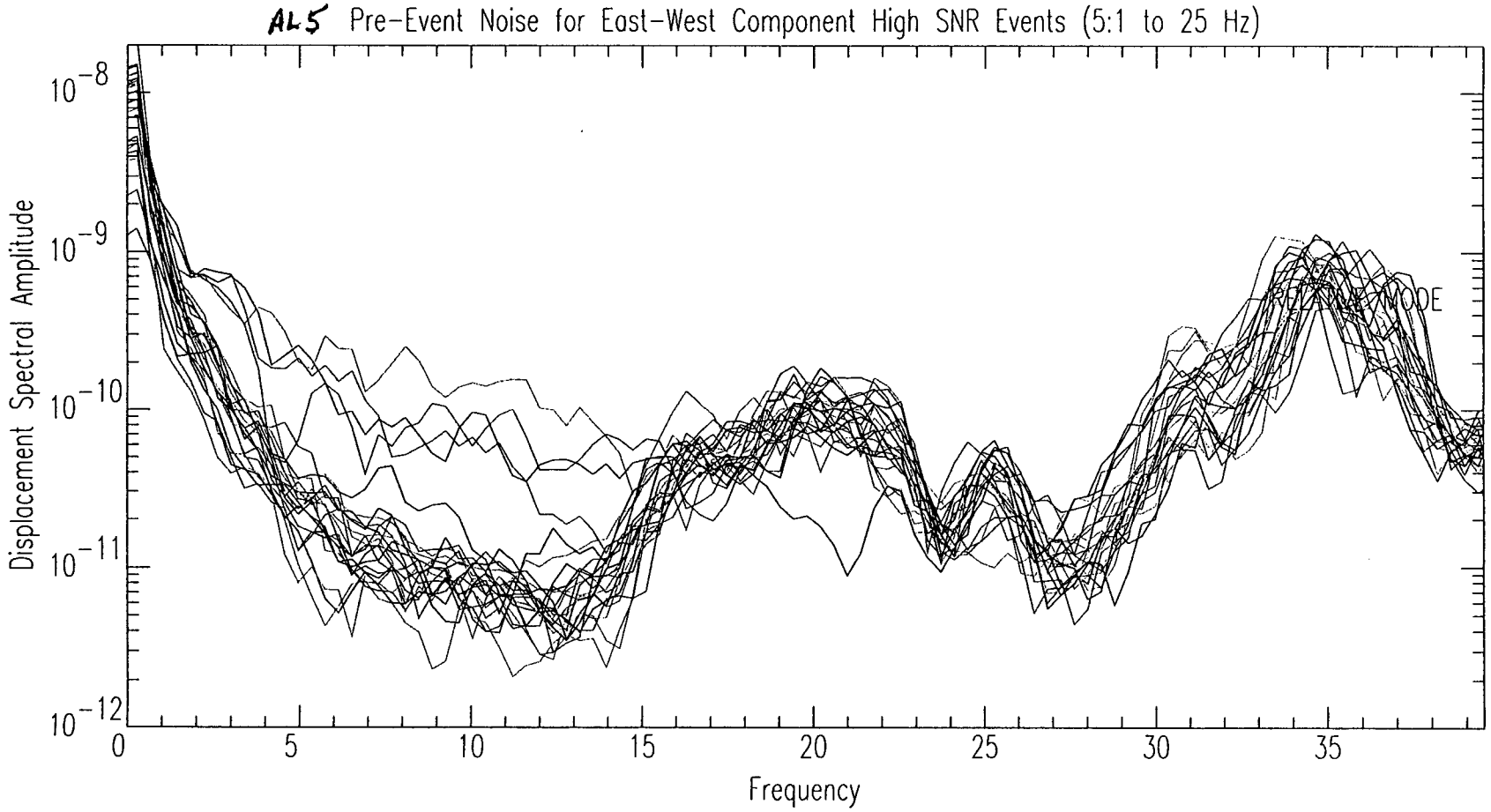
AL5 Pre-Event Noise for East-West Component High SNR Events (5:1 to 25 Hz)
Displacement Spectral Amplitude
10^{-8}
10^{-9}
10^{-10}
10^{-11}
10^{-12}
0
5
10
15
20
25
30
35
Frequency

Figure 13-16

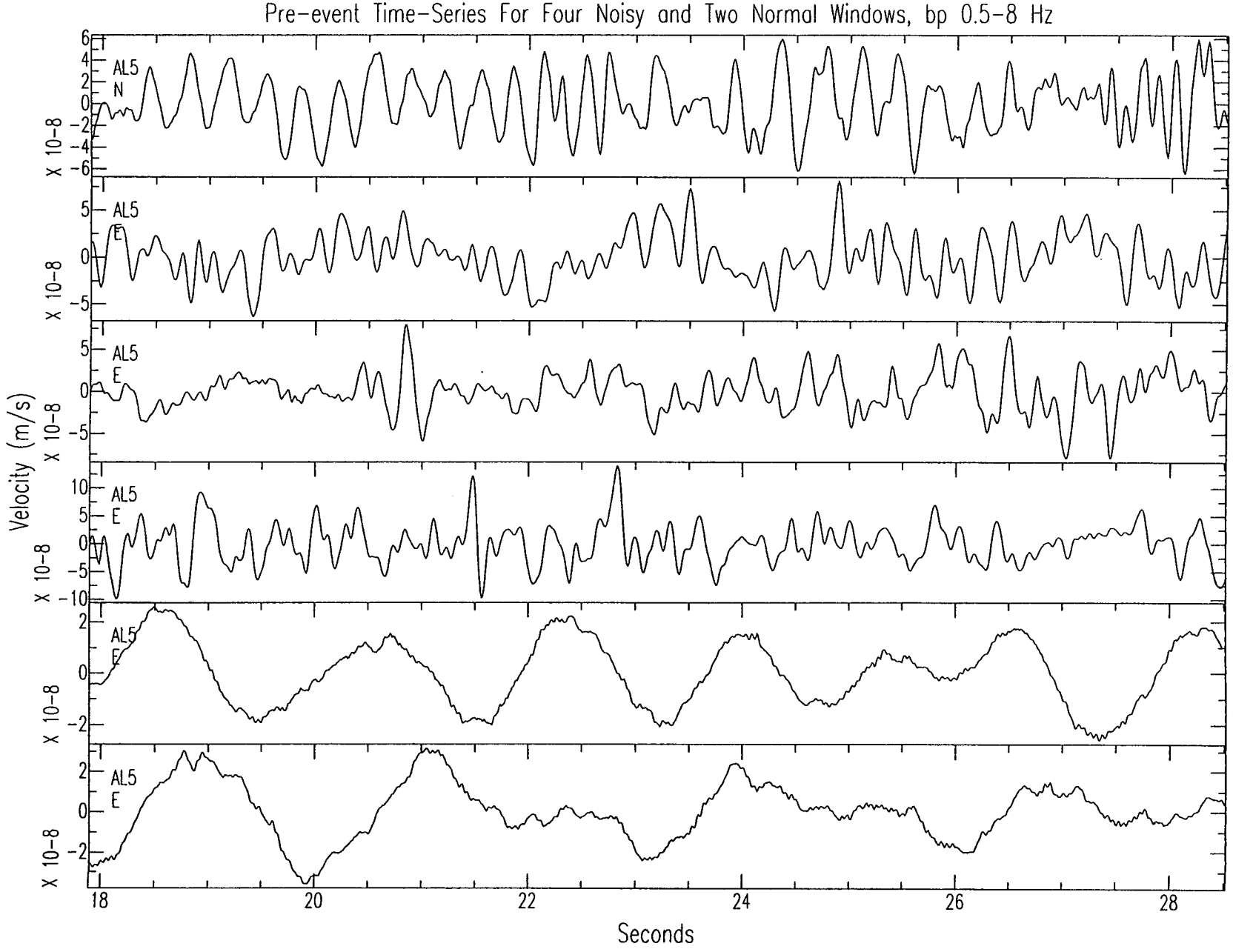
Pre-event Time-Series For Four Noisy and Two Normal Windows, bp 0.5-8 Hz
AL5
N
AL5
E
AL5
E
AL5
E
AL5
E
AL5
E
X 10-8
Velocity (m/s)
18
20
22
24
26
28
Seconds

Figure 13-17

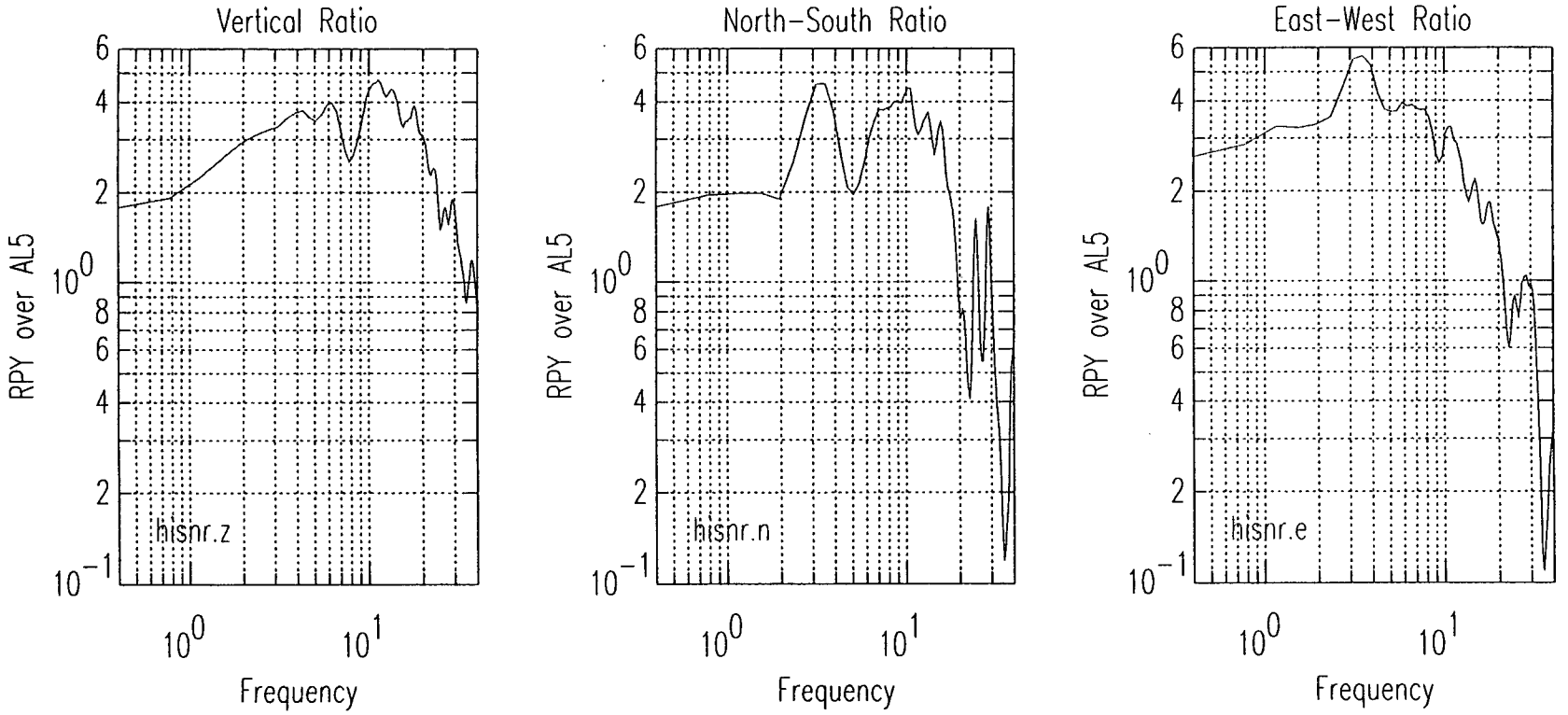
Vertical Ratio
North-South Ratio
East-West Ratio
RPY over AL5
Frequency
hisnr.z
hisnr.n
hisnr.e
6
4
2
10^0
8
6
4
2
10^{-1}
10^0
10^1

Figure 13-18

TABLE 3-2
YUCCA MOUNTAIN VELOCITY AND Q PROFILES

LAYER	DEPTH TO TOP (M)	V_S (KM/S)	V_P (KM/S)	DENSITY (G/CM^3)	Q_S	Q_P
1	0	0.6	1.8	1.7	25	80
2	40	1.2	2.5	2.0	40	120
3	80	1.5	2.9	2.3	40	120
4	220	1.9	3.2	2.4	70	150
5	1000	2.1	3.6	2.4	100	200

Source: Schneider *et al.* (1996)

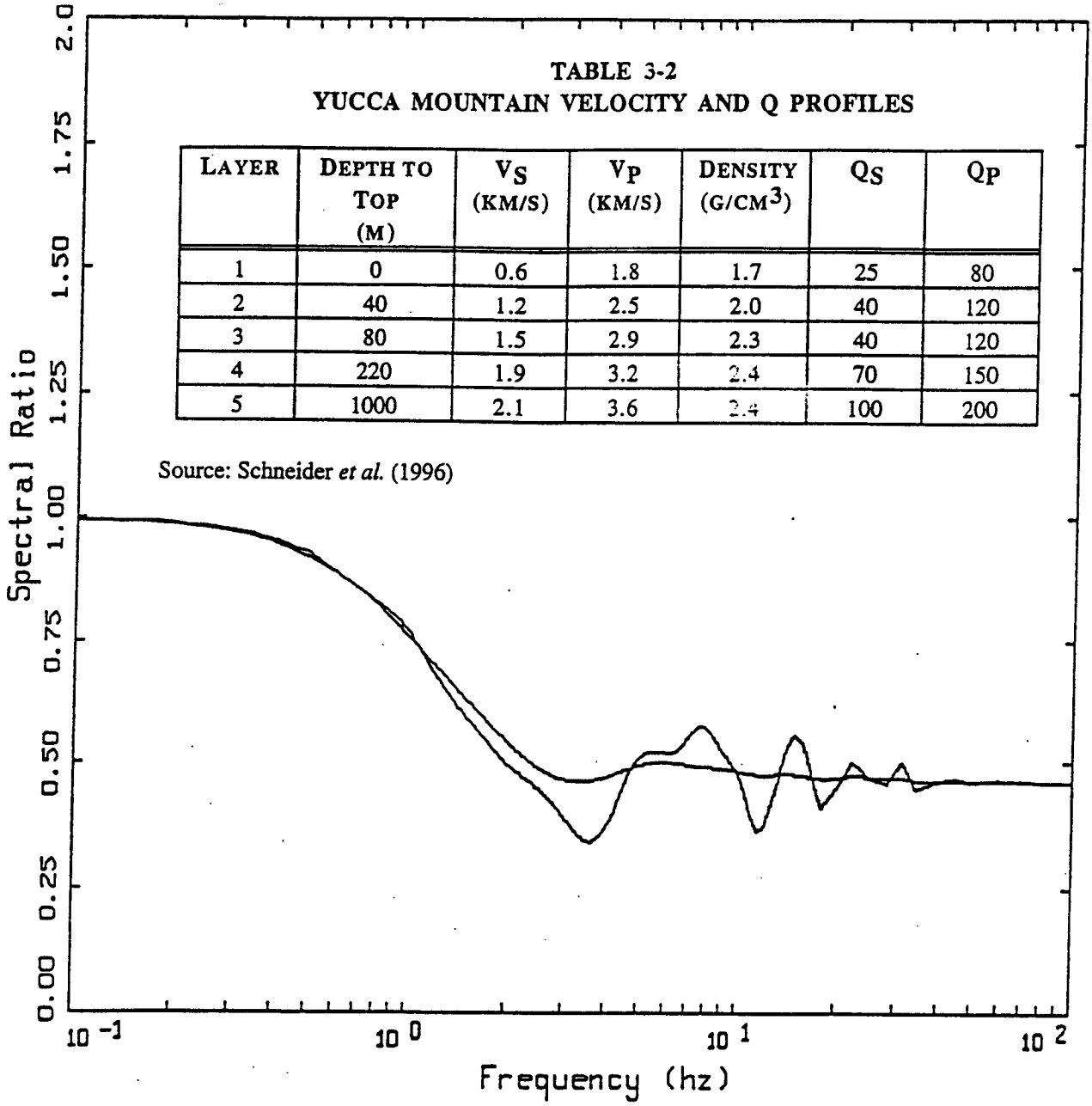

YUCCA 300M OUTCROP TO SURFACE
TRANSFER FUNCTION

LEGEND
5 %, TRANSFER FUNCTION
5 %, TRANSFER FUNCTION; 20 Hz smoothing

Figure 13-19

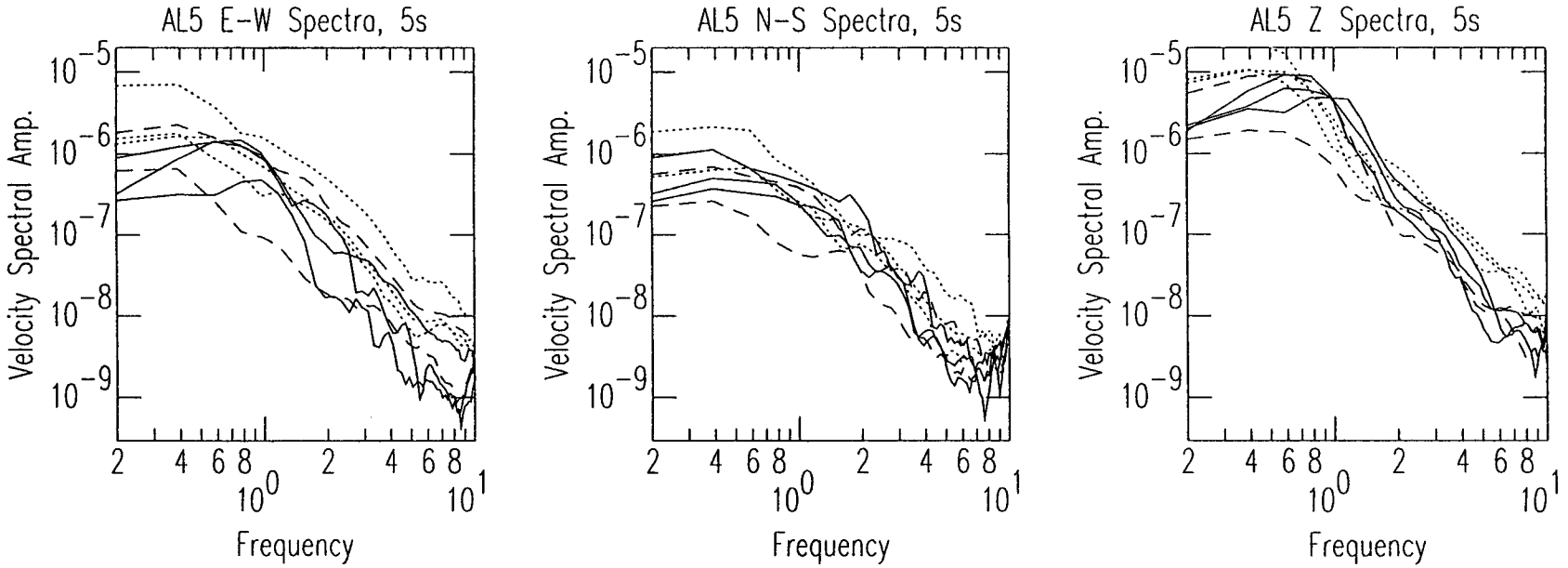
AL5 E-W Spectra, 5s
AL5 N-S Spectra, 5s
AL5 Z Spectra, 5s
Velocity Spectral Amp.
Frequency
10^{-5}
10^{-6}
10^{-7}
10^{-8}
10^{-9}
2 4 6 8 10^0 2 4 6 8 10^1

Figure 13-20

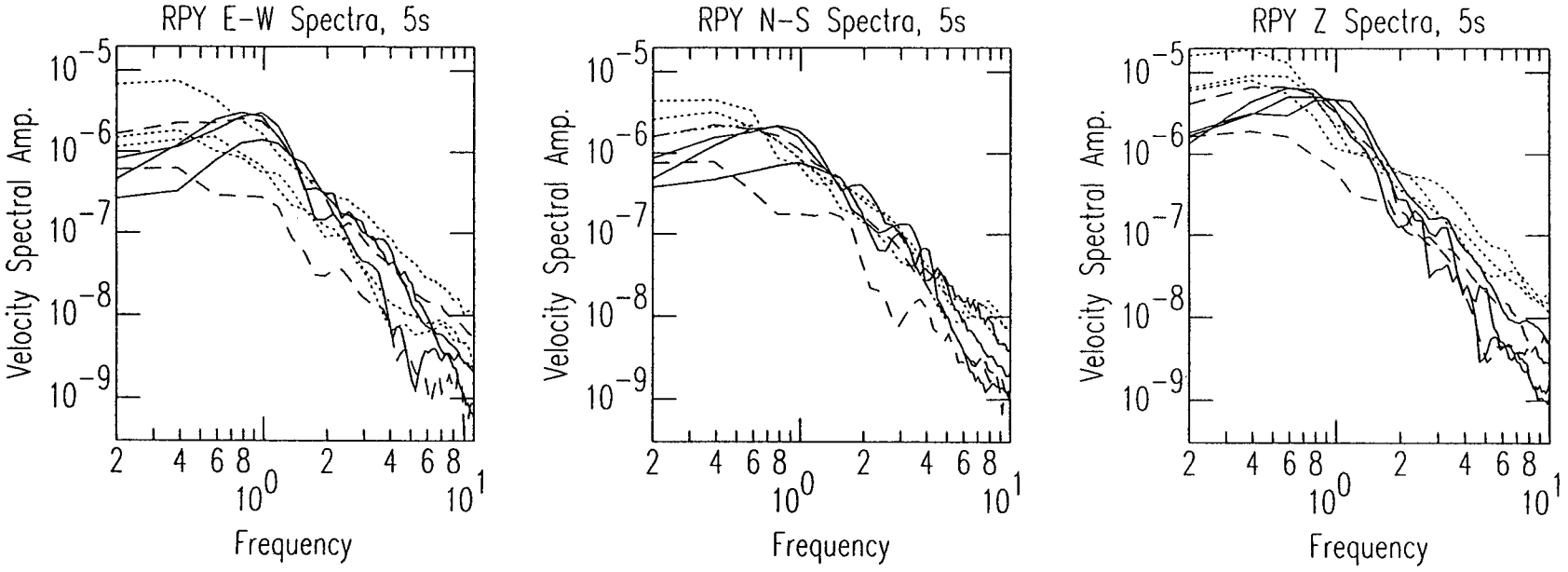
RPY E-W Spectra, 5s
RPY N-S Spectra, 5s
RPY Z Spectra, 5s
Velocity Spectral Amp.
Frequency
10^{-5}
10^{-6}
10^{-7}
10^{-8}
10^{-9}
2 4 6 8 10^{0} 2 4 6 8 10^{1}

Figure 13-21

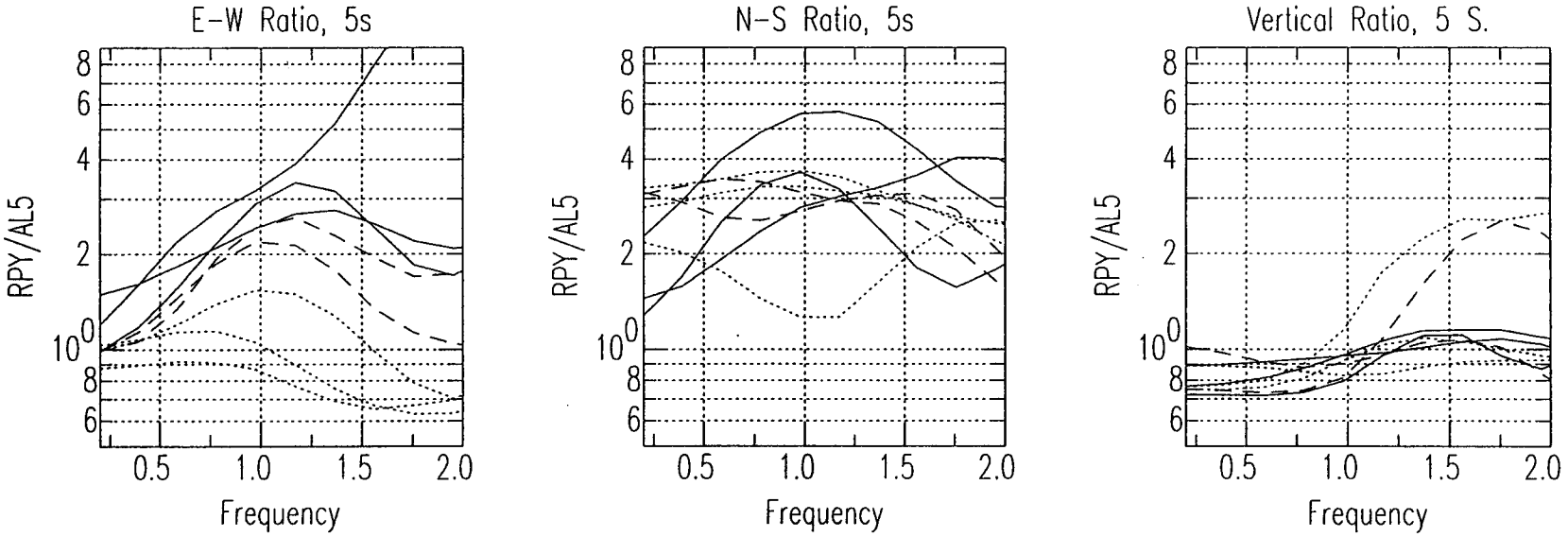
E-W Ratio, 5s
N-S Ratio, 5s
Vertical Ratio, 5 S.
RPY/AL5
Frequency
8
6
4
2
10^0
8
6
0.5
1.0
1.5
2.0

Figure 13-22

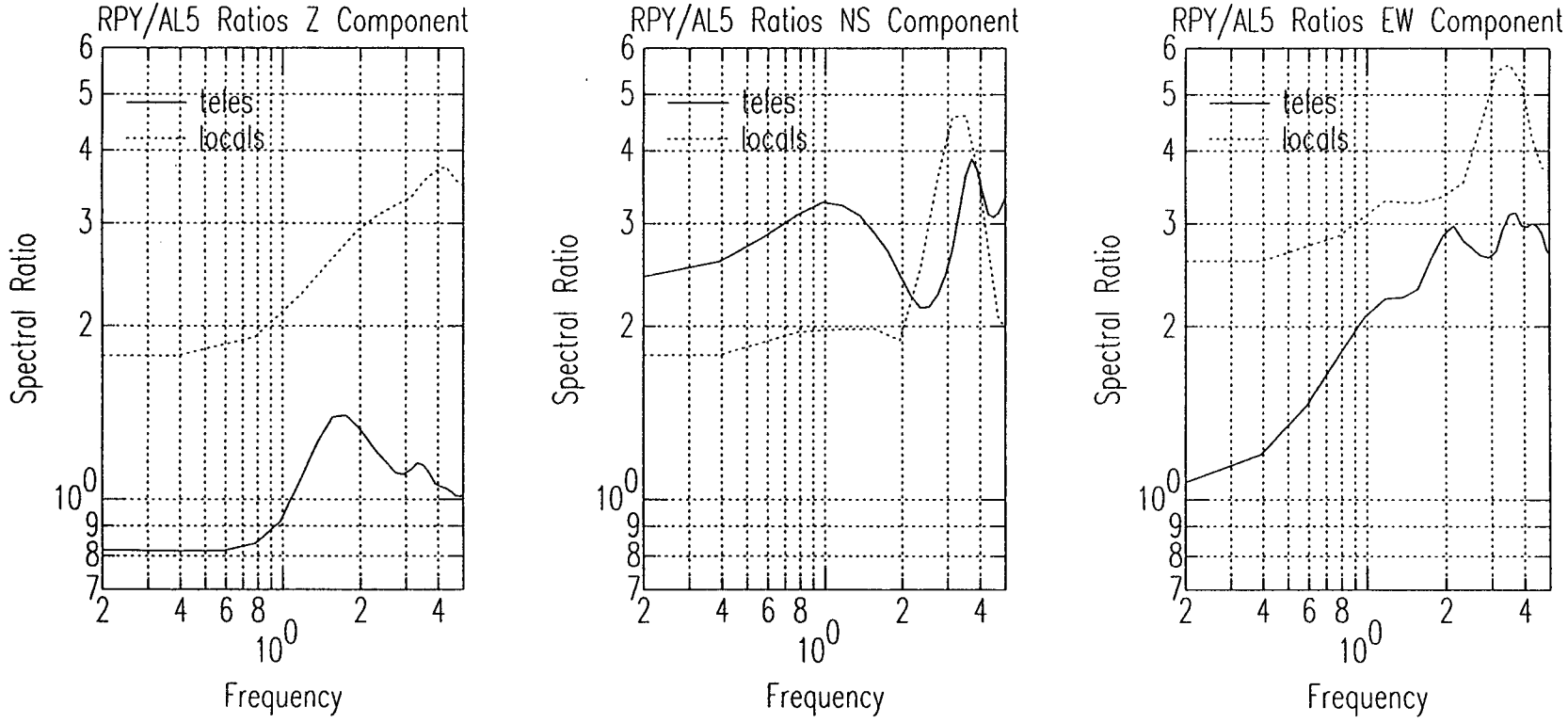
RPY/AL5 Ratios Z Component
RPY/AL5 Ratios NS Component
RPY/AL5 Ratios EW Component
teles
locals
Spectral Ratio
Frequency
6
5
4
3
2
10^0
9
8
7
2
4
6
8
2
4

Figure 13-23

Appendices

Appendix 1

Station Data and Description for the SGBDSN

code	station name and location	latitude north	longitude west	elevation km	on date	seismometer
AL5	Alcove 5, ESF, Southern NV	36.8596	116.4547	1.0660	1998252	Mark Products L4-3C
AMD	Amargosa Desert, Southern NV	36.4526	116.2809	0.7560	1997115	CMG-40 borehole
BTW	Beatty Wash, Southern NV	36.9978	116.5665	1.3910	1995230	Geotech S-13 Vertical
CAF	Calico Fan, NTS, Southern NV	36.8391	116.3377	1.1100	1995034	Geotech S-13 Vertical
CRF	Crater Flat, Southern NV	36.8118	116.5340	1.0320	1995165	Geotech S-13 Vertical
DOM	Dome Mountain, NTS, Southern NV	37.0021	116.4086	1.7110	1995333	Geotech S-13 Vertical
FMW	Forty Mile Wash, NTS, Southern NV	36.9021	116.3688	1.1460	1995165	Geotech S-13 Vertical
FRG	Fran Ridge, NTS, Southern NV	36.8169	116.4195	1.1550	1995165	Geotech S-13 Vertical
LSC	Little Skull Cliff, NTS, Southern NV	36.7307	116.3255	1.2380	1995034	Geotech S-13 Vertical
NCF	North Crater Flat, Southern NV	36.8899	116.5682	1.1510	1995034	Geotech S-13 Vertical
PUV	Plutonium Valley, NTS, Southern NV	36.9494	115.9633	1.2530	1995258	Geotech S-13 Vertical
RED	Red Mountain, NTS, Southern NV	36.6895	116.0930	1.1430	1996037	Geotech S-13 Vertical
RPY	Repository, NTS, Southern NV	36.8515	116.4563	1.3010	1996038	CMG-40 borehole
SCF	South Crater Flat, Southern NV	36.7568	116.5440	0.9090	1995034	Geotech S-13 Vertical
SGR	South Grapevine, Southern NV	36.9805	117.0327	1.5600	1998127	Geotech S-13 Vertical
SPC	Specter Range, NTS, Southern NV	36.6746	116.2030	1.0640	1996075	CMG-40 borehole
STC	Silent Canyon, NTS, Southern NV	37.2939	116.4358	1.9600	1995209	Geotech S-13 Vertical
STO	Solitario Canyon, Southern NV	36.8603	116.4742	1.3590	1995165	Geotech S-13 Vertical
SYM	South Yucca Mountain, NTS, Southern NV	36.7416	116.4460	0.9950	1995034	Geotech S-13 Vertical
TAR	Tarantula Canyon, Southern NV	36.8680	116.6322	1.2310	1996023	Geotech S-13 Vertical
TIM	Timber Mountain, NAFB, Southern NV	37.0667	116.4694	1.8710	1996143	CMG-40 borehole
TPW	Topopah Wash, NTS, Southern NV	36.9016	116.2519	1.5730	1995258	Geotech S-13 Vertical
TWP	Twin Peaks, NTS, Southern NV	37.2047	116.1234	1.5760	1995205	Geotech S-13 Vertical
TYM	Thirsty Mountain, NAFB, Southern NV	37.1441	116.7208	1.4570	1996275	CMG-40 borehole
WLD	Wildcat Mountain, Southern NV	36.7927	116.6257	0.9300	1995193	Geotech S-13 Vertical
YCW	Yucca Wash, NTS, Southern NV	36.9224	116.4756	1.4980	1996032	Geotech S-13 Vertical

Appendix 2
Downtime Log for the SGBDSN in FY98-99

Year	start		stop		comments
	Jday	hh:mm	jday	hh:mm	
--	---	-----	---	-- --	----------
97	295	20:25	295	20:40	dataServer hung -- no apparent reason
97	296	19:15	296	19:45	dataServer hung -- EW conflict? Buggy restart
97	306	22:53	306	23:36	disk full, Fish Lake Valley EQ
97	307	01:55	307	02:30	dataServer hung -- reason unknown
97	310	13:30	310	14:15	dataServer hung -- reason unknown
97	315	12:25	315	12:55	Y. M. node went down
97	318	05:40	318	06:05	dataServer hung -- reason unknown
97	328	16:53	328	17:03	adding modems in RT112 rack
97	329	01:00	329	01:15	connecting new station at Mammoth Lakes
97	364	12:40	364	13:20	dataServer hung -- reason unknown
97	364	18:50	364	19:10	dataServer hung -- modem bank 4 bad
98	018	13:30	018	16:55	gold1 spontaneous reboot; no page;reason unknown
98	031	22:25	032	01:15	dataServer hung -- no page due to alarm program
98	037	14:00	037	14:35	dataServer hung -- reason unknown
98	037	20:00	037	22:36	Power cycle on 112 rack (accidental), hung DataServer
98	059	20:25	059	20:40	Dataserver hung when second refraw was started by accident
98	086	21:34	086	21:54	Dataserver hung, refRaw killed by in-lab DAS
98	091	21:29	091	21:43	Software kernal patches
98	092	20:10	092	20:17	P.M.: reboot to impliment patches.
98	097	00:28	097	00:35	#1 112 hung; reset seemed to crash dataserver
98	105	18:10	105	18:55	dataServer hung -- reason unknown
98	106	01:40	106	01:53	dataServer hung -- reason unknown; promptly crashed again and restarted
98	106	08:20	106	08:40	dataServer hung -- reason unknown
98	107	21:10	107	21:50	dataServer hung -- reason unknown; did a complete RT112 reset to try and clear cause of recent crashes
98	108	13:50	108	14:20	dataServer hung -- same as above
98	128	18:35	128	18:45	bringing up station SGV
98	135	18:20	135	18:35	restarting refRaw to handle DAS 994
98	163	22:30	163	23:00	trying to bring up SHP station
98	164	00:00	164	00:15	problem with 3rd rack of RT112 --required a power cycle on RT112 to fix
98	166	15:50	166	16:10	data server hung-- reason unknown
98	166	21:55	166	22:05	bringing up station SHP
98	172	08:00	172	15:00	circuit breaker tripped, reconfig to /ymp7, times estimated only
98	173	08:25	173	14:30	reason unknown, times estimated only, alarm down due to ymp7 recording bug in alarm scripts
98	177	02:00	177	02:12	dataServer hung, reason unknown
98	177	02:23	177	02:31	dataServer hung, reason unknown
98	177	05:50	177	06:25	dataServer hung, reason unknown did power cycle, reset on all RT112's
98	223	15:15	223	17:50	dataServer hung
98	253	08:05	253	08:33	dataServer hung, reason unknown

98	285	18:40	285	18:50	RT112 disconnect -- fixing problem on bank 4
98	285	19:45	285	19:55	same as previous
98	298	21:55	298	22:05	rebooted gold1 -- numerous stagnant processes and machine not rebooted for 125 days
98	316	17:25	316	17:50	system taken down for rewiring of computer room
98	316	21:35	316	22:40	continuing outage for rewiring
98	334	17:20	334	17:45	resync RT112 modem bank 1
98	338	05:05	338	05:48	dataServer hung, reason unknown
98	339	19:50	339	21:20	dataServer hung, reason unknown -- rebooted gold1
98	340	07:52	340	15:02	dataServer hung, pager failure--forgot to reset it from vibrate to audible
98	358	07:40	340	09:15	dataServer hung, reason unknown
98	358	19:30	340	09:47	purposely aborted refRaw -- training exercise
99	004	23:15	004	23:40	dataServer hung, reason unknown
99	010	20:10	010	20:40	dataServer hung, reason unknown
99	010	21:05	010	21:25	dataServer hung, "modem 0" packet?
99	011	00:45	011	02:10	dataServer hung, "modem 0" packet?
99	070	06:35	070	07:05	dataServer hung, reason unknown
99	070	08:15	070	09:15	dataServer hung, "modem 0" packet? recycled power on modem bank 4 and reset RT112
99	071	10:15	071	10:30	resyncing modem bank 1 -- transmission problem
99	090	00:15	090	00:30	bringing 2 stations back online
99	113	19:05	113	19:57	Unknown; possibly due to /usr/local or local network maint.
99	113	21:25	113	21:53	Orb shutdown for maintenance; crashed dataserver (invalid portmask error)
99	114	08:45	114	09:17	dataServer hung, "modem 0" packet
99	116	13:20	116	13:58	dataServer hung, "modem 0" packet--recycled power on modem bank 4 and reset RT112
99	116	19:40	116	19:58	dataServer hung, "modem 0" packet
99	116	21:15	116	21:45	dataServer hung, "modem 0" packet--recycled power again on modem bank 4, reset and resync'd RT112
99	117	05:05	117	05:21	dataServer hung, "modem 0" packet--recycled power again on modem bank 4, reset and resync'd RT112
99	124	23:55	125	00:30	Rack 0 died; resetting the RT112 killed the data server. original RT112 problem unknown
99	183	12:15	183	12:57	dataServer hung, "modem 0" packet--recycled power on modem bank 4 and reset RT112
99	193	18:20	193	18:33	stopped to add modems to rack
99	193	18:40	193	18:47	stopped again -- fix slight problem
99	208	23:25	208	23:36	restart to accommodate a new station (DON)
99	214	00:50	214	01:25	Dataserver down, last line: RT112 Version: 02.80 (NodasID = 7896 packetID = 0)
99	214	02:20	214	02:28	Dataserver crashed by ref2orb reset.
99	214	21:50	214	22:15	UPS spontaneous outage.
99	216	05:00	216	05:45	Rack 3 problems. Two quick crashes - resync'd 112's
99	219	23:00	219	23:30	estimated times
99	223	19:10	223	19:35	DataServer crashed -- reason unknown
99	228	21:05	228	21:30	DataServer crashed -- reason unknown
99	228	23:15	228	23:30	DataServer crashed due to restart of ref2orb
99	231	00:30	231	01:00	DataServer crashed -- reason unknown
99	232	00:55	232	01:30	DataServer crashed -- reason unknown
99	232	03:05	232	03:15	DataServer crashed due to restart of ref2orb
99	232	13:30	232	14:10	DataServer crashed -- reason unk.—recycled power modem bank 4, reset RT112, resync'd modems

99	257	15:40	257	16:40	replacing internet router in computer room
99	258	17:04	258	17:18	reset modem bank 2 for "full" problem on DAS 1000
99	271	23:40	272	00:05	DataServer crashed -- reason unknown
99	272	00:28	272	00:41	DataServer crashed -- reason unknown

Notes:

Note 1: Downtimes are taken from on-line file entries.

Note 2: Times reported here cover intervals for which the entire data collection was down or inoperative due to software program failure, transmission failure, modem bank failure, or other hardware failure. It is not intended to cover individual station downtimes.

Note 3: Downtimes may be misleading. The DAS units in the field retain the data when the data collection program or modem bank is down and may send it all when they come back up.

Appendix 3
Catalog of FY98-99 Earthquakes

(listed as an electronic supplement)

Appendix 4
Events identified as blasts in FY98-99

year	julian_day	hour	minute	comments
1997	275	22	56	Near TAR
1997	279	23	05	Near TAR
1997	281	19	09	Near TAR
1997	283	19	04	Near TAR
1997	289	23	44	Near TAR
1997	293	19	04	Near TAR
1997	294	23	05	Near TAR
1997	296	23	04	Near TAR
1997	302	20	08	Near WLD, TAR
1997	308	00	05	
1997	309	00	05	
1997	310	00	06	
1997	314	20	08	
1997	317	00	00	
1997	323	00	05	
1997	328	00	02	
1997	336	00	03	
1997	336	23	56	
1997	339	00	00	
1997	342	23	01	
1997	343	00	02	
1997	346	00	01	
1997	351	23	19	
1997	357	00	30	
1997	357	21	27	
1998	006	00	05	
1998	009	19	57	First sta. @ WLD
1998	013	00	04	First sta. @ TAR
1998	013	22	01	First sta. @ WLD
1998	015	00	00	Near TAR
1998	018	21	54	First sta. @ TWP
1998	021	00	03	First sta. @ TAR
1998	022	00	04	Near TAR
1998	022	23	00	Near TAR
1998	026	10	53	First sta. @ STC
1998	027	18	40	First sta. @ STC
1998	027	20	04	First sta. @ TAR
1998	029	20	09	Near TAR
1998	034	00	05	First sta. @ TAR
1998	034	20	03	First sta. @ TAR
1998	036	23	57	First sta. @ TAR
1998	041	00	03	
1998	041	23	59	
1998	043	23	51	First sta. @ TAR
1998	050	20	05	First sta. @ TAR
1998	054	22	54	First sta. @ WLD
1998	057	00	05	First sta. @ WLD
1998	058	00	00	Near WLD
1998	063	00	07	First sta. @ WLD

year	julian_day	hour	minute	comments
1998	064	20	06	First sta. @ WLD
1998	064	06	32	First sta. @ WLD
1998	064	07	56	First sta. @ WLD
1998	069	20	04	
1998	070	12	58	First sta. @ STC
1998	073	19	31	
1998	076	00	00	
1998	076	22	50	Blast near CAF, TPW
1998	078	23	57	
1998	079	21	36	
1998	080	02	23	Near CAF
1998	080	20	12	Near CAF
1998	084	20	05	Near WLD
1998	086	00	00	
1998	091	00	00	
1998	092	23	56	First sta. @ WLD
1998	098	22	54	Near WLD
1998	099	08	00	Near STC
1998	099	22	56	Blast near WLD-Regional mixed in
1998	101	16	33	Near WLD
1998	105	23	04	Near WLD
1998	113	19	05	Near WLD
1998	117	22	58	Near WLD
1998	118	23	04	Near WLD
1998	121	02	56	Blast-no S, 0 depth, etc
1998	125	23	01	Near WLD
1998	126	21	43	Probable blast-all up, no S.
1998	132	23	03	Near WLD
1998	134	19	04	Near WLD
1998	139	16	58	Near WLD
1998	146	23	00	Near WLD
1998	148	23	04	Near WLD
1998	153	15	53	Blast near WLD
1998	153	22	34	Blast near WLD
1998	153	23	06	First sta. @ WLD
1998	155	07	49	First sta. @ WLD
1998	160	23	08	First sta. @ WLD
1998	161	23	05	First sta. @ WLD
1998	167	19	02	First sta. @ WLD
1998	169	23	10	First sta. @ WLD
1998	174	03	58	First sta. @ WLD
1998	174	19	08	First sta. @ WLD
1998	175	19	04	First sta. @ WLD
1998	176	21	57	First sta. @ WLD
1998	180	20	54	Near WLD
1998	182	20	06	First sta. @ WLD
1998	189	23	08	First sta. @ WLD
1998	195	23	09	First sta. @ WLD
1998	195	05	20	Collapse?
1998	197	23	42	Near STC
1998	201	23	08	First sta. WLD
1998	202	23	04	First sta. @ WLD
1998	208	23	11	First sta. @ WLD
1998	210	19	04	Near WLD
1998	216	23	09	First sta. @ WLD

year	julian_day	hour	minute	comments
1998	217	20	39	
1998	217	22	55	First sta. @ NCF
1998	218	21	19	First sta. @ TAR
1998	218	21	20	With previous event
1998	220	19	35	First sta. @ RED
1998	223	23	08	First sta. @ BTW
1998	229	23	13	First sta. @ TAR
1998	231	17	15	First sta. @ TAR
1998	233	00	24	First sta. @ TAR
1998	233	01	01	First sta. @ TAR
1998	240	18	18	First sta. @ TAR
1998	240	23	46	First sta. @ STC
1998	243	23	03	First sta. @ TAR
1998	244	19	00	First sta. @ TAR
1998	245	17	01	First sta. @ TAR
1998	246	19	03	First sta. @ TAR
1998	247	21	31	
1998	251	22	18	First sta. @ TAR
1998	256	23	40	First sta. @ TAR
1998	258	15	39	First sta. @ STC
1998	258	23	06	First sta. @ TAR
1998	259	19	19	First sta. @ TAR
1998	259	23	49	First sta. @ WLD
1998	261	05	20	First sta. @ STC
1998	261	05	43	First sta. @ STC
1998	261	07	52	First sta. @ TAR
1998	264	23	04	First sta. @ TAR
1998	266	16	00	First sta. @ TAR
1998	267	23	02	First sta. @ TAR
1998	271	20	05	First sta. TIM + STC
1998	271	23	05	First sta. @ TAR
1998	272	23	09	First sta. @ TAR
1998	273	23	08	First sta. @ PUV
1998	274	22	03	First sta. @ TWP
1998	274	23	05	First sta. @ WLD
1998	278	06	07	First sta. @ WLD
1998	278	06	21	First sta. @ WLD
1998	278	23	34	First sta. @ TAR
1998	280	19	04	First sta. @ TAR
1998	280	23	12	First sta. @ TAR
1998	281	23	09	First sta. @ TAR
1998	286	15	30	First sta. @ TAR
1998	287	19	13	First sta. @ TAR
1998	288	19	13	First sta. @ TAR
1998	293	19	10	First sta. @ TAR
1998	293	23	06	First sta. @ TAR
1998	295	19	06	First sta. @ TAR
1998	299	20	11	First sta. @ TAR
1998	302	20	10	
1998	306	20	08	First sta. @ TAR
1998	307	20	10	First sta. @ TAR
1998	308	20	02	First sta. @ TAR
1998	309	23	59	First sta. @ TAR
1998	310	00	00	
1998	313	17	21	First sta. @ TAR

year	julian_day	hour	minute	comments
1998	316	20	12	First sta. @ TAR
1998	316	14	58	First sta. @ TAR
1998	322	00	05	First sta. @ TAR
1998	323	20	05	First sta. @ TAR
1998	327	00	07	First sta. @ TAR
1998	327	20	05	First sta. @ TAR
1998	327	23	55	First sta. @ TAR
1998	328	23	16	First sta. @ TAR
1998	335	20	10	First sta. @ TAR
1998	336	00	03	First sta. @ TAR
1998	337	00	01	First sta. @ TAR
1998	337	00	30	
1998	338	00	03	First sta. @ TAR
1998	342	20	27	First sta. @ TAR
1998	344	00	08	First sta. @ TAR
1998	345	00	03	First sta. @ TAR
1998	350	17	25	First sta. @ TAR
1998	351	06	11	First sta. @ SYM
1998	351	20	29	First sta. @ TAR
1998	355	23	51	First sta. @ TAR
1998	363	00	34	First sta. @ TAR
1998	364	20	03	First sta. @ TAR
1998	365	00	30	First sta. @ TAR
1998	365	00	53	First sta. @ TAR
1998	365	20	01	First sta. @ TAR
1999	005	00	04	First sta. @ TAR
1999	008	00	00	First sta. @ TAR
1999	009	18	47	First sta. @ CAF
1999	009	20	35	First sta. @ CAF
1999	012	20	09	
1999	013	20	10	
1999	013	01	36	
1999	015	00	02	
1999	018	20	15	
1999	019	22	38	
1999	021	16	17	
1999	025	20	05	
1999	025	22	34	
1999	025	23	01	
1999	033	20	04	
1999	034	20	08	
1999	035	19	05	
1999	039	21	17	
1999	040	20	07	
1999	041	20	04	
1999	043	00	06	Near TAR
1999	047	17	50	
1999	048	00	11	
1999	049	00	07	
1999	054	20	06	
1999	055	20	07	
1999	057	08	06	
1999	061	00	08	
1999	061	20	08	
1999	063	00	04	

year	julian_day	hour	minute	comments
1999	063	23	50	
1999	068	21	49	
1999	070	20	07	Near TAR
1999	074	23	58	Near TAR
1999	075	11	42	Near TAR
1999	076	20	05	Near TAR
1999	076	00	00	Near WLD
1999	078	00	06	Near TAR
1999	082	20	04	First sta. @ TAR
1999	083	20	04	First sta. @ TAR
1999	085	00	03	First sta. @ TAR
1999	089	00	02	First sta. @ TAR
1999	089	20	08	Tele. mixed in-First sta. @ TAR
1999	091	00	07	First sta. @ TAR
1999	096	23	02	
1999	098	22	57	
1999	103	23	03	
1999	104	23	04	
1999	112	15	07	
1999	116	16	28	
1999	118	20	25	
1999	119	22	36	
1999	124	19	06	
1999	125	19	01	
1999	125	19	03	
1999	126	22	58	
1999	132	23	03	
1999	133	19	05	
1999	137	23	05	
1999	139	23	04	
1999	144	22	59	
1999	145	19	04	
1999	146	18	58	
1999	147	22	55	
1999	153	19	06	
1999	154	20	04	
1999	154	20	05	
1999	154	23	00	
1999	159	23	06	
1999	166	19	08	
1999	168	19	07	
1999	177	17	57	Near TAR
1999	180	17	24	
1999	182	19	02	
1999	190	22	45	
1999	200	19	06	Near TAR
1999	201	22	58	Near TAR
1999	203	20	58	Near TAR
1999	207	15	30	Near TAR
1999	212	17	47	Near TAR
1999	221	19	48	
1999	221	19	49	
1999	223	23	05	
1999	225	16	59	
1999	227	08	48	

year	julian_day	hour	minute	comments
1999	230	16	21	
1999	231	23	03	
1999	235	20	27	
1999	239	19	03	
1999	240	19	04	
1999	242	06	45	
1999	244	23	02	Near TAR
1999	250	16	24	Near TAR
1999	251	11	43	Near TAR
1999	252	23	01	Near TAR
1999	260	23	07	Near WLD
1999	271	23	01	
1999	273	23	06	Near TAR